



University  
of Glasgow

Crawford, Andrew Raymond (2013) *Iodoreboxetine: the development of a novel SPECT brain imaging tracer for the noradrenaline transporter*. PhD thesis.

<http://theses.gla.ac.uk/4226/>

Copyright and moral rights for this thesis are retained by the author

A copy can be downloaded for personal non-commercial research or study, without prior permission or charge

This thesis cannot be reproduced or quoted extensively from without first obtaining permission in writing from the Author

The content must not be changed in any way or sold commercially in any format or medium without the formal permission of the Author

When referring to this work, full bibliographic details including the author, title, awarding institution and date of the thesis must be given

**Iodoreboxetine:  
The Development of a Novel SPECT Brain Imaging  
Tracer for the Noradrenaline Transporter**

**Andrew Raymond Crawford**

B.Sc. (HONS): Biomedical Sciences, Durham University, 2005

Submitted in fulfilment of the requirements for the degree of:  
**Doctor of Philosophy**



**UNIVERSITY  
*of*  
GLASGOW**

**Institute of Neuroscience and Psychology  
Faculty of Medical, Veterinary, and Life Sciences  
University of Glasgow**

Garscube Estate, Bearsden Road, G61 1QH  
GLASGOW, SCOTLAND, UNITED KINGDOM

11 January 2013

## **Author's Declaration**

I declare that this thesis embodies the results of my own special work, that it has been composed by myself, and that it does not include work forming part of a thesis presented successfully for a degree in this or another University.

**Andrew Raymond Crawford.**

## Acknowledgements

I would like to extend my sincere thanks to the University of Glasgow and to Dr Deborah Dewar for selecting me for the research programme and for her guidance. My gratitude also to Dr William Holmes and Professor I Mhairi Macrae for their unwavering support, invaluable advice, and encouragement.

I greatly appreciate the staff and fellow students at the university for their help and support. Particular thanks are due to the laboratory staff, lead by Mrs Margaret Stewart, who provided assistance for a range of multidisciplinary techniques. Thanks are due, also, to Mrs Joan Stewart, Mrs Linda Carberry, Mrs Lindsay Gallagher, Mr Jim Mullin, Mrs Ann Marie Colquhoun, and Drs Rosemarie Spike, Mark McLaughlin, Hillary Carswell, Tracy Farr, Torsten Ruest, Kerrie Mulloy, and Rungrut Sutthiwarotamakun.

I had the pleasure of working with wonderful collaborators. Dr Andrew Sutherland, Dr Nicola Jobson, and Dr Sally Pimlott were indispensable partners throughout the ligand development project. Also, at YRING/PsyRING, I wish to thank Professor Judith Pratt, Professor Brian Morris, Dr Susan Cochran, Dr Antonio Ferra, Dr Matthew Kennedy, and Dr Allan McVie for sharing their knowledge and expertise during our schizophrenia collaboration.

The support and advice provided by my supervisory team at GlaxoSmithKline is much appreciated. Dr Thomas Bonasera, Dr Idriss Bennacef, and Dr Anthony Gee made my industrial placement both productive and enjoyable, and Dr Klara Valkó was very generous with her time.

The wonderful support of my loving family and dear friends has been invaluable. My parents have always encouraged my studies and have instilled the values that guide me through life. My sister, Carrie, always cheers my efforts, and my friends Dr Daniel and Mrs Victoria Growcott never cease to be uplifting. I also appreciate Dr Scott Whitaker for always being reassuringly cheerful about the future.

The author is indebted to the BBSRC, GlaxoSmithKline, and the University of Glasgow for providing the finance to support the research programme.

Finally, I wish to thank my wife, Nicola, for her love, patience, and unwavering support throughout. I dedicate this thesis and my life to her.

# List of Contents

<b>Title Page</b>	i
<b>Author's Declaration</b>	ii
<b>Acknowledgements</b>	iii
<b>List of Contents</b>	iv
<b>List of Figures</b>	ix
<b>List of Tables</b>	xii
<b>Thesis Summary</b>	xvii
<b>Abbreviations</b>	xxi
<b>Chapter 1: General Introduction</b>	<b>1</b>
1 Introduction	1
1.1 Monoamine systems	1
1.1.1 Noradrenaline system	1
1.1.2 Serotonin system	6
1.1.3 Dopamine system	6
1.1.4 Monoamine neurotransmitters, receptors, and transporters	10
1.2 Schizophrenia	15
1.2.1 Symptoms	15
1.2.2 Imaging in schizophrenia	16
1.2.3 Treatment and prognosis	19
1.2.4 Noradrenergic hypothesis	21
1.3 PCP-induced rat model of the metabolic hypofrontality observed in schizophrenia	24
1.3.1 Phencyclidine	24
1.3.2 Pathways implicated in schizophrenia and the PCP model	25
1.3.3 Hypothesis and study aims	29
1.4 Neuroimaging	30
1.4.1 The need for a SPECT brain imaging tracer for the NAT	30
1.4.2 Potential NAT-specific compounds for SPECT tracer development	32
1.4.3 Objectives for new iodoreboxetine analogues	38
1.5 Principles of <i>In Vivo</i> Imaging	39

1.5.1	Advantages of non-invasive SPECT and PET techniques	39
1.5.2	SPECT and PET Theory	40
1.5.3	SPECT vs. PET	43
1.5.4	Requirements for a SPECT brain imaging tracer for the noradrenaline transporter	44
1.6	Introduction to HPLC testing in tracer development	46
1.6.1	Lipophilicity ( $\log P$ or $\log P_{OCT}$ ) – blood-brain barrier penetration and nonspecific binding	47
1.6.2	Phospholipophilicity ( $\log D_{7.4 IAM}$ ) – predicting <i>in vivo</i> nonspecific binding	48
1.6.3	$\log BB$ – predicting blood brain barrier penetration	49
1.6.4	Immobilised protein chromatography ( $c\%PPB$ ) – predicting plasma protein binding <i>in vivo</i>	49
1.6.5	Reference Compounds: Successful and failed imaging tracers	50
1.7.	Thesis Aims	52
<b>Chapter 2: Methods</b>		<b>53</b>
2.1	PCP Study Methods	53
2.1.1.	Treatment regime	53
2.1.2.	Section Preparation	54
2.1.3.	Quantitative ligand binding autoradiography	54
2.1.4.	Radioligand binding	58
2.1.5.	<i>In situ</i> hybridisation	59
2.2.	Radioligand development	64
2.2.1.	Homogenate preparation protocol	66
2.2.2.	Competition binding experiments	68
2.2.3.	$K_i$ calculation and analysis	68
2.3.	<i>In Vitro</i> High Performance Liquid Chromatography (HPLC) Methodology	69
2.3.1	Chromatography System and Methods	69
2.3.2.	Determination of lipophilicity using C-18 column data	76
2.3.3	Determination of non-specific binding using IAM (phospholipid) column data	77

2.3.4	Determination of blood-brain barrier penetration using LUNA column data	77
2.3.5	Determination of plasma protein binding using HSA and AGP column data	78
<b>Chapter 3: Imaging Monoamine Transporters in the PCP-induced Rat Model of the Metabolic Hypofrontality Observed in Schizophrenia</b>		79
3.1	Results	79
3.1.1	[ <sup>3</sup> H]-nisoxetine binding to the NAT	79
3.1.2	[ <sup>3</sup> H]-WIN-35,428 binding to the DAT	90
3.1.3	[ <sup>3</sup> H]-citalopram binding to the SERT	101
3.1.4	<i>In situ</i> hybridisation results	112
3.2	Discussion/Conclusions	118
3.2.1.	The noradrenergic system	118
3.2.2.	The dopaminergic system	120
3.2.3.	The serotonergic system	120
3.3	Conclusions	122
<b>Chapter 4: Pharmacological Characterisation of Potential SPECT Brain Imaging Tracers for the Noradrenaline Transporter</b>		125
4.1.	Results	125
4.1.1.	Reboxetine affinity for the NAT	125
4.1.2.	Affinity of novel compounds for the NAT	127
4.1.3.	Serotonin Transporter Pharmacology	132
4.1.4.	Dopamine Transporter Pharmacology	138
4.1.5.	Monoamine Transporter Pharmacology (Summary)	144
4.2.	Discussion	147
4.2.1.	Summary of findings	147
4.2.2.	What alternative molecules are emerging?	148
4.2.3.	Identifying what the lead compound will be capable of imaging	151
4.2.4.	Next steps for NKJ-64 development	153

<b>Chapter 5: Using High-Performance Liquid Chromatography (HPLC) to Predict in vivo Characteristics of Tracer Candidates</b>	155
5.1 Results	155
5.1.1 Reboxetine Compounds	155
5.1.1.1 Lipophilicity ( $\log P_{OCT}$ )	155
5.1.1.2 Phospholipophilicity ( $\log D_{7.4 \text{ IAM}}$ )	157
5.1.1.3 Blood-brain barrier penetration (clog BB)	157
5.1.1.4 Plasma Protein Binding ( $c\%PPB$ )	157
5.1.2 Reference Compounds	161
5.1.2.1 Lipophilicity ( $\log P_{OCT}$ )	161
5.1.2.2 Phospholipophilicity ( $\log D_{7.4 \text{ IAM}}$ )	161
5.1.2.3 Blood-brain barrier penetration (clog BB)	161
5.1.2.4 Plasma Protein Binding ( $c\%PPB$ )	165
5.1.3 Combined Data Sets	167
5.1.3.1 Lipophilicity ( $\log P_{OCT}$ )	167
5.1.3.2 Phospholipophilicity ( $\log D_{7.4 \text{ IAM}}$ )	167
5.1.3.3 Blood-brain barrier penetration (clog BB)	170
5.1.3.4 Plasma Protein Binding ( $c\%PPB$ )	170
5.1.4 Summary	173
5.2. Discussion	175
5.2.1. Iodinated reboxetine compounds	175
5.2.2. Reference compounds (successful and failed tracers)	176
5.2.3. Conclusions	181
<b>Chapter 6: General Conclusions</b>	183
6.1. The NAT is not down-regulated in the PCP model of schizophrenic hypofrontality	183
6.2. The best pharmacology was demonstrated by NKJ-64, the ortho-position iodophenoxy ring compound	184
6.3. The best HPLC-derived predictors of in vivo behaviour were demonstrated by NKJ-64, the ortho-position iodophenoxy ring compound	185
6.4. Conclusions: NKJ-64, the ortho-position iodophenoxy ring compound, has been identified as the lead candidate for further development	185

6.5	Subsequent Work: radiolabelled compound	186
<b>Appendix I</b>		188
A1.1.	Do the groups have equal variances?	188
<b>Appendix II</b>		198
A2.1.	HPLC system calibrations	198
<b>References</b>		206
<b>Bibliography</b>		223

## List of Figures

<b>Figure 1-01:</b> The noradrenergic nerve terminal	4
<b>Figure 1-02:</b> Connections of the ventral tegmental area	9
<b>Figure 1-03:</b> The synthesis and metabolism of monoamine neurotransmitters	11
<b>Figure 1-04:</b> Coronal MRI sections from two sets of monozygotic twins	18
<b>Figure 1-05:</b> Clinical PET imaging of D <sub>2</sub> receptors with [ <sup>11</sup> C]-raclopride	20
<b>Figure 1-06:</b> The corticolimbothalamic circuitry that becomes deranged in schizophrenia	28
<b>Figure 1-07:</b> The Compartmental Model	42
<b>Figure 1-08:</b> The Simplified Three-compartment Model	42
<b>Figure 2-01:</b> PCP administration regime to establish the rat model of schizophrenic hypofrontality	53
<b>Figure 2-02:</b> NAT transporter-specific oligonucleotide probe sequences	60
<b>Figure 2-03:</b> DAT transporter-specific oligonucleotide probe sequences	60
<b>Figure 2-04:</b> SERT transporter-specific oligonucleotide probe sequences	60
<b>Figure 2-05:</b> Graphical representation of a Generic HPLC Run Timetable	73
<b>Figure 3-01:</b> [ <sup>3</sup> H]-nisoxetine binding to the NAT is unchanged	89
<b>Figure 3-02:</b> [ <sup>3</sup> H]-WIN-35,428 binding to the DAT is unchanged	100
<b>Figure 3-03:</b> [ <sup>3</sup> H]-citalopram binding to the SERT is selectively reduced	111
<b>Figure 3-04:</b> [ <sup>35</sup> S]-Oligonucleotide Hybridisation to Transporter-specific mRNA is Unchanged	117
<b>Figure 4-01:</b> Reboxetine displacement of [ <sup>3</sup> H]-nisoxetine binding to the noradrenaline transporter.	126
<b>Figure 4-02:</b> Iodophenyl ring iodoreboxetine analogues displacement of [ <sup>3</sup> H]-nisoxetine binding at the noradrenaline transporter.	128
<b>Figure 4-03:</b> Benzyl alcohol intermediate compounds displacement of [ <sup>3</sup> H]-nisoxetine binding at the noradrenaline transporter.	129
<b>Figure 4-04:</b> Iodophenoxy ring reboxetine analogues displacement of [ <sup>3</sup> H]-nisoxetine binding at the noradrenaline transporter.	131
<b>Figure 4-05:</b> Iodophenyl ring reboxetine analogues displacement of [ <sup>3</sup> H]-	133

citalopram binding at the serotonin transporter.	
<b>Figure 4-06:</b> ( <i>S,R</i> )- and ( <i>R,S</i> )- iodophenyl ring reboxetine analogues displacement of [ <sup>3</sup> H]-citalopram binding at the serotonin transporter.	134
<b>Figure 4-07:</b> Benzyl alcohol intermediate compounds displacement of [ <sup>3</sup> H]-citalopram binding at the serotonin transporter.	135
<b>Figure 4-08:</b> Iodophenoxy ring reboxetine analogues displacement of [ <sup>3</sup> H]-citalopram binding at the serotonin transporter.	137
<b>Figure 4-09:</b> Iodophenyl ring reboxetine analogues displacement of [ <sup>3</sup> H]-WIN-35,428 binding at the dopamine transporter.	139
<b>Figure 4-10:</b> ( <i>S,R</i> )- and ( <i>R,S</i> )- iodophenyl ring reboxetine analogues displacement of [ <sup>3</sup> H]-WIN-35,428 binding at the dopamine transporter.	140
<b>Figure 4-11:</b> Iodophenoxy ring reboxetine analogues displacement of [ <sup>3</sup> H]-WIN-35,428 binding at the dopamine transporter.	142
<b>Figure 5-01:</b> Measured lipophilicity of reboxetine analogues.	156
<b>Figure 5-02:</b> Measured phospholipophilicity ( $\log D_{7.4 \text{ IAM}}$ ) of reboxetine analogues.	158
<b>Figure 5-03:</b> Measured blood-brain barrier penetration predictors ( $\text{clog BB}$ ) for reboxetine analogues.	159
<b>Figure 5-04:</b> Plasma protein binding derived from a combination of HSA and AGP affinity determinations for reboxetine analogues.	160
<b>Figure 5-05:</b> Measured lipophilicity of the successful and failed imaging tracers comprising the reference compounds.	162
<b>Figure 5-06:</b> Measured phospholipophilicity ( $\log D_{7.4 \text{ IAM}}$ ) of the successful and failed imaging tracers comprising the reference compounds.	163
<b>Figure 5-07:</b> Measured blood-brain barrier penetration predictors ( $\text{clog BB}$ ) for the successful and failed tracers comprising the reference compounds.	164
<b>Figure 5-08:</b> Plasma protein binding derived from a combination of HSA and AGP affinity determinations for the successful and failed tracers comprising the reference compounds.	166
<b>Figure A2-01:</b> Calibration curve for the Luna (C-18) lipid column at pH 2.5.	199

<b>Figure A2-02:</b> Calibration curve for the Luna (C-18) lipid column at pH 10.5.	200
<b>Figure A2-03:</b> Calibration curve for the Luna (C-18) lipid column at pH 7.4.	201
<b>Figure A2-04:</b> Calibration curve for the immobilized artificial membrane (IAM) phospholipid column at pH 7.4.	202
<b>Figure A2-05:</b> Calibration curve for the Luna (C-18) column at pH 7.4 with a methanol elution.	203
<b>Figure A2-06:</b> Calibration curve for the immobilized $\alpha$ -acid glycoprotein (AGP) column at pH 7.4.	204
<b>Figure A2-07:</b> Calibration curve for the immobilized human serum albumin (HSA) column at pH 7.4.	205

## List of Tables

<b>Table 1-01:</b> Noradrenergic System Modulation	5
<b>Table 1-02:</b> Dopaminergic Projections	8
<b>Table 1-03:</b> Noradrenaline and Dopamine Transporter Specificities	12
<b>Table 1-04:</b> Monoamine Neurotransmitters, Receptors, and Effects	12
<b>Table 1-05:</b> Drugs Modulating Monoamine Systems	14
<b>Table 1-06:</b> Compounds modulating the noradrenaline system	23
<b>Table 1-07:</b> Monoaminergic Binding Profile of Reboxetine	34
<b>Table 1-08:</b> Candidate Compounds for <i>in vivo</i> imaging of the NAT	35
<b>Table 1-09:</b> NAT distribution in human brain and imaging tracer requirements	37
<b>Table 1-10:</b> Reference Compounds for Interpreting Predictors of <i>in vivo</i> Molecular Behaviour	51
<b>Table 2-01:</b> Monoamine transporter autoradiography reagents, buffers, and experimental schedules.	57
<b>Table 2-02:</b> Calculating oligonucleotide probe concentrations	62
<b>Table 2-03:</b> Reagents and quantities used with the Pharmacia probe labelling kit	62
<b>Table 2-04:</b> Reaction proportions for each slide containing 2-3 sections	62
<b>Table 2-05:</b> Iodoreboxetine Analogues and their Structure	65
<b>Table 2-06:</b> Assay conditions for radioligand competition experiments to determine the $K_i$ at monoamine transporters for iodoreboxetine compounds	67
<b>Table 2-07:</b> Technical specifications of HPLC columns used for <i>in vivo</i> behaviour predictors.	71
<b>Table 2-08:</b> Standards used to calibrate lipid and phospholipid columns and their respective CHI values for each column.	71
<b>Table 2-09:</b> Standards used to calibrate protein columns and their respective % binding for each column.	72
<b>Table 2-10:</b> Column run timetables	74
<b>Table 2-10:</b> Column run timetables (continued)	75

<b>Table 3-01:</b> The distribution of 3.0nM [ <sup>3</sup> H]-nisoxetine binding to the noradrenaline transporter in vehicle-treated and PCP-treated rat brain.	80
<b>Table 3-02:</b> 3.0nM [ <sup>3</sup> H]-nisoxetine binding to the noradrenaline transporter in sections of vehicle-treated and PCP-treated rat brain.	81
<b>Table 3-03:</b> 3.0nM [ <sup>3</sup> H]-nisoxetine binding to the noradrenaline transporter in sections of vehicle-treated and PCP-treated rat brain.	82
<b>Table 3-04:</b> 3.0nM [ <sup>3</sup> H]-nisoxetine binding to the noradrenaline transporter in sections of vehicle-treated and PCP-treated rat brain.	83
<b>Table 3-05:</b> 3.0nM [ <sup>3</sup> H]-nisoxetine binding to the noradrenaline transporter in sections of vehicle-treated and PCP-treated rat brain.	84
<b>Table 3-06:</b> 3.0nM [ <sup>3</sup> H]-nisoxetine binding to the noradrenaline transporter in sections of vehicle-treated and PCP-treated rat brain.	85
<b>Table 3-07:</b> 3.0nM [ <sup>3</sup> H]-nisoxetine binding to the noradrenaline transporter in sections of vehicle-treated and PCP-treated rat brain.	86
<b>Table 3-08:</b> 3.0nM [ <sup>3</sup> H]-nisoxetine binding to the noradrenaline transporter in sections of vehicle-treated and PCP-treated rat brain.	87
<b>Table 3-09:</b> 1.5nM [ <sup>3</sup> H]-nisoxetine binding to the noradrenaline transporter in sections of vehicle-treated and PCP-treated rat brain.	88
<b>Table 3-10:</b> The distribution of 10.0nMnM [ <sup>3</sup> H]-WIN-35,428 binding to the dopamine transporter in vehicle-treated and PCP-treated rat brain.	91
<b>Table 3-11:</b> [ <sup>3</sup> H]-WIN-35,428 binding to the dopamine transporter in sections of vehicle-treated and PCP-treated rat brain.	92
<b>Table 3-12:</b> [ <sup>3</sup> H]-WIN-35,428 binding to the dopamine transporter in sections of vehicle-treated and PCP-treated rat brain.	93
<b>Table 3-13:</b> [ <sup>3</sup> H]-WIN-35,428 binding to the dopamine transporter in sections of vehicle-treated and PCP-treated rat brain.	94
<b>Table 3-14:</b> [ <sup>3</sup> H]-WIN-35,428 binding to the dopamine transporter in sections of vehicle-treated and PCP-treated rat brain.	95
<b>Table 3-15:</b> [ <sup>3</sup> H]-WIN-35,428 binding to the dopamine transporter in sections of vehicle-treated and PCP-treated rat brain.	96
<b>Table 3-16:</b> [ <sup>3</sup> H]-WIN-35,428 binding to the dopamine transporter in sections of vehicle-treated and PCP-treated rat brain.	97
<b>Table 3-17:</b> [ <sup>3</sup> H]-WIN-35,428 binding to the dopamine transporter in sections of vehicle-treated and PCP-treated rat brain.	98

<b>Table 3-18:</b> [ <sup>3</sup> H]-WIN-35,428 binding to the dopamine transporter in sections of vehicle-treated and PCP-treated rat brain.	99
<b>Table 3-19:</b> The distribution of 2.0nM [ <sup>3</sup> H]-citalopram binding to the serotonin transporter in the vehicle-treated and PCP-treated rat brain.	102
<b>Table 3-20:</b> [ <sup>3</sup> H]-citalopram binding to the serotonin transporter in sections of vehicle-treated and PCP-treated rat brain.	103
<b>Table 3-21:</b> [ <sup>3</sup> H]-citalopram binding to the serotonin transporter in sections of vehicle-treated and PCP-treated rat brain.	104
<b>Table 3-22:</b> [ <sup>3</sup> H]-citalopram binding to the serotonin transporter in sections of vehicle-treated and PCP-treated rat brain.	105
<b>Table 3-23:</b> [ <sup>3</sup> H]-citalopram binding to the serotonin transporter in sections of vehicle-treated and PCP-treated rat brain.	106
<b>Table 3-24:</b> [ <sup>3</sup> H]-citalopram binding to the serotonin transporter in sections of vehicle-treated and PCP-treated rat brain.	107
<b>Table 3-25:</b> [ <sup>3</sup> H]-citalopram binding to the serotonin transporter in sections of vehicle-treated and PCP-treated rat brain.	108
<b>Table 3-26:</b> [ <sup>3</sup> H]-citalopram binding to the serotonin transporter in sections of vehicle-treated and PCP-treated rat brain.	109
<b>Table 3-27:</b> [ <sup>3</sup> H]-citalopram binding to the serotonin transporter in sections of vehicle-treated and PCP-treated rat brain.	110
<b>Table 3-28:</b> The distribution of [ <sup>35</sup> S]-oligonucleotide <i>in situ</i> hybridisation probe binding to monoamine transporter mRNA in vehicle-treated rat brain.	113
<b>Table 3-29:</b> <i>In situ</i> hybridisation imaging of DAT-specific mRNA in the ventral tegmental area (VTA) of control rat brains.	114
<b>Table 3-30:</b> <i>In situ</i> hybridisation imaging of SERT-specific mRNA in the dorsal raphe nuclei (DRN) of control rat brains.	115
<b>Table 3-31:</b> <i>in situ</i> hybridisation imaging of NAT-specific mRNA in the locus coeruleus (LC) of control rat brains.	116
<b>Table 4-01:</b> Affinity of iodinated reboxetine analogues for the NAT	131
<b>Table 4-02:</b> Affinity of iodinated reboxetine analogues for the SERT	137
<b>Table 4-03:</b> Affinity of iodinated reboxetine analogues for the DAT	143
<b>Table 4-04:</b> Novel Iodoreboxetine Compound Affinities	145
<b>Table 4-05:</b> Novel Iodoreboxetine Compound Selectivity	146

<b>Table 4-06:</b> NAT affinity of emerging brain imaging tracer compounds	150
<b>Table 4-07:</b> Binding Potential Estimations for NAT-specific SPECT Brain Imaging Tracer Candidates	152
<b>Table 5-01:</b> Lipophilicity ( $\log P_{\text{OCT}}$ ) of reboxetine-like compounds and reference compounds comprised of both successful and failed tracers.	168
<b>Table 5-02:</b> Phospholipophilicity ( $\log D_{7.4 \text{ IAM}}$ ) of reboxetine-like compounds and reference compounds comprised of both successful and failed tracers.	169
<b>Table 5-03:</b> Blood-brain barrier penetration ( $\text{clog BB}$ ) of reboxetine-like compounds and reference compounds comprised of both successful and failed tracers.	171
<b>Table 5-04:</b> Plasma protein binding ( $\text{c\%PPB}$ ) of reboxetine-like compounds and reference compounds comprised of both successful and failed tracers.	172
<b>Table 5-05:</b> HPLC-measured predictors for <i>in vivo</i> molecular behaviour of reboxetine analogues and the successful and failed brain imaging tracers comprising the reference compounds.	174
<b>Table 5-06:</b> HPLC-derived predictors for <i>in vivo</i> molecular behaviour of reboxetine analogues and the successful and failed brain imaging tracers comprising the reference compounds. Determined values have been converted into general descriptors.	174
<b>Table A1-01:</b> Summary of T-test and F-test to determine statistical differences between means and variances for [ $^3\text{H}$ ]-ligand binding to monoamine transporters in control and PCP-treated rat brain.	189
<b>Table A1-02:</b> T-test and F-test of [ $^3\text{H}$ ]-nisoxetine binding data.	190
<b>Table A1-02 (continued):</b> T-test and F-test of [ $^3\text{H}$ ]-nisoxetine binding data.	191
<b>Table A1-02 (continued):</b> T-test and F-test of [ $^3\text{H}$ ]-nisoxetine binding data.	192
<b>Table A1-03:</b> T-test and F-test of [ $^3\text{H}$ ]-WIN-35,428 binding data.	193
<b>Table A1-03 (continued):</b> T-test and F-test of [ $^3\text{H}$ ]-WIN-35,428 binding data.	194
<b>Table A1-04:</b> T-test and F-test of [ $^3\text{H}$ ]-citalopram binding data.	195

<b>Table A1-04 (continued):</b> T-test and F-test of [ <sup>3</sup> H]-citalopram binding data.	196
<b>Table A1-04 (continued):</b> T-test and F-test of [ <sup>3</sup> H]-citalopram binding data.	197

## Thesis Summary

The noradrenaline system is extensively innervated throughout the brain, implicated in the aetiology of a wide range of psychiatric conditions, and the pharmacological modulation of the noradrenaline system has had a positive influence upon the alleviation of symptoms for those suffering psychiatric or neurological disease. Clinical imaging of the brain with technologies such as Single Photon Emission Computed Tomography (SPECT) can provide clinicians and researchers with valuable information for elucidating disease aetiology, monitoring patient condition, and also confirming the mechanism of action for drug development through occupancy studies. However, to date, there is no SPECT brain imaging tracer for the noradrenaline transporter in regular clinical use.

This thesis is a body of work to develop a novel SPECT brain imaging tracer for the noradrenaline transporter with compounds that are iodinated forms of reboxetine, the selective noradrenergic reuptake inhibitor and clinically used antidepressant. From the compounds synthesised and tested, the one which demonstrated the best pharmacological affinity and selectivity for the noradrenaline transporter was NKJ-64. This same compound also displayed many of the HPLC-derived properties predicting *in vivo* molecular behaviour that are associated with successful brain imaging tracers. Therefore, NKJ-64 was recommended for radiolabelling and further study.

### **PCP Model of the Metabolic Hypofrontality Observed in Schizophrenia**

The metabolic hypofunction observed in the prefrontal cortex of schizophrenic patients is mimicked in a rat model via repeated, low-dose phencyclidine administration. The neural mechanisms underlying this hypofrontality are unclear. Whilst dopaminergic transmission is classically associated with aberrant activity in schizophrenia, modulation of noradrenergic neurotransmission is correlated with the alleviation of negative symptoms. Furthermore, the noradrenaline transporter rather than the dopamine transporter functions as the dominant dopaminergic reuptake mechanism in the prefrontal cortex. It was hypothesised that repeated phencyclidine administration in the rat would induce a down-regulation of the NAT.

Ligands labelled with [<sup>3</sup>H] were used for autoradiographic imaging of the noradrenaline, dopamine, and serotonin transporters in phencyclidine-treated and control groups, and [<sup>35</sup>S]-labelled oligonucleotide probes specific for the mRNA of each transporter were used for *in situ* hybridisation. The binding densities of the noradrenaline and dopamine transporters were unaltered in the model, however significant selective reductions of serotonin transporter binding sites were measured. The densities of mRNA for all three monoamine transporters were unaltered, so the unaltered densities of noradrenaline and dopamine transporter binding sites and the changes in serotonin transporter binding densities were not the result of altered gene expression.

Although the noradrenaline transporter was not directly affected in this model of one particular aspect of schizophrenia and the model is not ideal for demonstrating the capability of a SPECT tracer for the NAT, this does not imply that the noradrenaline transporter is uninvolved in the disease aetiology of schizophrenia or of diminished importance to future schizophrenia studies. The aforementioned correlation of noradrenaline transporter modulation to the alleviation of negative symptoms emphasises the importance of acquiring the clinical ability to assess the density and/or occupancy of the noradrenaline transporter by developing a useful SPECT brain imaging tracer for this site.

### **Pharmacological Characterisation of Potential SPECT Brain Imaging Tracers for the Noradrenaline Transporter**

*In vivo* imaging of the noradrenaline transporter was previously limited to peripheral tracers such as metaiodobenzylguanidine (MIBG), which does not cross the blood-brain barrier, and neuroligands such as radiolabelled desipramine, which demonstrated problematically high nonspecific binding. Recent efforts in the literature have focused upon modified reboxetine analogues, and some progress was made with the *S,S*-isomer of iodophenoxy-ring reboxetine, referred to as both INER and IPBM in publication (Tamagnan et al. 2007; Kanegawa et al. 2006).

Synthesised iodophenyl-ring compounds in *S,S*-, *R,R*-, *S,R*-, and *R,S*-isomers were evaluated for their affinity for the NAT. The *R,S*-isomer demonstrated a very similar level of binding to the *S,S*-isomer and so this was explored in an

iodophenoxy isomer to determine if improvement upon the characteristics of lead iodinated reboxetine compounds in the literature was possible.

The *R,S*-isomer iodophenoxy reboxetine analogues were synthesised with the iodine in the ortho, meta, and para positions of the phenoxy ring and assigned the designations NKJ-64, NKJ-67, and NKJ-68, respectively. NKJ-64 has strong affinity and selectivity for the noradrenaline transporter, with a  $K_D$  of  $8.4 \pm 1.7$  nM, a 6-fold selectivity for the noradrenaline transporter over the serotonin transporter, and a 63-fold selectivity for the noradrenaline transporter over the dopamine transporter. From the compounds synthesised and tested, NKJ-64 has the most suitable pharmacology to be developed further as a SPECT brain imaging tracer for the noradrenaline transporter and has an affinity in the same order of magnitude as iodinated compounds in the literature, such as the aforementioned INER/IPBM.

### **Using High-Performance Liquid Chromatography (HPLC) to Predict *in vivo* Characteristics of Tracer Candidates**

The development of any candidate tracer compound must include an evaluation of its *in vivo* properties. To streamline this process and select only the most viable compounds for further testing, predictors of *in vivo* molecular characteristics are used to conserve research effort. Measures such as lipophilicity, phospholipophilicity, and plasma protein binding, used to estimate the potential for blood-brain barrier penetration, nonspecific binding, and the likelihood of serum availability would be very time-intensive to determine via traditional bench-top methodologies.

High-performance liquid chromatography (HPLC) is a quick, precise, and reliable technique that is a rapid and high-throughput automatable process with exceptional precision that does not rely on the bench-top proficiency of an individual experimenter. The optimisation of gradient elution protocols and formulae to interpret sample retention times on commercially available columns into reproducible standardised units has allowed for the efficient evaluation of tracer candidate compounds.

The iodinated reboxetine compounds were compared to examples of both successful and failed neuroimaging tracers. Generally, the evaluations of the successful and failed neuroimaging tracers validated the combined methodologies of the HPLC-derived predictors of in vivo molecular behaviour. In applying these methodologies to the synthesised iodoreboxetine compounds, NKJ-64 displayed many of the HPLC-determined properties that are consistent with successful tracers.

## Abbreviations

<b>AAP</b>	Abraham H-bond Acidity Parameter
<b>AGP</b>	$\alpha$ -acid glycoprotein
<b>BBB</b>	Blood-brain barrier
<b><math>\beta</math>-CIT</b>	2 $\beta$ -carbomethoxy-3 $\beta$ -(4-iodophenyl)tropane
<b>B<sub>max</sub></b>	Maximum binding capacity
<b>BP</b>	Binding potential
<b>c%PPB</b>	Calculated percentage of plasma protein binding
<b>C<sub>1</sub></b>	Plasma compartment. Used in compartmental modelling for <i>in vivo</i> imaging.
<b>C<sub>2</sub></b>	Free compartment. Used in compartmental modelling for <i>in vivo</i> imaging.
<b>C<sub>2</sub>'</b>	Non-specifically bound compartment. Used in compartmental modelling for <i>in vivo</i> imaging.
<b>C<sub>3</sub></b>	Specifically bound compartment. Used in compartmental modelling for <i>in vivo</i> imaging.
<b>CHI</b>	Chromatographic Hydrophobicity Index
<b>CHI<sub>2.5</sub></b>	Chromatographic Hydrophobicity Index at pH 2.5
<b>CHI<sub>7.4</sub></b>	Chromatographic Hydrophobicity Index at pH 7.4
<b>CHI<sub>7.4(MeOH)</sub></b>	Chromatographic Hydrophobicity Index at pH 7.4 with MeOH elution
<b>CHI<sub>10.5</sub></b>	Chromatographic Hydrophobicity Index at pH 10.5
<b>CHI<sub>IAM</sub></b>	Chromatographic Hydrophobicity Index on an IAM column

<b>CMR</b>	Calculated molecular refractivity (a measurement of molecular size)
<b>CNS</b>	Central nervous system
<b>DPM</b>	Disintegrations per minute
<b>DAT</b>	Dopamine transporter
<b>FIAU</b>	<b>Fialuridine</b> 1-(2-deoxy-2-fluoro-1-D-arabinofuranosyl)-5-iodouracil
<b>HPLC</b>	High performance liquid chromatography
<b>HSA</b>	Human serum albumin
<b>5-IA-85380</b>	3-[2(S)-2-azetidylmethoxy]pyridine
<b>IAM</b>	Immobilized artificial membrane
<b>INER/IPBM</b>	( <i>S,S</i> )-2-( $\alpha$ -(2-iodophenoxy)benzyl)morpholine (Kanegawa et al. 2006; Tamagnan et al. 2007)
<b>K<sub>D</sub></b>	Dissociation constant
<b>K<sub>i</sub></b>	Inhibition constant
<b>k<sub>IAM</sub></b>	Solute capacity factor on the IAM column
<b>K<sub>m</sub></b>	Membrane partition coefficient
<b>k<sub>off</sub></b>	<i>In vitro</i> dissociation rate constant
<b>k<sub>on</sub></b>	<i>In vitro</i> association rate constant
<b>K<sub>1</sub></b>	Rate constant for diffusion from plasma across the blood brain barrier to the free compartment in the brain. Used in compartmental modelling for <i>in vivo</i> imaging.
<b>K<sub>2</sub></b>	Rate constant for diffusion from the free compartment in the brain across the blood brain barrier to the plasma. Used in compartmental modelling for <i>in vivo</i> imaging.
<b>K<sub>3</sub></b>	Rate constant for diffusion from the free compartment in the brain to the specifically

	bound compartment. Used in compartmental modelling for <i>in vivo</i> imaging.
<b>K<sub>4</sub></b>	Rate constant for diffusion from the specifically bound compartment in the brain to the free compartment. Used in compartmental modelling for <i>in vivo</i> imaging.
<b>K<sub>5</sub></b>	Rate constant for diffusion from the free compartment in the brain to the non-specifically bound compartment. Used in compartmental modelling for <i>in vivo</i> imaging.
<b>K<sub>6</sub></b>	Rate constant for diffusion from the non-specifically bound compartment in the brain to the free compartment. Used in compartmental modelling for <i>in vivo</i> imaging.
<b>Log D</b>	Distribution coefficient
<b>Log D<sub>OCT</sub></b>	Distribution coefficient determined to reflect Log D as estimated by octanol-water partition
<b>Log P</b>	Partition coefficient
<b>MAO</b>	Monoamine oxidase
<b>MIBG</b>	<b>Metaiodobenzylguanidine</b> 1-(3-iodobenzyl)guanidine
<b>MW</b>	Molecular weight
<b>NAT</b>	Noradrenaline transporter
<b>PBS</b>	Phosphate buffered saline
<b>PET</b>	Positron emission tomography
<b>P-gp</b>	P-glycoprotein
<b>PK11195</b>	1-(2-chlorophenyl)- <i>N</i> -methyl- <i>N</i> -(1-methylpropyl)-3-isoquinolinecarboxamide
<b>PPB</b>	Plasma protein binding
<b>Reboxetine</b>	2-[ $\alpha$ -(2-ethoxyphenoxy)benzyl]morpholine

<b>rpm</b>	Rotations per minute
<b>(R,R)-QNB</b>	3-quinuclidinyl-4-iodobenzilate
<b>SD</b>	Standard deviation
<b>SEM</b>	Standard error of mean
<b>SERT</b>	Serotonin transporter
<b>SNRI</b>	Selective noradrenergic reuptake inhibitor
<b>SPECT</b>	Single photon emission computed tomography
<b>UV</b>	Ultra-violet

# Chapter 1

## General Introduction

### 1. Introduction

Monoamine transmission plays an important role in a variety of CNS functions ranging from mood, sleep regulation, the initiation of movement, and modulation of pathways tasked with executive function (Bear et al. 2001; Moore & Bloom 1979). The extensive projections of monoamine systems can also become implicated in the aetiology of a similarly wide range of diseases such as clinical depression, severe anxiety, Parkinson's disease, learning and memory disorders, aberrant sleep and schizophrenia (De Sarro et al. 1987; Yamamoto & Hornykiewicz 2004; Hipolide et al. 2005).

Currently, a SPECT brain imaging tracer for the noradrenaline transporter (NAT) is not available for clinical use and, until one is developed, imaging studies *in vivo* will remain limited to probing with radiolabelled substrates (Eisenhofer 2001). It is expected that the production of successful SPECT and/or PET ligands for imaging of the NAT in the CNS will be derived from compounds structurally related to nisoxetine (Hadrich et al. 1999a) and indeed, early efforts have focused upon iodinated forms of reboxetine, the clinically used selective noradrenergic reuptake inhibitor and antidepressant. Nisoxetine itself cannot be used because compounds radiolabelled with [ $^{123/125}$ I] for SPECT imaging have lacked selectivity for the NAT (Kiyono et al. 2004; Kung et al. 2004) and nisoxetine-like compounds radiolabelled with [ $^{11}$ C] for PET imaging have demonstrated poor *in vivo* kinetics such as slow brain uptake and rapid metabolism (Tamagnan et al. 2007; Ding et al. 2005).

#### 1.1. Monoamine systems

##### 1.1.1. Noradrenaline system

The noradrenergic system projects from the locus coeruleus to many anatomical structures including – but not limited to – the neocortical mantle (prefrontal cortex included), thalamus, hippocampus, amygdala, hypothalamus, nucleus accumbens,

the cingulum (cingulate anterior), cerebellar cortex, reticular core of the lower brain stem, and spinal cord (Yamamoto & Hornykiewicz 2004; Moore & Bloom 1979).

Noradrenergic innervation is received by more widespread areas of the cerebrum than is dopaminergic innervation and, furthermore, noradrenaline is the predominant monoamine in many of the aforementioned brain regions – the nucleus accumbens being one of the noteworthy exceptions (Hipolide et al. 2005; Andersen et al. 2005).

The effect of noradrenaline, like many neurotransmitters, depends upon the receptors through which it exerts its action (see Figure 1-01). Action upon postsynaptic  $\beta$ -adrenoceptors stimulates adenylate cyclase, which catalyses the reaction to convert ATP to cAMP. Rising intracellular levels of cAMP opens  $\text{Ca}^{2+}$  channels and allows a  $\text{Ca}^{2+}$  influx that will facilitate vesicle fusion with the presynaptic membrane to exocytose stored neurotransmitter into the synaptic cleft. Auto-inhibition is achieved through presynaptic  $\alpha_2$ -adrenoceptors, which inhibit adenylate cyclase – thus inhibiting the conversion of ATP to cAMP and thereby preventing the opening of the  $\text{Ca}^{2+}$  channels that promote quantal release of noradrenaline. Pharmacological modulation of the noradrenergic system can also be achieved directly through  $\alpha_2$ -adrenoceptors (Table 1-01).

Activity of the noradrenergic locus coeruleus neurons is correlated with states of vigilance (Yamamoto & Hornykiewicz 2004): highest activity is apparent in an alert waking state, with activity declining through drowsy wakefulness, slow-wave sleep states, and finally silent during rapid eye movement sleep. Observations in non-human primates, felines, and rats that were exposed to arousing stimuli have provided evidence to support the theory that noradrenergic locus coeruleus neurons are essential to sustain vigilance. Furthermore, noradrenaline has been shown to increase in the brain during times of stress or in anticipation of stress (Tanaka 1999; Tanaka et al. 2000), and is implicated in depression and the treatment of depression (Brunello et al. 2002). Indeed, pharmacological modulation of the noradrenergic system can result in disturbances of sleep, attention, stress sensitivity, and social interaction (Yamamoto & Hornykiewicz 2004). Noradrenaline is also important in the periphery and is integrated into the sympathetic nervous system, and noradrenaline increases are also correlated with

peripheral stress responses such as an increased heart rate and elevated blood pressure.

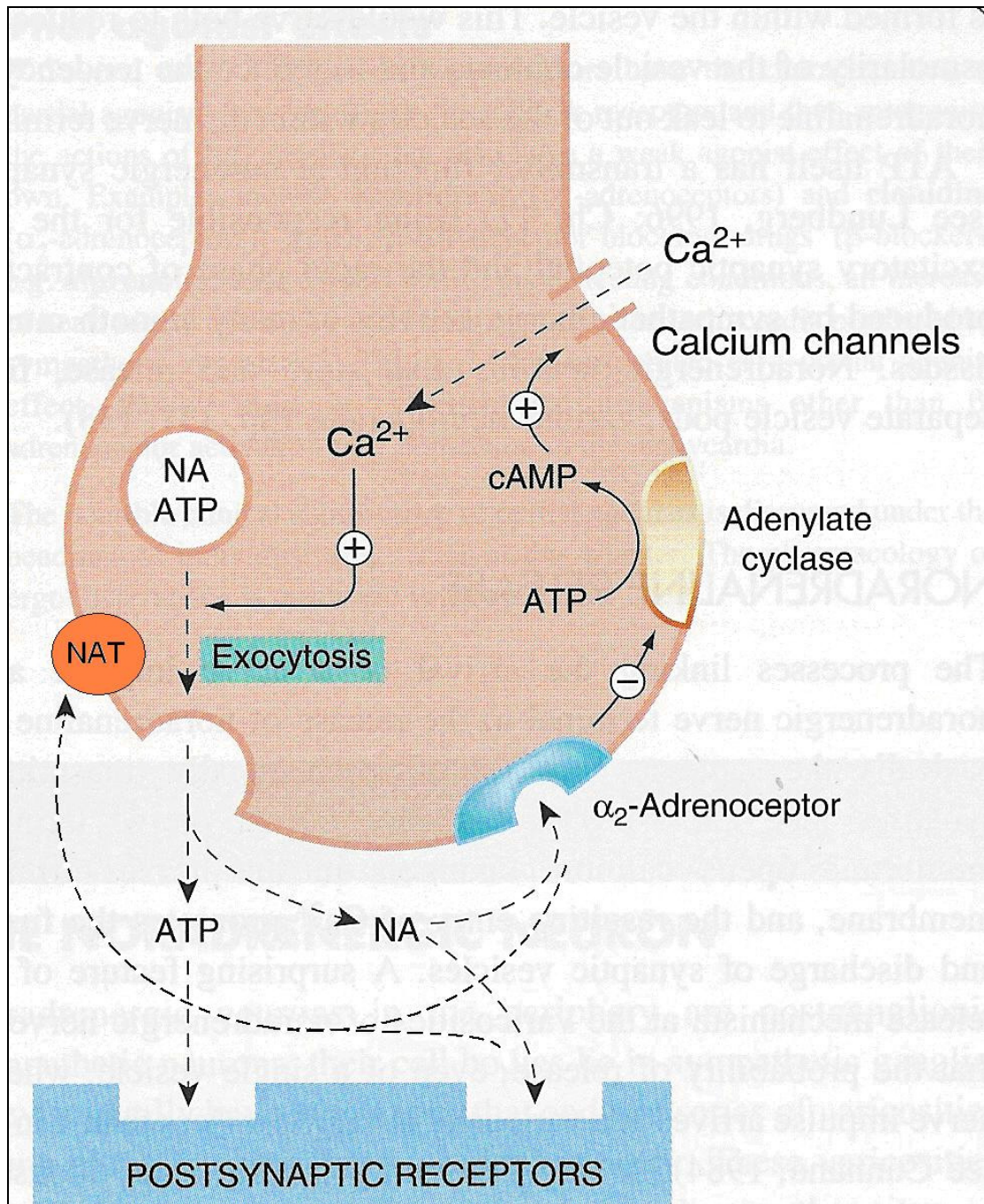


**Figure 1-01:** The noradrenergic nerve terminal (adapted from: Rang et al. 2003). Following an action potential, increases in cAMP stimulate calcium influxes that cause excitation of noradrenaline into the synaptic cleft where they simultaneously stimulate postsynaptic adrenergic receptors as well as pre-synaptic α<sub>2</sub> autoreceptors that regulate the termination of the noradrenergic release. Free noradrenaline (NA) in the synapse is transported back into the presynaptic neuron by the noradrenaline transporter (NAT) or metabolised by monoamine oxidase (MAO) and catechol-O-methyltransferase (COMT).

<b>Table 1-01: Noradrenergic System Modulation</b>		
<b>Pharmacological modulation</b>	<b>Injection site</b>	<b>Effect</b>
$\alpha_2$ -adrenoceptor agonist (e.g. clonidine)	Third ventricle	<ul style="list-style-type: none"> <li>• Inhibition of synaptic noradrenaline release</li> <li>• Induction of behavioural sedation</li> <li>• Induction of sleep</li> <li>• Induction of EEG synchronization.</li> </ul>
$\alpha_2$ -adrenoceptor antagonist (e.g. yohimbine)	Intraventricularly, or into the locus coeruleus	<ul style="list-style-type: none"> <li>• Stimulation of synaptic noradrenaline release</li> <li>• Induction of behavioural arousal</li> <li>• Stimulation of locomotion</li> <li>• Stimulation of exploratory behaviour</li> <li>• Induction of EEG desynchronization.</li> </ul>

**Table 1-01:** Effects of pharmacological modulation of the noradrenergic system (adapted from De Sarro et al. 1987).

### **1.1.2. Serotonin system**

The serotonergic system projects from the extensively innervated raphe nuclei to diverse regions throughout the brain (Adell et al. 2002). Significant densities of the serotonin transporter have been localised to the raphe nuclei themselves as well as other structures such as the amygdala, hippocampus, hypothalamus, locus coeruleus, striatum, substantia nigra, thalamus, and superior colliculi (D'Amato et al. 1987).

The effects of released serotonin (5-hydroxytryptamine or 5-HT) are varied and depend greatly upon the receptor class and subtype it is activating (Rang et al. 2003; Barnes & Sharp 1999). The serotonin receptors 5-HT<sub>1A</sub>, 5-HT<sub>1B</sub>, 5-HT<sub>1D</sub>, 5-HT<sub>4</sub>, and 5-HT<sub>7</sub> all mediate their effects through the down-regulation of cAMP. Serotonin receptors 5-HT<sub>2A</sub>, and 5-HT<sub>2C</sub> both mediate their effects through the up-regulation of IP<sub>3</sub>/DAG and 5-HT<sub>3</sub> is a ligand-gated potassium channel.

The serotonin system has been implicated in psychiatric diseases such as depression, schizophrenia (Abi-Dargham 2007; Frankle et al. 2005a; Ohuoha et al. 1993), and the modulation of it with selective serotonin reuptake inhibitors such as fluoxetine, paroxetine, and citalopram have been used in treatment programmes for clinical depression (Whittington et al. 2004).

### **1.1.3. Dopamine system**

The dopaminergic system can be subdivided into two major systems; the nigrostriatal system and the mesocorticolimbic system (Adell & Artigas 2004; Table 1-02). The nigrostriatal system projects from the substantia nigra to the striatum and has great relevance to Parkinson's disease, where the onset of symptoms is correlated to the death of dopaminergic neurons in the substantia nigra (Przuntek et al. 2004). The mesocorticolimbic system projects from the ventral tegmental area (VTA) and can be further subdivided into the paranigral and parabrachial pathways (Adell & Artigas 2004). The paranigral pathway is part of the mesolimbic system and projects from the VTA to the nucleus accumbens, while the parabrachial pathway is part of the mesocortical system and projects from the VTA to the cortical structures. The paranigral pathways are associated

with reward and locomotor activity while the parabrachial pathways are associated with the modulation of cognitive function.

Other systems – notably serotonergic, cholinergic, and noradrenergic – have modulatory effects upon dopaminergic neurotransmission. Dopaminergic neurons of the VTA (Figure 1-02) receive stimulatory modulation from noradrenergic neurons of the locus coeruleus and cholinergic neurons of the brainstem, while serotonergic neurons of the raphe nuclei offer both stimulatory and inhibitory modulation through the differing 5-HT receptor subtypes. One interesting point is that dopaminergic neurons have D<sub>2</sub> autoreceptors in the VTA that provide a tonic inhibition of further action potentials from a dopaminergic neuron. For example, noradrenergic innervations of the VTA cannot increase the rate of dopaminergic cell firing unless this tonic inhibition is pharmacologically blocked by D<sub>2</sub> receptor antagonists.

The effects of dopamine are mediated by dopamine receptors, of which there are two main categories (Neal 2002): the D<sub>1</sub> (and D<sub>1</sub>-like) receptors and the D<sub>2</sub> (and D<sub>2</sub>-like) receptors. There are five types of dopamine receptors, all of which are 7-transmembrane G-protein-coupled receptors: with D<sub>1</sub> and D<sub>5</sub> belong to the D<sub>1</sub> category, while D<sub>2</sub>, D<sub>3</sub>, and D<sub>4</sub> belong to the D<sub>2</sub> category. The D<sub>2</sub>-like dopamine receptors are involved in presynaptic, postsynaptic, and extrasynaptic inhibition. The D<sub>2</sub> receptor is the dominant dopamine receptor subtype in the human brain by both number and influence, with the majority of these occurring in the mesocorticolimbic system. The mass activation of D<sub>2</sub>-like receptors (or autoreceptors) leads to an increase in potassium conductance which hyperpolarizes the membrane of dopaminergic neurons and prevents the generation or propagation of an action potential. Therefore, D<sub>2</sub>-like receptor agonists diminish the rate of dopaminergic neuronal firing and D<sub>2</sub>-like receptor antagonists such as classical neuroleptics enhance (or enable modulatory systems to enhance) the rate of dopaminergic neuronal firing (Adell & Artigas 2004). The D<sub>1</sub>-like dopamine receptors are involved mainly in postsynaptic inhibition and it has been found that most classical neuroleptic drugs also block D<sub>1</sub>-like receptors as well as D<sub>2</sub>-like receptors (Abi-Dargham et al. 2002).

<b>Table 1-02: Dopaminergic Projections</b>			
<b>Nigrostriatal system</b>		Substantia nigra	→ Striatum
<b>Mesocorticolimbic system</b>	<b>Paranigral pathways</b>	VTA	→ Nucleus accumbens
	<b>Mesocortical pathways</b>	VTA	→ Cortical structures

**Table 1-02:** Subdivisions of dopaminergic system projections (adapted from: Adell & Artigas 2004).

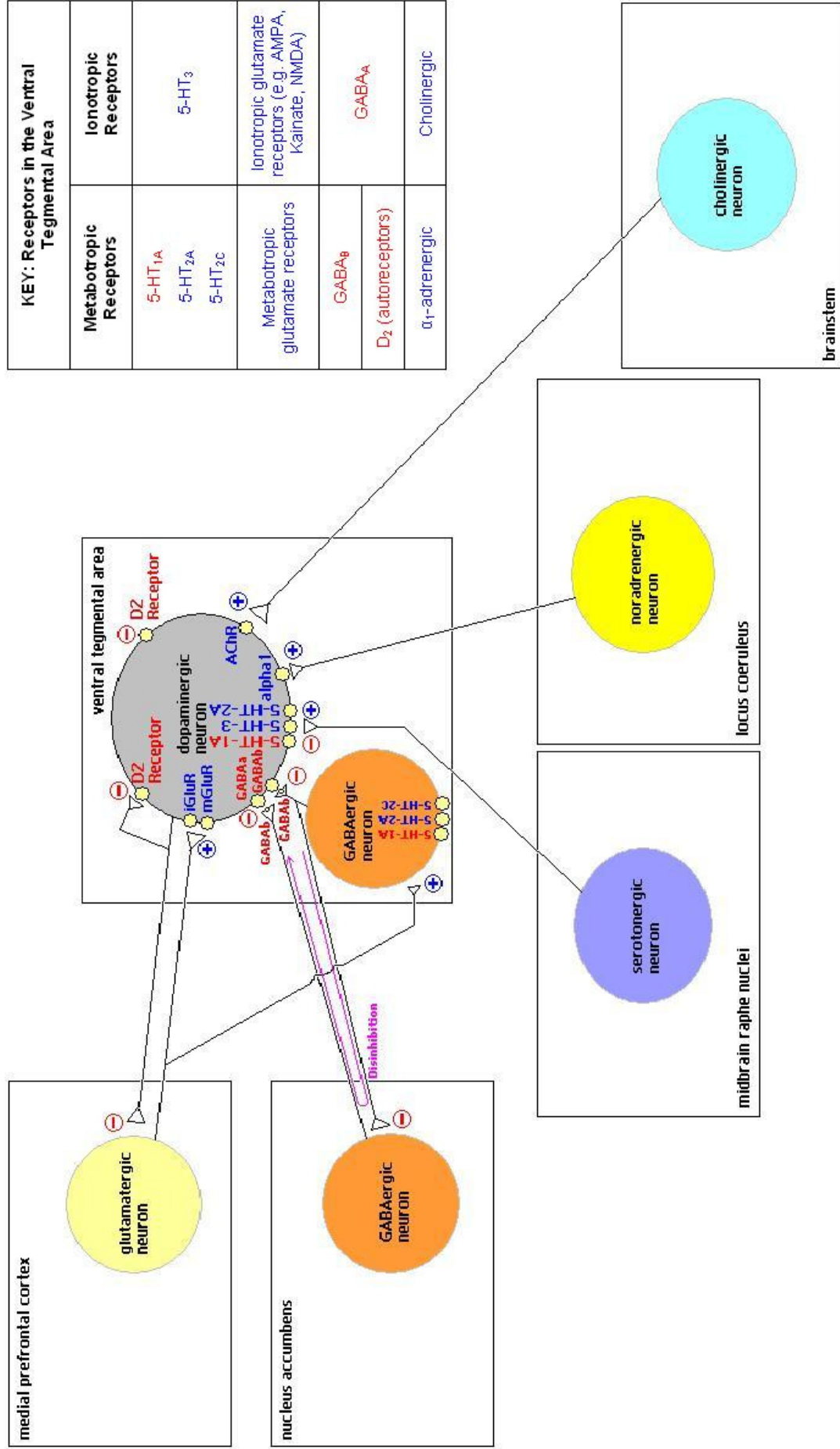


**Figure 1-02:** Connections of the ventral tegmental area. Excitatory receptors are assigned blue labels and inhibitory receptors are assigned red labels. Note that for noradrenergic modulation of the VTA, the activation of α<sub>1</sub>-adrenoceptors can only increase dopaminergic neuronal firing after a blockade of the D<sub>2</sub> autoreceptors. (adapted from Adell & Artigas 2004).

#### **1.1.4. Monoamine neurotransmitters, receptors, and transporters**

The monoamine transmitters noradrenaline (also known as norepinephrine) and dopamine share a synthesis path, whilst that of serotonin (also known as 5-hydroxytryptamine or 5-HT) is separate (Figure 1-03). Tyrosine hydroxylase is the rate-limiter in the synthesis of noradrenaline and dopamine, and tryptophan 5-hydroxylase (tryptophan 5-monoxygenase) limits the rate of synthesis for serotonin (Haavik et al. 2008). Monoamine transmitters are modulatory and can either cause neuronal excitation or inhibition depending upon which receptor they activate (Table 1-04). In the cases of noradrenaline and dopamine, their effects are usually mediated by the upregulation or downregulation of cAMP, while serotonin has receptors linked to cAMP, IP<sub>3</sub>/DAG, and ligand-gated K<sup>+</sup> channels (Barnes & Sharp 1999).

Monoamine transporters are known to be relatively non-selective and will transport other monoamines in addition to that which binds most strongly or is most commonly transported (Graefe & Bönisch 1988). Given this, it is not surprising to see that the dopamine transporter has greater affinity for dopamine than for noradrenaline – although it is interesting to find that the noradrenaline transporter also shares this order of affinity for these monoamines (Table 1-03). Furthermore, the noradrenaline transporter has been shown to be the dominant mechanism of dopaminergic reuptake in the prefrontal cortex (Moron et al. 2002) and that blockers of the noradrenaline transporter increase levels of dopamine specifically in the prefrontal cortex region of the neocortical mantle (Valentini et al. 2004). This data can be used to explain the reasons behind reduced reliance of the dopaminergic mesocorticolimbic system upon the dopamine transporter for neurotransmitter clearance in comparison to the dopaminergic nigrostriatal system while maintaining comparable levels of dopaminergic innervation.

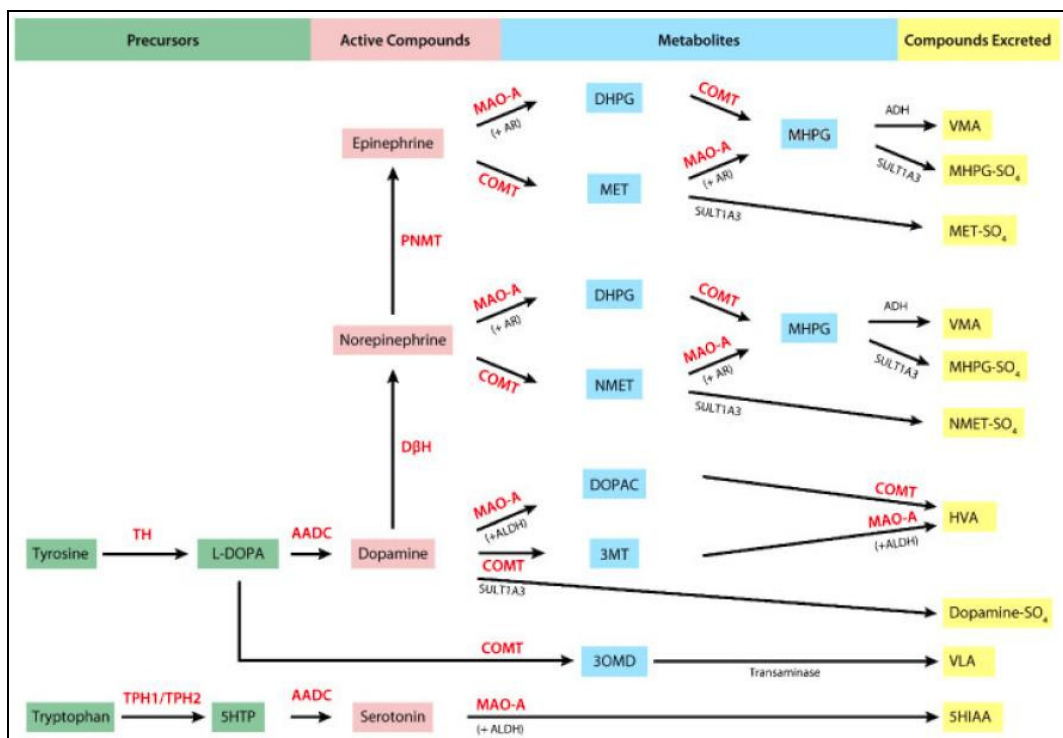


**Figure 1-03:** The synthesis and metabolism of monoamine neurotransmitters (adapted from Haavik et al. 2008). MAO-A and COMT are important mechanisms for reducing extracellular concentrations of monoamine neurotransmitters that are not recovered by presynaptic monoamine transporters following quantal release.

**Abbreviations for enzymes:**

- TH: tyrosine 3-hydroxylase or tyrosine 3-monoxygenase
- TPH1: tryptophan 5-hydroxylase isoform1 / tryptophan 5-monoxygenase isoform1
- TPH2: tryptophan 5-hydroxylase isoform2 / tryptophan 5-monoxygenase isoform2
- AADC: aromatic L-amino acid decarboxylase
- DβH: dopamine β-hydroxylase
- PNMT: phenylethanolamine N-methyltransferase
- MAO-A: monoamine oxidase A
- ALDH: aldehyde / aldose dehydrogenase/oxidoreductase
- AR: aldehyde / aldose reductase
- ADH: alcohol dehydrogenase
- COMT: catechol O-methyltransferase
- SUNLT1A3: sulfotransferase type 1A3

**Abbreviations for metabolites:**

- DHPG: 3,4-dihydrophenylglycol
- DOPAC: dihydroxyphenylacetic acid
- 5HTP: 5-hydroxytryptophan
- 5HIAA: 5-hydroxyindoleacetic acid
- HVA: homovanillic acid
- L-DOPA: 3,4-dihydroxyphenylalanine
- MET: metanephrine
- MHPG: 3-methoxy-4-hydroxyphenylglycol
- 3MT: 3-methoxytryptamine
- 3OMD: 3-O-methyldopa
- NMET: normetanephrine
- SO<sub>4</sub>: sulphate
- VMA: vanillylmandelic acid
- VLA: vanillactic acid

<b>Table 1-03: Noradrenaline and Dopamine Transporter Specificities</b>			
<b>Transporter</b>	<b>Substrate Specificity (K<sub>m</sub> value as μmol/L)</b>		
	<b>Dopamine</b>	<b>Noradrenaline</b>	<b>Serotonin</b>
Noradrenaline Transporter	0.1	0.4	8.6
Dopamine Transporter	0.3	1.9	8.5

**Table 1-03:** The substrate specificity of noradrenaline and dopamine transporters (adapted from Graefe & Bönisch 1988).

<b>Table 1-04: Monoamine Neurotransmitters, Receptors, and Effects</b>			
<b>Monoamine</b>	<b>CNS Receptor</b>	<b>Main effects</b>	<b>Second Messenger (if applicable)</b>
Noradrenaline	α <sub>2</sub>	Neuronal inhibition	↓cAMP
	β <sub>2</sub>	Neuronal excitation	↑cAMP
Dopamine	D <sub>1</sub> (D <sub>1</sub> -type)	Neuronal excitation	↑cAMP
	D <sub>5</sub> (D <sub>1</sub> -type)	Neuronal excitation	↑cAMP
	D <sub>2</sub> (D <sub>2</sub> -type)	Neuronal inhibition	↓cAMP
	D <sub>3</sub> (D <sub>2</sub> -type)	Neuronal inhibition	↓cAMP
	D <sub>4</sub> (D <sub>2</sub> -type)	Neuronal inhibition	↓cAMP
Serotonin (5-hydroxytryptamine)	5-HT <sub>1A</sub>	Neuronal inhibition	↓cAMP
	5-HT <sub>1B</sub>	Presynaptic inhibition	↓cAMP
	5-HT <sub>1D</sub>	Cerebral vasoconstriction	↓cAMP
	5-HT <sub>2A</sub>	Neuronal excitation	↑IP <sub>3</sub> /DAG
	5-HT <sub>2C</sub>	Neuronal excitation CSF secretion	↑IP <sub>3</sub> /DAG
	5-HT <sub>3</sub>	Neuronal excitation	N/A ( <i>ligand-gated K<sup>+</sup> channel</i> )
	5-HT <sub>4</sub>	Neuronal excitation	↑cAMP
	5-HT <sub>5</sub>		
	5-HT <sub>6</sub>		
	5-HT <sub>7</sub>		↑cAMP

**Table 1-04:** Monoamine receptors, their function and mechanism of action (adapted from Rang et al. 2003; Barnes & Sharp 1999).

The transporters – presynaptic reuptake mechanisms – of monoamine neurotransmitters have also been demonstrated as the sites of action for a variety of psychostimulants such as cocaine in various forms, amphetamine, and methamphetamine (Elliott & Beveridge 2005; Sora et al. 2009). Drugs binding to these systems can and do cause widespread modulation or disruption of brain function. There is a potential for using drugs based on the pharmacologies of such psychostimulants to modulate the rate of monoamine transporters uptake, and thus adjust synaptic concentrations of neurotransmitter. However, the ability to do so without causing unwanted side effects requires that various structural modifications of the compounds are explored. The effects of any drug given as treatment over time must also be evaluated and monitored, so therefore the modulation (Table 1-05), evaluation, and monitoring of monoamine systems is very important for the investigation, diagnosis, treatment, and follow-up of many neuropsychiatric disorders – as well as being useful for drug development itself (Tatsumi et al. 1997; Tatsumi et al. 1999; Brunello et al. 2002).

<b>Table 1-05: Drugs Modulating Monoamine Systems</b>			
<b>Monoamine System</b>	<b>Target Site</b>	<b>Drug</b>	<b>Condition</b>
<b>Noradrenaline</b>	NAT	Reboxetine (SNRI)	Clinical depression
	$\alpha_2$ -receptor partial agonist	Clonidine	Hypertension and migraine
	NAT > SERT >> DAT	Zotepine	Schizophrenia
<b>Serotonin (5-HT)</b>	SERT	Citalopram (SSRI)	Clinical depression
	SERT	Paroxetine (SSRI)	Clinical depression
<b>Dopamine</b>	D <sub>2</sub> -receptor antagonist	Haloperidol	Schizophrenia
	D <sub>2</sub> -receptor agonist	Bromocriptine	Parkinson's disease

**Table 1-05:** Examples of drugs used to modulate monoamine systems (Tatsumi et al. 1997; Tatsumi et al. 1999; Bear et al. 2001; Rang et al. 2003).

## **1.2. Schizophrenia**

Schizophrenia is a serious mental illness that afflicts 7.2 per 1,000 individuals during their lifetime, and there are 15.2 per 100,000 new cases reported each year (Saha et al. 2005). The Saha meta-analysis also highlights that the prevalence of schizophrenia in richer countries is higher than that of the prevalence in poorer ones, that the sexes are equally at risk to developing schizophrenia in their lifetime, and that migrants are at greater risk than native-born individuals in a given country. In the modern world, increasing numbers of people are living and working abroad – thus exposing them to this migrant risk factor.

As of 2006, the global human population reached 6.5 billion inhabitants, with that figure set to surpass 7 billion by 2012 (United Nations Population Division 2006) – using the prevalence calculations of the Saha meta-analysis, this equates to an existing global population of 46.8 million schizophrenia sufferers and a 2012 projection exceeding 50 million. Apart from the human factor, there is also an economic factor encouraging the furtherance of research into mental disease such as schizophrenia. An economic evaluation of the impact of schizophrenia put United States expenditure on schizophrenia alone at \$65 billion in 1991 (Wyatt et al. 1995) – this equates to approximately \$92-96 billion in today's money after adjustment for inflation (Cyr 2005; Friedman 2000).

### **1.2.1. Symptoms**

The onset of symptoms in schizophrenic patients usually occurs during late adolescence to early adulthood (Morris et al. 2005; Saha et al. 2005). The exact cause of schizophrenia has not yet been discovered, although risk factors such as genes that give a biological predisposition have been identified – such as Disrupted In Schizophrenia 1 (DISC1), a gene that contributes to schizophrenia predisposition as well as other mental illnesses (Hennah et al. 2006; Porteous et al. 2006) – and it is thought that the environmental conditions (i.e. ambience or social setting) a person is exposed to during childhood years of neural development, as well as acute environmental conditions in later life, can influence (for better or worse) the risk of developing schizophrenia (Hollister et al. 2006).

Clinical presentation is characterised by both 'positive' / 'type I' and 'negative' / 'type II' symptoms (Hollister et al. 2006; Abi-Dargham & Guillin 2007; Morris et al. 2005; Yamamoto & Hornykiewicz 2004). 'Positive' symptoms are described as being additive to normal experiences, for example: hallucinations (e.g. auditory, visual, tactile, olfactory, etc...), delusions (e.g. intense paranoia), thought broadcasting (the belief that others are listening or stealing one's thoughts), thought insertion (the belief that others are inserting their thoughts into one's mind), and deranged logic in thought. 'Negative' symptoms are described as being subtractive from normal experiences, for example: depression, affective flattening (the reduction in range and intensity of emotional experiences), anhedonia (incapacity for pleasure), self-neglect, reduced motivation, social withdrawal, alogia (poverty of speech) and cognitive deficits in working memory, selective attention, and mental flexibility (i.e. planning and strategizing) (Javitt 1987; Montgomery 1979).

### **1.2.2. Imaging in schizophrenia**

There are no specific biomarkers per se that will confirm that a patient has schizophrenia, so diagnosis remains limited to performance testing and psychiatric evaluation using such criteria as the Brief Psychiatric Rating Scale (BPRS) and the Comprehensive Psychopathological Rating Scale (CPRS) (Montgomery 1979; Yamamoto & Hornykiewicz 2004). However, while not used as diagnostic tools, there are several biomarker trends that can be identified in the schizophrenia sufferer.

Following reports that schizophrenia patients may exhibit enlarged cerebral ventricles, a neuroimaging study of monozygotic twins discordant for schizophrenia used magnetic resonance imaging (MRI) to reveal significant reductions of hippocampal volume and significant increases in lateral and third ventricle volume (Suddath et al. 1990; Figure 1-04). The increases in ventricular volume are regarded to be secondary to the atrophy of hippocampal and grey matter tissue rather than a primary process of dilation. It is uncertain whether the initial loss of tissue itself is primary or secondary to the pathogenesis of schizophrenia, although it appears not to be secondary to the treatment regimes of schizophrenic patients due to the extent and duration of neuroleptic exposure exhibiting poor correlation to the findings.

Researchers also discovered as early as the 1980's that noradrenaline levels in the cerebrospinal fluid of schizophrenic patients are elevated (Sternberg et al. 1981; Gomes et al. 1980; Lake et al. 1980), with paranoid schizophrenics demonstrating the most striking differences compared to those of normal healthy individuals (Kemali et al. 1985; Kemali et al. 1982). Furthermore, noradrenaline concentrations have been shown to be elevated in the blood plasma of schizophrenics – correlated to CPRS diagnoses, emergence of positive symptoms, and exhibition of paranoid phenotypes (Bondy et al. 1984; Dajas et al. 1983).

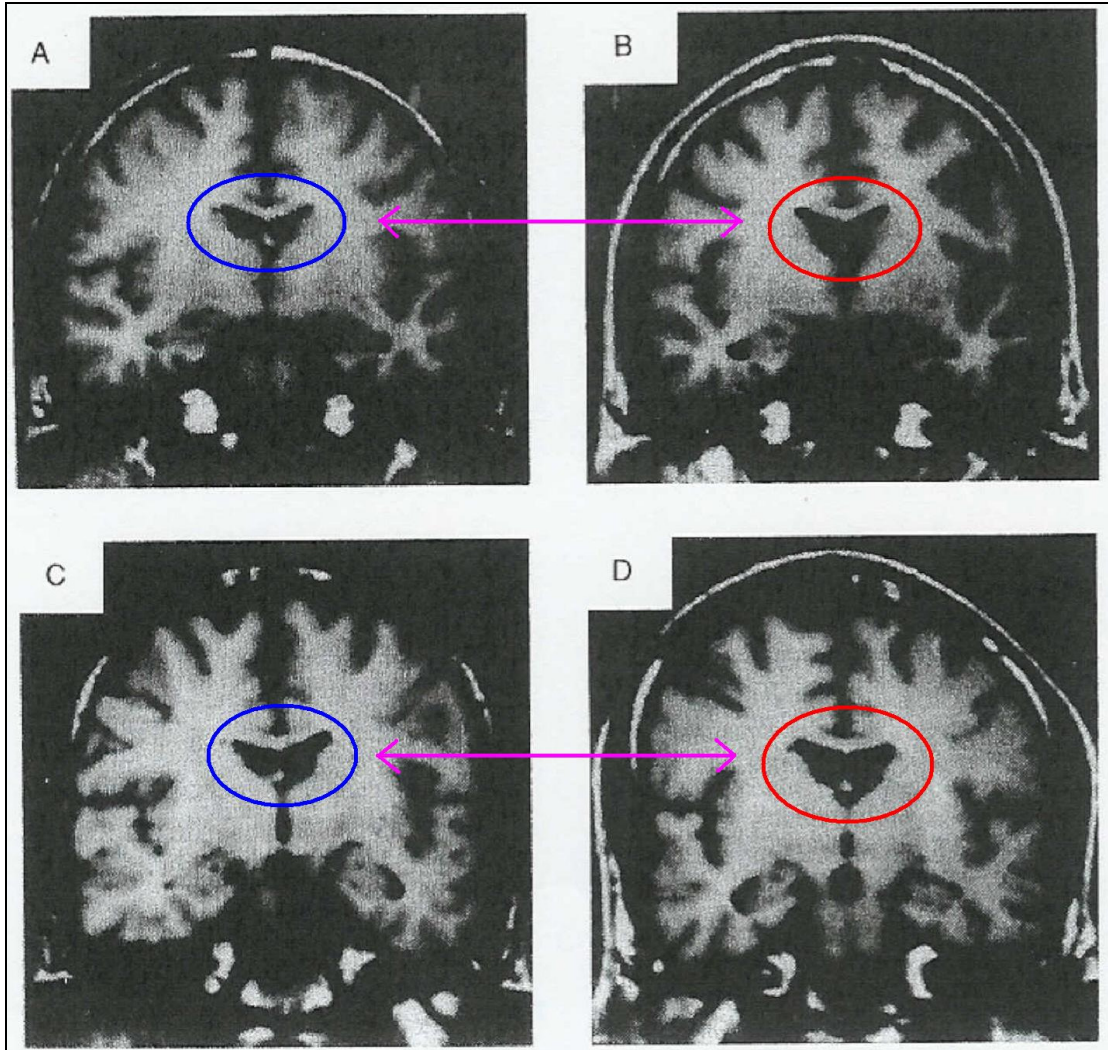


**Figure 1-04:** Coronal MRI sections from two sets of monozygotic twins (paired by purple arrows) discordant for schizophrenia (Adapted from Suddath et al. 1990). The lateral ventricles in the affected twins (B and D, red circles) are visibly enlarged in comparison to those of the healthy twins (A and C, blue circles).

### 1.2.3. Treatment and prognosis

The clearance of monoamines from the synapses of monoamine nerve terminals, thereby terminating stimulation of synaptic receptors, is primarily achieved through reuptake through monoamine transporters. Many examples of effective antipsychotics have been shown to exert at least part of their action through the blockade of the monoamine transporters: the noradrenaline transporter, the dopamine transporter, and the serotonin transporter (Tatsumi et al. 1999).

Neuroleptic drugs – antagonists for dopaminergic neurotransmission, particularly  $D_2$  receptors – control many of the symptoms of schizophrenia, although the negative symptoms such as social withdrawal are less responsive to treatment (Abi-Dargham & Laruelle 2005). Typical neuroleptics, such as haloperidol (Morita et al. 2000; Carlsson & Lindqvist 1963), were among the first drugs used to treat schizophrenic patients, but many carry adverse side effects, ranging from sensitivity reactions, haemolytic anaemias, rashes, cholestatic jaundice, photosensitisation, retinal degeneration, to severe movement disorders. Atypical neuroleptics are characterised by having lower incidences of movement disorders and are also better tolerated by patients than other anti-psychotics. Clozapine is considered to be one of the few ‘true’ atypical neuroleptics because it is sometimes effective in patients whose conditions were non-responsive to typical neuroleptics (Morita et al. 2000; Neal 2002).

It is noteworthy that in the cited examples of haloperidol (typical) and clozapine (atypical), while the typical neuroleptic instigates a near-total blockade of  $D_2$  receptors, the atypical neuroleptic causes only a partial  $D_2$  receptor occupancy (Farde et al. 1992; Figure 1-05). It has been postulated that the lower  $D_2$  receptor occupancy and lower specificity of clozapine contributes to the antipsychotic efficacy with reduced extrapyramidal side effects. Not only does this give us an indication of the differences between haloperidol and clozapine, but it is also a clear demonstration of how powerful *in vivo* imaging can be in improving our understanding of a disease state, demonstrating the pharmacology of existing drugs in a clinical patient, and assisting future drug design.

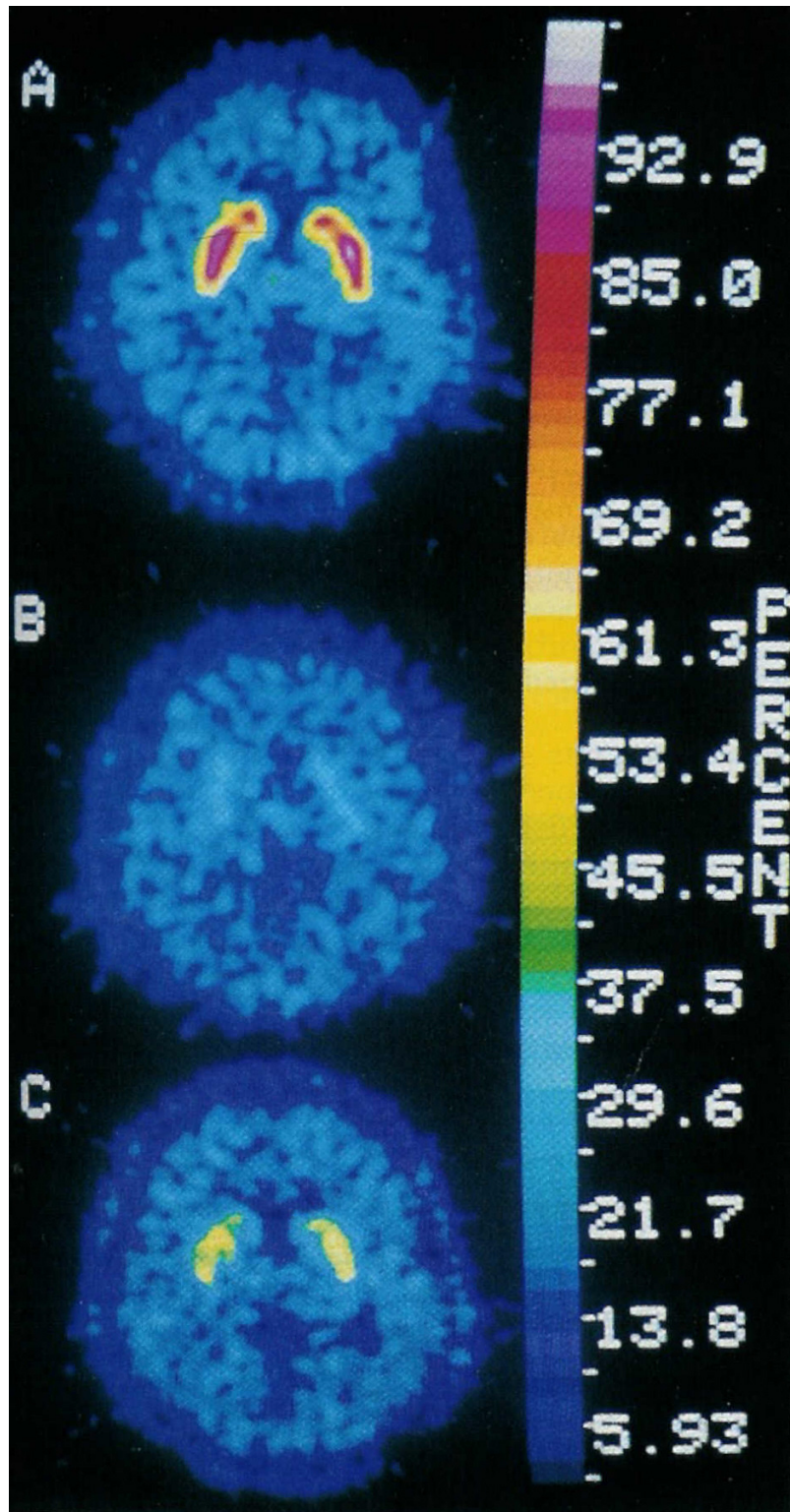


**Figure 1-05:** Clinical PET imaging of D<sub>2</sub> receptors with [<sup>11</sup>C]-raclopride (Reproduced from: Farde et al. 1992): a healthy medication-free volunteer (A), a schizophrenic treated with the typical neuroleptic haloperidol (B), and a schizophrenic treated with the atypical neuroleptic clozapine (C). The colour scale indicates D<sub>2</sub> receptor occupancy by [<sup>11</sup>C]-raclopride and is expressed as a percentage of maximum occupancy. Haloperidol exhibits a high D<sub>2</sub> receptor occupancy and competes for the majority of [<sup>11</sup>C]-raclopride binding sites, while the comparatively lesser competition for D<sub>2</sub> receptor binding sites by clozapine is indicative of a much lower D<sub>2</sub> receptor occupancy.

An example of another prominent atypical neuroleptic is zotepine, which although is believed to exert its effects primarily through dopamine and serotonin receptors also has notable affinity for the noradrenaline and serotonin transporters. The selectivity for the noradrenaline and serotonin transporters over the dopamine transporter is profound and affinities are reported as 20nM, 45nM, and 2.4µM, respectively (Tatsumi et al. 1999). This raises the question as to whether zotepine's mechanism of action is at least in part mediated by the blockade of the noradrenaline and/or serotonin transporters.

Currently, it is estimated that only 13% of global schizophrenic suffering is effectively alleviated or managed and that, given investment to improve our current medical interventions, it is reasonable to anticipate just under a doubling of the benefits provided by medical intervention. Unfortunately, due to limitations by current medical progress, current knowledge would be unable to impact up to three-quarters of schizophrenic disability – regardless of a theoretical unlimited investment in applying existing medical interventions (Andrews et al. 2004; Saha et al. 2005). Clearly, the focus of the research community is required for the development of more specific and medical intervention with greater efficacy, and the first step towards doing this is to further our knowledge of the molecular mechanisms, failed pathways, and deranged systems that underpin this debilitating condition.

#### **1.2.4. Noradrenergic hypothesis**

The precise molecular mechanisms, pathways, and deranged systems that underpin the pathology of schizophrenia are largely unknown although there are many circulating hypotheses involving many different neurotransmitters such as dopamine, serotonin, glutamate, GABA, acetylcholine, brain-derived neurotrophic factor, and noradrenaline (Lewis & Hashimoto 2007; Martin & Freedman 2007; Guillin et al. 2007; Bressan et al. 2005; Yamamoto & Hornykiewicz 2004; Laruelle et al. 2000). The most popular and heavily researched of the theories is the dopaminergic hypothesis of schizophrenia, which proposes hyperactivity in the dopaminergic mesolimbic and/or mesocortical pathway – supported by evidence that the most effective pharmacological interventions to alleviate schizophrenic suffering to date rely upon the antagonism of dopaminergic neurotransmission

(Neal 2002). However, strong evidence for a noradrenergic involvement is emerging.

A noradrenergic hypothesis to schizophrenia was first proposed in 1971 (Stein & Wise) but has received insufficient attention due to the limited interpretation that the D<sub>2</sub>-blocking actions of clinically effective neuroleptic drugs constituted conclusive evidence that the dopaminergic system was the most important system to investigate in schizophrenia research (Yamamoto & Hornykiewicz 2004).

Acute schizophrenic illness is usually accompanied by severe insomnia, and animal experimentation has shown that the injection of  $\alpha_2$ -adrenoceptor agonists and antagonists directly affect noradrenergic release, attention, sleep, exploratory behaviour, and locomotion (De Sarro et al. 1987; Table 1-01). Agonists of the noradrenergic system have been shown to exacerbate the positive symptoms and ameliorate the negative symptoms of schizophrenia upon acute administration (Jimerson et al. 1980). Conversely, antagonists of the noradrenergic system ameliorate positive symptoms and exacerbate the negative symptoms of schizophrenia upon acute administration (Hecht & Landy 2012; Svensson 2003) (Table 1-06). In the cases of chronic abuse of compounds such as methamphetamine, cocaine, or ephedrine – all noradrenergic agonists – negative symptoms are caused rather than prevented. Therefore, modulation or induced dysfunction of the noradrenergic system has been demonstrated to impose an influence upon both the positive and negative symptoms coupled with schizophrenic illness. This integrated involvement of noradrenaline in higher brain function, and similar symptomatology to schizophrenia upon disruption, suggests that noradrenergic neurotransmission may play an important part in schizophrenia's pathology (Yamamoto & Hornykiewicz 2004).

As aforementioned (Table 1-02), transporters transport more than just the monoamine that they are most commonly, the noradrenaline transporter has been shown to be the dominant mechanism of dopaminergic reuptake in the prefrontal cortex (Moron et al. 2002) and blockers of the noradrenaline transporter increase levels of dopamine specifically in the prefrontal cortex region of the neocortical mantle (Valentini et al. 2004).

<b>Table 1-06: Compounds modulating the noradrenaline system</b>		
<b>Method of action (direct or indirect)</b>	<b>Properties</b>	<b>Ligands</b>
<b>Mixed dopaminergic/noradrenergic modulating ligands</b>	<b>Agonists</b>	<ul style="list-style-type: none"> <li>• Amphetamine</li> <li>• Methamphetamine</li> <li>• Methylphenidate</li> <li>• L-DOPA</li> <li>• Cocaine</li> <li>• Monoamineoxidase Inhibitors</li> </ul>
	<b>Antagonists</b>	<ul style="list-style-type: none"> <li>• <math>\alpha</math>-methylparatyrosine</li> <li>• <math>\alpha</math>-methyldopa</li> <li>• Reserpine</li> </ul>
<b>Selective noradrenergic modulating ligands</b>	<b>Agonists</b>	<ul style="list-style-type: none"> <li>• Ephedrine</li> <li>• Yohimbine</li> <li>• Desipramine</li> <li>• Imipramine</li> <li>• Idazoxan</li> </ul>
	<b>Antagonists</b>	<ul style="list-style-type: none"> <li>• Clonidine</li> <li>• Propanolol</li> <li>• Oxypertine</li> </ul>

**Table 1-06:** Compounds that pharmacologically modulate the noradrenergic system (adapted from Yamamoto & Hornykiewicz 2004).

### **1.3. PCP-induced rat model of the metabolic hypofrontality observed in schizophrenia**

Schizophrenia is a complicated condition and furthering human knowledge of the disease is made that much more difficult due to the inability to perform a systematic characterisation of the disease in drug-free patients for ethical considerations. Therefore, an animal model of the disease is required to enable a full array of *in vitro* and *in vivo* techniques to be brought to bear and elucidate the aberrant mechanisms underlying schizophrenia. However, such is the complexity of the causes and progression of the disease that the field lacks universal agreement among schizophrenia researchers as to the best strategy for establishing a schizophrenic animal model and the models only mimic a aspects of the disease rather than schizophrenia in its entirety. Consequently, it is a combination of animal models mimicking various aspects of schizophrenia that will contribute to the understanding of the disease.

It is acknowledged that there are genetic models of the disease but, as aforementioned, while genetics may indeed impose a predisposition upon an individual to develop a schizophrenic psychosis, the evidence of monozygotic twins with discordance for the disease indicates that environmental factors are also prevalent. On this basis, this thesis will address the environmental factors through the pharmacological modelling of selected aspects of schizophrenia.

As with differing hypotheses as to which systems and neurotransmitters are most critically implicated in schizophrenia, there are also different pharmacological models to simulate schizophrenia – each with their advantages and disadvantages. The most often applied models are those established in rat by the chronic or acute administration of drugs that are known to have induced or exacerbated schizophrenic symptoms in humans or schizophrenic patients, respectively.

#### **1.3.1. Phencyclidine**

Phencyclidine (PCP) was initially developed as a surgical anaesthetic, but was abandoned due to patients exhibiting unacceptable side effects – including

hallucinations, disordered speech, delirium, agitation, and disorientation – during their recovery from surgery (Morris et al. 2005). Unfortunately, these symptoms proved attractive to the drug-abuse community and PCP became illicitly traded and abused under such names as “angel dust” and “hog”.

When it came to light that some drug users were mistaken for schizophrenics and as a result were treated with drug therapies as schizophrenics, the greater awareness of this potential for misdiagnosis resulted in better treatment for PCP addicts and a greater interest in PCP from the research community. PCP can therefore be said to induce a psychosis in normal healthy subjects and it has also been shown to exacerbate symptoms when administered to schizophrenic patients (Luby et al. 1959; Allen & Young 1978; Javitt 1987; Deutsch et al. 1989; Javitt & Zukin 1991; Morita et al. 2000). PCP reproduced not only the positive symptoms of schizophrenia, but also negative symptoms such as cognitive deficits – something that was not provided by the amphetamine models of schizophrenia that had been relied upon up until that point (Javitt & Zukin 1991; Deutsch et al. 1989; Javitt 1987).

### **1.3.2 Pathways implicated in schizophrenia and the PCP model**

The rat was chosen for establishing the animal model due to the widespread acceptance, easy availability, and commonplace use in research environments. This regular use of rat models has provided researchers with valuable experience and a thorough understanding of the biology, the advantages, and the limitations associated with the animal model.

Rats that have been subjected to PCP treatment regimes present with hyperlocomotion, ataxia, agitation, cognitive deficits, and impaired social interactions as well as decreased exploratory behaviour in a PCP-dose-dependent manner (Morita et al. 2000) – a behaviour that has been interpreted as modelling the reduced motivation seen in human schizophrenics. It has been argued that the extent to which the symptoms of PCP administration emulate those of schizophrenia is so far unequalled by alternative pharmacology (Morris et al. 2005). Many of these symptoms are alleviated by neuroleptics such as haloperidol and clozapine not only in rat but also in the more complex brains of non-human primates (Jentsch et al. 1997) with similar success rates to the clinical

treatment of schizophrenics – giving confidence to those applying the PCP model in their research paradigms.

The deranged pathways involved in schizophrenia involve a corticolimbothalamic circuitry (Figure 1-06) that is thought to also become defective following PCP administration, with hypometabolism in the prefrontal cortex and mediodorsal thalamus disturbing the circuit's positive feedback loop. Once disturbed, this positive feedback loop can prove difficult to restore. The prefrontal cortex has been shown to be important to schizophrenia through deoxyglucose studies (Cochran et al. 2003), where the prefrontal cortex was shown to have a reduced metabolic activity – referred to as the 'hypofrontality' of the schizophrenic phenotype. It is thought that the next generation of antipsychotic drugs to treat schizophrenia will be based on preparations that are demonstrated to be most capable of antagonising or reversing PCP-induced psychoses (Morita et al. 2000).

The PCP-induced rat model of the metabolic hypofrontality observed in schizophrenia is most similar to the alternative ketamine-induced rat model. Although while both ketamine- (Krystal et al. 1999) and PCP-induced psychoses can be reversed by clozapine and not haloperidol, unlike other NMDA receptor antagonist models, the PCP model in particular was able to mimic the metabolic deficit of the prefrontal cortex that does not respond to atypical neuroleptic treatment in the clinic (Cochran et al. 2003).

Recently, an attempt has been made to review, analyze, and standardize the treatment regime for the PCP model (Morris et al. 2005). The Morris laboratory examined acute, chronic, high- and low-dose PCP administration for establishing a PCP model of schizophrenia and devised an optimised protocol for most accurately replicating the schizophrenic phenotype in the model. Importantly, the PCP model optimised by Morris *et al* mimics the hypofrontality observed in schizophrenia without the temporal cortex lesions observed in the ketamine model and are not present in the clinical schizophrenic.

Acute PCP exposure in rodents has been shown to impair social interaction and induce cognitive deficits, although acute PCP exposure in humans is less likely to induce a schizophrenia-like psychosis than chronic exposure – therefore indicating that chronic PCP exposure in rodents may yield a more accurate model. Indeed,

chronic PCP exposure in rodents induces diminishing dopamine turnover within the prefrontal cortex, along with deficits in working memory and pathways reliant upon the prefrontal cortex.

When PCP administration is used in high-dose regimes, it has been demonstrated that neurodegeneration occurs in pyramidal neurons of the retrosplenial cortex – a pathology not observed in the post-mortem tissue of schizophrenic patients. In human schizophrenic patients, it is primarily the interneurons that are affected – thus indicating that high-dose PCP regimes are not appropriate for obtaining a PCP model of schizophrenia.

In light of these discussions, the PCP model applied in this thesis will use chronic, low-dose drug administration ( $2.58\text{mg}\cdot\text{kg}^{-1}\cdot\text{day}^{-1}$ ) in the rat to most accurately emulate the metabolic hypofrontality observed in both the human schizophrenic and the human PCP abuser (Cochran et al. 2003; Morris et al. 2005).

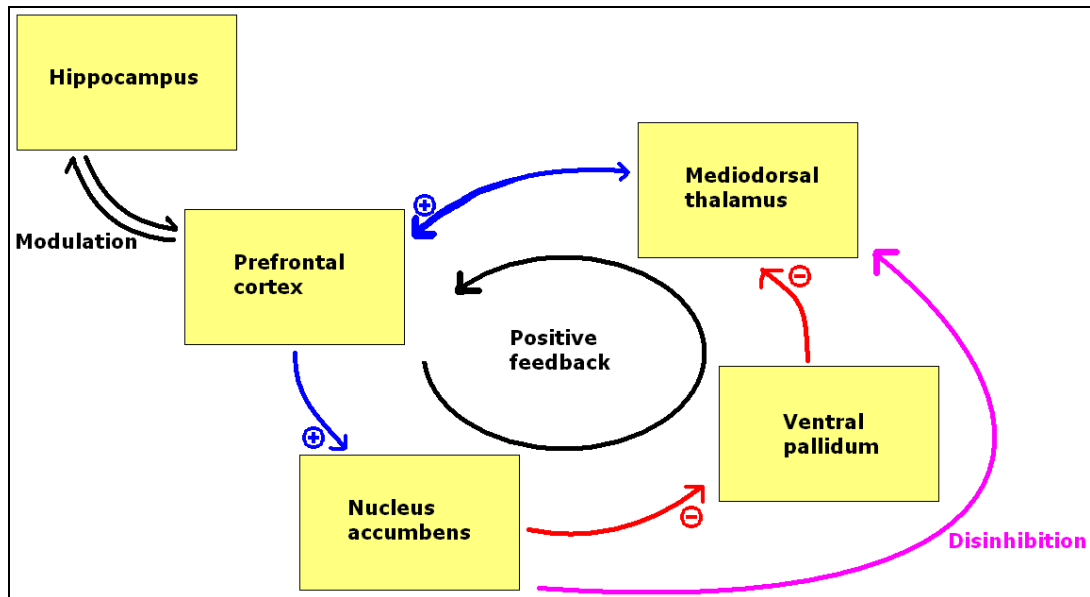


**Figure 1-06:** The corticolimbic circuitry that becomes deranged in schizophrenia (adapted from Morris et al. 2005). The hypometabolic function of the prefrontal cortex and mediodorsal thalamus disrupts the positive feedback of the corticolimbic circuitry.

### 1.3.3. Hypothesis and study aims:

The NAT is the dominant mechanism of dopaminergic reuptake in the prefrontal cortex (Moron et al. 2002) and blockers of the noradrenaline transporter increase levels of dopamine specifically in the prefrontal cortex region of the neocortical mantle (Valentini et al. 2004). It has been shown that PCP competes with [<sup>3</sup>H]-nisoxetine binding at the NAT in the periphery (Pubill et al. 1998; Rogers & Lemaire 1992) and also induces a metabolic hypofunction in the prefrontal cortex and other brain regions (Cochran et al. 2003; Morris et al. 2005). I therefore hypothesise that chronic low-dose PCP administration, as refined by Cochran et al 2003, will down-regulate the NAT in the prefrontal cortex.

In Chapter 3, the aims of the study are:

- [<sup>3</sup>H]-nisoxetine is considered a benchmark ligand that has been thoroughly validated for NAT imaging, so autoradiographic imaging using [<sup>3</sup>H]-nisoxetine will quantitatively determine the distribution and specific densities of the noradrenaline transporter in the PCP model of schizophrenic hypofrontality to ascertain whether noradrenaline reuptake mechanisms are perturbed. If changes are observed in NAT expression then this model may prove useful as a means of demonstrating the capabilities of a novel SPECT brain imaging tracer for the NAT.
- Use a noradrenaline transporter-specific [<sup>35</sup>S]-labelled oligonucleotide probe to qualitatively assess mRNA densities and ascertain whether noradrenaline transporter gene expression is perturbed in the PCP model of schizophrenic hypofrontality.
- Use a [<sup>3</sup>H]-nisoxetine competition assay with rat brain homogenates to confirm whether PCP competes for the [<sup>3</sup>H]-nisoxetine binding site on the noradrenaline transporter in the central nervous system as well as in the periphery.
- For comparison, image other monoamine transporters by using [<sup>3</sup>H]-WIN-35,428 and [<sup>3</sup>H]-citalopram autoradiographic imaging to quantitatively determine the distribution and specific densities of the dopamine and serotonin transporters, respectively, to ascertain whether

dopamine and serotonin reuptake mechanisms are perturbed in the PCP model of schizophrenic hypofrontality.

- For comparison, image other monoamine transporter mRNA by using dopamine and serotonin transporter-specific [<sup>35</sup>S]-labelled oligonucleotide probes to qualitatively assess mRNA densities and ascertain whether dopamine and serotonin transporter gene expression is perturbed in the PCP model of schizophrenic hypofrontality.

## **1.4 Neuroimaging**

### **1.4.1 The need for a SPECT brain imaging tracer for the NAT**

The noradrenergic system has wide-reaching projections throughout the brain (Moore & Bloom 1979), modulating both excitatory and inhibitory neurotransmission, with implications in diseases such as severe anxiety, clinical depression, disorders of sleep (De Sarro et al. 1987; Hipolide et al. 2005), and schizophrenia (Yamamoto & Hornykiewicz 2004). While my investigations into the involvement of the NAT in a pharmacological model of schizophrenia (see Chapter 3) did not demonstrate changes to the density or distribution of the NAT or changes in the expression of NAT-specific mRNA, published data shows that some pharmacological therapies for schizophrenia have significant affinities for the NAT (Tatsumi et al. 1999). Therefore, even in instances where the aetiology of the disease has not been shown to induce or arise from disturbed noradrenergic neurotransmission, pharmacological modulation of the noradrenergic system can still be used to alleviate the symptoms of disease. Consequently, the noradrenergic system presents itself as a logical target for pharmacological manipulation in the treatment of disease and a site of interest for imaging, as drug occupancy studies can be used to demonstrate the affinity of a newly developed drug at the NAT. Similarly, a NAT-specific SPECT imaging tracer can be used to characterise the occupancy of the NAT for drugs already in use to try to correlate their efficacy to NAT occupancy, such as is the case in the treatment of schizophrenia.

The NAT regulates synaptic levels of noradrenaline via uptake, so imaging the density and distribution of this important site will provide valuable information on

the potential for manipulation of the noradrenergic system by drugs targeted at the NAT. Where therapeutic action has been identified as mediated by selective noradrenergic reuptake inhibition, the ability to image the NAT will also aid future drug development and can act as a biomarker to demonstrate the efficacy of both new and existing drugs at the NAT. Competition for the binding site used by a NAT-specific tracer by emerging compounds will cause a decrease in binding by a NAT-specific tracer and so the affinity for the NAT by emerging compounds can be quantified. Where therapeutic action has been identified as mediated by selective noradrenergic reuptake inhibition, those compounds with greatest affinity and specificity for the NAT should have the greatest therapeutic effect with the least side effects.

As previously mentioned, there are several atypical neuroleptic drugs that show greater efficacy at the NAT than at the SERT or DAT (Tatsumi et al. 1999), so understanding the NAT occupancy of these drugs in the treatment of schizophrenia and even pharmacological models of the disease can further our understanding of how the modulation of noradrenergic neurotransmission may benefit schizophrenic patients and/or affect them in acute and chronic SNRI administration. For example, an increase or reduction in tracer binding to the NAT in the locus coeruleus could be used as a marker to ascertain how, and to what degree, noradrenergic neurotransmission has been affected by treatment regimes. Following an appropriate medication-free period in a long-term patient, increased NAT-specific tracer binding in the locus coeruleus could imply an overall upregulation of the NAT in response to long-term pharmacological blockade by chronic SNRI administration. Another use for a NAT-specific tracer could be to estimate pre- and post-medication administration NAT occupancy of the tracer to evaluate the NAT occupancy of the competing medication for a given dose.

Successful probing of the NAT in the CNS *in vitro* has been accomplished with [<sup>3</sup>H]-nisoxetine and radio-labelled desipramine (Lee & Snyder 1981), although excessive non-specific binding was problematic *in vivo* for the latter (Eisenhofer 2001). *In vivo* imaging of the NAT with single photon emission computed tomography (SPECT) and/or positron emission tomography (PET) imaging has previously been limited to the periphery with tracers such as MIBG in SPECT- and PET-ligand forms and has been a useful tool in the detection of NAT-overexpressing neuroendocrine tumors (Pryma & Divgi 2008). Unfortunately, as

MIBG is unable to cross the blood-brain barrier, it cannot be used for *in vivo* neuroimaging studies (Guilloteau et al. 1983b; - French language, cited by Baulieu et al. 1990).

#### 1.4.2 Potential NAT-specific compounds for SPECT tracer development

It might be expected that the production of successful SPECT and/or PET ligands for imaging of the NAT in the CNS will be derived from compounds structurally related to nisoxetine (Hadrich et al. 1999b). Unfortunately, although [<sup>11</sup>C]-nisoxetine displayed good affinity for NAT ( $K_i = 1.85$  nM), metabolism in the serum was more rapid than ideal and brain uptake kinetics were too slow so this meant that a low brain-to-serum ratio was achieved, and in the presence of unlabelled nisoxetine brain uptake was higher suggesting problematic high non-specific binding (Tamagnan et al. 2007; Ding et al. 2005). The measurements for uptake are different from the measurements for binding, and it could be that unlabelled nisoxetine also in the serum occupied a sequestering site at the blood-brain barrier to aid the uptake of more [<sup>11</sup>C]-nisoxetine into the brain, perhaps indicating an issue for labelled nisoxetine binding to an unintentional site at the blood-brain barrier. These unfavourable kinetics of [<sup>11</sup>C]-nisoxetine, in combination with the short half-life of PET radiolabels and high non-specific binding hampered its use as an *in vivo* imaging agent. Clearly, an alternative molecule for development was required. Furthermore, with *in vivo* kinetics posing a consistent problem for PET imaging of the NAT, it was hoped that SPECT-applicable tracer candidates would offer more likelihood for successful imaging of the NAT. Utilising [<sup>123/125</sup>I]-labelled ligands should enable maximal specific binding to be achieved prior to the decay rate of the isotope becoming problematic.

Tomoxetine (aka MIPP), structurally related to nisoxetine, was also explored for its potential as a SPECT brain imaging tracer and displayed good *in vitro* affinity for the NAT with a  $K_D$  of approximately 2nM, although only a 4.4-fold selectivity for the NAT over the SERT (Tatsumi et al. 1997). The iodinated tomoxetine (Kiyono et al. 2004; Kung et al. 2004), tomoxetine retains this lack of selectivity and the binding to the SERT as well as the NAT diminishes its value as a NAT-specific SPECT brain imaging tracer (Gehlert et al. 1995; Ding et al. 2005). Some groups even proposed an iodinated tomoxetine analogue as a SERT-specific brain imaging

tracer, however high nonspecific binding *in vivo* (Chumpradit et al. 1992) made it unsuitable for use as a brain imaging tracer.

Reboxetine is a highly selective noradrenergic reuptake inhibitor (Table 1-07) used in the treatment of clinical depression (Wong et al. 2000) and has been suggested as a basis for a NAT-specific *in vivo* imaging ligand. The inhibition constants of reboxetine demonstrated at monoamine receptors are particularly low, in the micromolar range for  $\alpha$ -adrenergic receptor subtypes, D<sub>2-4</sub> dopaminergic receptor subtypes, 5-HT<sub>1A</sub>, <sub>2A</sub> & <sub>2C</sub> receptor subtypes, and in millimolar range for  $\beta$ -adrenergic receptor subtypes, the D<sub>1</sub> dopamine receptor subtype, and 5HT<sub>3-7</sub> receptor subtypes (Wong et al. 2000; Table 1-07). At the dopamine transporter, there is no significant displacement noted against [<sup>3</sup>H]-WIN-35,428 (Wong et al. 2000; Table 1-07). Reboxetine exhibits notable affinity at the serotonin transporter in the hundred nanomolar range, although given the strong affinity at the noradrenaline transporter, the selectivity ratio of reboxetine is still greater than 120:1 (Wong et al. 2000; Table 1-07).

Recent research attention has therefore been focused upon the development of reboxetine-like compounds for *in vivo* imaging (Table 1-08). Many of the compounds labelled with the short half-life isotopes <sup>11</sup>C or <sup>18</sup>F are for PET imaging, and the relevant compounds for SPECT imaging have been labelled with the longer half-life isotopes <sup>123</sup>I or <sup>125</sup>I.

For example, [<sup>123/125</sup>I]- (S,S)-2-( $\alpha$ -(2-iodophenoxy)benzyl)morpholine, known by the acronyms INER and IPBM, has been determined to have good affinity for NAT (0.84nM and 4.22nM, Table 1-08) and good blood-brain barrier penetration at a favourable rate enabled maximum uptake at 30 minutes with a gradual decreases in brain concentration while serum concentrations were cleared more quickly – reaching a brain-to-blood ratio of 15.9:1 after an hour (Tamagnan et al. 2007; Kanegawa et al. 2006). Nisoxetine was also shown to displace specific binding in INER/IPBM *ex vivo* autoradiograms and it therefore shows some promise as a SPECT imaging tracer.

<b>Table 1-07: Monoaminergic Binding Profile of Reboxetine</b>	
<b>Monoamine Binding Site</b>	<b>K<sub>i</sub> (nM)</b>
Noradrenaline Transporter <i>(displacing [<sup>3</sup>H]-nisoxetine)</i>	1.1 ± 0.2
Adrenergic Receptors: α <sub>1</sub> Adrenergic α <sub>2</sub> Adrenergic β <sub>1</sub> Adrenergic β <sub>2</sub> Adrenergic	10,000 ± 2,000 43,000 ± 3,000 10,300,000 >10,000,000
Dopamine Transporter <i>(displacing [<sup>3</sup>H]-WIN-35,428)</i>	<i>No significant displacement at 10,000</i>
Dopaminergic Receptors: D <sub>1</sub> Dopamine D <sub>2</sub> Dopamine D <sub>3</sub> Dopamine D <sub>4</sub> Dopamine	>10,000,000 9,000 ± 5,000 20,000 ± 2,000 >49,000
Serotonin Transporter <i>(displacing [<sup>3</sup>H]-citalopram)</i>	129 ± 13
Serotonin Receptors: 5-HT <sub>1A</sub> 5-HT <sub>2A</sub> 5-HT <sub>2C</sub> 5-HT <sub>3</sub> 5-HT <sub>4</sub> 5-HT <sub>6</sub> 5-HT <sub>7</sub>	18,000 ± 3,000 7,300 ± 400 1,500 ± 500 >10,000,000 >10,000,000 >10,000,000 >10,000,000

**Table 1-07:** The monoaminergic binding profile of the selective noradrenergic reuptake inhibitor, reboxetine, established by the competitive displacement of various selective ligands (Adapted from: Wong et al. 2000).

<b>Table 1-08: Candidate Compounds for <i>in vivo</i> imaging of the NAT</b>				
<b>Compound</b>	<b>K<sub>i</sub> (nM)</b>	<b>Isotope</b>	<b>Technique</b>	<b>Reference</b>
2β,3α-(substituted phenyl) nortropanes	0.43 – 4.67	[ <sup>11</sup> C]	PET	(Zeng et al. 2007)
Methylreboxetine / MRB / MeNER	4.63 *	[ <sup>11</sup> C]	PET	(Logan et al. 2007; Ding et al. 2005)
3-Cl-methylreboxetine	6.11 *	[ <sup>11</sup> C]	PET	(Ding et al. 2005)
Fluororeboxetine		[ <sup>18</sup> F]	PET	(Ding et al. 2005)
Nisoxetine	1.85	[ <sup>11</sup> C]	PET	(Tatsumi et al. 1997)
Oxaprotiline	9.07 *	[ <sup>11</sup> C]	PET	(Ding et al. 2005)
Lortalamine	0.37 *	[ <sup>11</sup> C]	PET	(Ding et al. 2005)
(R)-MIPP / tomoxetine	1.16	[ <sup>125</sup> I]	SPECT	(Kiyono et al. 2004; Kung et al. 2004; Gehlert et al. 1995; Chumpradit et al. 1992)
Iodoreboxetine: a.k.a. INER; a.k.a. IPBM	0.84; 4.22	[ <sup>123</sup> I]; [ <sup>125</sup> I]	SPECT	(Tamagnan et al. 2007; Kanegawa et al. 2006)

**Table 1-08:** Candidate compounds for *in vivo* imaging of the NAT, their affinity for the NAT as defined by competition assays, their labelling isotope, and applicable imaging technology.

\* Reported relative to nisoxetine affinity and corrected here for an approximated K<sub>i</sub>.

The qualities required of a successful ligand are high affinity ( $K_d < 10\text{nM}$ ) and selectivity ( $\geq 10$ -fold) for the NAT, as well as stability in circulation (i.e. low rate of metabolism), blood-brain barrier penetrability, low *in vivo* non-specific binding, and favourable kinetics *in vivo* (i.e. rapid brain uptake). The isotope should also have a favourably low rate of decay, so as to permit maximum brain uptake prior to image acquisition and using SPECT-specific isotopes will provide this advantage over PET alternatives.

Schou et al (2007) examined previously successful PET brain imaging tracers for a variety of targets and determined that a simple binding potential estimation ( $B_{\text{max}}$  of target /  $K_d$  of ligand) greater than or equal to 12 would enable a ligand to yield valuable data from within a structure. Image acquisition is different on a PET scanner than it is on a SPECT scanner and there is the disadvantage of a more rapid rate of decay for the radioisotope sometimes necessitating image capture at a moment prior to that of ideal. A SPECT scanner, without this disadvantage, may not require a binding potential as great as 12 for valuable imaging of the NAT. However, as I am unable to determine what value would be appropriate 12 is an acceptable approximation for a simple analysis of INER/IPBM (Table 1-09).

<b>Table 1-09: NAT distribution in human brain and imaging tracer requirements</b>				
<b>Brain Structure</b>	<b>NAT B<sub>max</sub> as pmol/g wet weight, ~nM (Donnan et al. 1991)</b>	<b>Required K<sub>d</sub> to achieve simple binding potential estimations ≥12</b>	<b>Simple Binding Potential Estimation (B<sub>max</sub>/K<sub>d</sub>)</b>	
			<b>INER (aka IPBM) K<sub>d</sub> = 0.84nM (Tamagnan et al. 2007)</b>	<b>IPBM (aka INER) K<sub>d</sub> = 4.22nM (Kanegawa et al. 2006)</b>
Globus Pallidus	8.7	0.73	10.4	2.1
Ventral Pallidum	2.0	0.17	2.4	0.5
Bed Nucleus of the Striatum Terminalis	8.0	0.67	9.5	1.9
Thalamus	10.5	0.88	12.5	2.5
Hypothalamus	36.7	3.06	43.7	8.7
Red Nucleus	7.6	0.63	9.0	1.8
Substantia Nigra <i>pars compacta</i> <i>pars reticulata</i>	- 5.4	- 0.45	- 6.4	- 1.3
Edinger-Westphal Nucleus	18.4	1.53	21.9	4.4
Rostral Linear Nucleus	7.2	0.60	8.6	1.7
Caudal Linear Nucleus	50.5	4.21	60.1	12.0
Parabrachial Pigmented Nucleus	1.0	0.08	1.2	0.2
Paranigral Nucleus	4.6	0.38	5.5	1.1
Central Grey	18.0	1.50	21.4	4.3
Dorsal Raphe Nucleus	60.8	5.07	72.4	14.4
Medial Raphe Nucleus	47.3	3.94	56.3	11.2
Raphe Magnus Nucleus	7.1	0.59	8.5	1.7
Raphe Obscurus Nucleus	21.0	1.75	25.0	5.0
Raphe Pallidus Nucleus	10.2	0.85	12.1	2.4
Paramedian Raphe	68.6	5.72	81.7	16.3
Locus Coeruleus	70.8	5.90	84.3	16.8
Cerebellum	6.6	0.55	7.9	1.6
Dorsal Tegmental Nucleus	27.5	2.29	32.7	6.5
Subpenduncular Pigmented Nucleus	20.3	1.69	24.2	4.8

**Table 1-09:** The distribution of NAT in the human brain and simple estimations of binding potentials for NAT-specific prospective SPECT brain imaging tracers. Green shading indicates a simple binding potential estimation ≥12, and therefore indicative of a structure likely to be imaged successfully by the prospective tracer according to Schou et al (2007).

### 1.4.3 Objectives for new iodoreboxetine analogues

Candidate compounds, shown in Table 4-04, synthesised along novel routes by Nicola K. Jobson in the Sutherland Chemistry Laboratory (Jobson et al. 2008a; Jobson et al. 2008b; Jobson et al. 2009) are also structurally related to reboxetine and the iodophenoxy ring compounds have particularly strong structural similarities to [ $^{123/125}\text{I}$ ]-INER/IPBM. However, these compounds have novel routes of synthesis and some structural differences that distinguish them from previously reported molecules. The compounds were produced in three main groups (Table 4-04) with one group examining isomers of iodophenyl ring analogues, isomers of benzyl alcohol iodoamine analogues to determine the effect of deleting the phenoxy ring on binding properties, and the iodophenoxy ring analogues which examined iodine placement in a structural (*R,S*) confirmation that had not yet been fully explored by previous investigations in published literature.

As Tamagnan et al (2007) tested the (*S,S*)-isomer for the iodophenoxy ring reboxetine analogues, my investigations were of the (*R,S*)-isomer of these analogues to determine which of the reboxetine analogue isomers have the greatest potential as radioiodinated NAT-specific SPECT brain imaging tracers. The difference between each of the (*R,S*)-isomer analogues was the position of the iodine atom on the molecule, which will potentially influence the affinity and selectivity for NAT.

In Chapter 4, the affinity and selectivity for the NAT are determined via competitive radioligand binding assays with reference to structural differences in the chemistry of the candidate compounds. This will be accomplished by determining:

- Inhibition constants for all three monoamine transporters (NAT, SERT, and DAT) for the iodophenyl ring compounds to assess which isomers yield the greatest affinity and selectivity.
- Inhibition constants for benzyl alcohol amide intermediate compounds at all three monoamine transporters to discover whether the phenoxy ring is critical to molecular binding properties of iodinated reboxetine-analogues.
- Inhibition constants will be determined at all three monoamine transporters for the iodophenoxy ring compounds, how these compare to other

iodophenoxy ring compounds in the literature, and whether the position of the iodine atom greatly influences affinity and selectivity.

## **1.5 Principles of *In Vivo* Neuroimaging**

### **1.5.1 Advantages of non-invasive SPECT and PET techniques**

SPECT and PET imaging relies upon the development of radiolabelled 'tracer' compounds with which to probe binding sites of interest. For neuroimaging studies, these binding sites are usually found on neurotransmitter receptors or transporters and tracer ligands are normally administered in doses that are far exceeded by their  $K_D$  values for the sites of interest, so as not to perturb the system being studied either pharmacologically or become harmful in terms of the quantity of radioactivity being injected into the patient. Otherwise, the pharmacological effect of the ligand could modify the system under examination, too high a specific activity could inflict cellular damage, and would either be detrimental to the patient or fail to give a true reflection of the brain in its natural state – whether it is currently in good health or afflicted. In terms of the imaging itself, excessive binding of a ligand to noradrenaline transporters could have a pharmacological effect in the periphery to modulate vascular constriction and could have adverse effects upon the patient. Naturally, if the patient is stressed, then this could affect the results of the examination of occupancy and displacement studies upon targets in the noradrenergic system, which is implicated in stress and anxiety.

Selecting a non-invasive *in vivo* technique such as SPECT or PET provides the direct benefit of the imaging procedure being readily applied to patients in the clinic, and these neuroimaging techniques will take on an increasing importance in drug discovery in two main ways. Firstly, displacement of a tracer from a binding site by an existing therapeutic drug to treat disease will confirm the mechanisms of action for existing drugs. The mechanisms of action and specificities identified can be correlated with the known benefits and drawbacks of the therapeutic drug – thus identifying the most important targets in the brain for drug discovery and to what extent they must be manipulated to have the desired effect. Secondly, the displacement of a tracer from a binding site by a new drug candidate can be used as a biomarker to demonstrate the specificity for target site of the new compound

and demonstrate any long-term effects of the compound upon the system with follow-up scans.

### 1.5.2 SPECT and PET Theory

Single photon emission computed tomography (SPECT) and positron emission tomography (PET) scanners are able to detect gamma emissions from radiolabelled compounds that bind to receptors or transporters. The accumulation of compound in regions of the brain that express these functional protein structures results in an increased intensity of signal detected by the scanner and so reveals the distribution of the site of interest.

The theory of SPECT and PET neuroimaging (Frankle et al. 2005b) can be likened to a three-dimensional *in vivo* version of the *in vitro* technique autoradiography, although it is far more dynamic in nature. The difference between *in vitro* autoradiography and *in vivo* SPECT or PET is that, whilst using trace concentrations of ligand, it is not possible to directly calculate  $B_{\max}$  or  $K_D$  values if neither value is predetermined. The measure actually obtained via SPECT or PET scanner – termed the binding potential (BP) – is representative of  $B_{\max}$  and  $K_D$  and is equal to  $B_{\max}/K_D$  (Mintun et al. 1984). It is from this value, knowing the  $K_D$  of the tracer *in vitro*, that we are able to derive the  $B_{\max}$  of the tracer *in vivo* based on the assumption that the  $K_D$  of the tracer for the target site remains unchanged in the brain being imaged. Furthermore, a compound with a greater affinity will result in a greater binding potential during a scan for a given target site.

Neuroimaging with SPECT and PET theoretically segregates tracer concentrations into a compartmentalised system, with each compartment defined as an area where the concentration of radioactive tracer is assumed to be homogeneous (Frankle et al. 2005b).

The compartmental model (Figure 1-13) has representations for the homogeneous tracer concentration in the plasma ( $C_1$ ), free tracer in the intercerebral interstitium ( $C_2$ ), nonspecifically brain-bound tracer ( $C_2'$ ) and the specifically bound tracer at the brain site of interest ( $C_3$ ). Fractional rate constants  $K_{1-6}$  are said to be the fraction of the tracer concentration that moves from one compartment to the next in a given timeframe.  $K_1$  and  $K_2$  represent the fractional rate constants for

transversing the blood-brain barrier and are dependent upon blood flow and permeability (Frey et al. 1985; Gjedde & Wong 1990).  $K_3$  and  $K_4$  represent the fractional rate constant for association and dissociation from specific binding, while  $K_5$  and  $K_6$  represent the fractional rate constants for association and dissociation from nonspecific binding.

While the four-compartment model is the best representation for the theory of SPECT and PET imaging, the large number of parameters and variables for which to compensate make it difficult to put into practice - therefore, this is simplified to the three-compartment model (Figure 1-14). In the simplified three-compartment model, the plasma compartment ( $C_1$ ) is given the new designation of  $C_a$  to represent arteriole and capillary tracer concentrations. This is a practical improvement upon the full model in which tracer concentration is not deemed to be homogeneous between arteriole and capillary compartments, requiring modelling of arteriole concentrations, arteriole blood flow, capillary concentrations, and capillary flow (Frey et al. 1985). The assumption in the simplified model is that the equilibrium between free tracer in plasma and tracer bound to plasma proteins is rapidly reached and stable. Therefore, the assumed fraction of the total tracer free in the plasma is equivalent to  $C_a$  in the simplified model (Frankle et al. 2005b). Another assumption in the three-compartment model of neuroreceptor imaging is that immediately following tracer distribution the signal from the free fraction of tracer in the brain interstitium will be indistinguishable from the nonspecifically bound – especially in a PET analysis, which is conducted over a short time frame. Consequently, the assumed ‘free fraction’ is the combination of both the free tracer in brain interstitium ( $C_2$ ) and nonspecifically brain-bound tracer ( $C_2'$ ) to become the newly re-defined  $C_2$  (Frankle et al. 2005b).

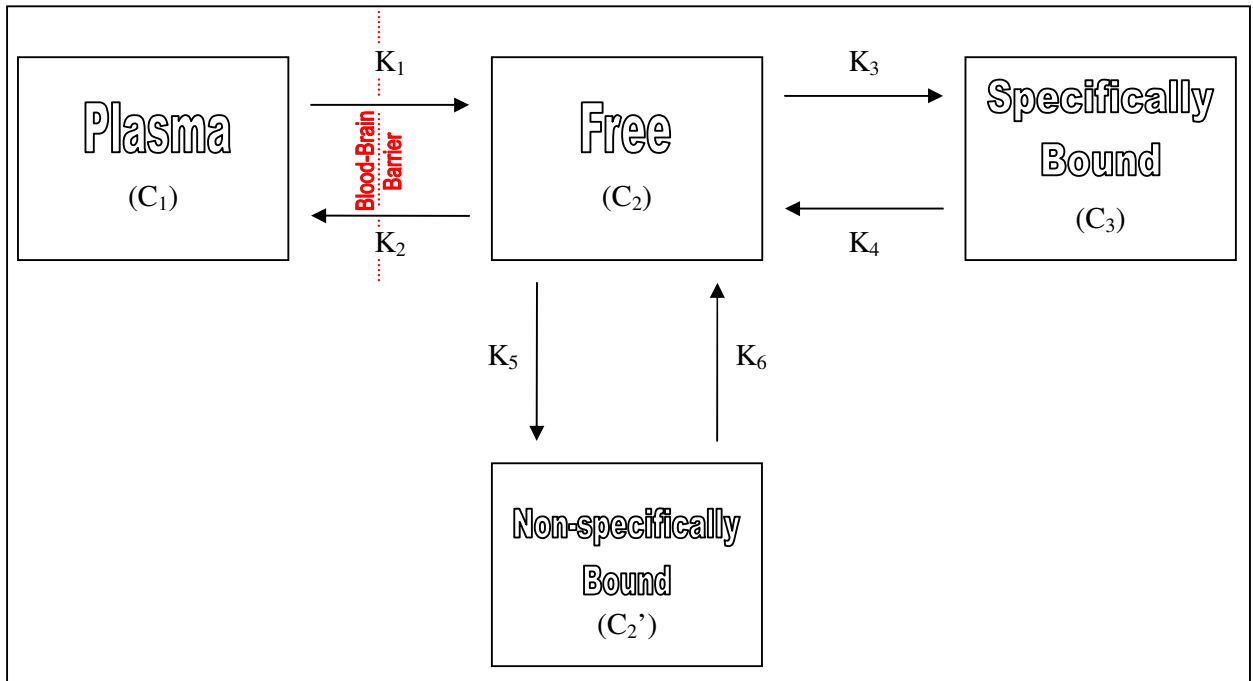


**Figure 1-07:** The Compartmental Model (adapted from Frankle et al. 2005). *In vivo* imaging with SPECT and PET separates concentrations of radiotracer into the theoretical compartments plasma ( $C_1$ ), free ( $C_2$ ), non-specifically bound ( $C_2'$ ), and specifically bound ( $C_3$ ), with fractional rate constants  $K_{1-6}$  representing the rate of movement between the compartments.

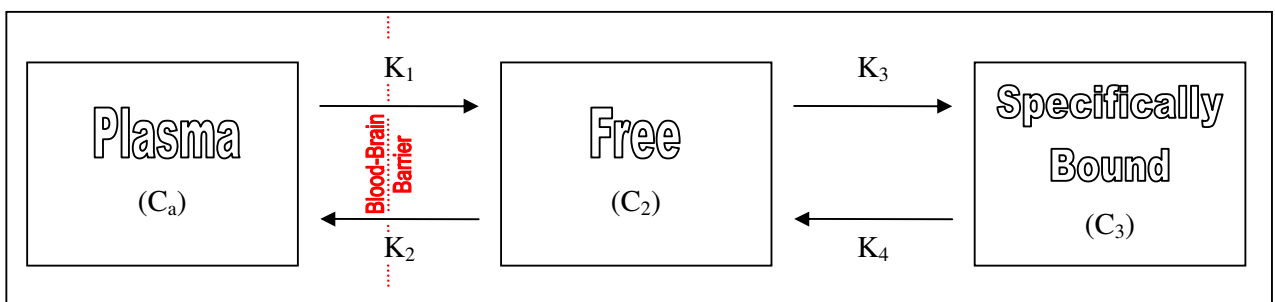


**Figure 1-08:** The Simplified Three-compartment Model (adapted from Frankle et al. 2005). *In vivo* imaging with SPECT and PET separates concentrations of radiotracer into the workable theoretical compartments plasma ( $C_a$ ), free ( $C_2$ ), and specifically bound ( $C_3$ ), with fractional rate constants  $K_{1-4}$  representing the rate of movement between the compartments.

### 1.5.3 SPECT vs. PET

PET imaging requires isotopes with rapid rates of decay, often measured in hours or days rather than weeks (Schmitz 2011), meaning that close proximity of the scanner to a cyclotron and a radiolabelling facility is necessary, adding expense to the method. SPECT imaging uses isotopes with a slower decay rate, enabling isotopes and radiolabelled ligands to be shipped after production. As such SPECT is less expensive and requires less computational modelling to interpret it. Currently, PET scanners have greater spatial resolution than SPECT scanners but investments in and advances of SPECT scanner hardware are negating that advantage and the lower costs involved with using longer-lived isotopes and less expensive hardware make SPECT imaging systems more affordable than their PET equivalents (Pimlott & Sutherland 2011).

Unfortunately, the half-life of a PET isotope also means signal to noise ratios will decrease dramatically if sufficient time elapses for free tracer clearance prior to image acquisition. Therefore, PET image acquisition must take place relatively quickly after injection and extensive computer modelling is used to determine what proportion of radioligand is bound and which is free. This makes distinguishing the specific binding from the free fraction (including nonspecific binding) more difficult with PET. The greater half-life of SPECT isotopes over those used in PET allow scans to be conducted over a longer period of time, enabling metabolism and systemic clearance mechanisms to reduce the concentration of free tracer (Pimlott & Sutherland 2011). The advantage inherent in SPECT is that before the isotopic decay rate becomes the limiting factor for completing image acquisition, the nonspecifically bound will constitute a greater proportion of the free fraction than in PET imaging. With computational modelling bearing greater importance in a PET assay than with SPECT, the reduced complexity of the modelling associated with SPECT can be thought of as a purer form of imaging and that provides greater confidence in the measurements.

#### 1.5.4 Requirements for a SPECT brain imaging tracer for the noradrenaline transporter

Tracer development itself can have many parallels to drug discovery. One approach is to take a molecule with known affinity for the target site, such as a well-characterised therapeutic drug that has high selectivity, and radiolabel the compound. However, the introduction of radioisotopes into the molecular structure of SPECT compounds can interfere with or modify the drug's binding properties and behaviour *in vivo*. Therefore, various analogues of the modified drug could be synthesised and applied through a series of experiments to determine which analogue has the greatest likelihood of success as an *in vivo* imaging agent.

SPECT imaging relies upon the development of radiolabelled 'tracer' compounds with which to probe binding sites of interest without perturbing the system being studied. For neuroimaging studies, these binding sites are usually found on neurotransmitter receptors or transporters. The dopamine and serotonin transporters have routinely been imaged with SPECT and PET in both clinical and research contexts (Varrone & Halldin 2010; Kupers et al. 2011). However, to date, there are no clinically used SPECT tracers for imaging the noradrenaline transporter in the CNS.

To briefly recap the qualities required of a successful SPECT tracer, they are: high affinity and selectivity for the target site, stability in circulation (i.e. low rate of metabolism), blood-brain barrier penetrability, low *in vivo* nonspecific binding, favourable radiological half-life (sufficiently long for uptake and image acquisition), and promising kinetics *in vivo* (i.e. rapid brain uptake, low metabolism). The *in vitro* affinity and selectivity of the ligand for the target site, as well as *in vitro* nonspecific binding should be ascertained via radioligand binding experiments. SPECT isotopes (e.g. [<sup>123/125</sup>I]) typically have long half-lives and are not limiting factors in image acquisition. The challenges of predicting the *in vivo* behaviour can be addressed by utilisation of rapid *in vitro* methodologies for compounds that have shown promise during earlier *in vitro* pharmacological testing.

A candidate compound likely to become a successful SPECT brain imaging tracer should satisfy the following general criteria (Chauveau et al. 2008; Kula et al. 1999; Petit-Taboue et al. 1991; Waterhouse 2003):

- Log P or log D < 3.5: while compounds require sufficient lipophilicity to cross the blood-brain barrier, higher lipophilicity and phospholipophilicity are associated with higher non-specific binding that would decrease the signal-to-noise ratio of a tracer and thus limit its utility.
- Molecular weight < 450 g/mol: smaller molecules are more likely to cross the blood-brain barrier through passive diffusion.
- An absence of functional groups that will strongly ionize at physiological pH: strongly ionized molecules are more likely to conjugate with lipid bilayers and the proteins comprising the blood-brain barrier and so are less likely to penetrate the brain.
- No appreciable affinity for efflux pumps (e.g. PGP): active transport interferes with the kinetics of the tracer penetrating and remaining in the brain. Affinity for an efflux pump would decrease the availability of an imaging tracer in the brain by returning it across the blood-brain barrier to the plasma.
- No appreciable affinity for specific binding sites for high capacity peripheral sites, including albumin or other plasma proteins: such an affinity would reduce the free concentration of tracer in the plasma and so decrease the amount of tracer to penetrate the brain.
- Not a substrate for enzymes at the blood-brain barrier: enzymatic metabolism of the tracer would remove its ability to bind to the target site in the brain and any metabolites that did cross the blood-brain barrier may just decrease the signal-to-noise ratio if the metabolites appear to the scanner as nonspecifically bound ligand.

These criteria would be very time-consuming to test for numerous compounds, and HPLC offers a high-throughput *in vitro* process by which to select the most likely compounds to be successful *in vivo* by measuring these various characteristics commonly associated with successful *in vivo* compounds.

## 1.6 Introduction to HPLC testing in tracer development

High-performance liquid chromatography (HPLC) is a quick, precise, and reliable technique that, through determining the binding properties of ligands to lipids and proteins that will be encountered *in vivo*, can model biological distribution of a drug. For example, among the main advantages to HPLC (measuring chromatographic hydrophobicity indexes to calculate log P) over traditional bench-top methodologies (measuring octanol-water partition coefficients to calculate log P) for the determination of lipophilicity are that very large numbers of samples can be assayed in a short space of time, sample concentration and purity does not greatly affect the outcome, and vastly increased precision and reproducibility that does not rely on the bench-top proficiency of an individual experimenter (Valkó et al. 1997; Valkó 2004). Using gradient elution protocols, the strength of the mobile phase is increased throughout the analysis to shorten the retention times of compounds that are strongly retained on the column – this reduces total analysis time, improves resolution, and maximises sensitivity (Valkó et al. 1997; Johnson & Stevenson 1978). The main disadvantage is that HPLC-derived measurements are not yet standardised and universally accepted in all circles of the scientific community, and the same terms (e.g. log P or log D) when determined under different conditions and using different formula are often not directly comparable. There is also great expense involved in the purchase and maintenance of an HPLC system, and retention times are not even directly comparable on the same system – though this is compensated for by calibrating every chromatographic run against known standards (Valkó et al. 1997; Valkó 2004). While time-consuming and highly dependent upon the proficiency of the individual experimenter, the octanol-water partition experiments have historically yielded Log P values that are more directly comparable between labs, and the equipment involved presents a smaller investment.

Recent efforts have attempted to bring greater standardisation to the terms calculated via HPLC and these techniques can be applied to screening tracer candidates as well as therapeutic drugs acting on the central nervous system. Commercially available columns immobilise lipids, phospholipids, albumins, and glycoproteins into the stationary phases of each column and longer retention times are indicative of greater interaction by tracer candidate with the stationary phase.

Compounds with known chromatographic hydrophobicity indexes and protein binding characteristics are run on the columns to act as standards and calibrate the system. The chromatographic hydrophobicity index (CHI) is the volumetric percentage of organic mobile phase necessary equally distribute a given compound between the mobile and stationary phases (Valkó et al. 1997). For most compounds, this will be between 0 and 100, though some can have extrapolated theoretical values outside of this range. This allows the conversion of retention times, which are arbitrary values and not comparable between two systems, into useful quantitative values such as:

- **lipophilicity** for uncharged molecules:  $\log P$  or  $\log P_{OCT}$  (Valkó 2004)
- **phospholipophilicity** interpreted as a nonspecific binding predictor:  $\log D_{7.4\text{ IAM}}$  (Valkó 2004; Hollósy et al. 2006)
- relative **blood-brain barrier penetration** predictor:  $\text{clog BB}$  (K. Valkó, 2008 - Personal Communication; Garg et al. 2008)
- **plasma protein binding** to predict availability in serum:  $\text{c\%PPB}$  (Valkó 2008; Oravcová et al. 1996).

### 1.6.1 Lipophilicity ( $\log P$ or $\log P_{OCT}$ ) – blood-brain barrier penetration and nonspecific binding

Lipophilicity ( $\log P$ ) is a measurement of compound affinity for lipid layers (Valkó 2004) and is measured using three C-18 lipid columns across three pH ranges: acidic (pH 2.5), neutral/physiological (pH 7.4), and alkaline (pH 10.5). If it is defined via octanol-water partitioning – the assay against which new methodologies are often measured – then it is generally expressed as  $\log P_{OCT}$  and will generally return a slightly higher value than one expressed in terms of  $\log P$  (Avdeef & Testa 2002). While the most easily comparable value for examining lipophilicity is  $\log P$  (often derived from computational modelling or HPLC),  $\log D$  (a common bench-top value) can also be encountered and is an expression of the lipophilicity for all species of a compound in a solution, usually at a given pH and returning a lower value than  $\log P$  (Avdeef & Testa 2002) when the molecule carries a charge.

The log  $P_{OCT}$  term is also applied to the HPLC technique when it is attempting to mimic the result of an octanol-water determination and the results are intended to be directly comparable, as with this thesis.

It is important to know whether a compound is lipophilic, because it is this property that will allow it to cross the blood-brain barrier and penetrate the brain. However, a compound that is too highly lipophilic may have a tendency to exhibit excessive levels of nonspecific binding – and thus would not be advantageous. An ‘ideal’ log  $P_{OCT}$  range, calculated from the chromatographic hydrophobicity index for the uncharged form of the compound is considered to be 1-3.5 (Waterhouse 2003; Valkó 2004), with blood-brain barrier penetration related to log  $P_{OCT}$  in a parabolic nature. Insufficient lipophilicity (below log  $P_{OCT}$  1) will result in insufficient permeability for compounds through the blood-brain barrier, and excessive lipophilicity (above log  $P_{OCT}$  3.5) is associated with elevated levels of nonspecific binding.

### **1.6.2 Phospholipophilicity (log $D_{7.4 \text{ IAM}}$ ) – predicting *in vivo* nonspecific binding**

Membrane binding *in vivo* can be a significant proportion of nonspecific binding for otherwise highly selective compounds, and this property is predicted using HPLC via an immobilized artificial membrane (IAM) column composed of phospholipids. It is important to note that the log  $D_{7.4 \text{ IAM}}$  value is very different from the log  $D_{7.4}$  lipophilicity calculation, with the addition of the phosphate heads in the column providing a very different surface in the stationary phase for the compounds suspended in the mobile phase to interact with.

Primarily, the binding to the phosphate heads models nonspecific binding to surface membranes *in vivo* and the log  $D_{7.4 \text{ IAM}}$  value can be used as a reference point to predict whether the membrane binding of a compound will be excessive and therefore problematic (Valkó 2004). This technique differs to the calculation for lipophilicity in that, while non-ionised compounds will roughly reflect the log  $P$  result, positively charged molecules will bind more strongly to an IAM column (Hollósy et al. 2006) and fills a gap left by the log  $P$  determination in our knowledge about positively charged tracer candidates. When a sufficiently comprehensive database is constructed containing these values in relation to

membrane binding contributing to overall nonspecific binding, ranges can be established to rapidly select for compounds that have a high probability of acceptable levels for nonspecific binding.

### **1.6.3 clog BB – predicting blood brain barrier penetration**

Blood brain barrier penetration can also be estimated using a formula incorporating data from the alkali C-18 acetonitrile-eluted column and a physiological pH C-18 with a methanol elution (K. Valkó, 2008 - Personal Communication).

Higher clog BB values are interpreted as indications of greater potential for successful brain penetration, whilst lower values are interpreted as a reduced potential for brain penetration (Garg et al. 2008). Negative values are theoretical numbers and are interpreted as an inability to cross the blood-brain barrier. The reason for incorporating a methanol elution into this estimation is to compensate for any relative variability in acetonitrile solubility between compounds by providing an alternative solvent for elution from the column (Kalendarev et al. 2001).

### **1.6.4 Immobilised protein chromatography (c%PPB) – predicting plasma protein binding *in vivo***

Drug and ligand binding to plasma transport proteins such as human serum albumin (HSA) and  $\alpha$ -acid glycoprotein (AGP) is an important part of the pharmacokinetic profile for the drug or ligand in clinical use (Oravcová et al. 1996; Valkó 2008; K. Valkó, 2008 - Personal Communication).

Plasma protein binding is directly correlated with lipophilicity and so availability of free tracer for the blood brain barrier penetration of a highly lipophilic compound may be compromised by excessive plasma protein binding (Vallabhajusola 2009). Benchtop methodologies including equilibrium dialysis, ultrafiltration, and ultracentrifugation can be used to determine protein-drug interactions – with equilibrium dialysis considered one of the ‘standard methods’. However, HPLC methods provide advantages such as speed, greater resolution, greater precision, and improved reproducibility without the traditional benchtop method drawbacks

such as ligand stability over time, leakage of drug or protein through membranes, and adsorption of ligands to the surface of dialysis devices and membranes. If high-throughput screening is to be rapid and cost-effective, then HPLC-based methods have the advantage over traditional benchtop assays.

Protein-binding displacement phenomena (Oravcová et al. 1996) may prove clinically significant for compounds that are highly bound to protein (>95% binding) and have small distribution volumes. Excessive protein binding such as this has been linked to reduced compound brain penetration (Valkó 2004) to the detriment of a compound's application to SPECT neuroimaging.

### **1.6.5 Reference Compounds: Successful and failed imaging tracers**

To provide a basis for comparison to the newly synthesised iodinated reboxetine analogues, it is important to examine a library of reference compounds comprised of both successful and failed brain imaging tracers (Table 1-10). Therefore, where similar values are found for each HPLC predictor, interpretations can be made as to the likelihood that the reboxetine analogues might behave in a similar manner.

<b>Table 1-10: Reference Compounds for Interpreting Predictors of <i>in vivo</i> Molecular Behaviour</b>				
<b>Reference Compound</b>	<b>Blood-Brain Barrier Penetration</b>	<b>Non-specific Binding</b>	<b>Is Plasma Protein Binding &lt;95%?</b>	<b>References</b>
5-I-A-85380	Yes	Low	Yes	(Fujita et al. 2000; Zoghbi et al. 2001; Ogawa et al. 2009)
$\beta$ -CIT	Yes	Low	Yes	(Al-Tikriti et al. 1995; Zoghbi SS et al 1998 - cited by Scanley et al. 2000; Kula et al. 1999; Scanley et al. 2000)
I-QNB	Yes	Moderate		(Varastet et al. 1992; Piggott et al. 2003)
CNS-1261	Yes	High	Yes	(Erlandsson et al. 2003; Knol et al. 2009)
PK11195	Yes	High	Yes	(Petit-Taboue et al. 1991; Lockhart et al. 2003; Chauveau et al. 2008)
MK-801	Yes	Not known (not a brain imaging agent)	Yes	(Wong et al. 1986; Owens et al. 1997; Murray et al. 2000; Erlandsson et al. 2003)
$\alpha$ -3-iodo-2-methyltyrosine	Yes (Active Transport)	Low	Yes	(Langen et al. 1991; Reimann et al. 2001; Shikano et al. 2004; Hellwig et al. 2008)
MIBG	No	Not discussed (not a brain imaging agent)		(Guilloteau et al. 1983b; Baulieu et al. 1990; DeGrado & Wang 1998; Raffel & Wieland 2001a; Tytgat et al. 2002)
FIAU	No	Not discussed (not a brain imaging agent)		(Tovell et al. 1988; Jacobs et al. 2001)
5-iodo-2'-deoxyuridine	No	Not discussed (not a brain imaging agent)	Too unstable to measure.	(Ghosh & Mitra 1991; Tjuvajev et al. 1994; Vaidyanathan & Zalutsky 1998; Khalili et al. 2003)

**Table 1-10:** Reference compounds, comprised of both successful and failed brain imaging tracers, to provide a basis for comparison of *in vivo* predictors to the newly synthesised iodinated reboxetine analogues.

## 1.7 Thesis Aims

The aim of this thesis is to develop a novel SPECT brain imaging tracer for the noradrenaline transporter, using compounds structurally related to reboxetine. This will be accomplished by:

1. Imaging the noradrenaline transporter in a model of psychiatric disease (Chapter 3). Autoradiography and *in situ* hybridisation will confirm the distribution of the NAT, investigate its potential role in the aetiology of the model, and highlight an instance where a SPECT tracer for the NAT would be beneficial. This model could then be used to demonstrate the *in vivo* capability of a SPECT imaging tracer for the noradrenaline transporter if the development of one is successful.
2. Ascertaining the NAT affinity and selectivity over other monoamine transporters for each candidate in a library of iodinated compounds that are structurally related to reboxetine (Chapter 4). Radioligand competition experiments will be used to select the molecule with the most desirable pharmacology for use as a SPECT brain imaging tracer for the NAT.
3. Using *in vitro* HPLC techniques to predict the *in vivo* molecular behaviour for the library of iodinated reboxetine-like compounds (Chapter 5). These experiments will be used to determine which of the molecules has the best balance of characteristics with regard to availability in the plasma for blood-brain barrier penetration, brain penetration kinetics, and measures to estimate *in vivo* non-specific binding.
4. Combining the data to recommend, if any are suitable, a lead candidate compound to be taken forward through development into a novel SPECT brain imaging tracer for the noradrenaline transporter (Chapter 6 – Conclusions).

## Chapter 2

### Methods

#### 2.1 PCP Study Methods

##### 2.1.1 Treatment regime

Adult male Hooded Long Evans rats (Harlan-Olac, UK) weighing approximately 240g were randomised into PCP-treated and control groups by assigning each rat a number with as little handling bias as possible and allocating the numbered rats to each group using a list of randomly generated numbers. The Hooded Long Evans rat strain was used because it was in this rat strain that the PCP-induced model for metabolic hypofrontality was established in the literature. PCP-treated animals (n=10) received single i.p. injections of  $2.58\text{mg}\cdot\text{kg}^{-1}\cdot\text{day}^{-1}$  PCP (Sigma-Aldrich) in normal saline for 5 days while control animals (n=10) received equivalent volumes of normal saline (Cochran et al. 2003). Normal saline is 154mM NaCl solution. The injection preparations were prepared by Susan Cochran using blinding codes to ensure my impartiality for the later data analysis. The brains were harvested two days after the final injection to allow sufficient time for the metabolism and clearance of the PCP from the brains. The rats underwent a Schedule 1 kill (Figure 2-01) in order to remove the brains, which were then coated in tissue tech, frozen in isopentane ( $-42^{\circ}\text{C}$ ), wrapped in tin foil, placed in an airtight plastic bag, and stored at  $-70^{\circ}\text{C}$  until sectioning.

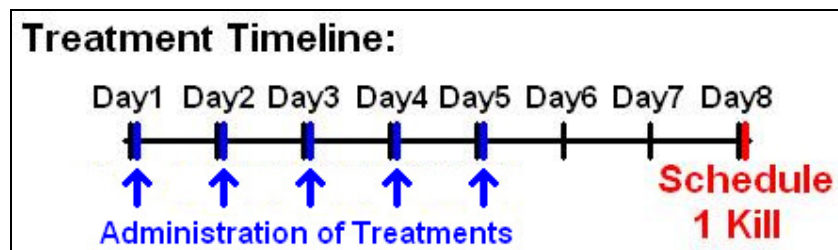


**Figure 2-01:** PCP administration regime to establish the rat model of schizophrenic hypofrontality.

### 2.1.2 Section Preparation

Frozen coronal sections, of 20 $\mu$ M thickness, were cut in a cryostat and thaw-mounted onto glass slides coated with poly-L-lysine for autoradiography or RNAase-free poly-L-lysine-coated glass slides for *in situ* hybridisation. Sections for autoradiography were air-dried for approximately 1 hour at room temperature and then stored at -70°C. Sections for *in situ* hybridisation were air dried for approximately 1 hour at room temperature, fixed in ice-cold 4% (w/v) paraformaldehyde solution (Sigma-Aldrich), processed through PBS, 70% EtOH, 95% EtOH, and 100% EtOH before storage in 100% EtOH at 4°C.

### 2.1.3 Quantitative ligand binding autoradiography

The noradrenaline transporter (NAT), the dopamine transporter (DAT), and the serotonin transporter (SERT) were labelled in selected sections throughout the brain with 3.0nM [<sup>3</sup>H]-nisoxetine (71.0 Ci/mmol, GE Healthcare), 10.0nM [<sup>3</sup>H]-WIN-35,428 (85.9 Ci/mmol, Perkin-Elmer), and 2.0nM [<sup>3</sup>H]-citalopram (83.0 Ci/mmol, GE Healthcare), respectively. Nonspecific binding was defined in adjacent sections in the presence of 10 $\mu$ M nortriptyline hydrochloride, 30 $\mu$ M nomifensine, and 20 $\mu$ M fluoxetine, respectively. Structures analysed included the prefrontal cortex (PFC), caudate putamen (CPu), anterior cingulate cortex (ACg), nucleus accumbens (N. acc.), bed nucleus of the striatus terminalis (BNST), anteroventral thalamic nucleus (AVTN), reticular thalamic nucleus (RTN), hippocampal structures CA1, CA2, CA3, and dentate gyrus (DG), ventral tegmental area (VTA), dorsal raphe nuclei (DRN), locus coeruleus (LC), and cerebellum (CBL). Due to the very high density of NAT in the locus coeruleus, sections containing this structure were incubated with 1.5nM [<sup>3</sup>H]-nisoxetine. Sections alongside calibrated [<sup>3</sup>H] microscalers (Amersham Bioscience) were exposed to Kodak BioMax MR for 7-weeks for sections labelled with [<sup>3</sup>H]-nisoxetine or [<sup>3</sup>H]-WIN-35,428, and for 5-weeks for sections labelled with [<sup>3</sup>H]-citalopram. Experimental schedules are presented in full in Table 2-01. Anatomical structures were identified in consultation with the Paxinos and Watson Rat Brain Atlas (2004) and delineated using MCID 7.0 Basic, the image analysis system. Prior to image analysis, a flat field correction was performed to account for any environmental

influences to the image or imperfections in, for example, the lightbox surface. The MCID 7.0 Basic image analysis system was used to convert average optical densities for delineated regions of each coded subject into fmol of bound ligand per mg of wet weight tissue by calibrating the measured optical densities with the delineations of [<sup>3</sup>H] microscales (Amersham Bioscience) exposed to the same piece of film. Corrections to account for the decay of the isotope in the ligand and in the microscales were performed via consultation of the specific product information sheet to each [<sup>3</sup>H] microscale – this included the manufacturer’s data on the wet weight tissue equivalence of radioactivity, precise date of manufacture, and the known decay profile for [<sup>3</sup>H], to ensure an accurate quantification of bound ligand. The ligand used was also corrected for isotopic decay, assuming standard rate of [<sup>3</sup>H] decay from the manufacture date of the ligand. Sections representing total binding were aligned in MCID 7.0 Basic’s digital Channel 1 with adjacent sections representing nonspecific binding in MCID 7.0 Basic’s digital Channel 2, so that identical coordinates were simultaneously assayed on each section when identified structures were delineated in the sections representing total binding. For measurements in the Caudate Putamen, thresholding was used to exclude white matter tracts that run through this structure. Blinding was used to ensure impartiality during image acquisition and data analysis, and each coded animal was represented by 6 measurements of each structure delineated from three sets of aligned total binding and non-specific binding sections. Microsoft Excel 2003 was used to perform the subtraction of nonspecific binding from total binding to ascertain specific binding and, for each coded animal, the specific binding measurements for each structure were averaged.

For each structure, each animal was assayed thusly:

total binding 1 – Nonspecific binding 1 = specific binding 1  
total binding 2 – Nonspecific binding 2 = specific binding 2  
total binding 3 – Nonspecific binding 3 = specific binding 3  
total binding 4 – Nonspecific binding 4 = specific binding 4  
total binding 5 – Nonspecific binding 5 = specific binding 5  
total binding 6 – Nonspecific binding 6 = specific binding 6

Measurements 1 and 2 were derived from the left and right hemispheres of the same aligned sections, measurements 3 and 4 were derived from the left and right

hemispheres of the same aligned sections, and measurements 5 and 6 were derived from the left and right hemispheres of the same aligned sections. For each animal, the measurements were averaged thusly:

$$( \text{specific binding 1} + \text{specific binding 2} + \text{specific binding 3} + \text{specific binding 4} + \text{specific binding 5} + \text{specific binding 6} ) / 6 = \text{average specific binding}$$

The average specific binding in  $\text{fmol.mg}^{-1}$  for each structure was taken as a single data point for that animal, and contributed to the group data. For analysing the group data, GraphPad Prism 4.0 was used to apply the Mann-Whitney statistical test, a non-parametric test due to the variances between the groups being unequal as determined by F-test, to determine whether differences between the groups are significant. F-test results, which determined that a parametric analysis would be inappropriate, are displayed in appendix I and autoradiograms are in Chapter 3.

<b>METHOD</b>	<b>FOR NAT IMAGING</b> (modified from: Hipolide et al. 2005)	<b>FOR DAT IMAGING</b> (modified from: Andersen et al. 2005)	<b>FOR SERT IMAGING</b> (modified from: Hebert et al. 2001)
<b>BINDING BUFFER</b>	50mM Tris-HCl 300mM NaCl 5mM KCl pH 7.4	25mM Na <sub>2</sub> HPO <sub>4</sub> 25mM NaH <sub>2</sub> PO <sub>4</sub> 50mM NaCl pH 7.7	50mM Tris-HCl 120mM NaCl 5mM KCl pH 7.4
<b>PREINCUBATION</b>	30 minutes at 4 °C in binding buffer	20 minutes at 4 °C in binding buffer	15 minutes at ~25 °C (RTP) in binding buffer
<b>INCUBATION</b>	4 hours (240 minutes) at 4 °C in binding buffer with:  <b>Ligand:</b> 3.0 nM [ <sup>3</sup> H]-nisoxetine  <b>Displacer:</b> 10.0 μM Nortriptyline Hydrochloride	2 hours (120 minutes) at 4 °C in binding buffer with:  <b>Ligand:</b> 10.0 nM [ <sup>3</sup> H]-WIN-35,428  <b>Displacer:</b> 30.0 μM Nomifensine	2 hours (120 minutes) at ~25 °C (RTP) in binding buffer with:  <b>Ligand:</b> 2.0 nM [ <sup>3</sup> H]-citalopram  <b>Displacer:</b> 20.0 μM Fluoxetine
<b>WASH 1</b>	5 minutes in buffer solution at 4 °C	30 seconds in buffer solution at 4 °C	2 minutes in buffer solution 4 °C
<b>WASH 2</b>	5 minutes in buffer solution at 4 °C	30 seconds in buffer solution at 4 °C	2 minutes in buffer solution 4 °C
<b>WASH 3</b>	5 minutes in buffer solution at 4 °C	30 seconds in buffer solution at 4 °C	2 minutes in buffer solution 4 °C
<b>WASH 4</b>	Rapid dip (10 seconds maximum) in dH <sub>2</sub> O at 4 °C	Rapid dip (10 seconds maximum) in dH <sub>2</sub> O at 4 °C	2 minutes in buffer solution 4 °C
<b>WASH 5</b>	N/A	N/A	Rapid dip (10 seconds maximum) in dH <sub>2</sub> O at 4 °C
<b>DRYING</b>	Dry overnight under cool fan	Dry overnight under cool fan	Dry overnight under cool fan
<b>FILM EXPOSURE</b>	7 weeks on Kodak BioMax MR with calibrated [ <sup>3</sup> H] microscaler (Amersham Bioscience) at ~25 °C (RTP).	7 weeks on Kodak BioMax MR with calibrated [ <sup>3</sup> H] microscaler (Amersham Bioscience) at ~25 °C (RTP).	5 weeks on Kodak BioMax MR with calibrated [ <sup>3</sup> H] microscaler (Amersham Bioscience) at ~25 °C (RTP).
<b>IMAGE ANALYSIS</b>	MCID 7.0 Basic / Microsoft Excel 2003 / GraphPad Prism 4.0	MCID 7.0 Basic / Microsoft Excel 2003 / GraphPad Prism 4.0	MCID 7.0 Basic / Microsoft Excel 2003 / GraphPad Prism 4.0

**Table 2-01:** Monoamine transporter autoradiography reagents, buffers, and experimental schedules.

#### 2.1.4 Radioligand binding

For determination of  $K_D$  values, triplicate aliquots of membrane suspensions (750-850 $\mu$ g of protein) were incubated in 0.5mL volumes in increasing concentrations of [ $^3$ H]-nisoxetine (71.0 Ci/mmol, GE Healthcare) and [ $^3$ H]-citalopram (83.0 Ci/mmol, GE Healthcare) for NAT and SERT, respectively. Non-specific binding was defined in the presence of 10 $\mu$ M Reboxetine (Tocris) and 20 $\mu$ M Fluoxetine (Tocris) for NAT and SERT, respectively. Reactions were terminated by rapid vacuum filtration through Whatman GF/B glass fibre filters pre-soaked in 0.5% polyethylenimine (PEI) in relevant binding buffer (Table 2-01) using a 24-well Brandel cell harvester. Filters received three rapid washes in ice-cold binding buffer, filter circle impressions were separated from the filter sheet and placed in glass scintillation vials containing 10mL liquid scintillant (National Diagnostics Ecoscint A). 20 $\mu$ L aliquots of the radioligand dilutions applied were added to additional glass scintillation vials containing 10mL liquid scintillant each, so that precise concentrations of each dilution could be confirmed. All vials were then vortexed 3 times for 3 seconds each and left for 24 hours to ensure chemiluminescence did not artificially inflate the liquid scintillation analysis. Liquid scintillation analysis was performed on a Packard 1900CA Tri-Carb Liquid Scintillation Analyzer that is calibrated against known [ $^3$ H] standards, automatically performs background subtraction, and presents raw data in disintegrations per minute (dpms).

Specific binding was expressed as fmol.mg<sup>-1</sup> protein, and the protein determination performed using a BioRad kit.  $K_D$  values for [ $^3$ H]-nisoxetine and [ $^3$ H]-citalopram were derived from nonlinear regression analysis using GraphPad Prism Version 4 (GraphPad Software Inc.). A  $K_D$  estimation for [ $^3$ H]-WIN-35,428 (5.0nM) binding to the high affinity site on the DAT was selected by a review of published literature (Reith & Coffey 1994; Kirifides et al. 1992). Data is presented as mean  $\pm$  SEM for at least three independent competition experiments with [ $^3$ H]-nisoxetine and at least two independent competition experiments with [ $^3$ H]-citalopram and [ $^3$ H]-WIN-35,428.

### 2.1.5 *In situ* hybridisation

Oligonucleotide probes were designed to be specific for the mRNA of each of the transporters studied by means of ligand binding autoradiography. The sequence for the mRNA of the rat noradrenaline transporter (Slc6a2 – Solute carrier family 6 member 2) was obtained via the NCBI Entrez Nucleotide online database. I selected a portion of the code that was a non-repeating part of the coding sequence of the mRNA for the NAT and the NCBI BLAST (Basic Local Alignment Search Tool) was used to confirm that this selected sequence would be specific for that specific gene only and that the secondary structure would be weak to prevent it from binding to itself. The reverse complementary sequence was obtained via extrapolations made by me as per figures 2-02, 2-03, and 2-04.

The rat dopamine transporter (Slc6a3) and rat serotining transporter (Slc6a4) mRNA sequences were obtained and checked by the same procedure, and their oligonucleotide probes designed in the same manner. Once designed by me, the probe sequences were used to create Sigma-Genosys Oligonucleotides (Sigma-Aldrich, United Kingdom), which were purchased.

Probes were [<sup>35</sup>S]-labelled for *in situ* hybridisation using a Pharmacia enzyme kit. Each probe was supplied as a powder, which was then combined with diethyl-pyrocabonate (DEPC, Sigma-Aldrich) treated water and vortex mixed to obtain a 100µM (1pmol/µl) stock solution. The stock solution was diluted to obtain a working concentration of 3.3nM (0.3pmol/µl or 5µg/µl) and concentration was precisely determined via measurement of optical density. Optical density was ascertained with 15µl samples using a pathlength of 10mm, compensation of 320mm, factor ssDNA of -37.0, probe length of 45mer, and background calibrated against DEPC-treated water. Probe concentration was determined in ng/µl (Table 2-02).

<b>NAT Probe:</b>																	
Targeted mRNA (5'-3'):	TCC	CCT	ATC	TCT	GCT	ACA	AGA	ATG	GTG	GTG	GTG	CCT	TCC	TGA	TTG		
Complementary Sequence (3'-5'):	AGG	GGA	TAG	AGA	CGA	TGT	TCT	TAC	CAC	CAC	CAC	GGA	AGG	ACT	AAG		
Reverse Complementary (5'-3') (i.e. Probe Sequence):	GAA	TCA	GGA	AGG	CAC	CAC	CAC	CAT	TCT	TGT	AGC	AGA	GAT	AGG	GGA		
Binds to Targeted mRNA (3'-5'):	CTT	AGT	CCT	TCC	GTG	GTG	GTG	GTA	AGA	ACA	TCF	TCT	CTA	TCC	CCT		

**Figure 2-02:** NAT transporter-specific oligonucleotide probe sequences. Targeted section of mRNA is shown highlighted in green and the reverse complementary sequence (the probe) is highlighted in yellow. The probe has a molecular weight of 13936.84, a melting temperature of 84.29°C, a percentage of GC content of 51.12, and a weak secondary structure.

<b>DAT Probe:</b>																	
Targeted mRNA (5'-3'):	GTG	TTG	TAA	GCA	TCT	GTT	TTT	TGT	GTC	TAT	AGC	CAG	TAC	CTT	GTG		
Complementary Sequence (3'-5'):	CAC	AAC	ATT	CGT	AGA	CAA	AAA	ACA	CAG	ATA	TCG	GTC	ATG	GAA	CAC		
Reverse Complementary (5'-3') (i.e. Probe Sequence):	CAC	AAG	GTA	CTG	GCT	ATA	GAC	ACA	AAA	AAC	AGA	TGC	TTA	CAA	CAC		
Binds to Targeted mRNA (3'-5'):	GTG	TTC	CAT	GAC	CGA	TAT	CTG	TGT	TTT	TTG	TCT	ACG	AAT	GTT	GTG		

**Figure 2-03:** DAT transporter-specific oligonucleotide probe sequences. Targeted section of mRNA is shown highlighted in green and the reverse complementary sequence (the probe) is highlighted in yellow. The probe has a molecular weight of 13816.87, a melting temperature of 76.74°C, a percentage of GC content of 40.00, and a weak secondary structure.

<b>SERT Probe:</b>																	
Targeted mRNA (5'-3'):	CAG	CTA	GCT	TCA	GGT	TTA	GAA	TTA	GGT	CTG	TGA	GAG	TCT	GTA	TCA		
Complementary Sequence (3'-5'):	GTC	GAT	CGA	AGT	CCA	AAT	CTT	AAT	CCA	GAC	ACT	CTC	AGA	CAT	AGT		
Reverse Complementary (5'-3') (i.e. Intended Probe Sequence):	TGA	TAC	AGA	CTC	TCA	CAG	ACC	TAA	TTC	TAA	ACC	TGA	AGC	TAG	CTG		
Binds to Targeted mRNA (3'-5'):	ACT	ATG	TCT	GAG	AGT	GTC	TGG	ATT	AAG	ATT	TFF	ACT	TCG	ATC	GAC		

**Figure 2-04:** SERT transporter-specific oligonucleotide probe sequences. Targeted section of mRNA is shown highlighted in green and the reverse complementary sequence (the probe) is highlighted in yellow. The probe has a molecular weight of 13765.71, a melting temperature of 76.08°C, a percentage of GC content of 42.23, and a weak secondary structure.

[<sup>35</sup>S]-d-ATP for the probe labelling was thawed from freezer storage at -20°C in a water bath heated to 37°C. The Pharmacia kit labelling reaction was prepared in RNAase-free Eppendorf tubes as follows, taking into account the unequal concentrations of the various probe preparations (Table 2-03):

The reaction mixture was vortex mixed and briefly centrifuged for a few seconds at low speed to aggregate the solution in the bottom of the reaction tubes. Terminal deoxynucleotide transferase (TdT) was kept on ice at all times until 0.6µl was added to each labelling mixture, taking extreme care not to introduce air bubbles which would degrade the enzyme. The completed reaction mixture was briefly stirred (not vortex mixed) and incubated in a water bath at 37°C for 30 minutes. The reaction was terminated at the end of the incubation with the addition of 40µl of room temperature DEPC-treated water.

Labelled probe was separated from the rest of the solution with the QIAquick Nucleotide Removal Kit (QIAGEN), consisting of columns and solutions PN, PE, and EB. This commercially available kit purifies the labelled probes by separating them from the remnants of the enzymatic reaction to label the oligonucleotides with the [<sup>35</sup>S]. The precise details of each solution are proprietary information of the manufacturer and are unavailable. 10 volumes of kit solution PN were added to 1 volume of terminated reaction and vortex mixed. Kit columns were set up with RNAase-free collection tubes and the sample-PN mixture was applied. The columns were centrifuged for 1 minute at 2,000 *g* and the elution was discarded. 500µl of kit solution PE was applied to the column before centrifuging for 1 minute at 2,000 *g* and the elution was discarded. The column was centrifuged for 1 minute at 9,500 *g* and the elution was discarded if any was found. New RNAase free Eppendorf tubes were prepared beneath the columns and 100µl of kit solution EB was applied to the column. After sitting for 30 seconds, each column was centrifuged for 1 minute at 9,500 *g* and the elution (containing the [<sup>35</sup>S]-labelled probe) was retained.

<b>Oligonucleotide probe concentrations</b>	
<b>Equation</b>	Optical density * cDNA co-efficient * pathlength correction = concentration (ng/μl)
<b>DAT-specific oligonucleotide probe</b>	$0.094 * 30 * 2 = 5.64 \text{ ng/}\mu\text{l}$
<b>NAT-specific oligonucleotide probe</b>	$0.092 * 30 * 2 = 5.52 \text{ ng/}\mu\text{l}$
<b>SERT-specific oligonucleotide probe</b>	$0.116 * 30 * 2 = 6.96 \text{ ng/}\mu\text{l}$

**Table 2-02:** The calculations applied to determining the oligonucleotide probe concentrations via optical density.

<b>Reagent</b>	<b>General rule of thumb</b>	<b>For DAT probe</b>	<b>For NAT probe</b>	<b>For SERT probe</b>
<b>DEPC-treated water</b>	0.9	1.18	1.14	1.60
<b>5x tailing buffer</b>	1.2	1.2	1.2	1.2
<b>12.5μg probe</b>	2.5 (at 5ng/μl)	2.22	2.26	1.80
<b>[<sup>35</sup>S]-d-ATP</b>	1.5	1.5	1.5	1.5

**Table 2-03:** Reagents and quantities (in μL) used with the Pharmacia probe labelling kit, for preparing each RNAase-free Eppendorf tube.

<b>Reaction preparations per slide</b>		
<b>Reactant</b>	<b>For slides with sections defining total binding</b>	<b>For slides with sections defining non-specific binding</b>
<b>Labelled probe preparation</b>	4μl	4μl
<b>1M DTT</b>	16μl	16μl
<b>Hybridisation buffer</b>	200μl	200μl
<b>Unlabelled probe from 100μM (1pmol/μl) stock preparation</b>	none	16μl

**Table 2-04:** Reaction proportions for each slide containing 2-3 sections. These volumes were scaled up as needed to cover all slides.

2µl of each probe sample was transferred into 4ml liquid scintillant (National Diagnostics Ecoscint A) in a scintillation tube and disintegrations per minute were determined to ensure that the probes had been labelled successfully with [<sup>35</sup>S]. Probes that were labelled successfully were combined with 4µl 1M Dithiothreitol (DTT, 1.5495g in 10ml DEPC-treated water), vortex mixed, and stored in a freezer at -20°C.

For *in situ* hybridisation, nonspecific labelling was defined in the presence of 1000-fold excess of unlabelled oligonucleotide probe and each slide required the preparation of reaction solutions (Table 2-04). Sections were removed from storage in 4°C ethanol and air dried for 30 minutes.

Selected slides were placed inside Petri dishes on horizontal toothpicks. The reaction mixtures were briefly vortex mixed just prior to application to sections. The sections were then covered with Parafilm, ensuring no air bubbles. 20x concentration saline-sodium citrate (SSC, containing 3M NaCl and 0.3M monosodium citrate) was prepared in DEPC-treated water. 4xSSC was used to soak paper towel wads to provide humidity inside the Petri dish during incubation. Petri dishes were sealed with Parafilm and incubated in and incubated overnight (approximately 18 hours) in an oven set to 42°C.

Following incubation, slides were removed from the Petri dishes, immersed in room temperature 1xSSC and the Parafilm strips covering the sections were removed. Slides were then incubated with gentle agitation in 60°C 1xSSC before being rinsed with gentle agitation in room temperature 1xSSC for 20 seconds, rinsed with gentle agitation in RTP 0.1xSSC for 20 seconds, rinsed with gentle agitation in RTP 70% EtOH for 20 seconds, rinsed with gentle agitation in RTP 95% EtOH for 20 seconds, and then air dried for 1 hour at RTP. Images were generated by exposing labelled sections to Kodak BioMax MR film for 10-14 days and processing with an automatic developer.

Anatomical structures were identified in consultation with the Paxinos and Watson Rat Brain Atlas (2004), the Allen Brain Atlas (Lein et al. 2007) and delineated using MCID 7.0 Basic, the image analysis system. The MCID 7.0 Basic image analysis system was used to measure average optical densities for delineated regions of each coded subject. Sections representing total binding were aligned in

digital Channel 1 with adjacent sections representing nonspecific binding in digital Channel 2, so that identical coordinates were simultaneously assayed on each section when identified structures were delineated in the sections representing total binding. Blinding was used to ensure impartiality during image acquisition and data analysis, and each coded animal was represented by 6 measurements of each structure delineated from three sets aligned total binding and non-specific binding sections. Microsoft Excel 2003 was used to perform the subtraction of nonspecific binding from total binding to ascertain specific binding. The qualitative specific binding measurements for each structure from each subject were averaged and contributed to the group data. GraphPad Prism 4.0 was used to apply the Mann-Whitney statistical test, a non-parametric test due to being unable to assume equivalent variances between the groups. The aforementioned blinding of the treatment groups was still in effect to ensure impartiality during image acquisition and data analysis, and the qualitative presentation as a percentage relative to the control group was done only after the blinding was lifted.

## **2.2 Radioligand Development**

All novel compounds (Table 2-05) were synthesised by Nicola Jobson (Sutherland Chemistry Laboratory, Glasgow University) and dissolved by Nicola Jobson to a concentration of 1mM in relevant binding buffer provided by me. These were transported to the Wellcome Surgical Institute at room temperature in a sealed glass vial.

Table 2-05: Iodoreboxetine Analogues and their Structure		
Type	Structure *	Names
Reference (Commercially Available)		<b>Reboxetine, prepared as racemic mix: (<i>S,S</i>)/(<i>R,R</i>)</b>  (2 <i>S</i> ,3 <i>S</i> )/(2 <i>R</i> ,3 <i>R</i> ) -2-[(2-Ethoxyphenoxy)phenylmethyl]morpholine
Iodo-phenyl ring reboxetine analogues		<b>(<i>S,R</i>)-iodoreboxetine</b>  (2 <i>S</i> ,3 <i>R</i> )-2-[(4-Iodophenyl)-(2-ethoxyphenoxy)methyl]morpholine
		<b>(<i>R,S</i>)-iodoreboxetine</b>  (2 <i>R</i> ,3 <i>S</i> )-2-[(4-Iodophenyl)-(2-ethoxyphenoxy)methyl]morpholine
		<b>(<i>S,S</i>)-iodoreboxetine</b>  (2 <i>S</i> ,3 <i>S</i> )-2-[(4-Iodophenyl)-(2-ethoxyphenoxy)methyl]morpholine
		<b>(<i>R,R</i>)-iodoreboxetine</b>  (2 <i>R</i> ,3 <i>R</i> )-2-[(4-Iodophenyl)-(2-ethoxyphenoxy)methyl]morpholine
Benzyl alcohol iodo-amide analogues		<b>NKJ-38</b>  (2 <i>S</i> ,3 <i>S</i> )-2-[α-Hydroxy-(4-iodophenyl)methyl]morpholine-5-one
		<b>NKJ-50</b>  (2 <i>R</i> ,3 <i>R</i> )-2-[α-Hydroxy-(4-iodophenyl)methyl]morpholine-5-one
Iodo-phenoxy ring reboxetine analogues		<b>NKJ-64</b>  (2 <i>R</i> ,3 <i>S</i> )-2-[(2-Iodophenoxy)phenylmethyl]morpholine
		<b>NKJ-67</b>  (2 <i>R</i> ,3 <i>S</i> )-2-[(3-Iodophenoxy)phenylmethyl]morpholine
		<b>NKJ-68</b>  (2 <i>R</i> ,3 <i>S</i> )-2-[(4-Iodophenoxy)phenylmethyl]morpholine

**Table 2-05:** Summary of the structures for Glasgow-synthesised iodoreboxetine analogues for binding to the noradrenaline transporter.

\* **Note:** Structures obtained from Jobson, NK (Ph.D. Thesis 2008).

### **2.2.1 Homogenate preparation protocol**

Brains were obtained via Schedule 1 kill from male adult Sprague-Dawley rats (Charles River) and the cerebellum removed. Sprague-Dawley rats were used because the expense of sourcing Hooded Long-Evans rats for these assays was not necessary as this homogenate was intended for ligand analysis and not investigations into the model of schizophrenic hypofrontality. Tissue was pooled and homogenised using a Polytron in ice-cold binding buffer (1g:10mL) for the relevant transporter (Table 2-06). Homogenates were centrifuged at 25,400g for 15 minutes at 4°C and the resulting pellet was washed in binding buffer three further times by centrifugation and resuspension. The final resuspension in binding buffer was stored in 500µL aliquots at -50°C until use.

Protein concentration of randomly selected sample aliquots was determined via a BioRad kit based upon the Bradford protein assay. Standards of known concentration (0mg/ml, 0.05mg/ml, 0.1mg/ml, 0.2mg/ml, 0.5mg/ml, and 0.6mg/ml) were prepared using bovine serum antigen (BSA). Sample aliquots were thawed, vortex mixed, sonic probed, and vortex mixed again. Reaction tubes contained 1.0ml mixed BioRad protein assay reagent with 5µl of BSA standard or 50µl sample homogenate. Reaction solutions were vortex mixed and incubated at 37°C for 30 minutes, cooled at room temperature for 5 minutes, poured into glass cuvettes and the absorbance at a wavelength of 562nm was read from a spectrophotometer.

<b>Transporter Assay</b>	<b>Radioligand</b>	<b>Binding Buffer and Incubation Conditions</b>
Noradrenaline Transporter (modified from Hipolide et al. 2005)	1.2nM [ <sup>3</sup> H]-nisoxetine (71.0 Ci/mmol, GE Healthcare)	50 mM Tris-HCl, pH 7.4 300 mM NaCl 5 mM KCl Incubation: 4 hours at 4 °C
Serotonin Transporter (modified from Andersen et al. 2005)	2.0nM [ <sup>3</sup> H]-citalopram (83.0 Ci/mmol, GE Healthcare)	50 mM Tris-HCl, pH 7.4 120 mM NaCl 5 mM KCl Incubation: 2 hours at RTP
Dopamine Transporter (modified from Hebert et al. 2001; Reith & Coffey 1994; Kirifides et al. 1992)	4.7nM [ <sup>3</sup> H]-WIN-35,428 (85.9 Ci/mmol, Perkin-Elmer)	25 mM NaH <sub>2</sub> PO <sub>4</sub> 25 mM Na <sub>2</sub> HPO <sub>4</sub> 50 mM NaCl pH 7.70 Incubation: 2 hours at 4 °C

**Table 2-06:** Assay conditions for radioligand competition experiments to determine the  $K_i$  at monoamine transporters for iodoreboxetine compounds.

## 2.2.2 Competition binding experiments

For determination of  $K_i$  values, membrane suspensions (750-850 $\mu$ g of protein) were incubated with the appropriate radioligand in the presence or absence of 12-20 concentrations of the competitor (range 1pM - 300 $\mu$ M). The range of competitor concentrations was chosen to most accurately assay the range of  $K_i$  values expected from a compound with the potential to be taken forward in development as a tracer candidate. Assays were performed in triplicate and the total incubation volume was 0.5ml. Non-specific binding was defined in the presence of 10 $\mu$ M reboxetine (Tocris), 20 $\mu$ M fluoxetine (Tocris), and 30 $\mu$ M nomifensine (Sigma-Aldrich) for NAT, SERT, and DAT assays, respectively. Reactions were terminated by rapid vacuum filtration through Whatman GF/B glass fibre filters pre-soaked in 0.5% polyethylenimine (PEI) in relevant binding buffer using a 24-well Brandel cell harvester. Filters received three rapid washes in ice-cold binding buffer then were added to 10ml liquid scintillant (National Diagnostics Ecoscint A), and [ $^3$ H] disintegrations per minute, including automatic background subtraction, were determined by liquid scintillation analysis (average over 3 cycles of 4 minutes count per vial).

## 2.2.3 $K_i$ calculation and analysis

Specific binding was expressed as a percentage of specific binding in the absence of competitor and  $K_i$  values were derived from nonlinear regression analysis using GraphPad Prism Version 4 (GraphPad Software Inc.), which to calculate the  $K_i$  from the  $IC_{50}$  uses the following equation (Cheng & Prusoff 1973):

$$K_i = IC_{50} / ( 1 + ( Ligand Concentration / K_D ) )$$

The  $K_d$  values determined under the same assay conditions for [ $^3$ H]-nisoxetine (1.7nM) and [ $^3$ H]-citalopram (2.1nM) binding to the NAT and SERT, respectively, were used in the calculation. A  $K_d$  value (5.0nM) for binding to the high affinity [ $^3$ H]-WIN-35,428 site on the DAT was selected by a review of published literature (Reith & Coffey 1994; Kirifides et al. 1992).  $K_i$  data is presented as mean  $\pm$  SEM for at least three independent competition experiments with [ $^3$ H]-nisoxetine and at

least two independent competition experiments with [<sup>3</sup>H]-citalopram and [<sup>3</sup>H]-WIN-35,428.

## **2.3 *In Vitro* High Performance Liquid Chromatography (HPLC) Methodology**

### **2.3.1 Chromatography System and Methods**

Determination of retention times were performed by reverse phase high performance liquid chromatography (HPLC) on an Agilent series 1200 HPLC system consisting of pump, degasser, autosampler, microinjector, and diode array detector. The diode array detector is a UV detector capable of recording variable wavelengths simultaneously, thus enabling UV peaks to be examined for purity – whether they are comprised of a single compound or more than one. The diode array detector also enables the clearest wavelength found to be used for analysis, which can be useful if the lambda max, the wavelength of greatest UV absorbance, is not known at the outset of the assay of the compound of interest. Each column used (Table 2-07) was temperature controlled to 30°C.

HPLC analysis used gradient methodology (Figure 2-05) to elute compounds. Details of the methodology for each column is outlined in Table 2-09, including column identification, mobile phase conditions, and gradient methodology flow rates for organic mobile phase. The conditions and flow rate gradients are identical to those used in the formulation of each equation by Klara Valkó and they were optimised for each column to be a standard procedure to enable repeated, high-throughput analyses. Wavelengths recorded on all columns were 210nm, 230nm, 245nm, 254nm, 275nm, 285nm, and 310nm – these were chosen by me to enable the retention times to be taken from the acquired wavelength closest to the  $\lambda_{MAX}$  for each sample. Software utilized for HPLC operation and analysis was Agilent ChemStation, which recorded the absorbances across the aforementioned wavelengths throughout the runs and allowed accurate determination of the retention times for each compound. After all runs on a particular column were completed, the column was flushed through with dH<sub>2</sub>O for 30 minutes prior to disconnection from the HPLC system, capping at both ends, and storage.

Standards of known CHI values (Tables 2-08 and 2-09) were prepared as  $\sim 1 \text{ mg} \cdot \text{mL}^{-1}$  solutions in a 50:50 mix of organic and aqueous mobile phase. These were filtered through a Whatman filter ( $0.45 \mu\text{m}$ ) prior to injection onto the column to prevent blockages caused by large particles or debris. HPLC is not dependent on concentration to achieve an accurate retention time so concentration and injection volumes are not important to standardize, provided the injection volume is not excessive (e.g.  $< 50 \mu\text{L}$ ) so as not to displace too much of the mobile phase and so as not to saturate the column. I selected  $1\text{-}20 \mu\text{L}$  volumes for each compound to achieve sharp peaks and absorbance intensities of  $\sim 200\text{-}1000 \text{ mAU}$  without saturating the column – the retention times of these molecules were used to calibrate the column. Calibration curves are displayed in Appendix II. The standards were run at the start and end of every automated sequence to ensure that the result was consistent throughout an assay. The standards always returned consistent retention times at the start and end of all runs.

Commercially available compounds were similarly prepared, however iodoreboxetine analogues were only available in binding solutions (50mM Tris-HCl, 120mM NaCl, 5mM KCl, pH 7.4) and compounds NKJ-64, NKJ-67, and NKJ-68 were heated to  $70^\circ\text{C}$  in a water bath for 20 minutes to ensure compound solubility. All iodoreboxetine compounds were injected in  $1\text{-}20 \mu\text{L}$  volumes to achieve absorbance peaks of approximately  $800\text{-}1000 \text{ mAu}$ . All preparations were filtered using a Whatman filter ( $0.45 \mu\text{m}$ ) prior to installation in the autosampler, and all samples were run concurrently on each run to ensure they were assayed under the same conditions and calibration.

Column	Dimensions	Supplier	Manufacturer Product Reference/Number
LUNA C-18	50 x 3mm, 5 microns	Phenomenex	00B-4252-Y0
Rexchrom Immobilized Artificial Membrane (IAM)	10cm x 4.6mm, 12 microns	Regis	IAM.PC.DD.2 / 774011
Human Serum Antigen (HSA)	50 x 3mm, 5 microns	ChromTech Ltd	HSA 50.3 07-G: 2506
$\alpha$ -acid glycoprotein (AGP)	50 x 3mm, 5 microns	ChromTech Ltd	AGP 50.3 07-33: 2407

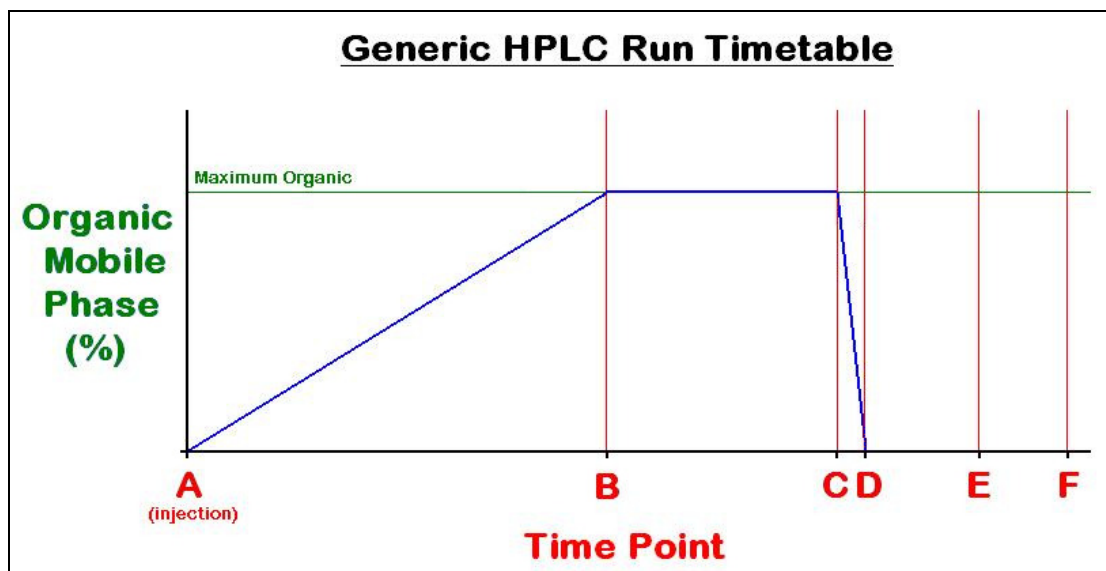
**Table 2-07:** Technical specifications of HPLC columns used for *in vivo* behaviour predictors. The LUNA C-18 columns were used in the calculation of  $\log P_{OCT}$  and  $c \log BB$ . The Rexchrom Immobilized Artificial Membrane Column was used in the calculation of  $\log D_{7.4(IAM)}$ . The Human Serum Antigen and  $\alpha$ -Acid Glycoprotein columns were used in the calculation of  $c\%PPB$ .

Table 2-08: Calibration standards for lipid and phospholipid columns					
Standard	Acidic Luna CHI (pH 2.5)	'Physiological' Luna CHI (pH 7.4)	Alkali Luna CHI (pH 10.5)	MeOH Luna CHI	IAM CHI
Acetanilide				54.50	11.50
Benzimidazole		34.30	30.61		
Indole	72.10	71.50	70.07		
Phenyltetrazole		23.60	15.98		
Phenyltheophylline	51.70	51.20	51.30		
Theophylline	6.30	18.40	4.97		
Acetophenone	64.10	65.10	64.12	69.17	17.20
Butyrophenone	87.30	87.50	87.33	83.53	32.00
Heptanophenone				93.95	45.70
Hexanophenone				91.32	41.80
Octanophenone				96.11	49.40
Propriophenone	77.40	77.40	77.42	78.29	25.90
Valerophenone	96.40	96.20	96.36	54.50	37.30

**Table 2-08:** Standards used to calibrate lipid and phospholipid columns and their respective CHI values for each compound in the conditions of the relevant column. These were run before and after every programmed autosampling run of each column. These CHI values were plotted against the retention time of each compound and the linear equation derived from that was used to convert the retention time of samples into CHI values.

<b>Table 2-09: Calibration standards for protein columns</b>		
<b>Standard</b>	<b>% Bound to HSA</b>	<b>% Bound to AGP</b>
Propranolol		86
Nizatidine	35	
Nicardipine	95	92
Warfarin (2 <sup>nd</sup> Peak)	98	
Carbamazepine	75	24
Piroxicam	94.5	
Imipramine		91

**Table 2-09:** Standards used to calibrate protein columns and their respective know percentage of protein binding for the protein immobilized in each column. These were run before and after every programmed autosampling run of each column. These were converted into log scale (as linearised log k) and plotted against the log of their retention times.  $\text{Log } k = \log ( \%PPB / 101 - \%PPB )$ . Sample retention times were then able to be processed by reverse of those steps.



**Figure 2-05:** Graphical representation of a Generic HPLC Run Timetable. *Time point A:* injection and the start of the gradient elution. *Time point B:* the maximum percentage of organic mobile phase to be used has been reached. *Time point C:* the end of the plateau of maximum organic mobile phase. *Time point D:* organic mobile phase is discontinued and aqueous mobile phase is restored to the column. *Time point E:* U.V. absorbance recordings were stopped for a given run. *Time point F:* re-equilibration of the column to prepare for the next automated injection occurred between points E and F, during which flow of aqueous mobile phase in the absence of organic mobile phase was utilised.

Column	Mobile Phase	Flow Rate (mL/min)	Time Point A and Organic	Time Point B and % Organic	Time Point C and % Organic	Time Point D and % Organic	Time Point E and % Organic	Time Point F and % Organic
Acidic LUNA	<b>Aqueous:</b> 10mM Phosphoric Acid, pH 2.5 <b>Organic:</b> 100% Acetonitrile	1.0	0.00 minutes (0%)	2.50 minutes (100%)	3.00 minutes (100%)	3.20 minutes (0%)	4.00 minutes (0%)	10.00 minutes (0%)
Alkali LUNA	<b>Aqueous:</b> 50mM Ammonium Acetate, pH 10.5 <b>Organic:</b> 100% Acetonitrile	1.0	0.00 minutes (0%)	2.50 minutes (100%)	4.00 minutes (100%)	4.20 minutes (0%)	5.00 minutes (0%)	10.00 minutes (0%)
LUNA	<b>Aqueous:</b> 50mM Ammonium Acetate, pH 7.4 <b>Organic:</b> 100% Acetonitrile	1.5	0.00 minutes (0%)	2.50 minutes (100%)	3.00 minutes (100%)	3.20 minutes (0%)	4.00 minutes (0%)	8.00 minutes (0%)
IAM	<b>Aqueous:</b> 50mM Ammonium Acetate, pH 7.4 <b>Organic:</b> 100% Acetonitrile	2.549	0.00 minutes (0%)	2.50 minutes (70%)	3.00 minutes (70%)	3.20 minutes (0%)	4.00 minutes (0%)	10.00 minutes (0%)
MeOH LUNA	<b>Aqueous:</b> 50mM Ammonium Acetate, pH 7.4 <b>Organic:</b> 100% Methanol	1.5	0.00 minutes (0%)	2.50 minutes (100%)	3.00 minutes (100%)	3.20 minutes (0%)	4.00 minutes (0%)	6.00 minutes (0%)

**Table 2-10 (continued below):** Column run timetables showing column identification, mobile phase conditions, and gradient methodology flow rates for organic mobile phase (Smith & Valkó-Slegel 2004; Valkó-Slegel 2004; Valkó 2008; K. Valkó, 2008 - Personal Communication). In conjunction with figure 2-05.

Column	Mobile Phase	Flow Rate (mL/min)	Time Point A and % Organic	Time Point B and % Organic	Time Point C and % Organic	Time Point D and % Organic	Time Point E and % Organic	Time Point F and % Organic
AGP	<b>Aqueous:</b> 50mM Ammonium Acetate, pH 7.4 <b>Organic:</b> 100% Propan-2-ol	1.5	0.00 minutes (0%)	3.00 minutes (25%)	5.00 minutes (25%)	5.10 minutes (0%)	6.00 minutes (0%)	10.00 minutes (0%)
HSA	<b>Aqueous:</b> 50mM Ammonium Acetate, pH 7.4 <b>Organic:</b> 100% Propan-2-ol	1.8	0.00 minutes (0%)	3.00 minutes (25%)	5.00 minutes (25%)	5.10 minutes (0%)	6.00 minutes (0%)	10.00 minutes (0%)

**Table 2-10 (Continued from above):** Column run timetables showing column identification, mobile phase conditions, and gradient methodology flow rates for organic mobile phase (Smith & Valkó-Slegel 2004; Valkó-Slegel 2004; Valkó 2008; K. Valkó, 2008 - Personal Communication). In conjunction with figure 2-05.

### 2.3.2 Determination of lipophilicity using C-18 column data

The retention times for the iodoreboxetine compounds are compared to the C-18 column retention times of 'standard' compounds for which the chromatographic hydrophobicity index (CHI) was known. The CHI for a test compound is derived from comparing the retention time of the test compound to that of the retention times for a series of compounds with known CHI values. The CHIN is the CHI of the uncharged molecule and will be the greatest measured CHI across acidic (2.5), physiological (7.4), and alkaline (10.5) pH levels (Table 2-09) – as non-polar molecules will more readily transverse both the positive and negative regions of lipid layers.

The log  $D$  at a given pH can be calculated via the following linear equation, which was formulated via plotting the CHI of a large library of compounds against log  $D_{pH}$  (Valkó et al. 1997; K. Valkó, 2008 - Personal Communication).

$$\log D_{pH} = 0.0525 \times \text{CHI} - 1.467$$

Where,

CHI = Chromatographic Hydrophobicity Index at a given pH  
0.0525 = The gradient  
-1.467 = The Y-axis intercept

The log  $D_{pH}$  of the compound has a linear relationship with its CHI at that given pH. The log  $P$ , an estimation of partition coefficients for the uncharged molecule, and the log  $P_{\text{OCT}}$ , an estimation of the octanol/water bench-top determination of partition coefficients for the uncharged molecule, are calculated via the following linear equations (Valkó et al. 1997; K. Valkó, 2008 - Personal Communication):

$$\log P = 0.0525 \times \text{CHIN} - 1.467$$

Where,

CHIN = Chromatographic Hydrophobicity Index of the unionised form of the molecule (this will be the greatest CHI measured across acidic, physiological, and alkali pH conditions)  
0.0525 = The gradient  
-1.467 = The Y-axis intercept

$$\log P_{\text{OCT}} = (0.054 \times \text{CHIN}) + (1.319 \times \text{AAP}) - 1.877$$

Where,

CHIN = Chromatographic Hydrophobicity Index of the unionised form of the molecule (this will be the greatest CHI measured across acidic, physiological, and alkali pH conditions)

AAP = Abraham Acidity Parameter, calculated by ADAMANTIS (GSK's proprietary software)

0.054 = The gradient

$(1.319 \times \text{AAP}) - 1.877$  = the specific Y-axis intercept for that molecule, accounting for its AAP

### 2.3.3 Determination of non-specific binding using IAM (phospholipid) column data

Non-specific binding *in vivo* can be predicted using HPLC via an immobilized artificial membrane (IAM) column composed of phospholipids. As with the C-18 column assays, standards with known CHI values were used to convert the retention times of test compounds into CHI values. The  $\log D_{7.4 \text{ (IAM)}}$  was calculated using the following linear equations (Valkó et al. 2000; Valkó 2004; Hollósy et al. 2006), which were derived from a library of compounds by Klara Valkó (GSK):

$$\log D_{7.4 \text{ (IAM)}} = (2.07 \times \log k_{\text{IAM}}) + (1.09 \times \text{AAP}) + 0.52$$

Where,

AAP = Abraham Acidity Parameter, calculated by ADAMANTIS (GSK's proprietary software)

2.07 = The gradient

$(1.09 \times \text{AAP}) + 0.52$  = The specific Y-axis intercept for that molecule, accounting for its AAP

$$\log k_{\text{IAM}} = (0.046 \times \text{CHI}_{\text{IAM}}) + 0.42$$

Where,

$\text{CHI}_{\text{IAM}}$  = Chromatographic Hydrophobicity Index on IAM column

0.046 = The gradient

0.42 = The Y-axis intercept

### 2.3.4 Determination of blood-brain barrier penetration index using LUNA column data

Blood brain barrier penetration can be estimated using a formula incorporating data from the alkali LUNA C-18 acetonitrile-eluted column and a physiological pH

LUNA C-18 with a methanol elution. The calculated log BB was determined using the equation below (K. Valkó, 2008 - Personal Communication).

$$c \log BB = (0.017 \times CHI_{10.5}) + (0.048 \times CHI_{7.4 (MeOH)}) - (0.129 \times CMR) - 3.11$$

Where,

$CHI_{10.5}$  = Chromatographic Hydrophobicity Index at pH 10.5, acetonitrile elution

$CHI_{7.4 (MeOH)}$  = Chromatographic Hydrophobicity Index, MeOH elution at pH 7.4

CMR = calculated molecular refractivity (a measurement of size), determined by ADAMANTIS (GSK's proprietary software)

Higher values are interpreted as greater potential for successful brain penetration, whilst lower values are interpreted as reduced brain penetration (Garg et al. 2008), negative c log BB values are theoretical and interpreted as an inability to penetrate the brain.

### 2.3.5 Determination of plasma protein binding using HSA and AGP column data

Compound binding to plasma transport proteins such as human serum albumin (HSA) and  $\alpha$ -acid glycoprotein (AGP) are used to estimate plasma protein binding (c%PPB) by inputting column data into the following equation (Valkó et al. 2011; Hollósy et al. 2006), which had been updated via personal communication to reflect the ongoing refinement of it:

$$c\%PPB = (0.87 \times \log k_{HSA}) + (0.17 \times \log k_{AGP}) + (0.06 \times CMR) - 0.27$$

Where,

CMR = calculated molecular refractivity (a measurement of size), calculated by ADAMANTIS (GSK's molecular predictor software).

$$\log k_{HSA} = \log ( \%PPB_{HSA} / 101 - \%PPB_{HSA} )$$

Note:  $\%PPB_{HSA} = [ ( 101 * 10^{\log k_{HSA}} ) / ( 1 + 10^{\log k_{HSA}} ) ]$

$$\log k_{AGP} = \log ( \%PPB_{AGP} / 101 - \%PPB_{AGP} )$$

Note:  $\%PPB_{AGP} = [ ( 101 * 10^{\log k_{AGP}} ) / ( 1 + 10^{\log k_{AGP}} ) ]$

# Chapter 3

## Imaging Monoamine Transporters in the PCP-induced Rat Model of the Metabolic Hypofrontality Observed in Schizophrenia

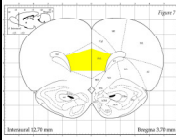
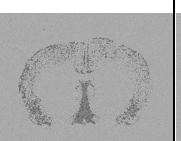
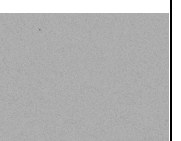
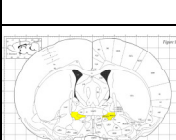
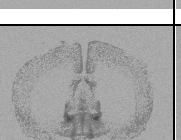
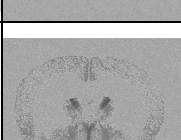
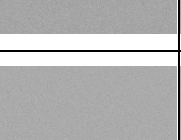
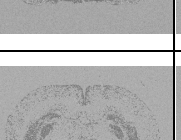
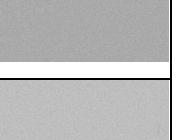
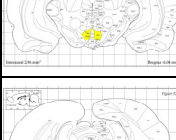
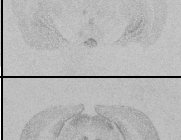
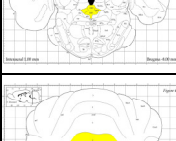
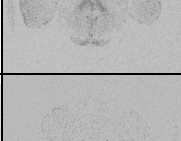
### 3.1 Results:

#### 3.1.1 [<sup>3</sup>H]-nisoxetine binding to the NAT

The distribution of [<sup>3</sup>H]-nisoxetine binding to the NAT (Table 3-01, Tables 3-02 to 3-10) is widespread throughout cortical regions (Tables 3-02 to 3-08), and low NAT binding was detected in the CA1 (Table 3-06). Moderate binding densities were localized to the RTN (Table 3-05), hippocampal regions CA2, CA3, and DG (all Table 3-06), and DRN (Table 3-08) and high NAT binding densities were localized in the BNST (Table 3-04) and AVN (Table 3-05). The highest densities for binding to NAT were found in the LC (Table 3-09), from where all noradrenergic projections originate. NAT binding in the LC and CBL appears visually lower relative to the other regions due to using half the concentration of [<sup>3</sup>H]-nisoxetine on these sections due to the extremely high density of NAT in the LC. Binding was extremely low in the caudate putamen and nucleus accumbens (both Table 3-03).

Imaging with [<sup>3</sup>H]-nisoxetine provided clear delineation of most assayed structures with the exception of the caudate putamen and nucleus accumbens (both Table 3-03). White matter tracts could sometimes be distinguished with [<sup>3</sup>H]-nisoxetine binding and non-specific binding was very low throughout the brain.

There were no statistically significant differences detected in the [<sup>3</sup>H]-nisoxetine binding to the NAT of control and PCP-treated rats (Figure 3-01). The LC and CBL were imaged with 1.5nM [<sup>3</sup>H]-nisoxetine rather than 3.0nM [<sup>3</sup>H]-nisoxetine due to the intense NAT density in the LC, so these regions have a greater density of [<sup>3</sup>H]-nisoxetine binding sites than is immediately apparent from a cursory glance of the data.

Table 3-01: The Distribution of the Noradrenaline Transporter (Overview)					
Structures	Paxinos and Watson plate	Group B		Group A	
		Total Binding in Vehicle-Treated	Nonspecific Binding in Vehicle-Treated	Total Binding in PCP-Treated	Nonspecific Binding in PCP-Treated
Prefrontal Cortex (PrL; aka PFC)					
Caudate Putamen (CPu), Cingulate Anterior (Cg1; aka ACg), Nucleus Accumbens (AcbC; aka N.acc.)					
Bed Nucleus of the Striatum Terminalis (BSTMV and BSTLV; together aka BNST)					
Anteroventral Thalamic Nucleus (AVDM and AVVL; together aka AVTN), Reticular Thalamic Nucleus (Rt; aka RTN)					
Hippocampus CA1 (CA1), Hippocampus CA2 (CA2), Hippocampus CA3 (CA3), Hippocampus Dentate Gyrus (DG)					
Ventral Tegmental Area (VTA)					
Dorsal Raphe Nuclei (DRD, DRV, and DRVL; together aka DRN)					
Locus Coeruleus (LC), Cerebellum (2; aka CBL)					

**Table 3-01:** The distribution of 3.0nM [<sup>3</sup>H]-nisoxetine binding (1.5nM for LC and CBL) to the noradrenaline transporter in the vehicle-treated and PCP-treated rat brain. Non-specific binding was defined in the presence of 10.0μM nortriptyline hydrochloride. Structures that were assayed to determine quantitative differences are specified for each level and are highlighted on the adapted Paxinos and Watson plates. This overview allows the overall distribution of the NAT throughout the brain to be observed. The caudate putamen appears to be a promising reference region to define an absence of binding for *in vivo* scanning with SPECT or PET, rather than the commonly used cerebellum.

Table 3-02: The Distribution of the Noradrenaline Transporter		
	Total Binding	Nonspecific Binding
Vehicle-Treated		
PCP-Treated		
Paxinos and Watson Plate with Structures	<p>Figure 7</p> <p>Interaural 12.70 mm      Bregma 3.70 mm</p> <p>Prefrontal Cortex (PrL; aka PFC)</p>	

**Table 3-02:** 3.0nM [<sup>3</sup>H]-nisoxetine binding to the noradrenaline transporter in sections of vehicle-treated and PCP-treated rat brain. Non-specific binding was defined in the presence of 10.0μM nortriptyline hydrochloride. Structures that were assayed to determine quantitative differences are specified for this level and are highlighted on the adapted Paxinos and Watson plate.

Table 3-03: The Distribution of the Noradrenaline Transporter		
	Total Binding	Nonspecific Binding
Vehicle-Treated		
PCP-Treated		
Paxinos and Watson Plate with Structures	<p>Caudate Putamen (CPu), Cingulate Anterior (Cg1; aka ACg), Nucleus Accumbens (AcbC; aka N.acc.)</p>	

**Table 3-03:** 3.0nM [<sup>3</sup>H]-nisoxetine binding to the noradrenaline transporter in sections of vehicle-treated and PCP-treated rat brain. Non-specific binding was defined in the presence of 10.0μM nortriptyline hydrochloride. Structures that were assayed to determine quantitative differences are specified for this level and are highlighted on the adapted Paxinos and Watson plate.



Table 3-05: The Distribution of the Noradrenaline Transporter		
	Total Binding	Nonspecific Binding
Vehicle-Treated		
PCP-Treated		
Paxinos and Watson Plate with Structures	<p>Anteroventral Thalamic Nucleus (AVDM and AVVL; together aka AVTN), Reticular Thalamic Nucleus (Rt; aka RTN)</p>	

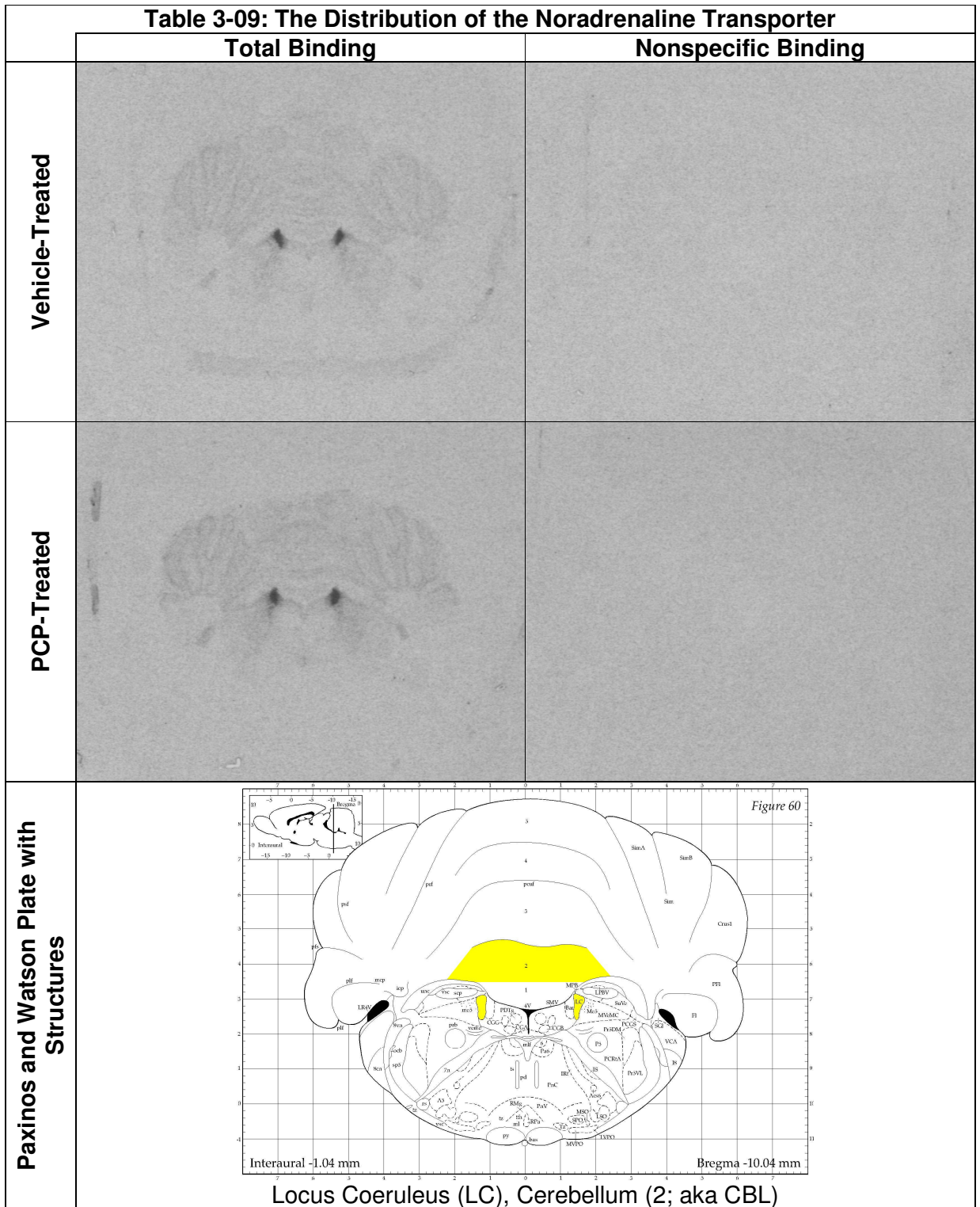
**Table 3-05:** 3.0nM [<sup>3</sup>H]-nisoxetine binding to the noradrenaline transporter in sections of vehicle-treated and PCP-treated rat brain. Non-specific binding was defined in the presence of 10.0μM nortriptyline hydrochloride. Structures that were assayed to determine quantitative differences are specified for this level and are highlighted on the adapted Paxinos and Watson plate.



Table 3-07: The Distribution of the Noradrenaline Transporter		
	Total Binding	Nonspecific Binding
Vehicle-Treated		
PCP-Treated		
Paxinos and Watson Plate with Structures	<p style="text-align: center;">Ventral Tegmental Area (VTA)</p>	

**Table 3-07:** 3.0nM [<sup>3</sup>H]-nisoxetine binding to the noradrenaline transporter in sections of vehicle-treated and PCP-treated rat brain. Non-specific binding was defined in the presence of 10.0μM nortriptyline hydrochloride. Structures that were assayed to determine quantitative differences are specified for this level and are highlighted on the adapted Paxinos and Watson plate.





**Table 3-09:** 1.5nM [<sup>3</sup>H]-nisoxetine binding to the noradrenaline transporter in sections of vehicle-treated and PCP-treated rat brain. This is a lower concentration of ligand used in comparison to other regions due to the high intensity of binding to NAT in the LC. Non-specific binding was defined in the presence of 10.0μM nortriptyline hydrochloride. Structures that were assayed to determine quantitative differences are specified for this level and are highlighted on the adapted Paxinos and Watson plate.

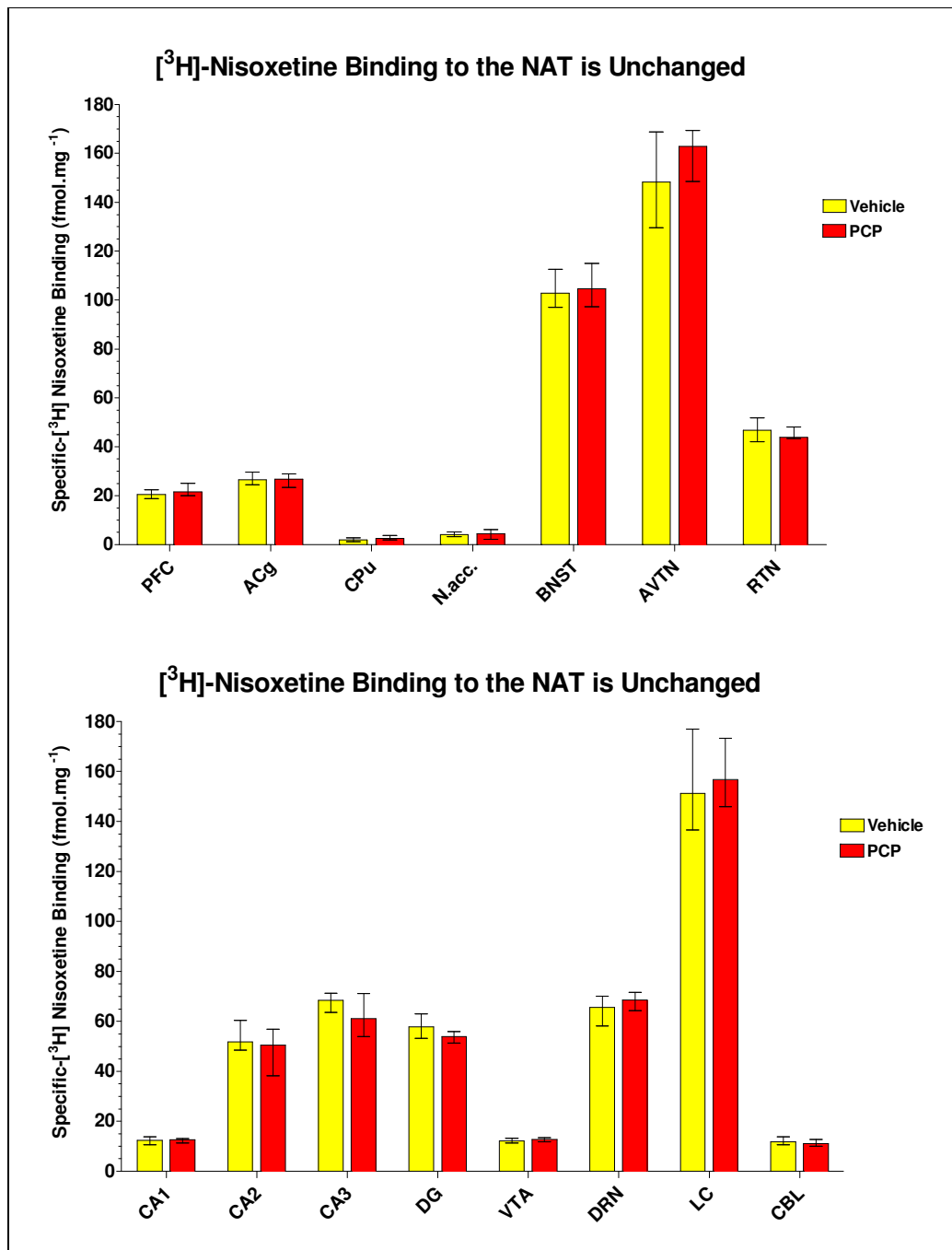


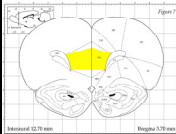
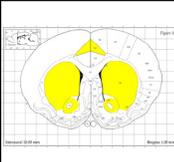
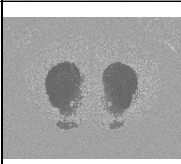
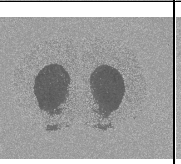
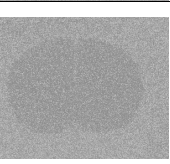
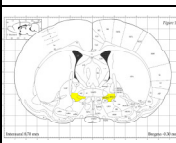
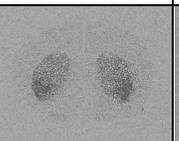
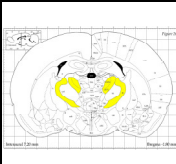
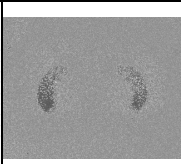
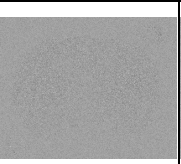
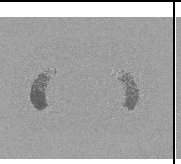
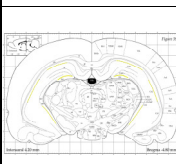
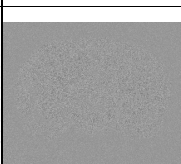
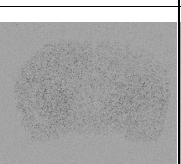
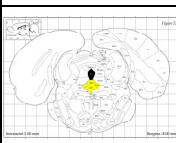
**Figure 3-01:** Shown as medians of each group for each structure with error bars representing interquartile range. No statistically significant differences, as  $P > 0.05$  (Mann-Whitney) across all structures. Structures assayed: prefrontal cortex (PFC), anterior cingulate cortex (ACg), caudate putamen (CPu), nucleus accumbens (N. acc.), bed nucleus of the striatus terminalis (BNST), anteroventral thalamic nucleus (AVTN), reticular thalamic nucleus (RTN), hippocampal regions: CA1, CA2, CA3, & dentate gyrus (DG), ventral tegmental area (VTA), dorsal raphe nuclei (DRN), locus coeruleus (LC), and cerebellum (CBL). All structures imaged with 3.0nM [<sup>3</sup>H]-Nisoxetine except LC and CBL, which were imaged with 1.5nM [<sup>3</sup>H]-Nisoxetine due to the high density of noradrenaline transporters in the LC.

### 3.1.2 [<sup>3</sup>H]-WIN-35,428 binding to the DAT

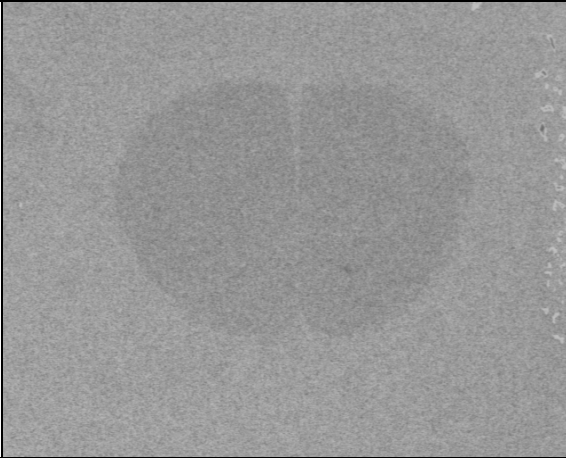
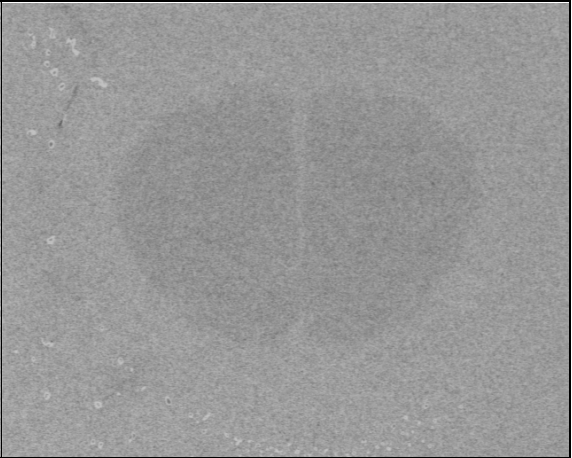
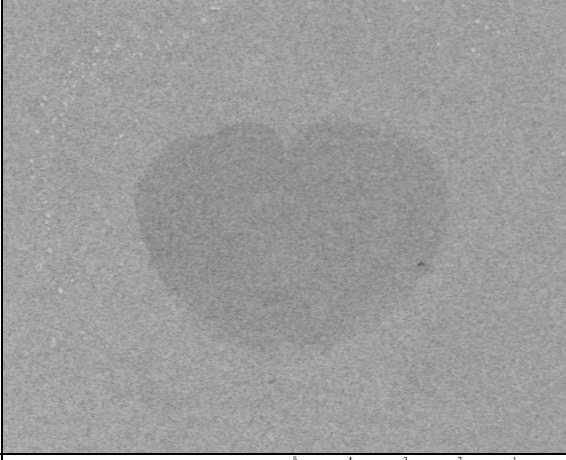
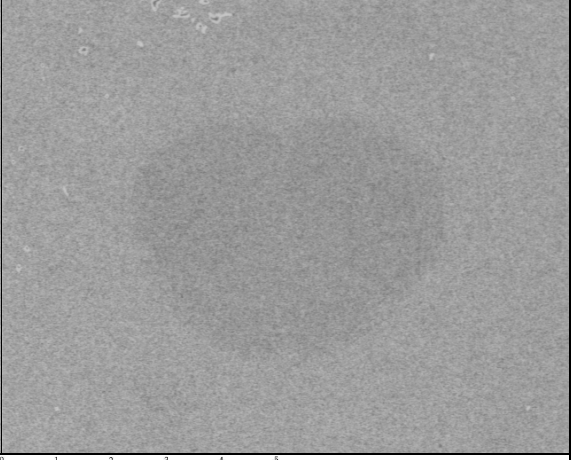
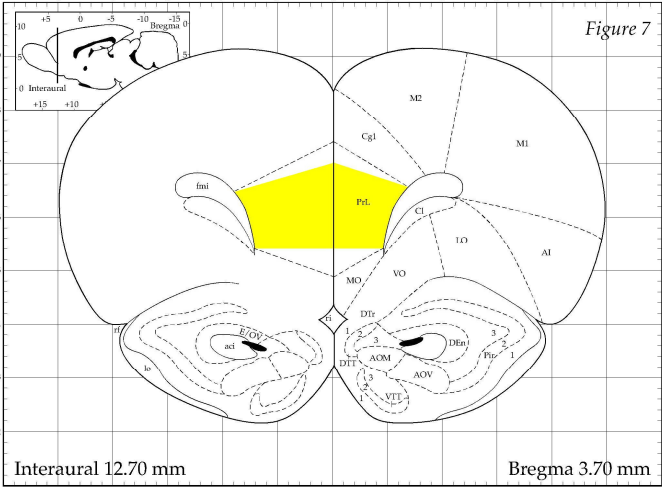
The distribution of [<sup>3</sup>H]-WIN-35,428 binding to the DAT (Table 3-10, Tables 3-11 to 3-18) was high throughout the caudate putamen and the nucleus accumbens (both Table 12), and it was in these structures that the highest binding densities were found. The next highest densities were found in the VTA (Table 3-16) and then the DRN (Table 3-17), and LC (Table 3-18). It was interesting to note that, unlike the distribution of the NAT, the highest binding density was not found in the cell bodies from whence dopaminergic projections originate. Binding to DAT was absent in the hippocampal regions CA1, CA2, CA3, and DG (all Table 3-15), as well as in the cerebellum (Table 3-18).

Imaging with [<sup>3</sup>H]-WIN-35,428 did not offer particularly clear delineation of assayed structures with the exception of the caudate putamen, nucleus accumbens (both Table 3-12), and VTA (Table 3-16) - the substantia nigra (Table 3-16) was also discernable but not assayed. White matter tracts were difficult to distinguish with [<sup>3</sup>H]-WIN-35,428 binding and non-specific binding appeared higher than was observed with [<sup>3</sup>H]-nisoxetine and [<sup>3</sup>H]-citalopram, but higher nonspecific binding was consistent with the use of a relatively higher ligand concentration (10nM) that exceeded the  $K_D$  (5nM) for the binding site on the DAT when compared to the NAT or SERT imaging.

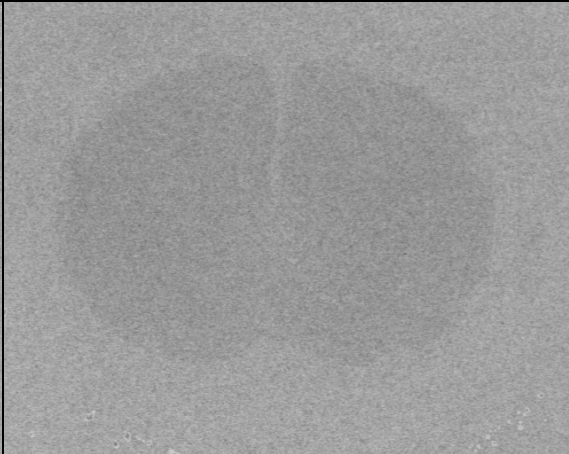
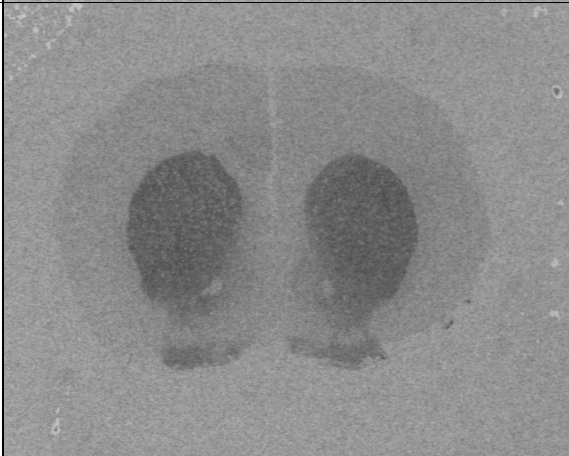
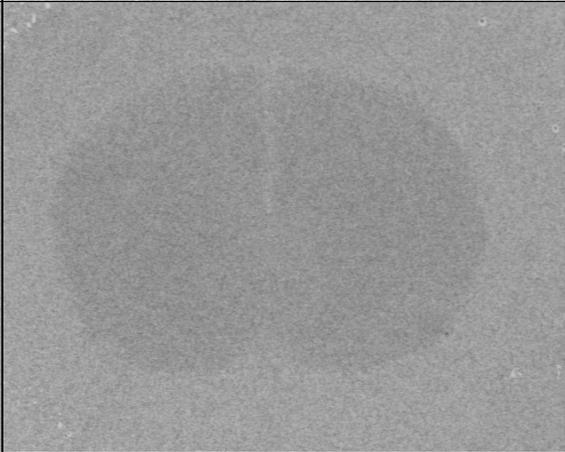
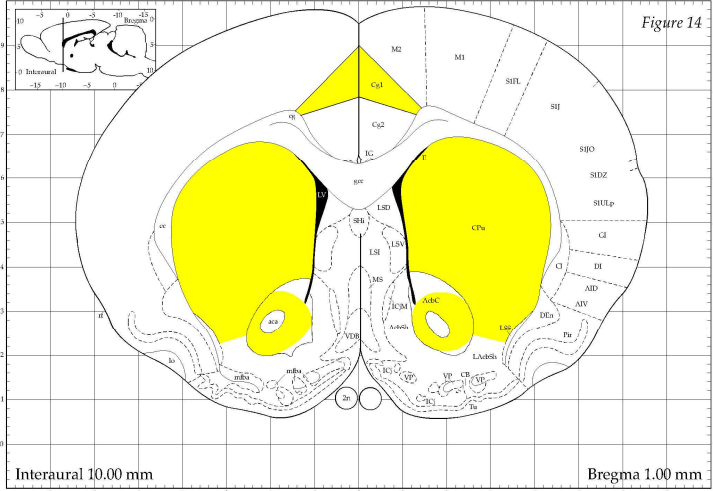
There were no statistically significant differences detected between [<sup>3</sup>H]-WIN-35,428 binding to the DAT in control and PCP-treated rats (Figure 3-02). Hippocampal areas CA1, CA2, CA3, and DG, and the CBL are either devoid of [<sup>3</sup>H]-WIN-35,428 binding sites or are of such low density they are below the detection threshold for the assay.

Table: 3-10: The Distribution of the Dopamine Transporter (Overview)					
Structures	Paxinos and Watson plate	Group B		Group A	
		Total Binding in Vehicle-Treated	Nonspecific Binding in Vehicle-Treated	Total Binding in PCP-Treated	Nonspecific Binding in PCP-Treated
Prefrontal Cortex (PrL; aka PFC)					
Caudate Putamen (CPu), Cingulate Anterior (Cg1; aka ACg), Nucleus Accumbens (AcbC; aka N.acc.)					
Bed Nucleus of the Striatum Terminalis (BSTMV and BSTLV; together aka BNST)					
Anteroventral Thalamic Nucleus (AVDM and AVVL; together aka AVTN), Reticular Thalamic Nucleus (Rt; aka RTN)					
Hippocampus CA1 (CA1), Hippocampus CA2 (CA2), Hippocampus CA3 (CA3), Hippocampus Dentate Gyrus (DG)					
Ventral Tegmental Area (VTA)					
Dorsal Raphe Nuclei (DRD, DRV, and DRVL; together aka DRN)					
Locus Coeruleus (LC), Cerebellum (2; aka CBL)					

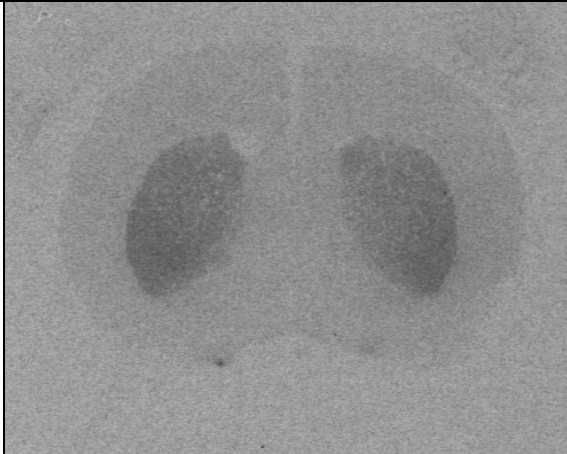
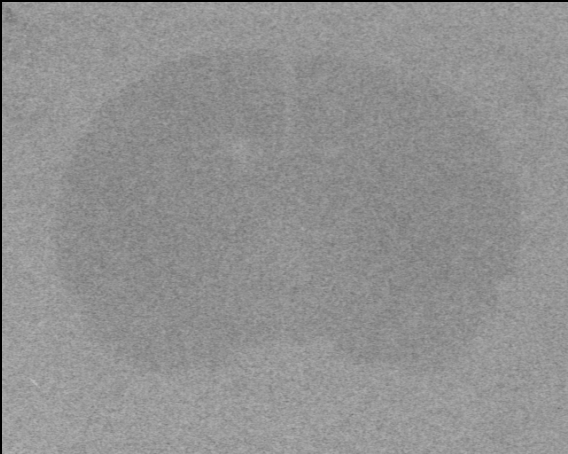
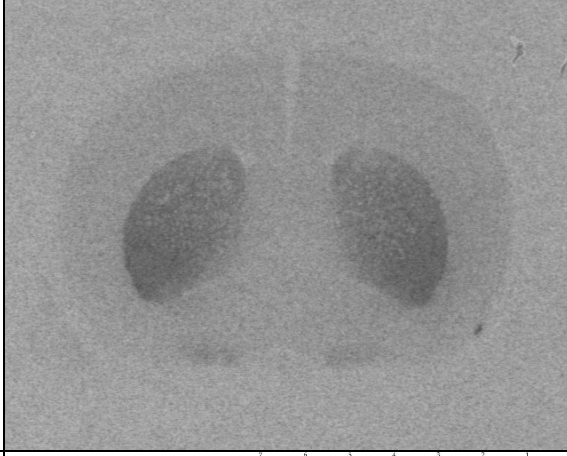
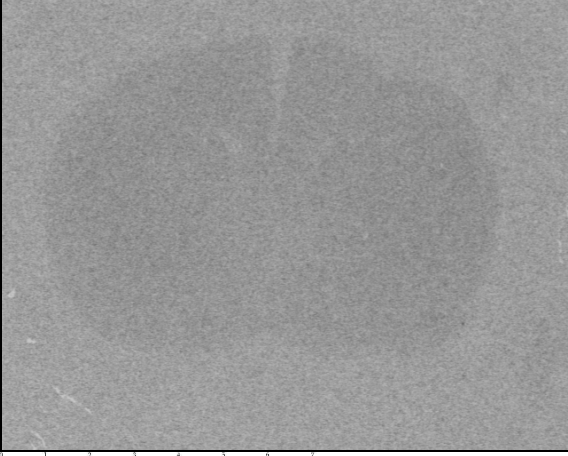
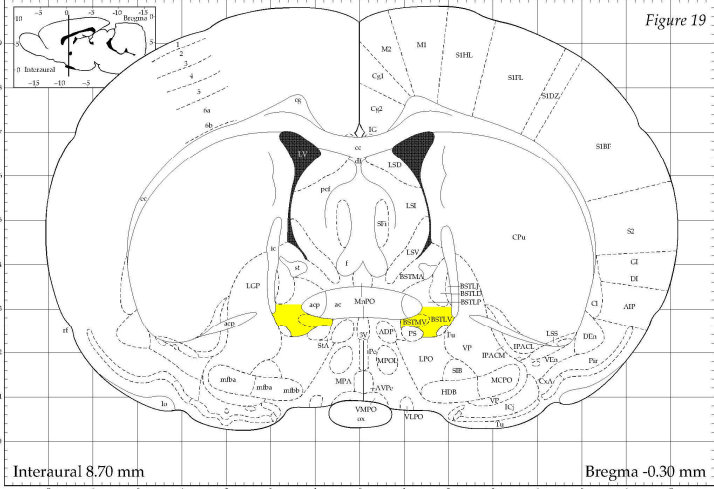
**Table 3-10:** The distribution of 10.0nM [<sup>3</sup>H]-WIN-35,428 binding to the dopamine transporter in the vehicle-treated and PCP-treated rat brain. Non-specific binding was defined in the presence of 30.0μM nomifensine. Structures that were assayed to determine quantitative differences are specified for each level and are highlighted on the adapted Paxinos and Watson plates. This overview allows the overall distribution of the DAT throughout the brain to be observed.

Table 3-11: The Distribution of the Dopamine Transporter		
	Total Binding	Nonspecific Binding
Vehicle-Treated		
PCP-Treated		
Paxinos and Watson Plate with Structures	 <p style="text-align: center;">Prefrontal Cortex (PrL; aka PFC)</p>	

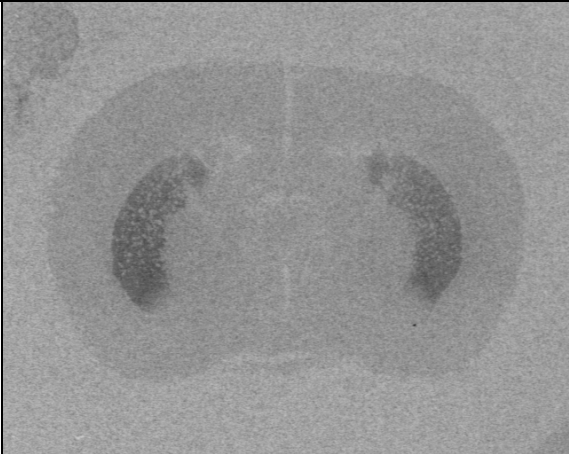
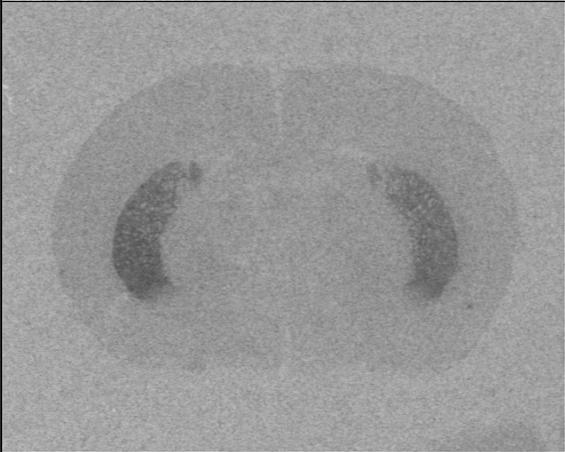
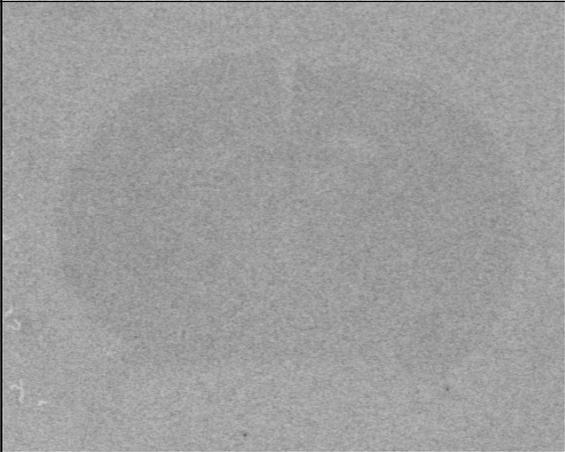
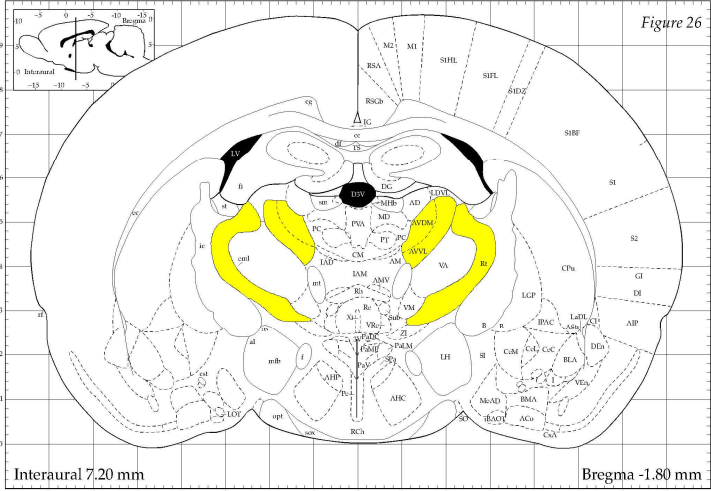
**Table 3-11:** [<sup>3</sup>H]-WIN-35,428 binding to the dopamine transporter in sections of vehicle-treated and PCP-treated rat brain. Non-specific binding was defined in the presence of 30.0μM nomifensine. Structures that were assayed to determine quantitative differences are specified for this level and are highlighted on the adapted Paxinos and Watson plate.

Table 3-12: The Distribution of the Dopamine Transporter		
	Total Binding	Nonspecific Binding
Vehicle-Treated		
PCP-Treated		
Paxinos and Watson Plate with Structures	 <p>Figure 14</p> <p>Interaural 10.00 mm</p> <p>Bregma 1.00 mm</p> <p>Caudate Putamen (CPu), Cingulate Anterior (Cg1; aka ACg), Nucleus Accumbens (AcbC; aka N.acc.)</p>	

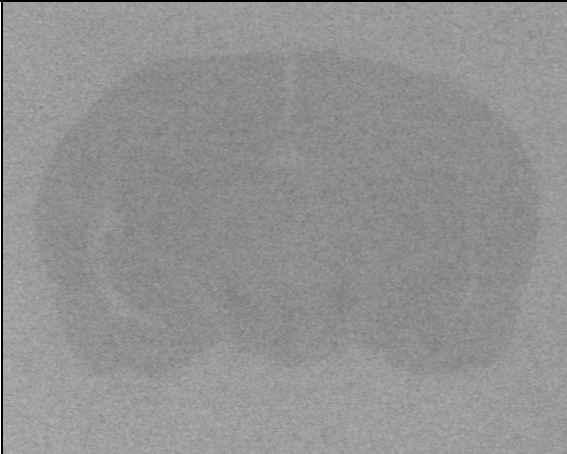
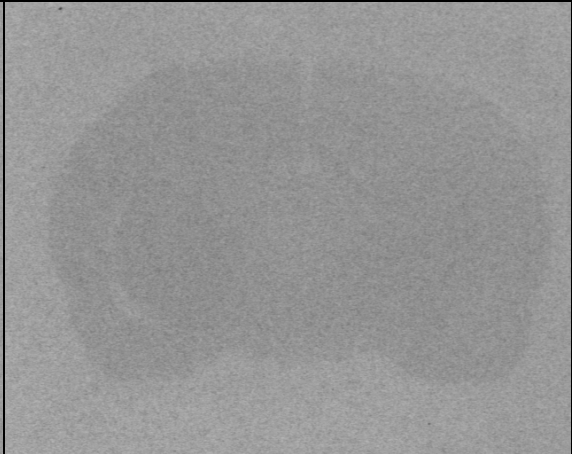
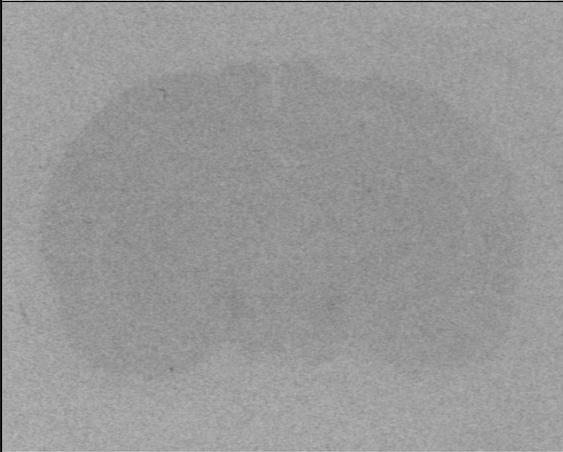
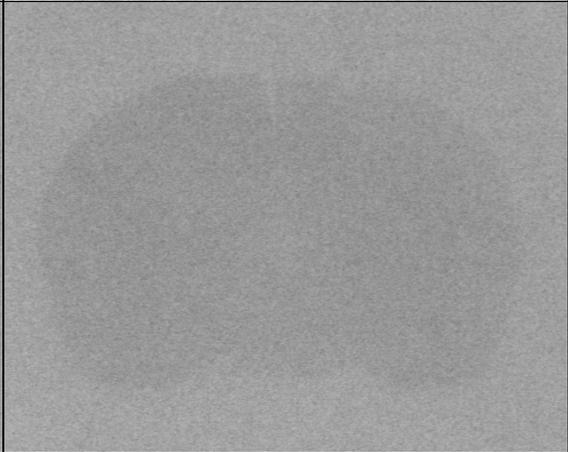
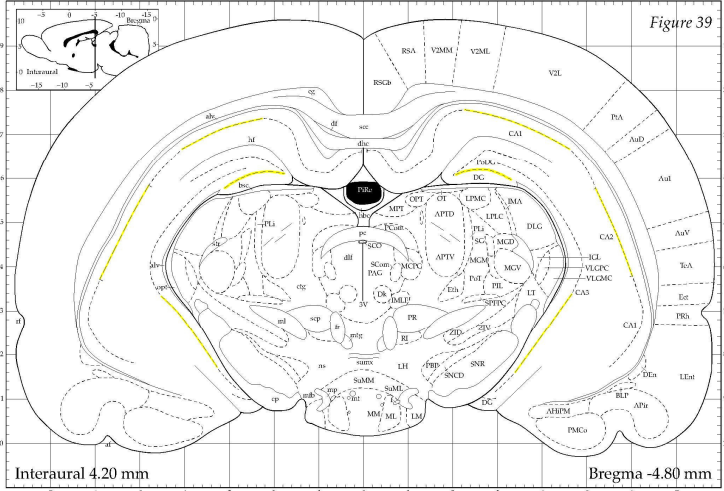
**Table 3-12:** [<sup>3</sup>H]-WIN-35,428 binding to the dopamine transporter in sections of vehicle-treated and PCP-treated rat brain. Non-specific binding was defined in the presence of 30.0μM nomifensine. Structures that were assayed to determine quantitative differences are specified for this level and are highlighted on the adapted Paxinos and Watson plate.

Table 3-13: The Distribution of the Dopamine Transporter		
	Total Binding	Nonspecific Binding
Vehicle-Treated		
PCP-Treated		
Paxinos and Watson Plate with Structures	 <p style="text-align: right;">Figure 19</p> <p style="text-align: center;">Bed Nucleus of the Striatum Terminalis (BSTMV and BSTLV; together aka BNST)</p>	

**Table 3-13:** [<sup>3</sup>H]-WIN-35,428 binding to the dopamine transporter in sections of vehicle-treated and PCP-treated rat brain. Non-specific binding was defined in the presence of 30.0μM nomifensine. Structures that were assayed to determine quantitative differences are specified for this level and are highlighted on the adapted Paxinos and Watson plate.

Table 3-14: The Distribution of the Dopamine Transporter		
	Total Binding	Nonspecific Binding
Vehicle-Treated		
PCP-Treated		
Paxinos and Watson Plate with Structures	 <p>Anteroventral Thalamic Nucleus (AVDM and AVVL; together aka AVTN), Reticular Thalamic Nucleus (Rt; aka RTN)</p>	

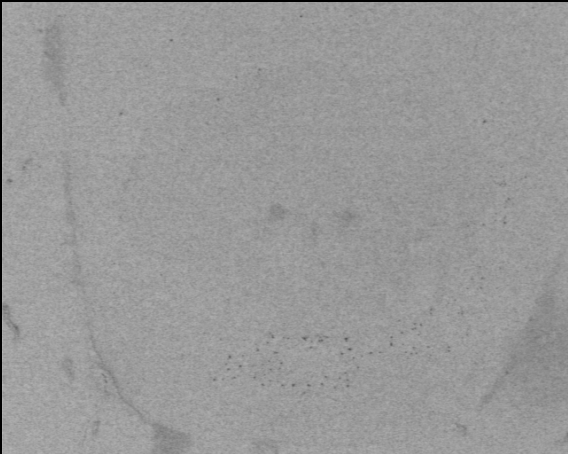
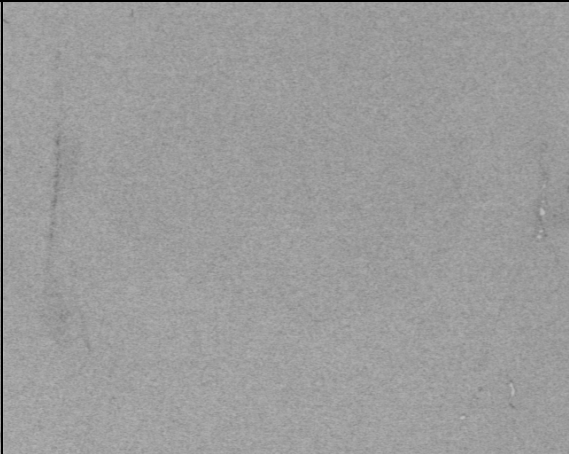
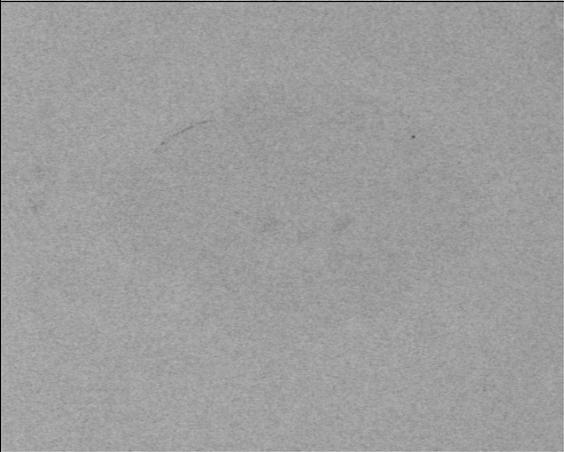
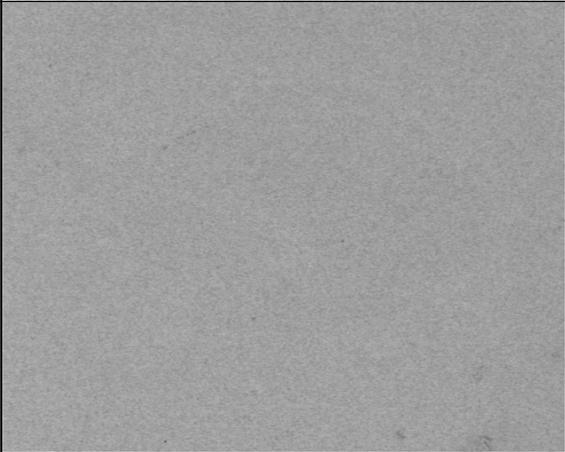
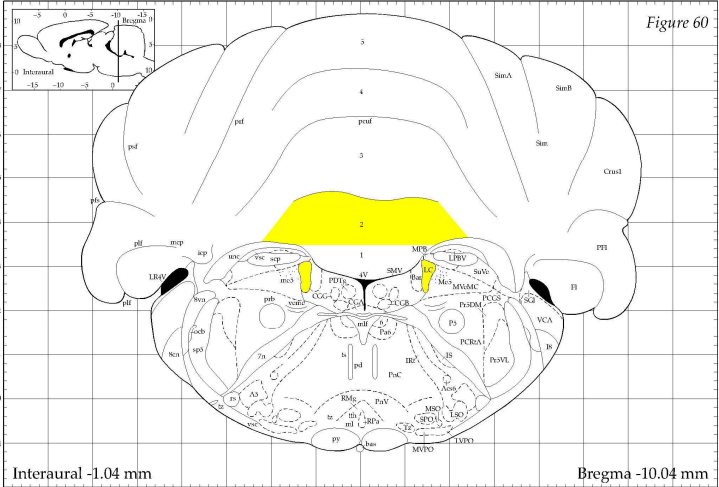
**Table 3-14:** [<sup>3</sup>H]-WIN-35,428 binding to the dopamine transporter in sections of vehicle-treated and PCP-treated rat brain. Non-specific binding was defined in the presence of 30.0μM nomifensine. Structures that were assayed to determine quantitative differences are specified for this level and are highlighted on the adapted Paxinos and Watson plate.

Table 3-15: The Distribution of the Dopamine Transporter		
	Total Binding	Nonspecific Binding
Vehicle-Treated		
PCP-Treated		
Paxinos and Watson Plate with Structures	 <p>Hippocampus CA1 (CA1), Hippocampus CA2 (CA2), Hippocampus CA3 (CA3), Hippocampus Dentate Gyrus (DG)</p>	

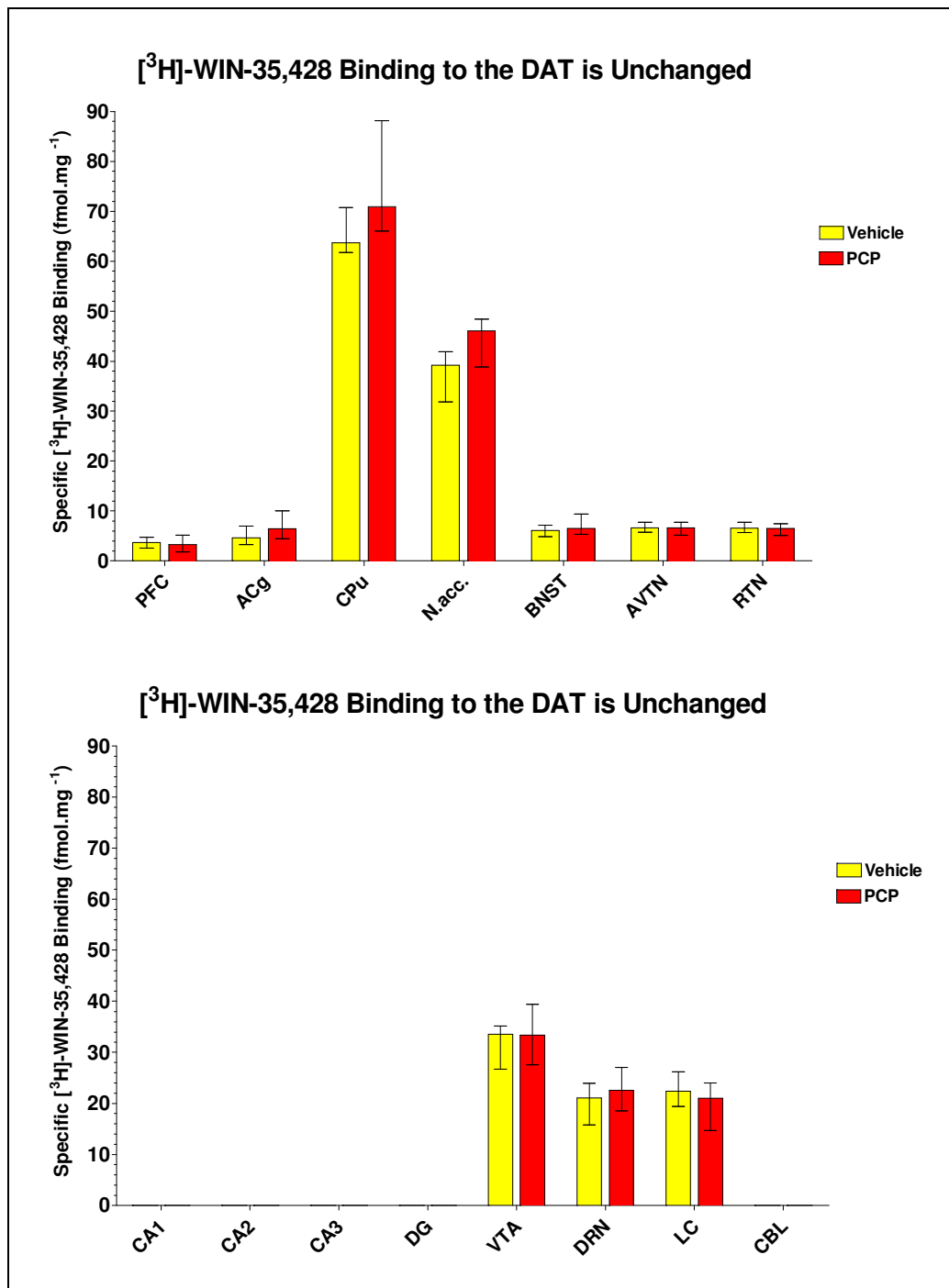
**Table 3-15:** [<sup>3</sup>H]-WIN-35,428 binding to the dopamine transporter in sections of vehicle-treated and PCP-treated rat brain. Non-specific binding was defined in the presence of 30.0μM nomifensine. Structures that were assayed to determine quantitative differences are specified for this level and are highlighted on the adapted Paxinos and Watson plate.





Table 3-18: The Distribution of the Dopamine Transporter		
	Total Binding	Nonspecific Binding
Vehicle-Treated		
PCP-Treated		
Paxinos and Watson Plate with Structures	 <p style="text-align: center;">Locus Coeruleus (LC), Cerebellum (2; aka CBL)</p>	

**Table 3-18:** [<sup>3</sup>H]-WIN-35,428 binding to the dopamine transporter in sections of vehicle-treated and PCP-treated rat brain. Non-specific binding was defined in the presence of 30.0μM nomifensine. Structures that were assayed to determine quantitative differences are specified for this level and are highlighted on the adapted Paxinos and Watson plate.



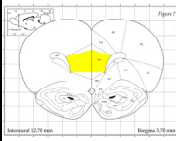
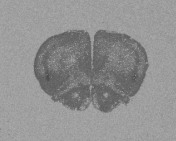
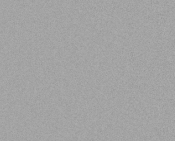
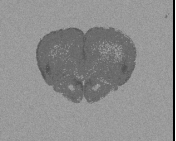
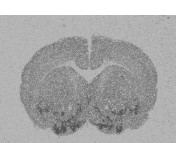
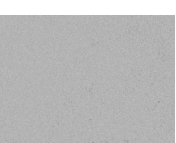
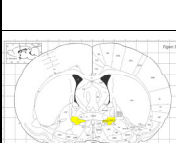
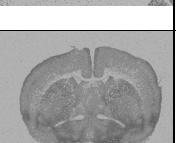
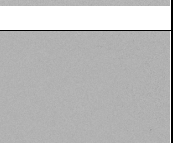
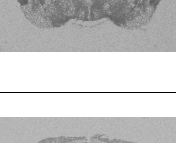
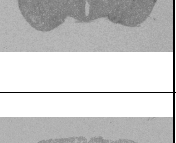
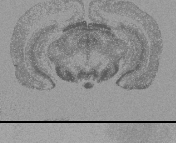
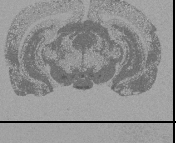
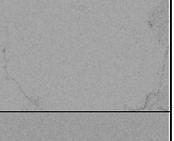
**Figure 3-03:** Shown as medians of each group for each structure with error bars representing interquartile range. No statistically significant differences, as  $P > 0.05$  (Mann-Whitney) across all structures. Structures assayed: prefrontal cortex (PFC), anterior cingulate cortex (ACg), caudate putamen (CPu), nucleus accumbens (N. acc.), bed nucleus of the striatus terminalis (BNST), anteroventral thalamic nucleus (AVTN), reticular thalamic nucleus (RTN), hippocampal regions: CA1, CA2, CA3, & dentate gyrus (DG), ventral tegmental area (VTA), dorsal raphe nuclei (DRN), locus coeruleus (LC), and cerebellum (CBL). All structures imaged with 10.0nM [<sup>3</sup>H]-WIN-35,428. Structures with no [<sup>3</sup>H]-WIN-35,428 binding reported (CA1, CA2, CA3, DG, and CBL) were either devoid of dopamine transporter binding sites or did not contain sufficient density of binding sites to meet the detection threshold for the assay.

### 3.1.3. [<sup>3</sup>H]-citalopram binding to the SERT

The distribution of [<sup>3</sup>H]-citalopram binding to the SERT (Table 3-19, Tables 3-20 to 3-27) was widespread throughout the brain, with the exception of the cerebellum (Table 3-27) where it was absent. Higher binding densities were found in structures housing the cell bodies from whence monoaminergic projections originate, such as the VTA (Table 3-25), DRN (Table 3-26), and LC (Table 3-27), with the highest binding density localized to the DRN, from whence serotonergic projections originate.

Imaging with [<sup>3</sup>H]-citalopram provided exceptionally clear delineation of all assayed structures with the sole exception of the cerebellum (Table 3-27). White matter tracts were easily distinguishable with [<sup>3</sup>H]-citalopram binding and non-specific binding was very low throughout the brain.

Selective statistically significant reductions in [<sup>3</sup>H]-citalopram binding densities were decreased 12% in the anterior cingulate cortex, decreased 11% caudate putamen, decreased 15% nucleus accumbens, and decreased 9% and decreased 15% in hippocampal areas CA2 and CA3, respectively, indicating either a change in affinity or a change in number for the [<sup>3</sup>H]-citalopram binding sites on the serotonin transporter in these structures (Figure 3-03). There were no statistically significant differences detected in any remaining structures assayed.

Table 3-19: The Distribution of the Serotonin Transporter (Overview)					
Structures	Paxinos and Watson plate	Group B		Group A	
		Total Binding in Vehicle-Treated	Nonspecific Binding in Vehicle-Treated	Total Binding in PCP-Treated	Nonspecific Binding in PCP-Treated
Prefrontal Cortex (PrL; aka PFC)					
Caudate Putamen (CPu), Cingulate Anterior (Cg1; aka ACg), Nucleus Accumbens (AcbC; aka N.acc.)					
Bed Nucleus of the Striatum Terminalis (BSTMV and BSTLV; together aka BNST)					
Anteroventral Thalamic Nucleus (AVDM and AVVL; together aka AVTN), Reticular Thalamic Nucleus (Rt; aka RTN)					
Hippocampus CA1 (CA1), Hippocampus CA2 (CA2), Hippocampus CA3 (CA3), Hippocampus Dentate Gyrus (DG)					
Ventral Tegmental Area (VTA)					
Dorsal Raphe Nuclei (DRD, DRV, and DRVL; together aka DRN)					
Locus Coeruleus (LC), Cerebellum (2; aka CBL)					

**Table 3-19:** The distribution of 2.0nM [<sup>3</sup>H]-citalopram binding to the serotonin transporter in the vehicle-treated and PCP-treated rat brain. Non-specific binding was defined in the presence of 20.0μM fluoxetine. Structures that were assayed to determine quantitative differences are specified for each level and are highlighted on the adapted Paxinos and Watson plates. This overview allows the overall distribution of the SERT throughout the brain to be observed.

Table 3-20: The Distribution of the Serotonin Transporter		
	Total Binding	Nonspecific Binding
Vehicle-Treated		
PCP-Treated		
Paxinos and Watson Plate with Structures	<p style="text-align: center;">Prefrontal Cortex (PrL; aka PFC)</p>	

**Table 3-20:** [<sup>3</sup>H]-citalopram binding to the serotonin transporter in sections of vehicle-treated and PCP-treated rat brain. Non-specific binding was defined in the presence of 20.0μM fluoxetine. Structures that were assayed to determine quantitative differences are specified for this level and are highlighted on the adapted Paxinos and Watson plate.

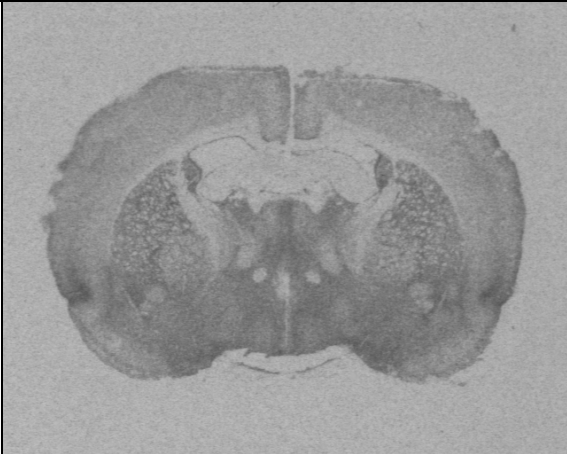
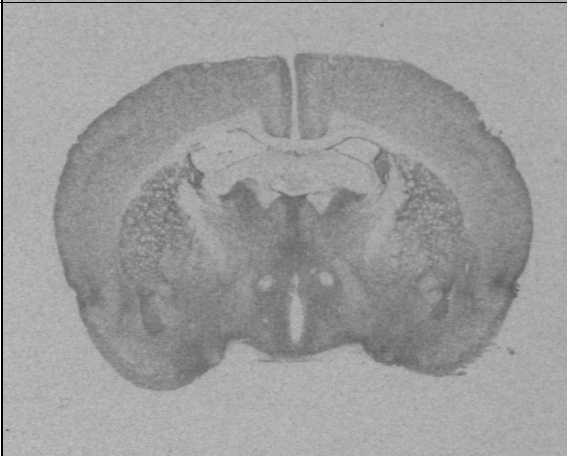
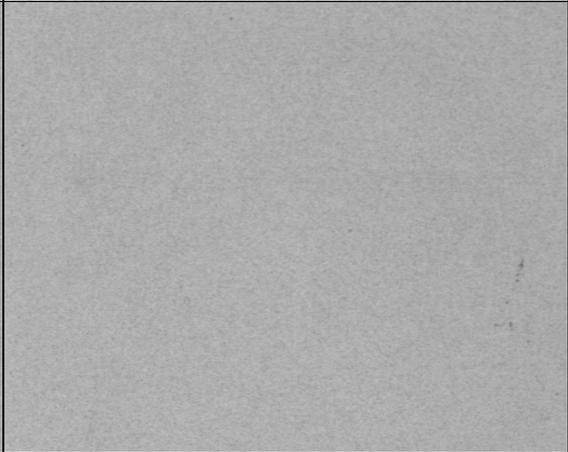
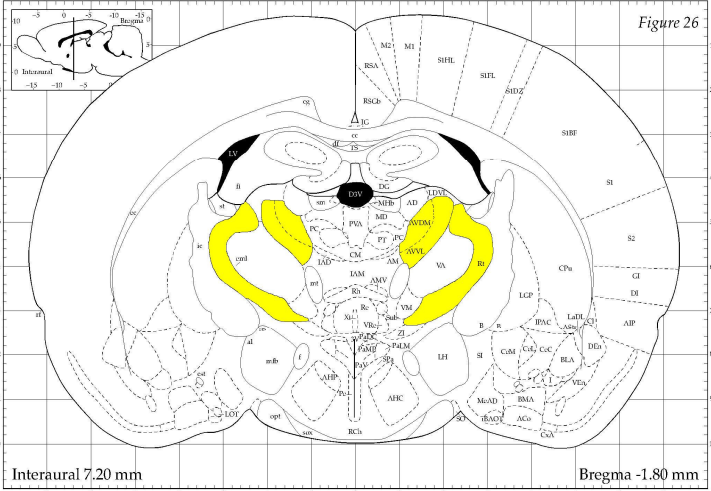
Table 3-21: The Distribution of the Serotonin Transporter		
	Total Binding	Nonspecific Binding
Vehicle-Treated		
PCP-Treated		
Paxinos and Watson Plate with Structures	<p>Figure 14</p> <p>Interaural 10.00 mm</p> <p>Bregma 1.00 mm</p> <p>Caudate Putamen (CPu), Cingulate Anterior (Cg1; aka ACg), Nucleus Accumbens (AcbC; aka N.acc.)</p>	

**Table 3-21:** [<sup>3</sup>H]-citalopram binding to the serotonin transporter in sections of vehicle-treated and PCP-treated rat brain. Non-specific binding was defined in the presence of 20.0μM fluoxetine. Structures that were assayed to determine quantitative differences are specified for this level and are highlighted on the adapted Paxinos and Watson plate.

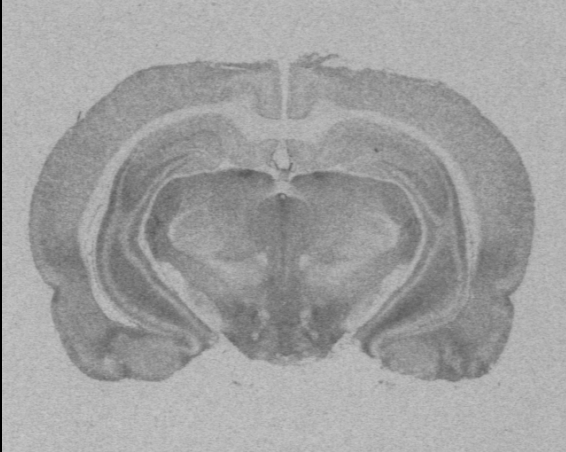
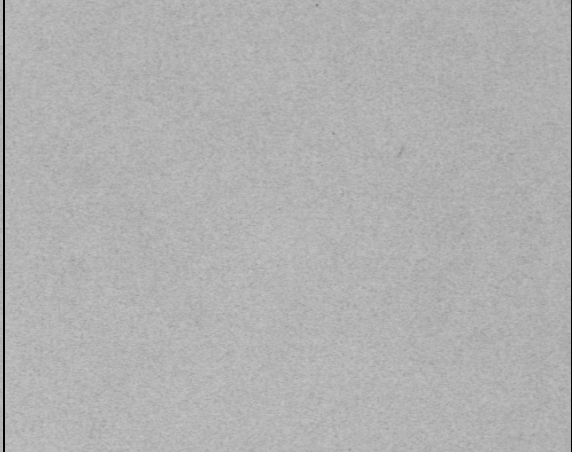
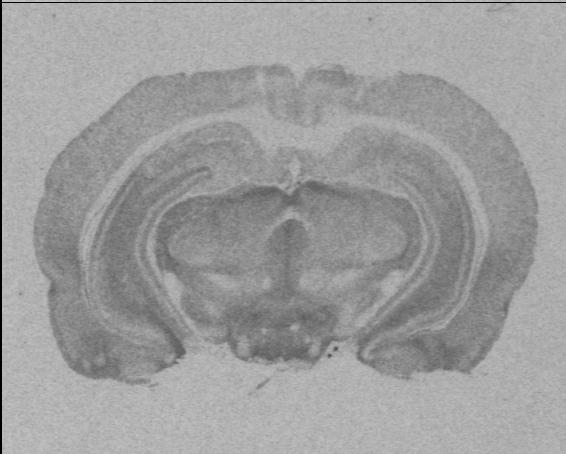
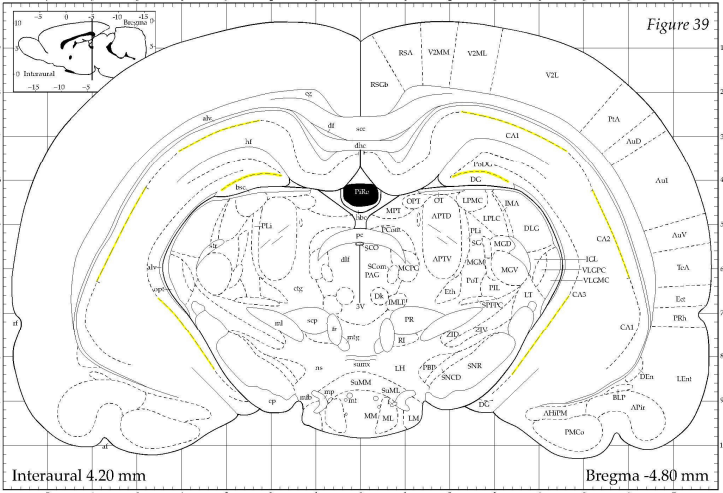
Table 3-22: The Distribution of the Serotonin Transporter		
	Total Binding	Nonspecific Binding
Vehicle-Treated		
PCP-Treated		
Paxinos and Watson Plate with Structures		

Bed Nucleus of the Striatum Terminalis (BSTMV and BSTLV; together aka BNST)

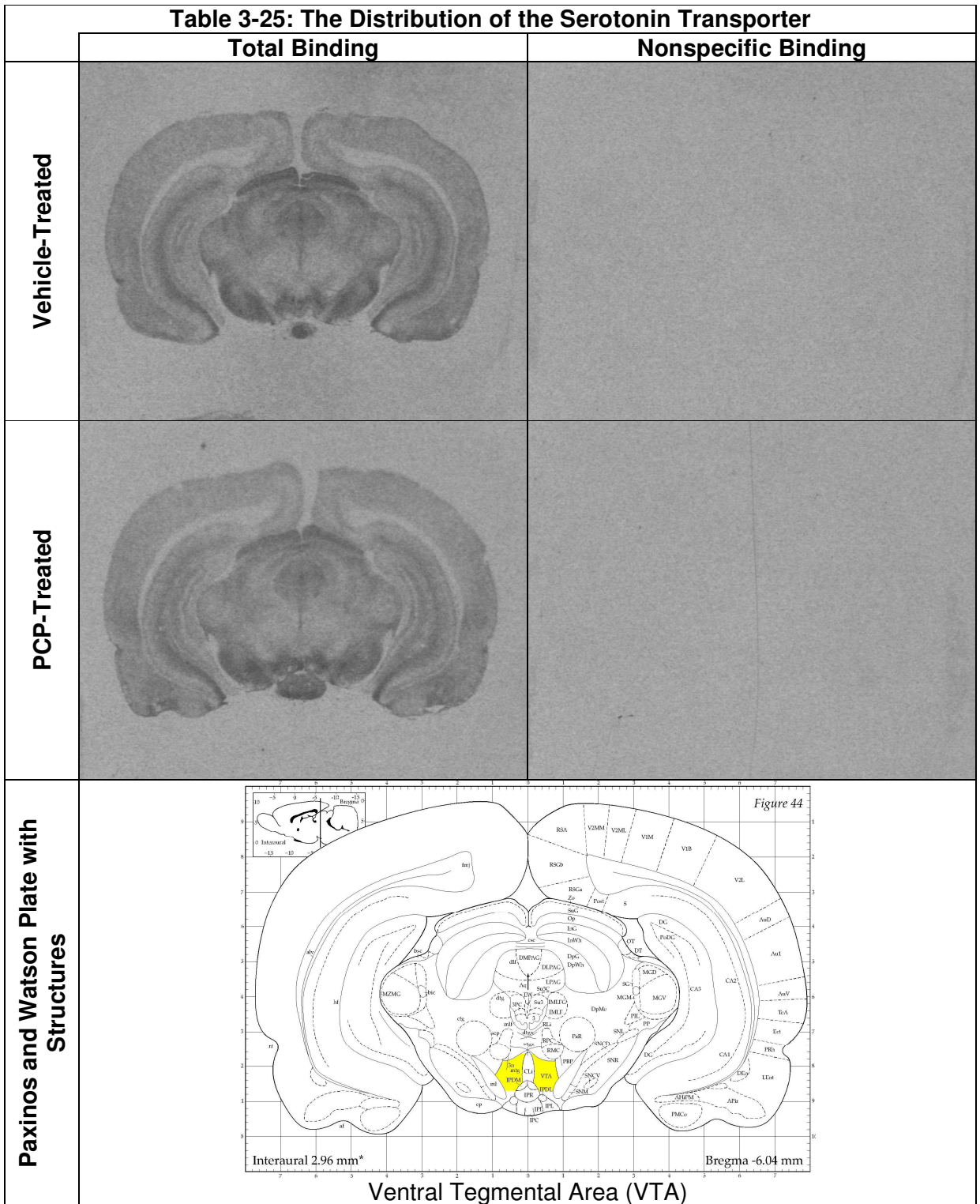
**Table 3-22:** [<sup>3</sup>H]-citalopram binding to the serotonin transporter in sections of vehicle-treated and PCP-treated rat brain. Non-specific binding was defined in the presence of 20.0μM fluoxetine. Structures that were assayed to determine quantitative differences are specified for this level and are highlighted on the adapted Paxinos and Watson plate.

Table 3-23: The Distribution of the Serotonin Transporter		
	Total Binding	Nonspecific Binding
Vehicle-Treated		
PCP-Treated		
Paxinos and Watson Plate with Structures	 <p>Anteroventral Thalamic Nucleus (AVDM and AVVL; together aka AVTN), Reticular Thalamic Nucleus (Rt; aka RTN)</p>	

**Table 3-23:** [<sup>3</sup>H]-citalopram binding to the serotonin transporter in sections of vehicle-treated and PCP-treated rat brain. Non-specific binding was defined in the presence of 20.0μM fluoxetine. Structures that were assayed to determine quantitative differences are specified for this level and are highlighted on the adapted Paxinos and Watson plate.

Table 3-24: The Distribution of the Serotonin Transporter		
	Total Binding	Nonspecific Binding
Vehicle-Treated		
PCP-Treated		
Paxinos and Watson Plate with Structures	 <p>Hippocampus CA1 (CA1), Hippocampus CA2 (CA2), Hippocampus CA3 (CA3), Hippocampus Dentate Gyrus (DG)</p>	

**Table 3-24:** [<sup>3</sup>H]-citalopram binding to the serotonin transporter in sections of vehicle-treated and PCP-treated rat brain. Non-specific binding was defined in the presence of 20.0μM fluoxetine. Structures that were assayed to determine quantitative differences are specified for this level and are highlighted on the adapted Paxinos and Watson plate.



**Table 3-25:** [<sup>3</sup>H]-citalopram binding to the serotonin transporter in sections of vehicle-treated and PCP-treated rat brain. Non-specific binding was defined in the presence of 20.0μM fluoxetine. Structures that were assayed to determine quantitative differences are specified for this level and are highlighted on the adapted Paxinos and Watson plate.





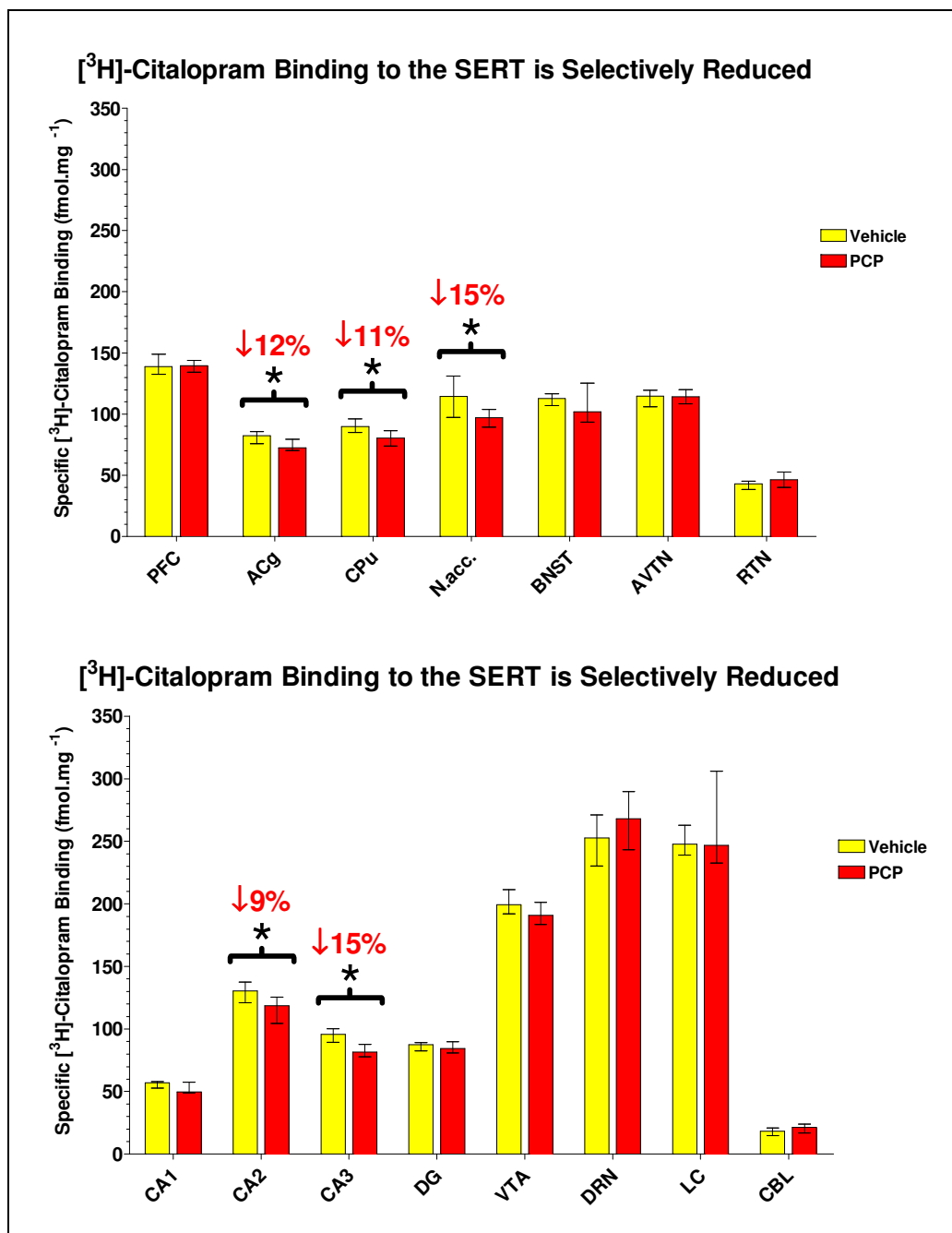


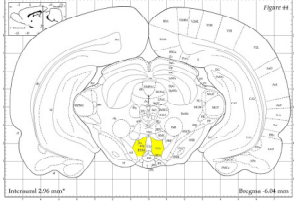
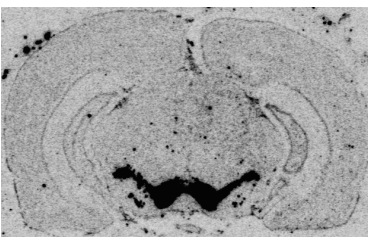
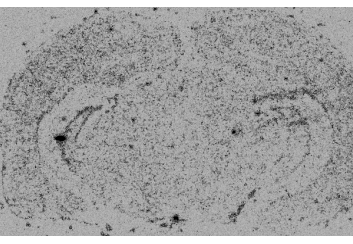
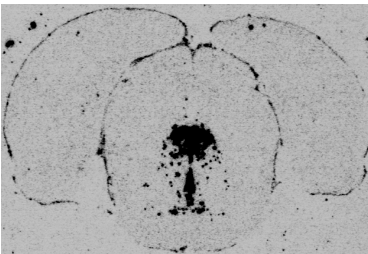
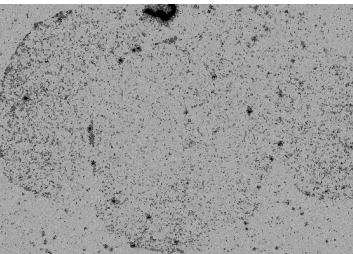
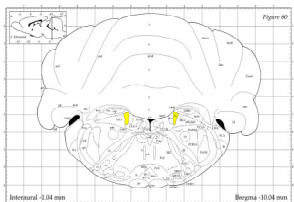
**Figure 3-04:** Shown as medians of each group for each structure with error bars representing interquartile range. Asterisks indicate statistically significant differences, where  $P < 0.05$  (Mann-Whitney), with their percentage reductions also shown. Structures assayed: prefrontal cortex (PFC), anterior cingulate cortex (ACg), caudate putamen (CPu), nucleus accumbens (N. acc.), bed nucleus of the striatus terminalis (BNST), anteroventral thalamic nucleus (AVTN), reticular thalamic nucleus (RTN), hippocampal regions: CA1, CA2, CA3, & dentate gyrus (DG), ventral tegmental area (VTA), dorsal raphe nuclei (DRN), locus coeruleus (LC), and cerebellum (CBL). All structures imaged with 2.0nM [<sup>3</sup>H]-Citalopram.

#### 3.1.4. *In situ* hybridisation results

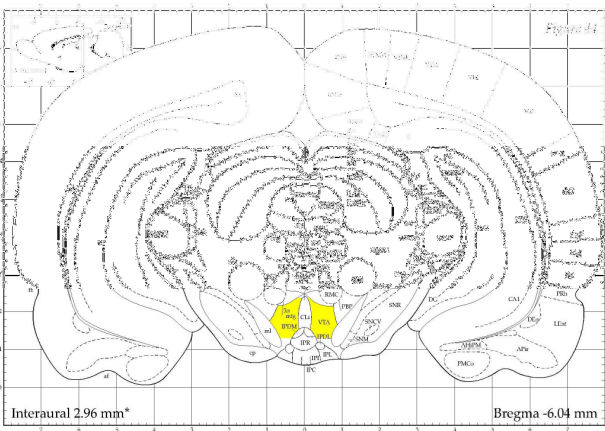
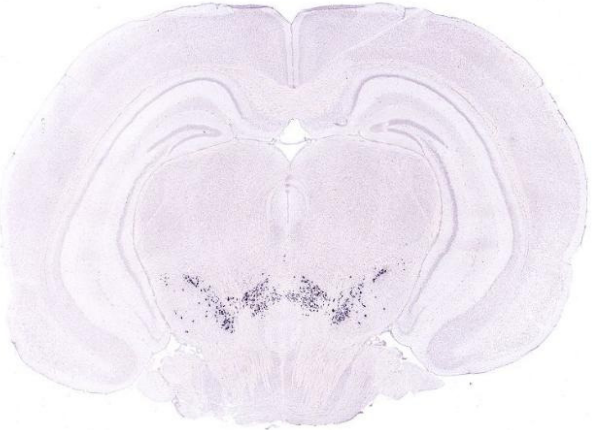
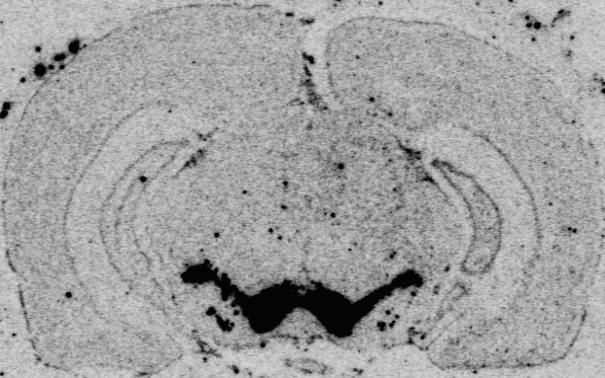
In all instances *in situ* hybridisation (Table 3-28) revealed highly specific and localised binding to the cell bodies of monoaminergic neurones, from whence monoaminergic projections originate. The NAT-specific [<sup>35</sup>S]-oligonucleotide probe binding to mRNA is both highly specific and localised to the locus coeruleus in high density (Table 3-31) and NAT-specific mRNA is also apparent in the cerebellar lobules, possibly in the granule cell layers. The DAT-specific [<sup>35</sup>S]-oligonucleotide probe binding to mRNA is both highly specific and localised to the ventral tegmental area and substantia nigra in high density (Table 3-29). The SERT-specific [<sup>35</sup>S]-oligonucleotide probe binding to mRNA is both highly specific and localised to the dorsal raphe nuclei in high density (Table 3-30).

Qualitative differences between the levels of monoaminergic transporter mRNA in control and PCP-treated animals (Figure 3-04) were not statistically significant, following a Mann-Whitney non-parametric analysis. Consequently, the unchanged levels of monoamine transporter mRNA mean that the selective reductions of [<sup>3</sup>H]-citalopram binding to the SERT is not the result of SERT-specific mRNA downregulation. Furthermore, while NAT-specific mRNA expression in the LC appeared to be slightly increased by approximately 5% relative to controls, this change was not significant.

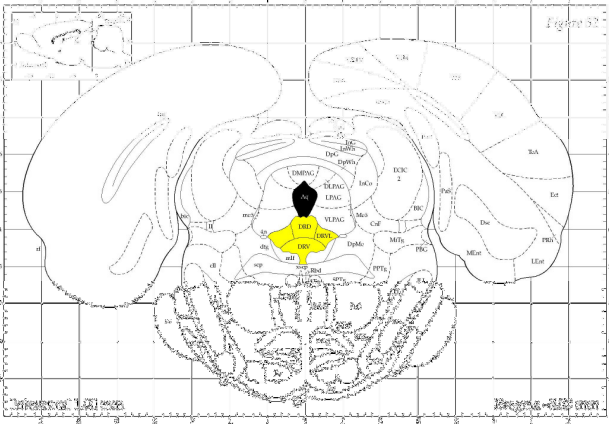
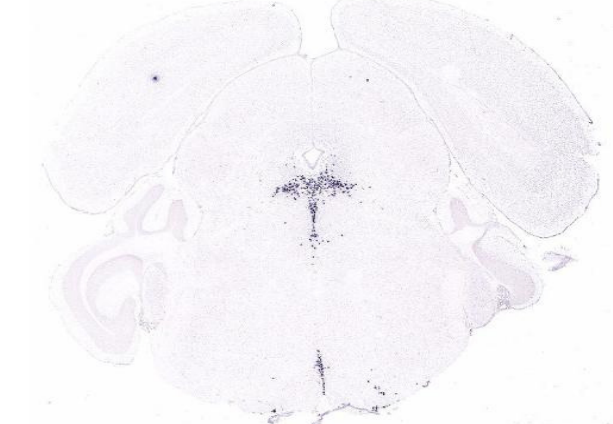
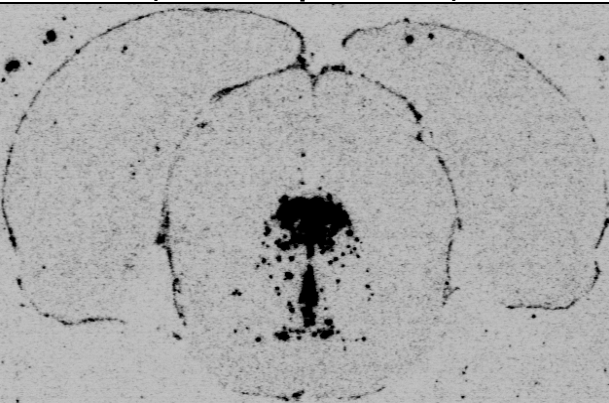
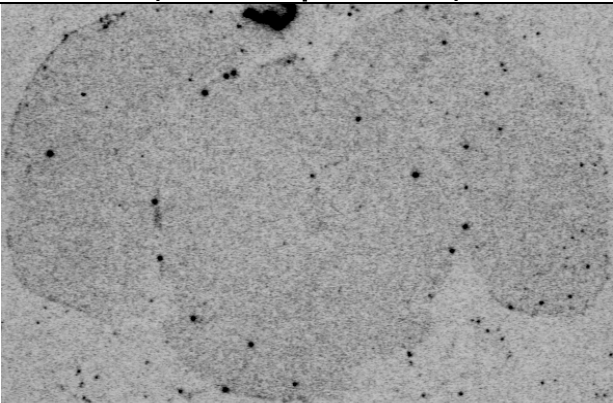
The finding that NAT mRNA is present in the cerebellum indicates that the noradrenaline transporter is being translated there rather than merely trafficked from the locus coeruleus. Therefore, the mRNA itself may have been trafficked there, or there may be cell bodies for non-locus coeruleus origin noradrenergic neurons in the cerebellum.

<b>Table 3-28: The Distribution of Monoamine Transporter mRNA</b>			
<b>Target mRNA</b>	<b>Paxinos and Watson plate with structures</b>	<b>Total Binding in Vehicle-Treated</b>	<b>Nonspecific Binding in Vehicle-Treated</b>
DAT	 <p>Ventral Tegmental Area (VTA)</p>		
SERT	 <p>Dorsal Raphe Nuclei (DRD, DRV, and DRVL; together aka DRN)</p>		
NAT	 <p>Locus Coeruleus (LC)</p>		

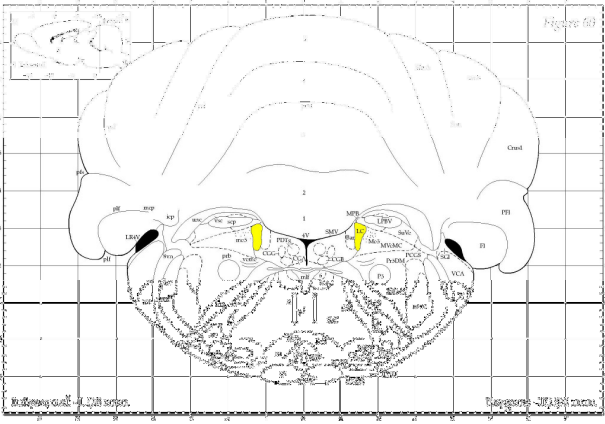
**Table 3-28:** The distribution of [<sup>35</sup>S]-oligonucleotide *in situ* hybridisation probe binding to monoamine transporter mRNA in vehicle-treated rat brain. Structures that were assayed to determine qualitative differences are specified for each level and are highlighted on the adapted Paxinos and Watson plates. There was no discernable difference between the sections of vehicle-treated and PCP-treated rat brains.

Table 3-29: <i>In situ</i> Hybridisation of DAT-specific mRNA	
Paxinos and Watson Rat Brain Atlas Anatomical Reference (Ventral Tegmental Area)	Allen Brain Atlas: DAT mRNA <i>in situ</i> Hybridisation Specific Binding (Ventral Tegmental Area in Mouse Brain)
	
DAT mRNA <i>in situ</i> Hybridisation Total Binding (Ventral Tegmental Area)	DAT mRNA <i>in situ</i> Hybridisation Non-Specific Binding (Ventral Tegmental Area)
	

**Table 3-29:** *In situ* hybridisation imaging of DAT-specific mRNA in the ventral tegmental area (VTA) of control rat brains. The optical density of [<sup>35</sup>S]-oligonucleotide probe binding in the VTA was qualitatively assayed and Mann-Whitney statistical analysis determined no statistical differences. PCP-treated rat brains are also visually indistinguishable from controls.

<b>Table 3-30: <i>In situ</i> Hybridisation of SERT-specific mRNA</b>	
<b>Paxinos and Watson Rat Brain Atlas Anatomical Reference (Dorsal Raphe Nuclei)</b>	<b>Allen Brain Atlas: SERT mRNA <i>in situ</i> Hybridisation Specific Binding (Dorsal Raphe Nuclei in Mouse Brain)</b>
	
<b>DAT mRNA <i>in situ</i> Hybridisation Total Binding (Dorsal Raphe Nuclei)</b>	<b>DAT mRNA <i>in situ</i> Hybridisation Non-Specific Binding (Dorsal Raphe Nuclei)</b>
	

**Table 3-30:** *In situ* hybridisation imaging of SERT-specific mRNA in the dorsal raphe nuclei (DRN) of control rat brains. The optical density of [<sup>35</sup>S]-oligonucleotide probe binding in the DRN was qualitatively assayed and Mann-Whitney statistical analysis determined no statistical differences. PCP-treated rat brains are also visually indistinguishable from controls.

<b>Table 3-31: <i>In situ</i> Hybridisation of NAT-specific mRNA</b>	
<b>Paxinos and Watson Rat Brain Atlas Anatomical Reference (Locus Coeruleus)</b>	<b>Allan Brain Atlas: NAT mRNA <i>in situ</i> Hybridisation Specific Binding (Locus Coeruleus in Mouse Brain)</b>
	
<b>NAT mRNA <i>in situ</i> Hybridisation Total Binding (Locus Coeruleus)</b>	<b>NAT mRNA <i>in situ</i> Hybridisation Non-Specific Binding (Locus Coeruleus)</b>
	

**Table 3-31:** *in situ* hybridisation imaging of NAT-specific mRNA in the locus coeruleus (LC) of control rat brains. The optical density of [<sup>35</sup>S]-oligonucleotide probe binding in the LC was qualitatively assayed and Mann-Whitney statistical analysis determined no statistical differences. PCP-treated rat brains are also visually indistinguishable from controls.

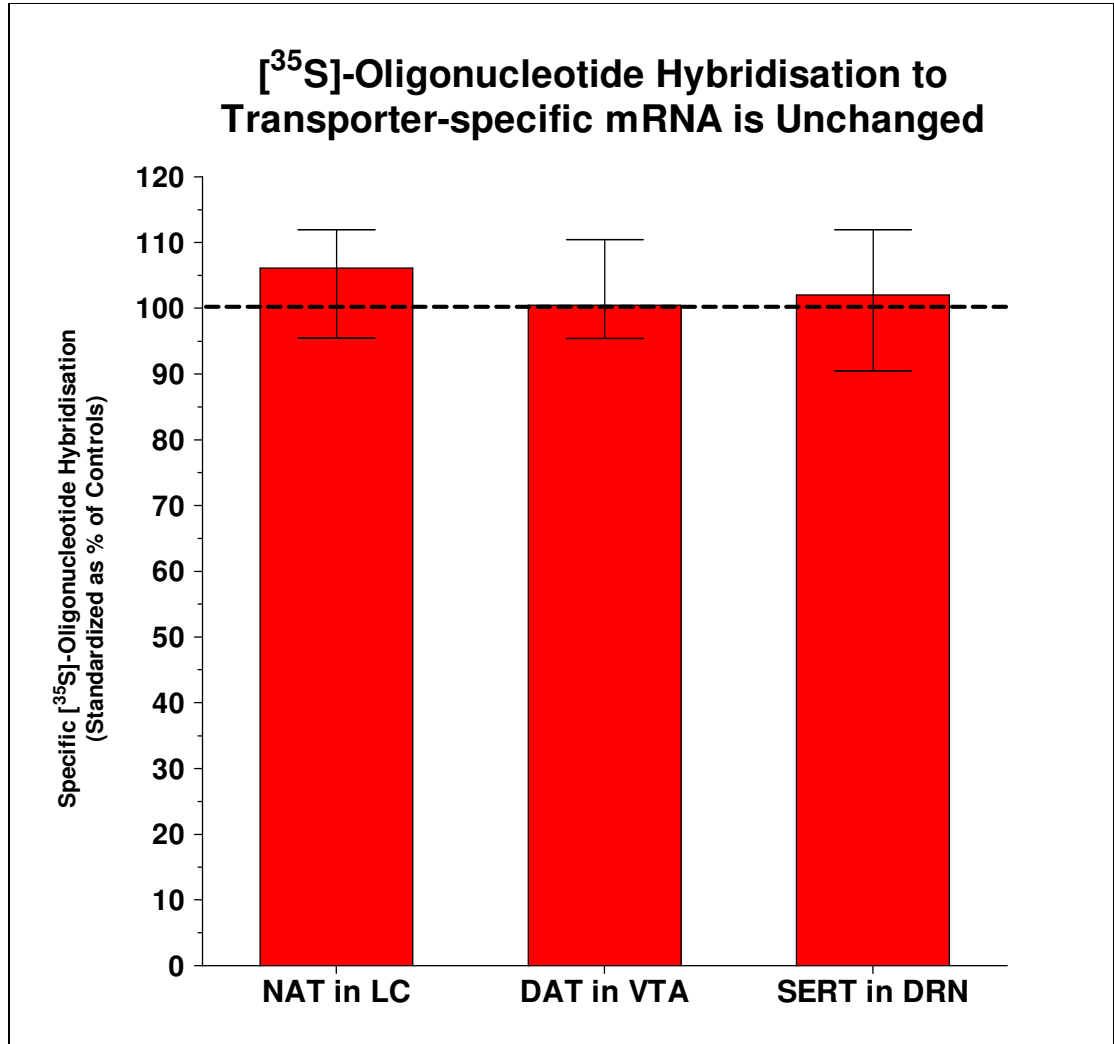


**Figure 3-04:** Shown as medians of the PCP-treated group for the locus coeruleus (LC), ventral tegmental area (VTA) and dorsal raphe nuclei (DRN) relative to the median of the vehicle-treated group. Error bars represent interquartile range. No statistically significant differences between the groups, as  $P > 0.05$  (Mann-Whitney). Transporter-specific mRNA localisations imaged with [<sup>35</sup>S]-labelled oligonucleotide probes.

## **3.2 Discussion/Conclusions**

### **3.2.1 The noradrenergic system**

It was hypothesized that the NAT would have been down-regulated in the prefrontal cortex (PFC) because the dopaminergic hypothesis of schizophrenia proposes hypoactivity in dopaminergic projections to the PFC (van Rossum 1966; Carlsson & Lindqvist 1963; Frankle et al. 2005b; Marek 2007; Laruelle et al. 2005; Abi-Dargham 2004), hypometabolism has been demonstrated in the PFC in both schizophrenia and in the PCP-induced model, and the NAT is the dominant dopamine reuptake mechanism in the PFC (Moron et al. 2002). Similarly, other areas, such as the thalamic regions where a reduction in metabolism has been demonstrated (Cochran et al. 2003; Morris et al. 2005) and hippocampal regions where tissue atrophy is known to occur (Suddath et al. 1990), have also shown no significant difference in NAT binding densities indicating that NAT number and affinity remain unperturbed in this model. If a change in binding densities had been detected, it could indicate either a change in affinity between the ligand and binding site or a change in binding site number. A decrease in NAT expression in these regions would have indicated that noradrenergic neurones projecting into them are less active, thus reducing the modulation exacted upon these regions by the noradrenaline system. It was also apparent that the unchanged qualitative measurements of NAT-specific mRNA indicated that there were no upregulations of mRNA to compensate for the downregulated NAT concentrations that were hypothesized but not found. It would be interesting to know whether synaptic concentrations of noradrenaline are effected in any of these areas or if the apparent normality of NAT density is indicative of undisrupted noradrenergic neurotransmission to these critical structures. Noradrenaline has been shown to be depleted by the administration of PCP (Tonge & Leonard 1972), so a follow-up on noradrenaline concentrations in this particular model could make an interesting future study. If NAT concentrations are unchanged while noradrenaline concentrations decrease, then this would reduce the duration of stimulation by noradrenaline of the postsynaptic receptors upon quantal release into the synapse. Conversely, if NAT concentrations are unchanged while noradrenaline concentrations increase, then the stimulation of postsynaptic receptors by

noradrenaline could be prolonged following a slower synaptic clearance if reuptake and metabolism mechanisms are overwhelmed.

As the NAT is located on presynaptic neurons, the biological significance of the highest binding density for [<sup>3</sup>H]-nisoxetine detected in the locus coeruleus means that this structure is where the majority of noradrenergic modulation occurs – noradrenergic interneurons communicating with other nearby neurons within the locus coeruleus. Consequently, there is an argument that the primary brain region of interest in the noradrenergic system and the most important one for any potential SPECT tracer to image is the locus coeruleus.

It is important to note that despite the sections containing the locus coeruleus and the cerebellum receiving a lower concentration of [<sup>3</sup>H]-Nisoxetine, the lowest binding density reported for the NAT was not in the cerebellum but in the caudate putamen (CPu). This is highly relevant to *in vivo* NAT imaging because in both SPECT and PET imaging, a reference region is selected to determine the nonspecific binding of the ligand and the cerebellum is a common choice for many ligands. Indeed, where NAT imaging is concerned, the cerebellum clearly demonstrates specific binding to the NAT and thus is not suitable for use as a reference region. Given the extremely low specific NAT binding density reported in the CPu, this would make a far more acceptable structure to use as a reference region.

Interestingly, mRNA for the noradrenaline transporter was detected in the cerebellum. The cerebellum receives noradrenergic innervation from the locus coeruleus (Kolasiewicz et al. 2011) and stimulates the firing of globular and Golgi cells (Hirono et al. 2012). Therefore, there is the possibility that in the instance of the cerebellum that NAT mRNA is trafficked to the cerebellum from the locus coeruleus rather than the NAT protein itself. The electrophysiology experiments of Hirono et al, which showed that noradrenaline stimulates cells in the cerebellum, would suggest that noradrenaline transporters in the cerebellum are probably functional as there is a need for them to be there – clearance of released noradrenaline from synapses would be slow if the sole mechanism for this was metabolism by MAO and COMT.

### 3.4.2 The dopaminergic system

It was hypothesized that changes in the binding density for the DAT would have been detected in agreement with the dopaminergic hypothesis for schizophrenia proposing hyperactivity in mesolimbic and/or mesocortical pathways and the mechanism for many traditional neuroleptics is the antagonism of dopaminergic neurotransmission. However, although there was a general trend across many limbic structures to indicate an increase in the density of DAT binding in these regions, no measurements demonstrated a significant difference, corresponding to published data (Laruelle et al. 2000). Another hypothesis that was not fulfilled was the one of areas demonstrating hypometabolism to have expressed changes in the binding density of DAT, but no significant differences were detected and furthermore no statistically insignificant trends were identified either. The qualitative measurement of DAT-specific mRNA in the VTA indicated no significant differences between control and PCP-treated rats, indicating that no upregulation took place to compensate for the hypothesized downregulations of DAT. It would be interesting to know whether synaptic concentrations of dopamine are affected in any of these areas or if the apparent normality of DAT density is indicative of undisrupted noradrenergic neurotransmission to such structures.

It is important to note that DAT was not detected in any hippocampal structures for either the control or PCP-treated groups, so although this area appears to play a role – either primary or secondary – in the pathology of schizophrenia, it is unlikely that the DAT is involved in these structures. The absence of detectable DAT concurs with published autoradiographic studies using [<sup>3</sup>H]-WIN-35,428 (Andersen et al. 2005) and PET studies imaging DAT (Goodman et al. 2000).

The binding densities of [<sup>3</sup>H]-WIN-35,428 to the DAT were also below that of the detection threshold in the cerebellum, indicating that while this structure would not be suitable for use as a reference region for NAT, it would be perfectly adequate as such for *in vivo* imaging of the DAT with SPECT or PET scanning technologies.

### 3.4.3 The serotonergic system

The selective reductions in the hippocampus correlate anatomically to regions shown through MRI imaging and *post mortem* analyses to be compromised in

schizophrenia. Broadly, this correlates with previous studies that have also found selective decreases of SERT binding in areas of the forebrain (Joyce et al. 1993; Ohuoha et al. 1993; Laruelle et al. 1993). In areas with unchanged levels of [3H]-citalopram binding in the forebrain, the binding levels and overall autoradiograph appearance correlated well with published literature (Hipolide et al. 2005). Further correlating with published data, there were no statistically significant changes detected in the hindbrain structures (Laruelle et al. 2000). Where there was some variation with the literature, Dean *et al* ( 1995) found an increase in affinity, but no change in the density, of SERT binding sites in the hippocampus. PCP administration in rat has been shown to directly deplete noradrenaline and its metabolites (Tonge & Leonard 1972), so if a similar effect occurs in the serotonergic system then this might explain why fewer SERTs are maintained.

As discussed earlier in this thesis, the serotonin system is the most widely innervated of all the monoamine systems and the abundance of SERT labelled throughout the brain was not unforeseen. The assayed region with the lowest density of SERT detected was the cerebellum, and would perhaps make a suitable reference region for *in vivo* SERT imaging.

In the corticolimbothalamic circuitry known to be deranged in schizophrenia (Morris et al. 2005), the prefrontal cortex stimulates the nucleus accumbens, which inhibits the ventral pallidum, which inhibits the thalamus – disinhibition – to enable thalamic stimulation of the prefrontal cortex and thus complete a circuit of positive feedback. Meanwhile, the prefrontal cortex and the hippocampus modulate one another. These results, in context, would indicate that a 15.3% reduction in SERT affinity or number in the nucleus accumbens might cause some of the disinhibition of the thalamus to be removed, thus reducing the positive feedback on the prefrontal cortex. However, binding of all three monoamine transporters seem unaffected in thalamic structures. The binding reductions found in the hippocampus, a structure involved in mutual modulation with the prefrontal cortex proves interesting. The dentate gyrus is the ‘gateway’ to the hippocampus and yet binding densities here are normal. Internally, in the CA2 and CA3, selective reductions in SERT binding were found but it is difficult to see how this would impact the prefrontal cortex unless the dentate gyrus was involved as well.

Although these are statistically significant reductions and do affect some key regions in the deranged circuitry involved in the pathogenesis of schizophrenia, it begs the question as to whether a reduction of up to only 15% of the transporters for only one of the monoamine systems has a biological significance. It is already known that monoamine transporters are promiscuous with the monoamines they uptake, and with the complexity of monoamine systems and their intermodulation in the brain, it seems as though such small reductions may very well be within the tolerances provided by natural redundancies in the brain. It has also been noted that SERT binding densities are not significantly correlated with the severity of symptoms (Abi-Dargham 2007). Furthermore, the decreased SERT affinity in the hippocampus and decreased density in the frontal cortical regions reported by *post mortem* studies were not confirmed by *in vivo* studies where no significant differences were observed in SERT expression (Frankle et al. 2005a) – so this aspect of the model may very well mimic an artefact of post mortem tissue that is not relevant in the living schizophrenic.

Interestingly, there appeared to be no significant differences in the levels of SERT-specific mRNA in the DRN to attempt to compensate for the reductions in SERT found in the PCP model of the metabolic hypofrontality associated with schizophrenia. As with the synaptic concentrations of noradrenaline and dopamine, it would be interesting to know what the concentrations of serotonin were in the regions where selective reductions were detected and whether the selective reductions in SERT have produced a corresponding rise in the concentrations of neurotransmitter following neuronal activation, or whether the reductions in SERT appear to have occurred following a reduction of serotonin release.

#### **3.4.4 Conclusions**

The PCP-induced rat model mimics the metabolic hypofrontality observed in schizophrenia and is not a complete reproduction of all aspects involved in the human disease. Interestingly, aspects of the model appear to correlate *post mortem* examination of schizophrenic patients, while reductions of serotonin transporter expression were not apparent during an *in vivo* scan of living medication-free schizophrenic patients. However, this may very well be explained

by the changes in SERT density being too small and beneath the detection threshold for PET imaging.

It had been hypothesised that down-regulation of the NAT would be observed, particularly in the pre-frontal cortex, of the PCP-induced rat model of the metabolic hypofrontality observed in schizophrenia. However, the NAT distribution and density remained unchanged by chronic low-dose PCP administration, so the model does not yield itself as an obvious choice for first demonstration of an emerging NAT-specific SPECT brain imaging tracer. While there were no changes detected in NAT levels or NAT-specific mRNA in this model, pharmacological intervention exerting influence at the noradrenaline transporter is beneficial in modulating monoaminergic neurotransmission in both the model and in the human disease, so it is clear that the NAT is important in how schizophrenia treatment is approached. In order to ensure a wider access to *in vivo* imaging techniques in research, a SPECT tracer would be preferable to a PET tracer due to the lower costs involved in SPECT imaging associated with using more readily available isotopes with longer half-lives. Currently, there is no SPECT imaging tracer for imaging the noradrenaline transporter *in vivo* so NAT levels in the medication-free schizophrenic patient cannot yet be compared to those of the model to determine whether the model holds true.

Furthermore, in the development of new antipsychotic drugs to treat schizophrenia, it will be important to have a readily available biomarker of *in vivo* NAT occupancy to demonstrate dose-occupancy and therapeutic benefit, as has been done at other antipsychotic drug targets in the brain – such as the SERT (Takano et al. 2006). Therefore, compounds structurally related to the clinically-approved selective noradrenergic reuptake inhibitor reboxetine will be examined for their suitability for radiolabelling with SPECT-applicable isotopes and potential for use as SPECT brain imaging tracers.

It had been hoped that if changes in NAT expression were present in this model then it would have presented itself as a valuable opportunity for validating and demonstrating the imaging capabilities of a future NAT-specific SPECT tracer, however another model that can demonstrate a clear difference in NAT density will have to be sought for that purpose. Nevertheless, the PCP model of

schizophrenic hypofrontality still provides valuable insight into aspects of schizophrenia.

## Chapter 4

# Pharmacological Characterisation of Potential SPECT Brain Imaging Tracers for the Noradrenaline Transporter

### 4.3 Results

#### 4.3.1 Reboxetine affinity for the NAT

The  $K_i$  of Reboxetine, a commercial available *S,S*-/*R,R*- racemic mixture available as a mesylate salt, against [ $^3\text{H}$ ]-nisoxetine binding at the NAT was determined as  $6.9 \pm 1.6$  nM (Figure 1). This is in the same order of magnitude as, and therefore compares favourably to, the published value of  $1.1 \pm 0.2$  nM (Wong et al. 2000). Given the highly selectivity (>100-fold) of reboxetine for the NAT, and published data in the literature on its monoamine binding profile, it was deemed unnecessary to repeat this validation at the SERT or the DAT in this thesis.

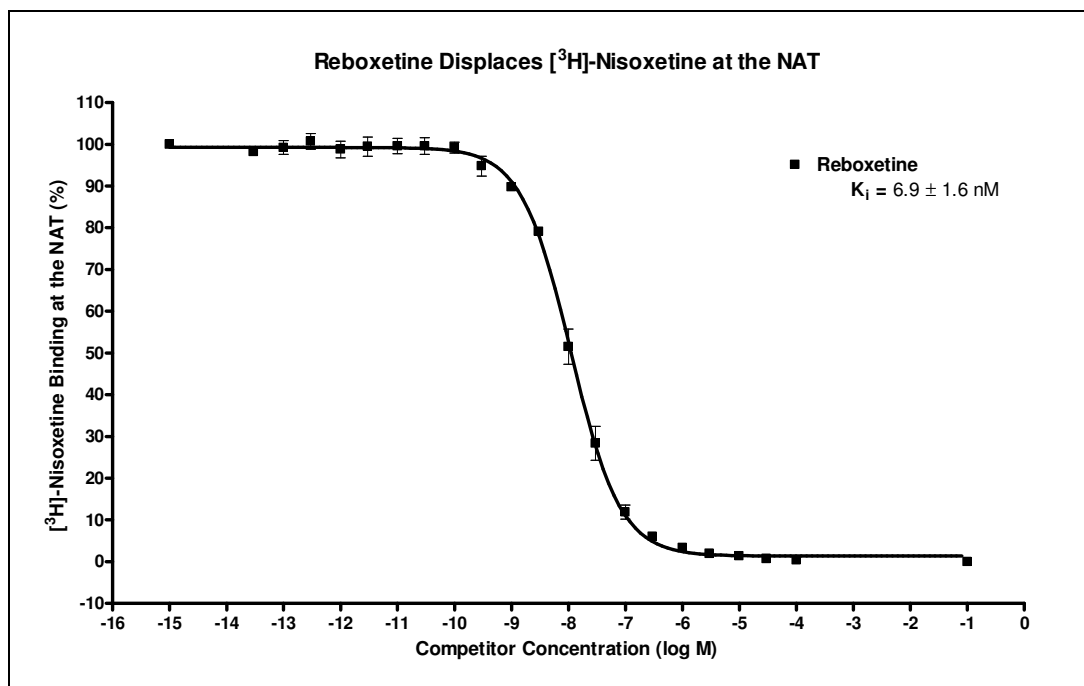


**Figure 4-01:** Reboxetine competes for [<sup>3</sup>H]-nisoxetine binding to the noradrenaline transporter. Points are means of 3 independent repetitions and error bars represent standard error of the mean. K<sub>i</sub> value is represented as the mean of 3 independent determinations ± the standard deviation, and was calculated from the IC<sub>50</sub> using the Cheng-Prusoff equation in GraphPad Prism 4.0.

#### 4.1.2 Affinity of novel compounds for the NAT

The iodophenyl ring compounds (Figure 4-02) demonstrated greatest affinity for the NAT in the *S,S*-, *R,S*-, and *R,R*-isomers with  $K_i$  values of  $53.8 \pm 2.7$  nM,  $58.2 \pm 9.4$  nM, and  $64.0 \pm 2.4$  nM, respectively. The *S,R*-isomer was an order of magnitude greater at  $321 \pm 9$  nM, so this conformation obviously does not allow the molecule to bind effectively to the [<sup>3</sup>H]-nisoxetine binding site. While the curve clearly shows that these compounds are offering specific displacement of [<sup>3</sup>H]-nisoxetine at the NAT, a  $K_i$  of ~54nM is not sufficiently high affinity for a SPECT brain imaging tracer.

While none of the iodophenyl ring compounds have sufficient affinity for the NAT, the differing affinities with structural modification are enlightening. For the next generation of candidate compounds, no further *S,R*- conformations were synthesised, as it was clear this conformation is not suitable for binding to the reboxetine binding site on the NAT. As expected, the *S,S*- and *R,R*- conformations both showed better affinity and the *S,S*- conformation molecule is what is being taken forward by other groups in the literature as the INER/IPBM molecule. The *R,S*- conformation molecule has not yet been developed in the literature, and perhaps an INER/IPBM-like molecule in this conformation would yield a promising candidate for SPECT imaging of the NAT. For further elucidation of important aspects to the molecular structure of potential NAT tracers, several of the intermediate compounds in the synthetic process were also evaluated for their affinity to the NAT.

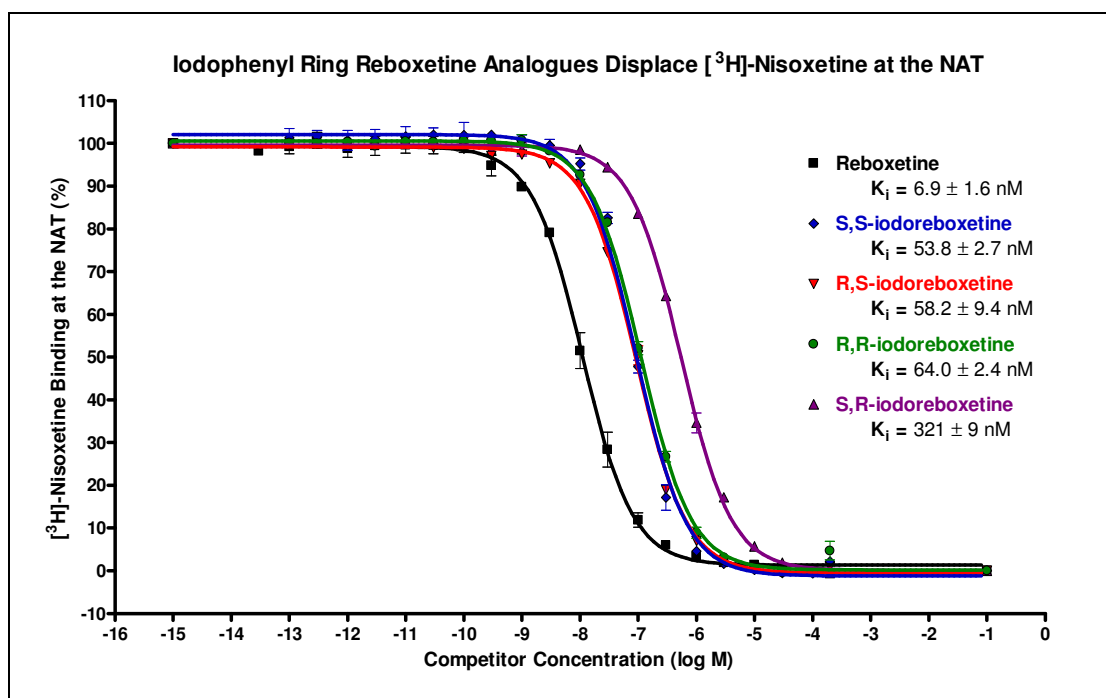


**Figure 4-02:** Iodophenyl ring iodoreboxetine analogues displacement of [<sup>3</sup>H]-nisoxetine binding at the noradrenaline transporter. Data points are means of 3 independent repetitions and error bars represent standard error of the mean. Total binding (1.2nM [<sup>3</sup>H]-nisoxetine) plotted as competitor concentration  $10^{-15}$ M and non-specific binding (1.2nM [<sup>3</sup>H]-nisoxetine + 10  $\mu$ M reboxetine) plotted as  $10^{-1}$ M.  $K_i$  values are represented as the mean of 3 independent determinations  $\pm$  the standard deviation, and was calculated from the  $IC_{50}$  using the Cheng-Prusoff equation in GraphPad Prism 4.0.

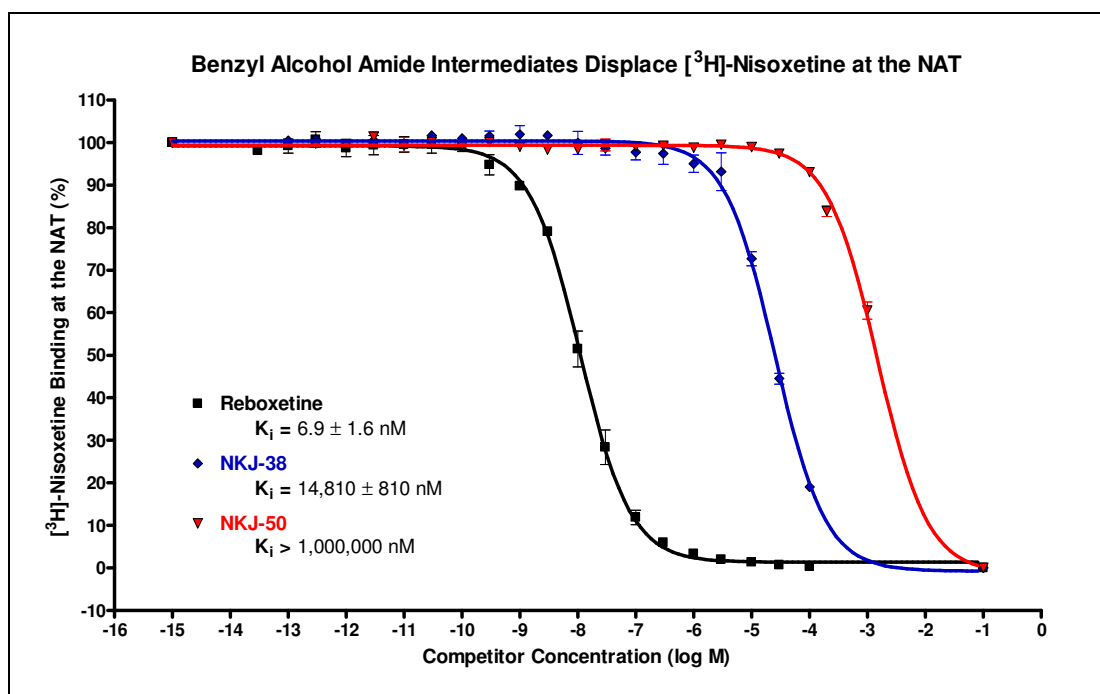


**Figure 4-03:** Benzyl alcohol intermediate compounds displacement of [<sup>3</sup>H]-nisoxetine binding at the noradrenaline transporter. Data points are means of 3 independent repetitions and error bars represent standard error of the mean. Total binding (1.2nM [<sup>3</sup>H]-nisoxetine) plotted as competitor concentration  $10^{-15}$ M and non-specific binding (1.2nM [<sup>3</sup>H]-nisoxetine + 10  $\mu$ M reboxetine) plotted as  $10^{-1}$ M.  $K_i$  values are represented as the mean of 3 independent determinations  $\pm$  the standard deviation, and was calculated from the  $IC_{50}$  using the Cheng-Prusoff equation in GraphPad Prism 4.0.

The benzyl alcohol amides demonstrated particularly poor affinity ( $K_i = \mu\text{M}$ -mM range) for the NAT (Figure 4-03) and the loss of the phenoxy ring appears to have destroyed the ability of the compound to bind to the NAT, highlighting the importance of this ring in reboxetine-like compound pharmacology.

*R,S*- conformation iodophenoxy compounds (Figure 4-04) demonstrated excellent affinity when the iodine was in the ortho position in the NKJ-64 ( $K_i = 8.4\text{nM}$ ), yet poor affinity otherwise. The poor binding exhibited when the phenoxy ring's iodine was in the meta and para positions for NKJ-67 ( $K_i = 1.1\mu\text{M}$ ) and NKJ-68 ( $K_i = 1.7\mu\text{M}$ ), respectively, is further evidence of this ring conferring binding affinity to the NAT and that there is an ideal position (ortho) for the iodine in order to maintain affinity of the compound for the [ $^3\text{H}$ ]-nisoxetine binding site on the NAT.

Of the iodinated compounds synthesised and tested (Table 4-01), NKJ-64 yielded the most potent affinity for NAT ( $K_i = 8.4 \pm 1.7 \text{ nM}$ ), was in the same order of magnitude as reboxetine ( $K_i = 6.9 \pm 1.6 \text{ nM}$ ), and looks to be the most promising compound tested here.

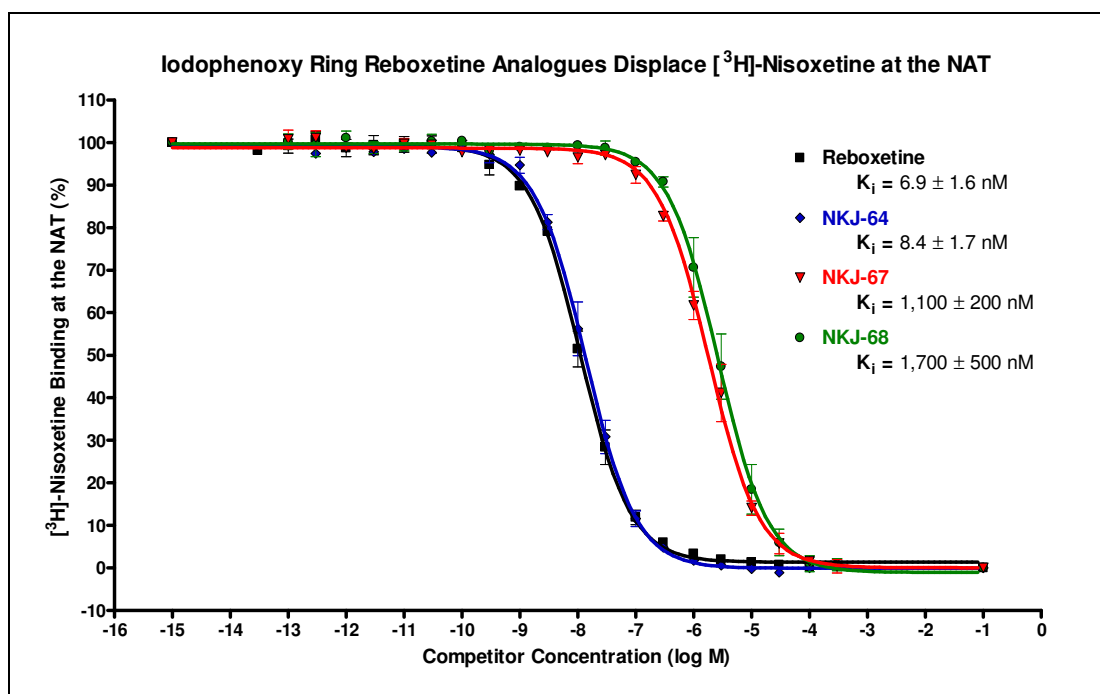


**Figure 4-04:** Iodophenoxy ring reboxetine analogues displacement of [<sup>3</sup>H]-nisoxetine binding at the noradrenaline transporter. Data points are means of 3 independent repetitions and error bars represent standard error of the mean, except for NKJ-64 which is derived from 5 independent repetitions. Total binding (1.2nM [<sup>3</sup>H]-nisoxetine) plotted as competitor concentration 10<sup>-15</sup>M and non-specific binding (1.2nM [<sup>3</sup>H]-nisoxetine + 10 μM reboxetine) plotted as 10<sup>-1</sup>M. K<sub>i</sub> values are represented as the mean of 3 independent determinations ± the standard deviation, except for NKJ-64 which is derived from 5 independent determinations. All K<sub>i</sub> values were calculated from the IC<sub>50</sub> using the Cheng-Prusoff equation in GraphPad Prism 4.0.

Table 4-01: Affinity of iodinated reboxetine analogues for the NAT		
Group	Compounds	NAT K <sub>i</sub>
Iodophenyl ring analogues	( <i>S,R</i> )-iodoreboxetine	321 ± 9 nM
	( <i>R,S</i> )-iodoreboxetine	58.2 ± 9.4 nM
	( <i>S,S</i> )-iodoreboxetine	53.8 ± 2.7 nM
	( <i>R,R</i> )-iodoreboxetine	64.0 ± 2.4 nM
Benzyl alcohol amide intermediates	NKJ-38	14,810 ± 810 nM
	NKJ-50	> 1,000,000 nM
Iodophenoxy ring analogues	NKJ-64	8.4 ± 1.7 nM
	NKJ-67	1,700 ± 500 nM
	NKJ-68	1,100 ± 200 nM

**Table 4-01:** Summary of affinity of novel iodoreboxetine compounds for the NAT.

### 4.1.3 Serotonin Transporter Pharmacology

The iodophenyl ring compounds (Figure 4-05) demonstrated greatest affinity for the SERT in the (*R,R*)-isomer with a  $K_i$  of  $646 \pm 146$  nM and, consequently, the (*S,S*)-isomer shows greater promise as a NAT-specific tracer with a much lower affinity for the [ $^3$ H]-citalopram binding site and a  $K_i$  of approximately 2.8  $\mu$ M.

Unfortunately, depleted stocks for the (*S,R*)- and (*R,S*)- isomers of the iodophenyl ring compounds resulted in the inability to ascertain their inhibition constants at the SERT through a comprehensive displacement protocol, so a pilot experiment was conducted to determine if there was any affinity for the SERT (Figure 4-06), revealing minimal displacement of [ $^3$ H]-citalopram binding to the SERT. Reboxetine was shown to displace virtually all [ $^3$ H]-citalopram binding at the SERT when applied in both 10 $\mu$ M and 100 $\mu$ M concentrations. Both of the iodinated reboxetine analogues demonstrated less affinity for the SERT than reboxetine. The *S,R*- isomer demonstrated less affinity for the SERT than the *R,S*- isomer, however the precise affinity of these compounds was not able to be determined with the solution stocks remaining following assays at other monoamine transporter sites. Additional compound could be synthesised for a comprehensive characterisation, but the poor NAT affinity of the *S,R*- isomer precludes further development as a NAT tracer and makes a comprehensive characterisation of these particular compounds inconsequential.

The benzyl alcohol amides are intermediate compounds in the production of the iodophenoxy reboxetine analogues and their characterisation aids in determining which aspects of reboxetine-like compounds are contributing to the pharmacological properties of the molecule. The benzyl alcohol amide intermediates demonstrated particularly poor affinity for the SERT and both  $K_i$  values were greater than 100 $\mu$ M (Figure 4-07). The loss of the phenoxy ring appears to have destroyed the ability of the compound to bind to the SERT as well as the NAT, once again confirming the importance of this aspect of reboxetine-like compounds to monoamine transporter pharmacology.

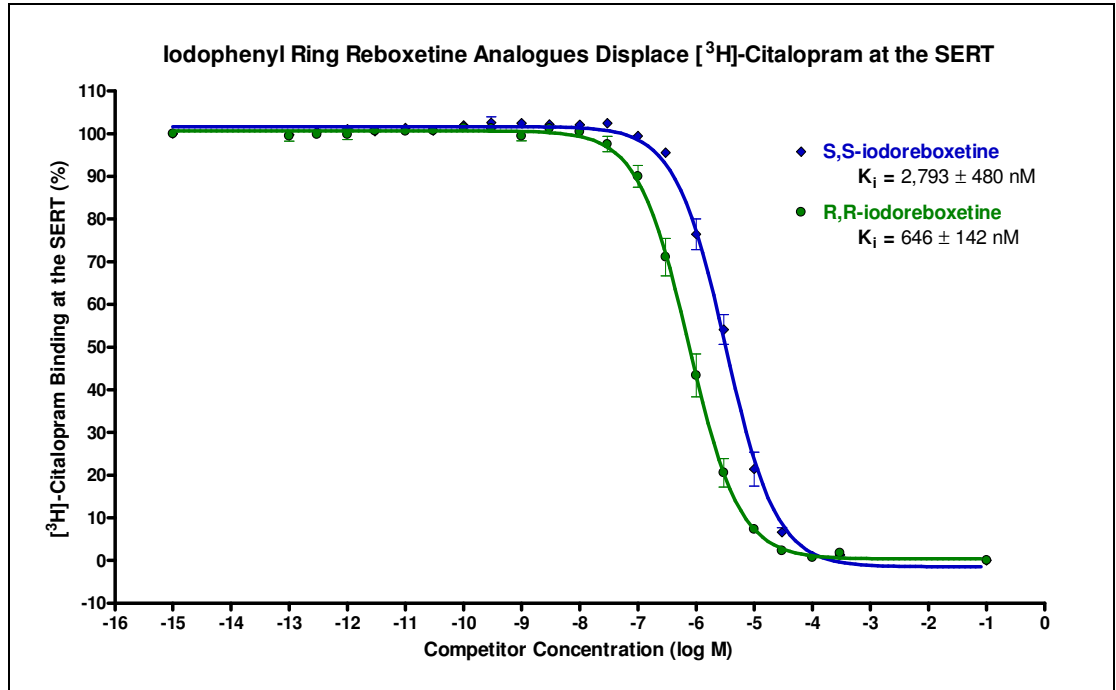


**Figure 4-05:** Iodophenyl ring reboxetine analogues displacement of [<sup>3</sup>H]-citalopram binding at the serotonin transporter. Data points are means of 2 independent repetitions and error bars represent standard error of the mean. Total binding (2.0nM [<sup>3</sup>H]-citalopram) plotted as competitor concentration 10<sup>-15</sup>M and non-specific binding (2.0nM [<sup>3</sup>H]-citalopram + 20 μM fluoxetine) plotted as 10<sup>-1</sup>M.  $K_i$  values are represented as the mean of 2 independent determinations ± the standard deviation, and are calculated from the IC<sub>50</sub> using the Cheng-Prusoff equation in GraphPad Prism 4.0.

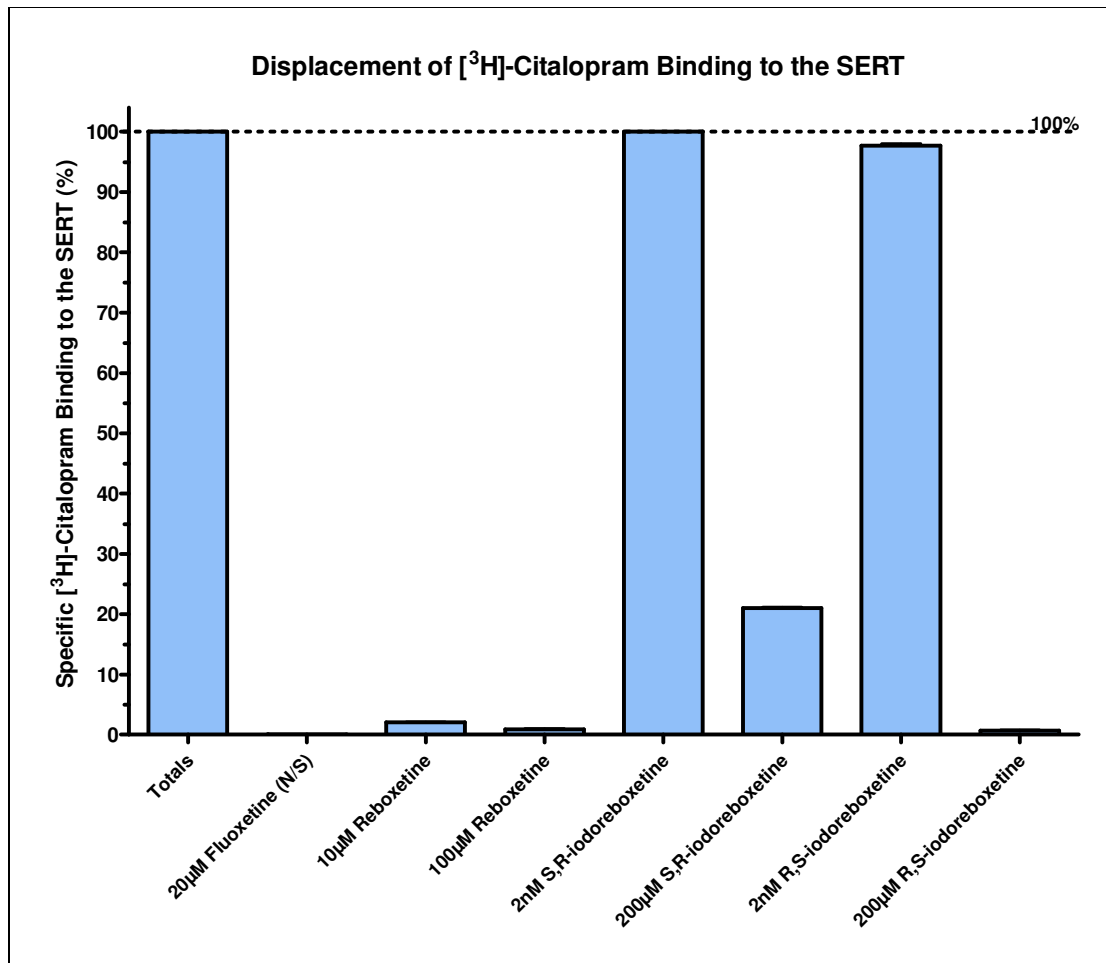


**Figure 4-06:** (*S,R*)- and (*R,S*)- iodophenyl ring reboxetine analogues displacement of [<sup>3</sup>H]-citalopram binding at the serotonin transporter. Bars representative one determination and error bars represent standard error of samples in triplicate for that single assay only. Total binding was defined with 2.0nM [<sup>3</sup>H]-citalopram and non-specific binding was defined with 2.0nM [<sup>3</sup>H]-citalopram in the presence of 20 µM fluoxetine.  $K_i$  values cannot be accurately determined from this data set.

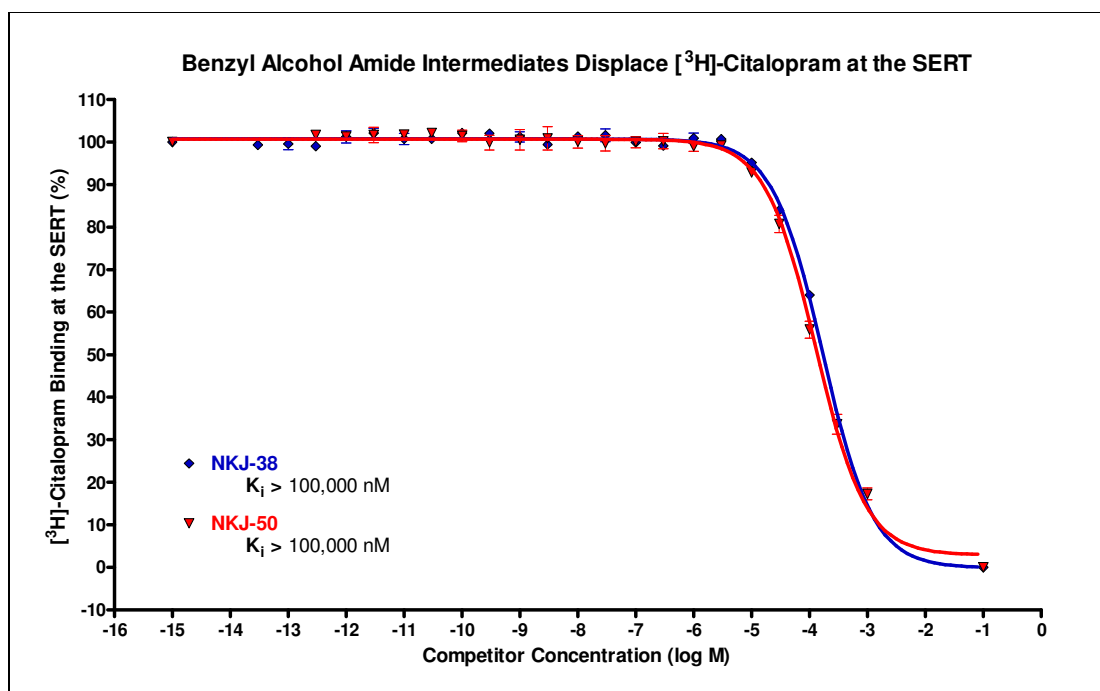


**Figure 4-08:** Benzyl alcohol intermediate compounds displacement of [<sup>3</sup>H]-citalopram binding at the serotonin transporter. Data points are means of 3 independent repetitions and error bars represent standard error of the mean. Total binding (2.0nM [<sup>3</sup>H]-citalopram) plotted as competitor concentration 10<sup>-15</sup>M and non-specific binding (2.0nM [<sup>3</sup>H]-citalopram + 20 μM fluoxetine) plotted as 10<sup>-1</sup>M. K<sub>i</sub> values are represented as the mean of 3 independent determinations ± the standard deviation, and was calculated from the IC<sub>50</sub> using the Cheng-Prusoff equation in GraphPad Prism 4.0. For these compounds, the bottom of the graph (i.e. 0% binding) was ill-defined, so IC<sub>50</sub> and K<sub>i</sub> could not be accurately calculated. Greater concentrations of competitor were not available and the K<sub>i</sub> values are approximately stated as > 100,000 nM.

The iodophenoxy ring reboxetine analogues as a group actually show greater overall affinity for the SERT than they do the NAT. The highest SERT affinity of these compounds was displayed by the NKJ-68 with a  $K_i$  of  $34.5 \pm 1.7$  nM, following by the NKJ-64 with a  $K_i$  of  $51.5 \pm 8.4$  nM, and finally the NKJ-67 has the lowest affinity with a  $K_i$  of  $154 \pm 12$  nM (Figure 4-08).

Elucidation of the SERT-binding properties for the (*R,S*)-conformation iodophenoxy compounds demonstrated that although the ortho-position compound, NKJ-64, demonstrated notable affinity for the SERT, it was approximately 6-fold more selective for the NAT and therefore may yet make an acceptable NAT brain imaging tracer. The meta-position compound, NKJ-67 demonstrated poor affinity for SERT as well as for NAT. Interestingly, the para-position molecule, NKJ-68, which demonstrated poor affinity at the NAT, showed some affinity for SERT. Should this prove highly selective for the SERT, it may have had potential as a SERT brain imaging tracer if not for superior affinity, pre-existing compounds already in use for both clinical and research contexts.

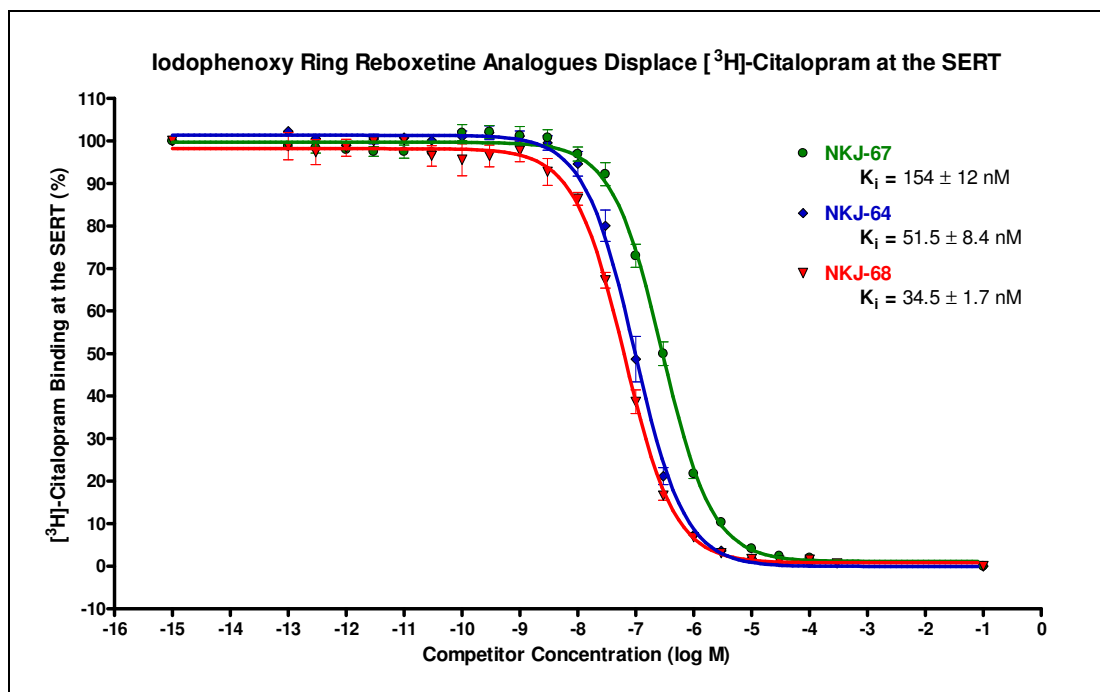


**Figure 4-08:** Iodophenoxy ring reboxetine analogues displacement of [<sup>3</sup>H]-citalopram binding at the serotonin transporter. Data points are means of 3 independent repetitions and error bars represent standard error of the mean. Total binding (2.0nM [<sup>3</sup>H]-citalopram) plotted as competitor concentration 10<sup>-15</sup>M and non-specific binding (2.0nM [<sup>3</sup>H]-citalopram + 20 μM fluoxetine) plotted as 10<sup>-1</sup>M. K<sub>i</sub> values are represented as the mean of 3 independent determinations ± the standard deviation, and was calculated from the IC<sub>50</sub> using the Cheng-Prusoff equation in GraphPad Prism 4.0.

Table 4-02: Affinity of iodinated reboxetine analogues for the SERT		
Group	Compounds	SERT K <sub>i</sub>
Iodophenyl ring analogues	( <i>S,R</i> )-iodoreboxetine	-
	( <i>R,S</i> )-iodoreboxetine	-
	( <i>S,S</i> )-iodoreboxetine	2,793 ± 480 nM
	( <i>R,R</i> )-iodoreboxetine	646 ± 142 nM
Benzyl alcohol amide intermediates	NKJ-38	> 100,000 nM
	NKJ-50	> 100,000 nM
Iodophenoxy ring analogues	NKJ-64	51.5 ± 8.4 nM
	NKJ-67	154 ± 12 nM
	NKJ-68	34.5 ± 1.7 nM

**Table 4-02:** Summary of affinity of novel iodoreboxetine compounds for the SERT. Broadly, the iodophenoxy ring analogues had the highest SERT affinity, the iodophenyl ring analogues were either untested or had poor affinity, and the benzyl alcohol amide intermediates had no noteworthy SERT affinity at all.

The affinity of the iodophenyl ring reboxetine analogues were reasonably low for the SERT (Table 4-02) and thus were highly specific for the NAT – however their inadequate affinity for the NAT is still problematic. The benzyl alcohol amide intermediates have no notable affinity for the SERT. Although the iodophenoxy ring analogues as a group demonstrated notable affinity for the SERT, the 6-fold selectivity of NKJ-64 for the NAT means it still has potential as a SPECT brain imaging tracer for the noradrenaline transporter.

#### 4.1.4 Dopamine Transporter Pharmacology:

To complete the pharmacological binding profile for monoamine transporters and elucidate the specificity for each compound, the dissociation constants of the produced compounds for which there were stocks remaining were determined at the DAT.

The iodophenyl ring compounds demonstrated encouragingly low affinity for the DAT (Figure 4-09), although displayed the greatest affinity in the (*R,R*)-isomer with a  $K_i$  value of  $716 \pm 20$  nM. The (*S,S*)-isomer yielded a  $K_i$  of approximately 1.4  $\mu$ M and so is the more favourable molecule in the group from the perspective of a NAT brain imaging tracer.

Unfortunately, depleted stocks for the (*S,R*)- and (*R,S*)- isomers of the iodophenyl ring compounds resulted in the inability to ascertain their inhibition constants at the DAT, although a pilot experiment was conducted and demonstrated low affinity for the [ $^3$ H]-WIN-35,428 binding site on the DAT (Figure 4-10).

Reboxetine was shown to displace virtually all [ $^3$ H]-WIN-35,428 binding at the DAT when applied in both 10 $\mu$ M and 100 $\mu$ M concentrations. Relative to reboxetine, (*R,S*)-iodoreboxetine demonstrated less affinity for the DAT and there was no significant displacement in the nanomolar range. Unfortunately, from this data set, it is difficult to draw comparative observations against reboxetine with (*S,R*)-iodoreboxetine, but there was no significant displacement in the nanomolar range.

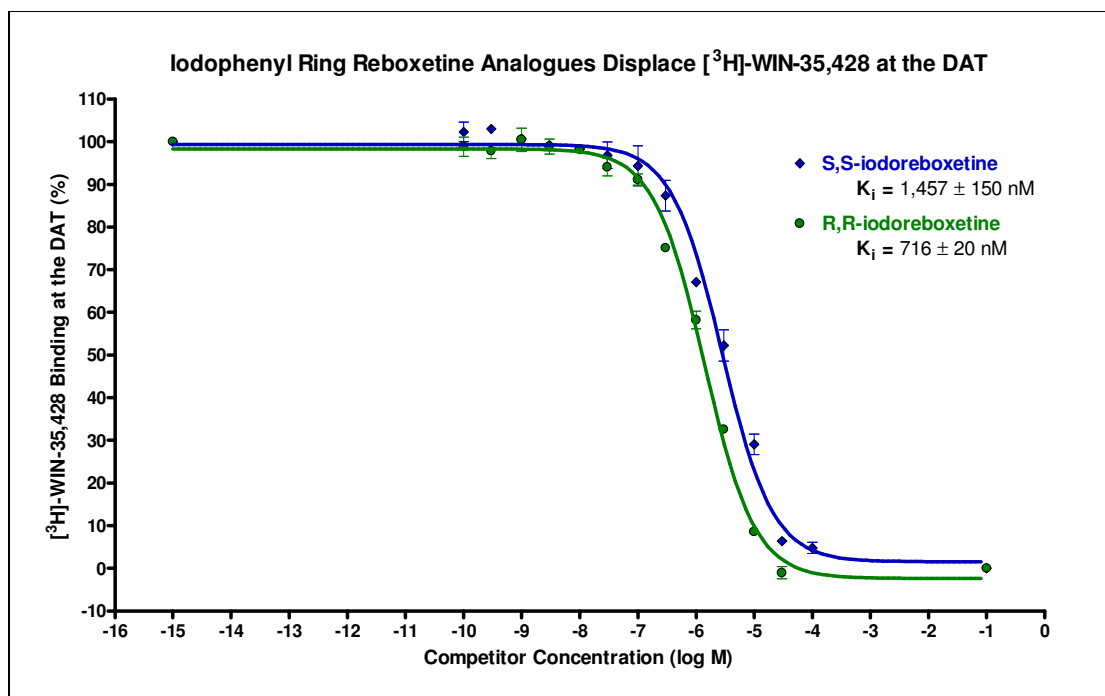


**Figure 4-09:** Iodophenyl ring reboxetine analogues displacement of [<sup>3</sup>H]-WIN-35,428 binding at the dopamine transporter. Data points are means of 2 independent repetitions and error bars represent standard error of the mean.  $K_i$  values are represented as the mean of 2 independent determinations  $\pm$  the standard deviation, and are calculated from the  $IC_{50}$  using the Cheng-Prusoff equation in GraphPad Prism 4.0.

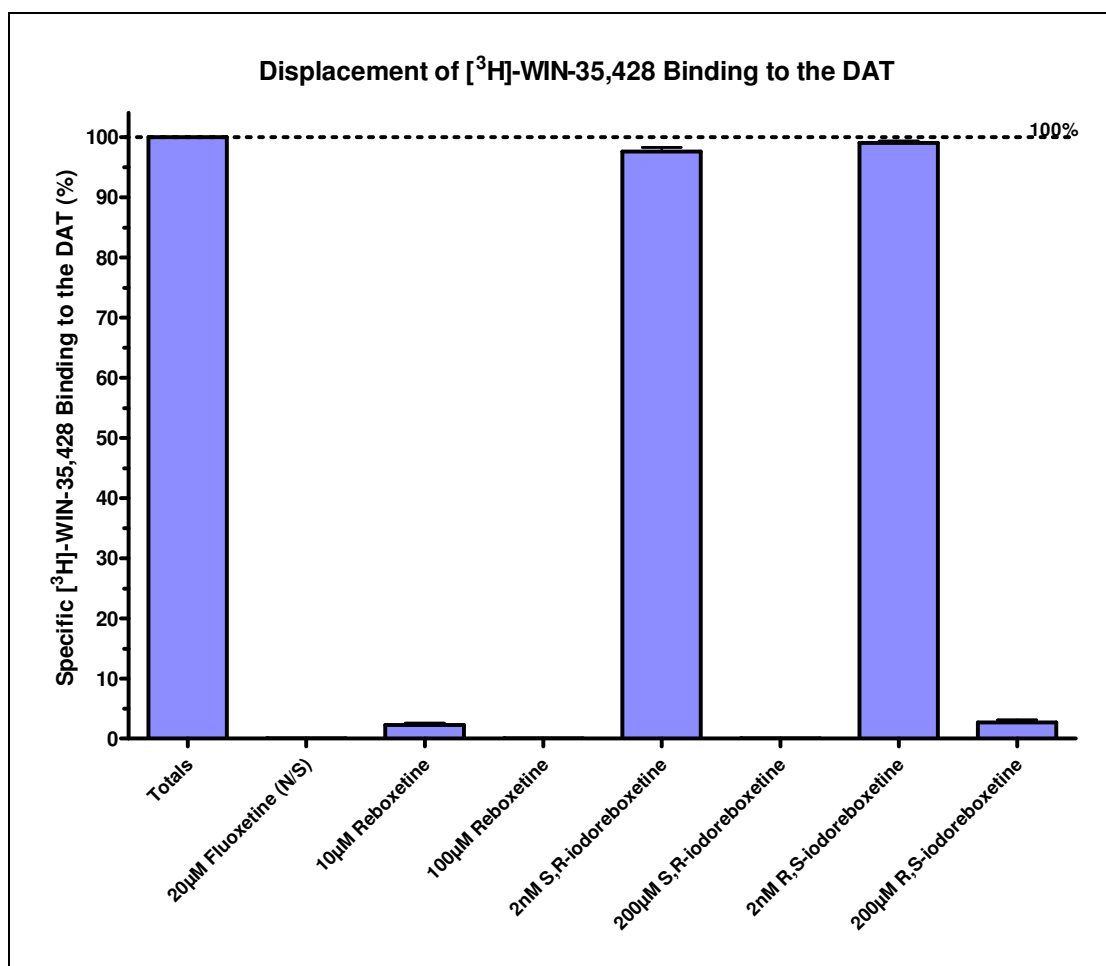


**Figure 4-10:** (*S,R*)- and (*R,S*)- iodophenyl ring reboxetine analogues displacement of [<sup>3</sup>H]-WIN-35,428 binding at the dopamine transporter. Bars representative one determination and error bars represent standard error of samples in triplicate for that single assay only.  $K_i$  values cannot be accurately determined from this data set.

Benzyl alcohol amides stocks had precipitated out of solution and their inhibition constants at the DAT were not ascertained, and nor was any sort of affinity established via pilot experiment. The distinct lack of any notable affinity for either the NAT or the SERT meant that preparing more of these compounds for analysis at the DAT was not a worthwhile endeavour. For monoamine pharmacology of reboxetine-like molecules, the trends seem to indicate that the phenoxy ring is the critical aspect conferring monoamine transporter affinity and it is predicted that the loss of this would have similarly destroyed affinity at the DAT.

Elucidation of the DAT-binding properties for the (*R,S*)-conformation iodophenoxy analogues revealed poor affinity for the DAT from all three compounds (Figure 4-12).

For [<sup>3</sup>H]-WIN-35,428 binding, there is a high affinity and low affinity binding site on the DAT. The curves for the iodophenoxy ring reboxetine analogues seem less traditionally shaped for a one-site competition than the curves on the iodophenyl ring reboxetine analogue competition assays. It is possible that this form of the molecule has a greater affinity for the low-affinity binding site, thus affecting the shape of the curve. Regardless, the compounds' affinity for the DAT in the range of 0.5 – 2.1 μM should mean that images of the NAT will not be disturbed by the influence of DAT binding.

None of the compounds showed any problematic affinity for the [<sup>3</sup>H]-WIN-35,428 binding site on the DAT (Table 4-03) and it appears that the minimal binding at this monoaminergic target will not detract from the selectivity of the compounds for the NAT.

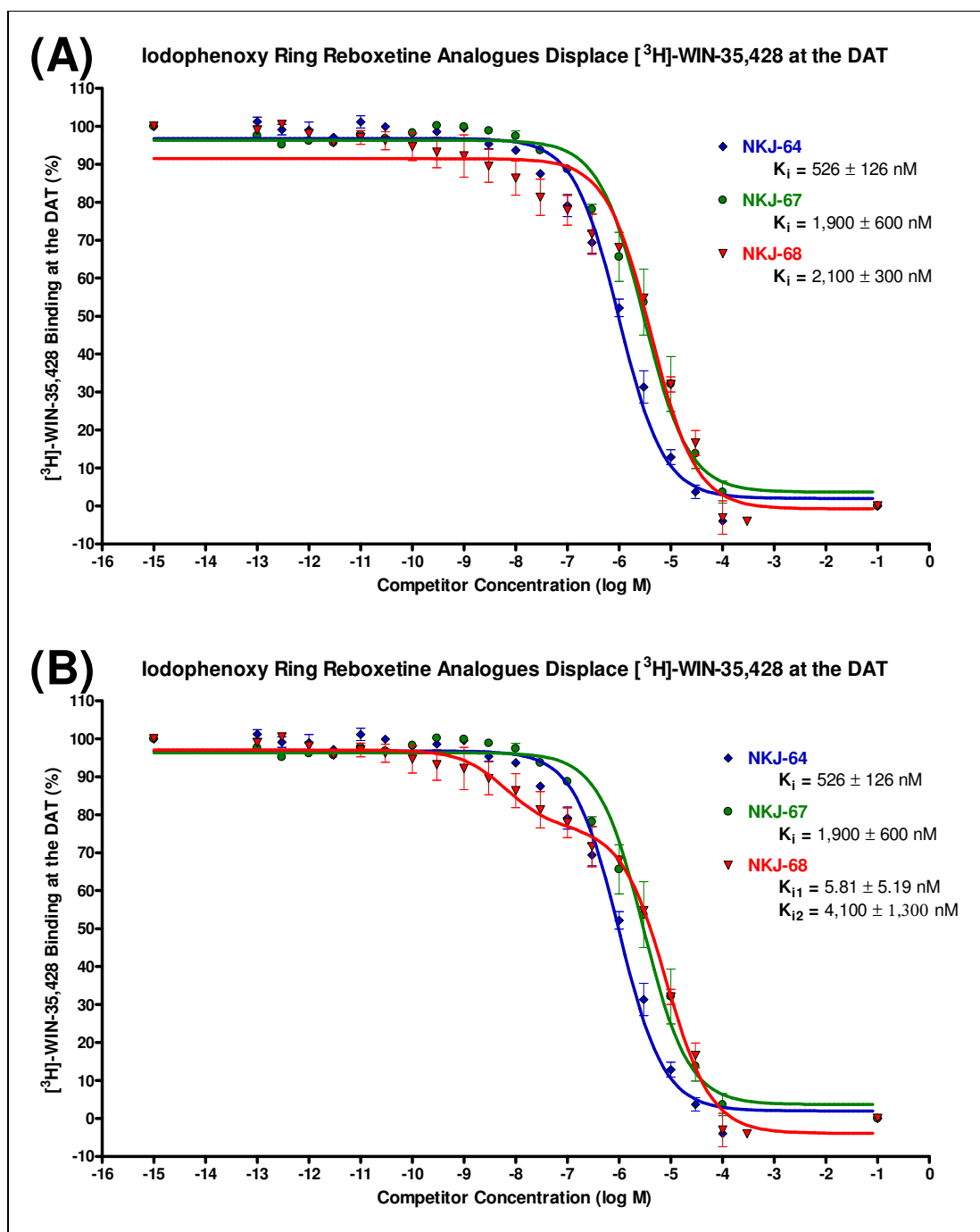


**Figure 4-11:** Iodophenoxy ring reboxetine analogues displacement of [<sup>3</sup>H]-WIN-35,428 binding at the dopamine transporter **(A)**. NKJ-68 appears to have affinity for more than one binding site on the DAT and this has been reanalysed and represented with the other iodophenoxy compounds to demonstrate both  $K_i$  values **(B)**. Data points for both graphs are means of 3 independent repetitions and error bars represent standard error of the mean.  $K_i$  values are represented as the mean of 3 independent determinations  $\pm$  the standard deviation, and are calculated from the  $IC_{50}$  using the Cheng-Prusoff equation in GraphPad Prism 4.0.

<b>Table 4-03: Affinity of iodinated reboxetine analogues for the DAT</b>		
<b>Group</b>	<b>Compounds</b>	<b>DAT K<sub>i</sub></b>
Iodophenyl ring analogues	( <i>S,R</i> )-iodoreboxetine	-
	( <i>R,S</i> )-iodoreboxetine	-
	( <i>S,S</i> )-iodoreboxetine	1,457 ± 150 nM
	( <i>R,R</i> )-iodoreboxetine	716 ± 20 nM
Benzyl alcohol amide intermediates	NKJ-38	-
	NKJ-50	-
Iodophenoxy ring analogues	NKJ-64	526 ± 126 nM
	NKJ-67	1,900 ± 600 nM
	NKJ-68	5.81 ± 5.19 nM & 4,100 ± 1,300 nM

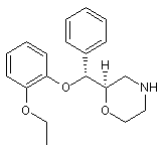
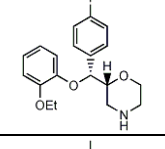
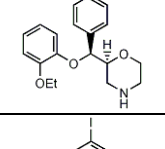
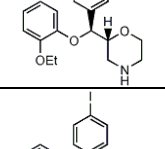
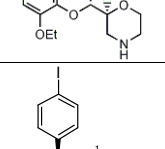
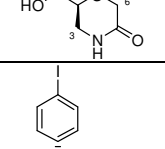
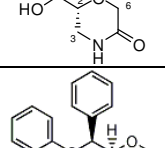
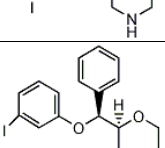
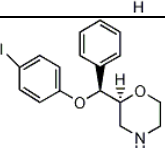
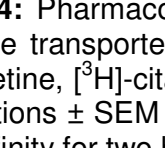
**Table 4-03:** Summary of affinity of novel iodoreboxetine compounds for the DAT.

#### 4.1.5 Monoamine Transporter Pharmacology (Summary)

The data set for the pharmacological characterisation of the Glasgow-produced reboxetine-like compounds at monoamine transporters is summarised in Tables 4-04 and 4-05.

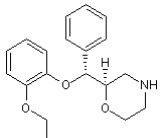
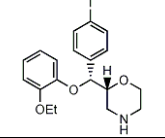
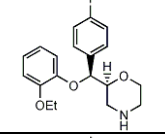
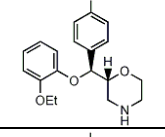
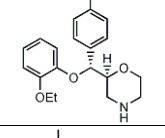
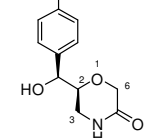
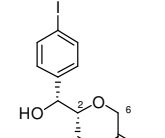
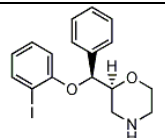
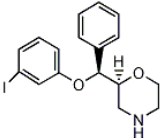
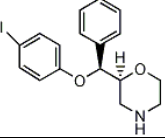
The iodophenyl ring reboxetine analogues were very selective for NAT but the affinity was not sufficient for use as SPECT tracers for imaging the NAT. The benzyl alcohol analogues had poor affinity for all monoamine sites tested and it would seem that the phenyl ring is critical for conferring monoamine transporter binding. The iodophenoxy ring reboxetine analogues as a group were more selective for the SERT than they were for the NAT, however when the iodine was in the ortho position it conferred both affinity and selectivity for the NAT. The iodophenoxy ring compounds with the iodine in the para- and meta- positions had greatly diminished affinity to the NAT in comparison to the ortho-position compound. Therefore, based on pharmacological binding profiles, the placement of the iodine on the phenoxy ring is of critical importance to the affinity of the compound for the NAT. This indicates that placing the iodine in the para- and meta- positions on the phenoxy ring interferes with the ability of reboxetine to bind to the NAT and that these portions of the molecule are therefore important in conferring NAT affinity and selectivity. Based on these pharmacological binding profiles, the ortho-positioned compound, (2*R*,3*S*)-2-[(2-iodophenoxy)phenylmethyl]morpholine, also known as NKJ-64, is therefore the most promising candidate for further development as a SPECT brain imaging tracer to be used for studying the NAT.

Interestingly, the para-position iodophenoxy molecule, also known as NKJ-68 or (2*R*,3*S*)-2-[(4-iodophenoxy)phenylmethyl]morpholine, proved to have notable affinity for the SERT with an inhibition constant of 34.5nM. Furthermore, this compound demonstrated multiple affinities for the DAT, indicating that there were two distinct conformations or sites for NKJ-68 binding to the DAT.

Table 4-04: Novel Iodoreboxetine Compound Affinities					
Compound			Pharmacology ( $K_i$ in nM)		
Type	Structure *	Names	NAT	SERT	DAT
Reference		<b>Reboxetine, prepared as racemic mix: (S,S)/(R,R)</b>  (2S,3S)/(2R,3R)-2-[(2-Ethoxyphenoxy)phenylmethyl]morpholine	<b>6.9 ± 1.6</b>	<i>not tested</i>	<i>not tested</i>
Iodo-phenyl ring reboxetine analogues		<b>(S,R)-iodoreboxetine</b>  (2S,3R)-2-[(4-Iodophenyl)-(2-ethoxyphenoxy)methyl]morpholine	321 ± 9	<b>Pilot only:</b> 80% inhibition @ 200µM; no inhibition @ 2nM	<b>Pilot only:</b> 100% inhibition @ 200µM; inhibits <5% @ 2nM
		<b>(R,S)-iodoreboxetine</b>  (2R,3S)-2-[(4-Iodophenyl)-(2-ethoxyphenoxy)methyl]morpholine	58.2 ± 9.4	<b>Pilot only:</b> 100% inhibition @ 200µM; inhibits <5% @ 2nM	<b>Pilot only:</b> >95% inhibition @ 200µM; inhibits <5% @ 2nM
		<b>(S,S)-iodoreboxetine</b>  (2S,3S)-2-[(4-Iodophenyl)-(2-ethoxyphenoxy)methyl]morpholine	53.8 ± 2.7	2,793 ± 480 (2)	1,457 ± 150 (2)
		<b>(R,R)-iodoreboxetine</b>  (2R,3R)-2-[(4-Iodophenyl)-(2-ethoxyphenoxy)methyl]morpholine	64.0 ± 2.4	646 ± 142 (2)	716 ± 20 (2)
Benzyl alcohol iodo-amide intermediates		<b>NKJ-38</b>  (2S,3S)-2-[α-Hydroxy-(4-iodophenyl)methyl]morpholine-5-one	14,810 ± 810	>100,000 (2)	<i>not tested</i>
		<b>NKJ-50</b>  (2R,3R)-2-[α-Hydroxy-(4-iodophenyl)methyl]morpholine-5-one	>1,000,000	>100,000 (2)	<i>not tested</i>
Iodo-phenoxy ring reboxetine analogues		<b>NKJ-64</b>  (2R,3S)-2-[(2-Iodophenoxy)phenylmethyl]morpholine	<b>8.4 ± 1.7</b> (5)	51.5 ± 8.4	526 ± 126
		<b>NKJ-67</b>  (2R,3S)-2-[(3-Iodophenoxy)phenylmethyl]morpholine	1,700 ± 500	154 ± 12	1,900 ± 600
		<b>NKJ-68</b>  (2R,3S)-2-[(4-Iodophenoxy)phenylmethyl]morpholine	1,100 ± 200	34.5 ± 1.7	5.81 ± 5.19 & 4,100 ± 1,300

**Table 4-04:** Pharmacological binding profile summary for iodoreboxetine analogues at monoamine transporters in the CNS.  $K_i$  determined at the NAT, SERT, and DAT with [ $^3$ H]-nisoxetine, [ $^3$ H]-citalopram, and [ $^3$ H]-WIN-35,428, respectively. Data are means of 3 determinations ± SEM unless otherwise specified (bottom right corner). NKJ-68 appears to have affinity for two binding sites on the DAT and so two  $K_i$  determinations are listed.

\* **Note:** Structures from Jobson, NK (Ph.D. Thesis 2008).

Table 4-05: Novel Iodoreboxetine Compound Selectivity				
Compound			Selectivity	
Type	Structure *	Names	NAT:SERT	NAT:DAT
Reference		<b>Reboxetine, prepared as racemic mix: (S,S)/(R,R)</b>  (2 <i>S</i> ,3 <i>S</i> )/(2 <i>R</i> ,3 <i>R</i> )-2-[(2-Ethoxyphenoxy)phenylmethyl]morpholine	-	-
Iodo-phenyl ring reboxetine analogues		<b>(S,R)-iodoreboxetine</b>  (2 <i>S</i> ,3 <i>R</i> )-2-[(4-Iodophenyl)-(2-ethoxyphenoxy)methyl]morpholine	-	-
		<b>(R,S)-iodoreboxetine</b>  (2 <i>R</i> ,3 <i>S</i> )-2-[(4-Iodophenyl)-(2-ethoxyphenoxy)methyl]morpholine	-	-
		<b>(S,S)-iodoreboxetine</b>  (2 <i>S</i> ,3 <i>S</i> )-2-[(4-Iodophenyl)-(2-ethoxyphenoxy)methyl]morpholine	52 : 1	27 : 1
		<b>(R,R)-iodoreboxetine</b>  (2 <i>R</i> ,3 <i>R</i> )-2-[(4-Iodophenyl)-(2-ethoxyphenoxy)methyl]morpholine	10 : 1	11 : 1
Benzyl alcohol iodo-amide intermediates		<b>NKJ-38</b>  (2 <i>S</i> ,3 <i>S</i> )-2-[ $\alpha$ -Hydroxy-(4-iodophenyl)methyl]morpholine-5-one	7 : 1	-
		<b>NKJ-50</b>  (2 <i>R</i> ,3 <i>R</i> )-2-[ $\alpha$ -Hydroxy-(4-iodophenyl)methyl]morpholine-5-one	1 : 10	-
Iodo-phenoxy ring reboxetine analogues		<b>NKJ-64</b>  (2 <i>R</i> ,3 <i>S</i> )-2-[(2-Iodophenoxy)phenylmethyl]morpholine	6 : 1	63 : 1
		<b>NKJ-67</b>  (2 <i>R</i> ,3 <i>S</i> )-2-[(3-Iodophenoxy)phenylmethyl]morpholine	1 : 11	1 : 1
		<b>NKJ-68</b>  (2 <i>R</i> ,3 <i>S</i> )-2-[(4-Iodophenoxy)phenylmethyl]morpholine	1 : 32	-

**Table 4-05:** Pharmacological selectivity summary for iodoreboxetine analogues at monoamine transporters in the CNS. Data calculated via  $K_i$  data at the NAT, SERT, and DAT with [ $^3$ H]-nisoxetine, [ $^3$ H]-citalopram, and [ $^3$ H]-WIN-35,428, respectively. Where data is insufficient for calculation is denoted with a dash. Ratios accurate to nearest integer. NAT:DAT selectivity for NKJ-68 is not listed, as this compound appears to have affinity for two binding sites at the DAT. \* **Note:** Structures from Jobson, NK (Ph.D. Thesis 2008).

## 4.2 Discussion

### 4.2.1 Summary of findings

The main findings of this chapter are that the addition of the iodine atom to a reboxetine-like molecule lowered the binding affinity in every compound synthesised and the position of the iodine greatly affects the binding properties of the various analogues of iodoreboxetine. When the iodine atom is positioned on the phenyl ring, this enabled a NAT affinity of approximately 54nM in the most potent of these analogues, (*S,S*)-iodoreboxetine, and demonstrated excellent selectivity for NAT over DAT and SERT. However, the affinity of this iodophenyl ring reboxetine analogue was not high enough for SPECT imaging, as it would give a simple binding estimation of approximately 1.3, compared to the required value of approximately 12 (Schou et al. 2007). The benzyl alcohol iodo-amide intermediates are reboxetine-like molecules lacking the phenoxy ring and their extremely low affinity for NAT demonstrated how important this ring is for the binding properties of reboxetine and any future iodoreboxetine molecules. When the iodine is positioned on the phenoxy ring, this yielded the greatest affinity for NAT of all the compounds produced, NKJ-64 (8.4 nM), and acceptable selectivity – but the orientation of the iodine atom in the ortho-position on the ring is critical to maintaining the capability for binding to the NAT and other phenoxy ring analogues were not suitable.

NKJ-64's  $K_i$  at the NAT of 8.4nM compares favourably with the similarly-structured SPECT candidate compound INER/IPBM, which has  $K_i$  determinations of 0.84nM (Kanegawa et al. 2006) and 4.22nM (Tamagnan et al. 2007), and while the  $K_i$  measurement was higher it is in the same order of magnitude. A  $K_i$  of 8.4nM also compares favourably against the  $K_i$  determinations in the literature for methylreboxetine/MRB/MeNER, 3-Cl-methylreboxetine, and oxaprotiline, at 4.63nM, 6.11nM, and 9.07nM, respectively (Logan et al. 2007; Ding et al. 2005). Once again, NKJ-64 is within the same order of magnitude.

It was interesting to note that the  $K_i$  determined in this thesis for reboxetine was 6.9nM, compared to 1.1nM (Wong et al. 2000) in the literature. While this is approximately 6-fold higher, it is in the same order of magnitude and I haven't cause to doubt my determination. Pilot experiments showed that reboxetine itself

displayed affinity for the SERT and DAT. As aforementioned, the inhibition constant for reboxetine at the SERT was determined as  $129 \pm 13 \text{ nM}$  (Wong et al. 2000) and the pilot assay at the SERT merely confirmed that reboxetine is exhibiting displacement at this site, although the precise determination was not repeated. The inhibition constant for reboxetine at the DAT was not precisely determined but has previously been recorded as exhibiting no significant displacement at  $10 \mu\text{M}$  (Wong et al. 2000; Millan et al. 2001), so finding a significant blockade of [ $^3\text{H}$ ]-WIN-35,428 binding when this concentration was applied is interesting. Had the leading compound demonstrated significant affinity for the DAT then it may have been worthwhile performing a full displacement experiment with reboxetine against [ $^3\text{H}$ ]-WIN-35,428 at the DAT to determine to what extent the structural changes to the compound had affected the DAT affinity – positively or negatively. However, without problematic DAT binding in the lead compound, this curiosity was not attributed great importance and was not investigated further.

#### **4.4.2 What alternative molecules are emerging?**

Although several reboxetine analogues have since shown promise *in vitro* and been applied to PET imaging (Table 4-06), compounds such as (*S,S*)-[ $^{11}\text{C}$ ]-MeNER and (*S,S*)-[ $^{18}\text{F}$ ]-MeNER- $\text{D}_2$  exhibited similar *in vivo* problems to [ $^{11}\text{C}$ ]-nisoxetine, resulting in slow uptake, rapid radioisotope decay, and noisy images with poor contrast (Zeng et al. 2008).

Although the  $2\beta,3\alpha$ -(substituted phenyl) nortropane compound selected and developed by Zeng et al (2007) exhibited great affinity and selectivity *in vitro*, high uptake in the caudate meant that this compound did not present an acceptable reference region for *in vivo* imaging and thus was not suitable for further use. Similarly, (*S,S*)-MRB/MeNER/Methylreboxetine proved to have good affinity, specificity, displaceable binding, stability, metabolism, and suitable *in vivo* blood-brain barrier penetration, but unfortunately a low specific-to-nonspecific ratio due to high uptake in reference regions and an intrinsic PET-associated difficulty in accurately defining the specific binding meant that there was a low signal-to-noise ratio and the assessment of many low NAT concentration structures was difficult.

Turning to efforts on SPECT compounds, the nisoxetine analogues PYINXT and INXT / MIPP displayed high affinity and selectivity *in vitro* using cloned cell lines, however the non-specific binding and *in vivo* kinetics for [<sup>125</sup>I]-INXT were unacceptable (Lakshmi et al. 2008). Through modification of the molecule, [<sup>125</sup>I]-PYINXT demonstrated 67% specific binding *in vivo* and more favourable kinetics – placing the nonspecific binding of this molecule equivalent to that of [<sup>11</sup>C]MeNER (Lakshmi et al. 2008; Ding et al. 2005).

[<sup>125</sup>I]-INER/IPBM has been demonstrated as having favourable *in vivo* characteristics with maximal brain radioactivity achieved after 10 minutes following bolus injection and a slow washout over 2 hours with specifically displaceable regional distributions consistent with those known of the NAT (Tamagnan et al. 2007; Kanegawa et al. 2006). Nonspecific binding was approximately 40% and the compound therefore has potential as a SPECT brain imaging tracer for evaluating the NAT – however the aforementioned [<sup>125</sup>I]PYINXT, although slightly lower in NAT affinity, demonstrated superior specific binding and may therefore make a more valuable tracer once the *in vivo* stability of the molecule is determined.

<b>Table 4-06: NAT affinity of emerging brain imaging tracer compounds</b>				
<b>Compound</b>	<b>K<sub>i</sub> (nM) *</b>	<b>Isotope</b>	<b>Technique</b>	<b>References</b>
2β,3α-(substituted phenyl) nortropine	1.78	[ <sup>11</sup> C]	PET	Zeng 2007
Methylreboxetine / MeNER / MRB	0.95 – 5.0	[ <sup>11</sup> C], [ <sup>18</sup> F]	PET	Zeng 2009 Schou 2009; Zeng 2008; Logan 2007;
MENET / FENET / FPNET	1.02 – 3.68	[ <sup>11</sup> C], [ <sup>18</sup> F]	PET	Zeng 2009
(S,S)-S-methylreboxetine / MESNET	0.30 – 1.35	[ <sup>11</sup> C], [ <sup>18</sup> F]	PET	Zeng 2009; Zeng 2008
PYINXT	5.3 *	[ <sup>125</sup> I]	SPECT	Lakshmi 2008

**Table 4-06:** Recently emerging compounds characterised and suggested for *in vivo* imaging of the NAT.

\* **Note:** K<sub>i</sub> values determined against [<sup>3</sup>H]-nisoxetine, except for PYINXT, which was determined against [<sup>125</sup>I]-nisoxetine.

### 4.2.3 Identifying what the lead compound will be capable of imaging

Whilst the affinity of NKJ-64 is not as high as some compounds reviewed in the literature, the good selectivity combined with the reasonable affinity and novel routes of synthesis warrants further evaluation of this compound as a potential SPECT imaging tracer for the NAT. Reapplication of the simple  $B_{\max}/K_d$  calculation to approximate binding potential (Schou et al. 2007) to the quantitative autoradiographic *post mortem* data set of Donnan et al (1991) gives a rough guide (Table 4-07) to the *in vivo* imaging potential of NKJ-64 ( $K_i = 8.4 \pm 1.7$  nM). When the  $K_i$  for a competitive compound is defined at the  $K_d$  for the ligand it is competing against, the  $K_i$  of the competitor may be considered an approximation for its  $K_d$  to the same site. The  $K_i$  determinations for competitor compounds undertaken in this thesis have all occurred at or very near the  $K_d$  for each relevant ligand, and therefore  $B_{\max}/K_i$  for those compounds can be taken as an approximation of  $B_{\max}/K_d$  and appear in Table 4-07. This allows a rough approximation of binding potential for the lead candidate compound to be compared with other similar compounds such as INER/IPBM.

<b>Table 4-07: Binding Potential Estimations for NAT-specific SPECT Brain Imaging Tracer Candidates</b>			
<b>Structure</b>	<b>Regional B<sub>max</sub> of NAT in Human Brain (pmol/g wet weight, ~nM)</b>	<b>NKJ-64 B<sub>max</sub>/K<sub>d</sub></b>	<b>INER/IPBM B<sub>max</sub>/K<sub>d</sub> *</b>
Globus Pallidus	8.7	1.04	3.44
Ventral Pallidum	2.0	0.24	0.79
Bed Nucleus of the Striatum Terminalis	8.0	0.95	3.16
Thalamus	10.5	1.25	4.15
<b>Hypothalamus</b>	36.7	4.37	14.51
Red Nucleus	7.6	0.90	3.00
Substantia Nigra <i>pars compacta</i>	-	-	-
<i>pars reticulata</i>	5.4	0.64	2.13
Edinger-Westphal Nucleus	18.4	2.19	7.27
Rostral Linear Nucleus	7.2	0.86	2.85
<b>Caudal Linear Nucleus</b>	50.5	6.01	19.96
Parabrachial Pigmented Nucleus	1.0	0.12	0.40
Paranigral Nucleus	4.6	0.55	1.82
Central Grey	18.0	2.14	7.11
<b>Dorsal Raphe Nucleus</b>	60.8	7.24	24.03
<b>Medial Raphe Nucleus</b>	47.3	5.63	18.70
Raphe Magnus Nucleus	7.1	0.84	2.81
Raphe Obscurus Nucleus	21.0	2.50	8.30
Raphe Pallidus Nucleus	10.2	1.21	4.03
<b>Paramedian Raphe</b>	68.6	8.17	27.11
<b>Locus Coeruleus</b>	70.8	8.33	27.98
Cerebellum	6.6	0.79	2.61
Dorsal Tegmental Nucleus	27.5	3.27	10.86
Subpenduncular Pigmented Nucleus	20.3	2.42	8.02

**Table 4-07:** Distribution of the NAT in human brain and simple estimations of binding potentials for NAT-specific prospective SPECT brain imaging tracers. Green boxes indicate a simple binding potential estimation  $\geq 12$ , and therefore indicative of a structure likely to be imaged by the prospective tracer according to Schou et al (2007).

\* **Note:** INER/IPBM K<sub>d</sub> applied as an average of the literature-reported values, 2.53nM.

The NKJ-64 did not meet the binding potential calculation criteria, as suggested by Schou et al (2007), while INER/IPBM – the (S,S)-isomer of an ortho-position iodophenoxy reboxetine analogue – did so across 6 structures: the hypothalamus, the caudal linear nucleus, the dorsal raphe nucleus, the raphe magnus nucleus, the paramedian raphe, and of course the locus coeruleus. It should be noted that the ratio defined by Schou et al was on the basis of PET, not SPECT, radioligands and that this simple calculation does not account for the levels of non-specific binding – resulting in a lower binding potential measured *in vivo* than those estimated here. As SPECT ligand isotopes have a longer half-life compared to PET ligand isotopes, more time is afforded for achieving maximal specific binding for image acquisition and it is possible that the ratio required for a successful SPECT tracer is less than that of a useful PET tracer. In that context, the simple binding potential ratios calculated for NKJ-64 across the raphe nuclei and the locus coeruleus are not so disheartening and combined with favourable levels of non-specific binding could indicate the utility of this molecule as a SPECT tracer.

#### **4.2.4 Next steps for NKJ-64 development**

The *in vitro* evaluation of the NKJ-64 indicates that it possesses sufficient affinity and specificity for the NAT to warrant characterisation of its potential *in vivo*. Although the INER/IPBM molecule characterised in the literature by Tamagnan et al (2007) and Kanegawa et al (2006) has greater affinity for the NAT, it is not a foregone conclusion that the *in vivo* characteristics of this compound will also be more favourable and thus further study of NKJ-64 developed in this thesis is required to determine its *in vivo* potential. As previously discussed, it is not always the ligand with the greatest affinity that is the most viable and valuable as a SPECT brain imaging tracer. Should it be found that NKJ-64 possesses superior blood-brain barrier penetrability, lower non-specific binding, and/or reduced plasma protein association combined with stability in circulation, then it may yet prove a more valuable SPECT brain imaging tracer for the NAT than those described thus far in the literature.

The next phase of ligand development is to predict the *in vivo* characteristics of the lead molecules using high performance liquid chromatography (HPLC) techniques to provide justification for conducting *in vitro* assays with radiolabelled compound. Encouraging results at that phase, the development programme would progress to

*in vivo* assays in an animal model, and continue towards the ultimate goals of use in drug occupancy studies and clinical application.

## Chapter 5

### Using High-Performance Liquid Chromatography (HPLC) to Predict *in vivo* Characteristics of Tracer Candidates

#### 5.1 Results:

##### 5.1.1 Reboxetine Compounds

###### 5.1.1.1 Lipophilicity ( $\log P_{OCT}$ )

Reboxetine-like compounds (Figure 5-01) that fall inside the ideal  $\log P_{OCT}$  range of 1-3.5 (Waterhouse 2003) are: commercially available reboxetine mesylate ( $\log P_{OCT}$  2.81), the iodinated amide compounds NKJ-38 ( $\log P_{OCT}$  1.88) and NKJ-50 ( $\log P_{OCT}$  1.87), and the iodoreboxetine compound NKJ-64 ( $\log P_{OCT}$  3.40).

Reboxetine-like compounds (Figure 5-01) that were measured as outwith of the ideal  $\log P_{OCT}$  range of 1-3.5 are the iodoreboxetine compounds (*S,S*)-iodoreboxetine ( $\log P_{OCT}$  3.54), (*R,R*)-iodoreboxetine ( $\log P_{OCT}$  3.57), NKJ-67 ( $\log P_{OCT}$  3.68), and NKJ-68 ( $\log P_{OCT}$  3.62), which all demonstrated greater lipophilicity than the ideal range's upper threshold of  $\log P_{OCT}$  3.5.

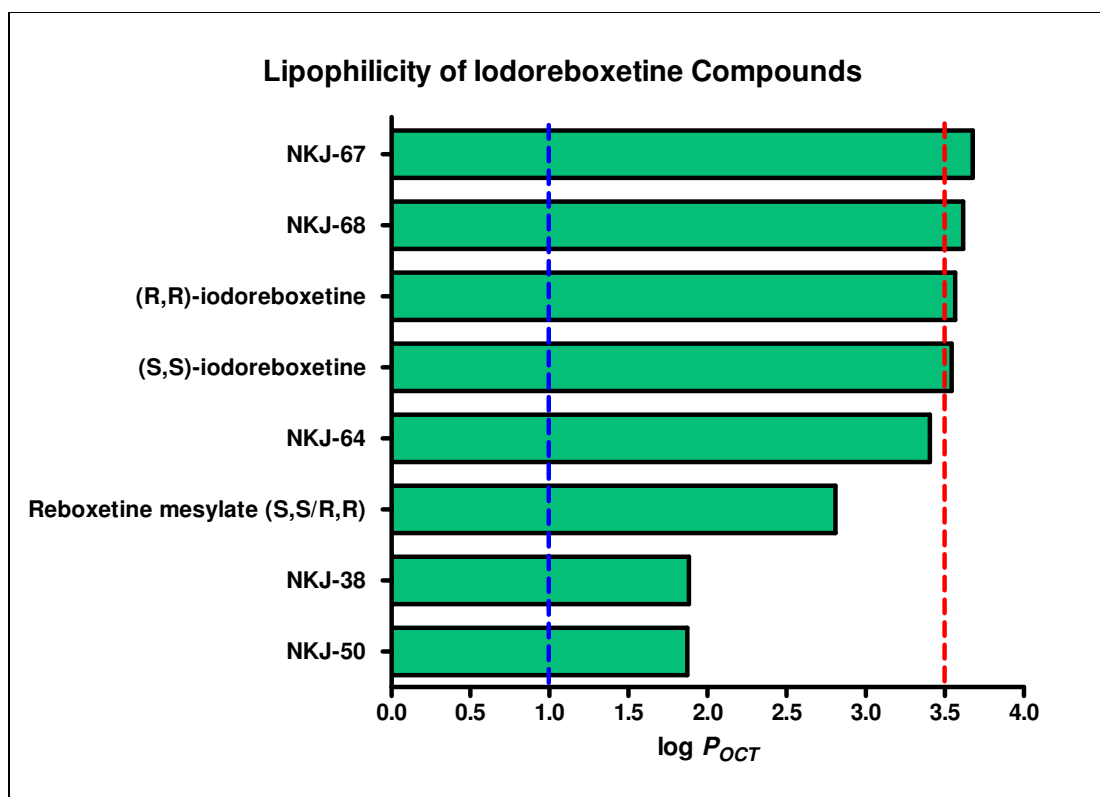


**Figure 5-01:** Measured lipophilicity of reboxetine analogues. The best blood-brain penetration without problematic non-specific binding is anticipated to be exhibited by compounds with log  $P_{OCT}$  values between 1.0 (dotted blue line) and 3.5 (dotted red line). Retention times used in CHI calculations, which were used in log  $P_{OCT}$  calculations, were highly reproducible and variance between determinations was not within the sensitivity of the assay.

### 5.2.1.1 Phospholipophilicity (log $D_{7.4 \text{ IAM}}$ )

The phospholipophilicity of reboxetine (Figure 5-02) was determined as log  $D_{7.4 \text{ IAM}}$  5.90. Relative to reboxetine, the iodinated reboxetine compounds (*S,S*)-iodoreboxetine (log  $D_{7.4 \text{ IAM}}$  7.08), (*R,R*)-iodoreboxetine (log  $D_{7.4 \text{ IAM}}$  7.08), NKJ-64 (log  $D_{7.4 \text{ IAM}}$  6.87), NKJ-67 (log  $D_{7.4 \text{ IAM}}$  7.38), and NKJ-68 (log  $D_{7.4 \text{ IAM}}$  7.17) were all more phospholipophilic. The iodinated amide compounds NKJ-38 (log  $D_{7.4 \text{ IAM}}$  4.14) and NKJ-50 (log  $D_{7.4 \text{ IAM}}$  4.14) were relatively less phospholipophilic, however do not have any notable affinity for the NAT (Chapter 4).

### 5.2.1.2 Blood-Brain Barrier Penetration (clog BB)

Blood brain barrier penetration of iodoreboxetine molecules (Figure 5-03) suggests that all iodoreboxetine compounds (clog BB 1.29-1.53) should penetrate the blood brain barrier more successfully than reboxetine (clog BB 0.88), with the exception of the iodoamide compounds (clog BB 0.23 each), which do not have any noteworthy affinity for the NAT (Chapter 4).

### 5.2.1.3 Plasma Protein Binding (c%PPB)

The plasma protein binding predictor for reboxetine (c%PPB 82.75) was determined to be below the threshold of 95%, above which it is thought the degree of plasma protein binding could be problematic (Figure 5-04). The iodination of reboxetine resulted in greater than a predicted plasma protein binding greater than 95% in all cases (c%PPB 97.49-98.60) with NKJ-64 exhibiting the lowest and most favourable measurement amongst them (c%PPB 97.49). The iodinated amides NKJ-38 (c%PPB 46.09) and NKJ-50 (c%PPB 44.15) had very low plasma protein binding predictors, however poor affinity for the NAT (Chapter 4) means they would not make suitable brain imaging tracers.

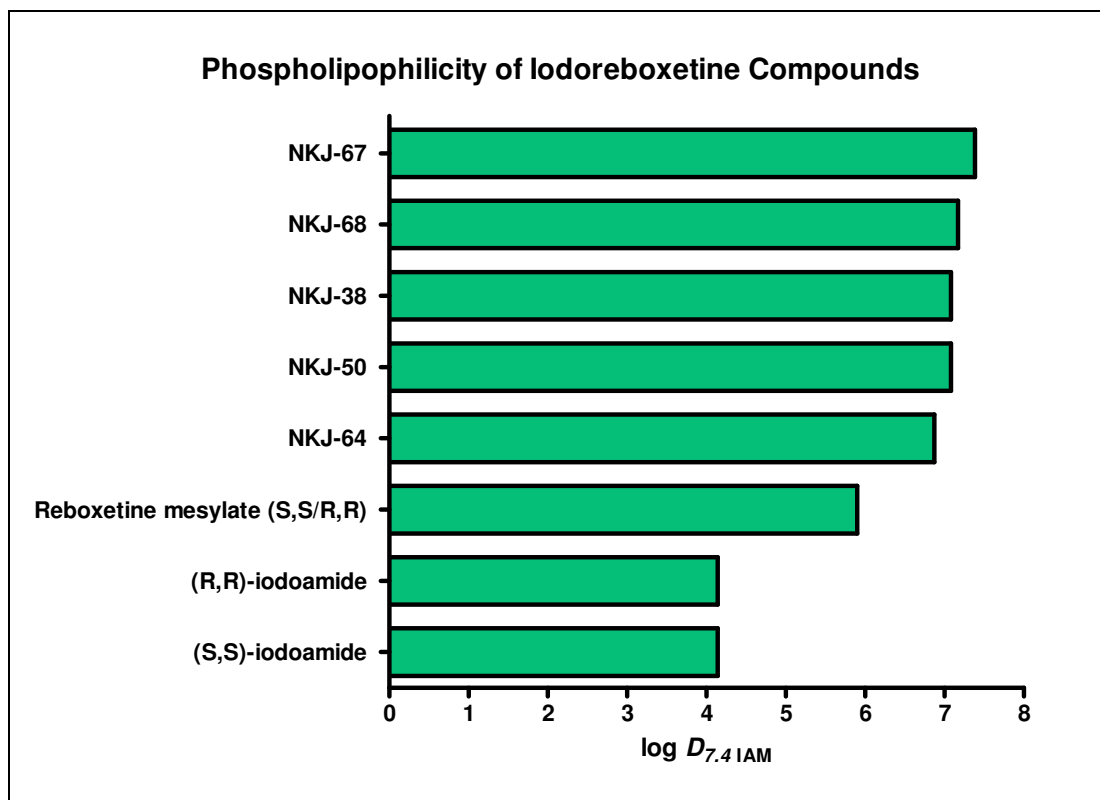


**Figure 5-02:** Measured phospholipophilicity ( $\log D_{7.4 \text{ IAM}}$ ) of reboxetine analogues. Phospholipophilicity is used as predictor of nonspecific binding and very high values may indicate problematic nonspecific binding. Retention times used in CHI calculations, which were used in  $\log D_{7.4 \text{ IAM}}$  calculations, were highly reproducible and variance between determinations was not within the sensitivity of the assay.

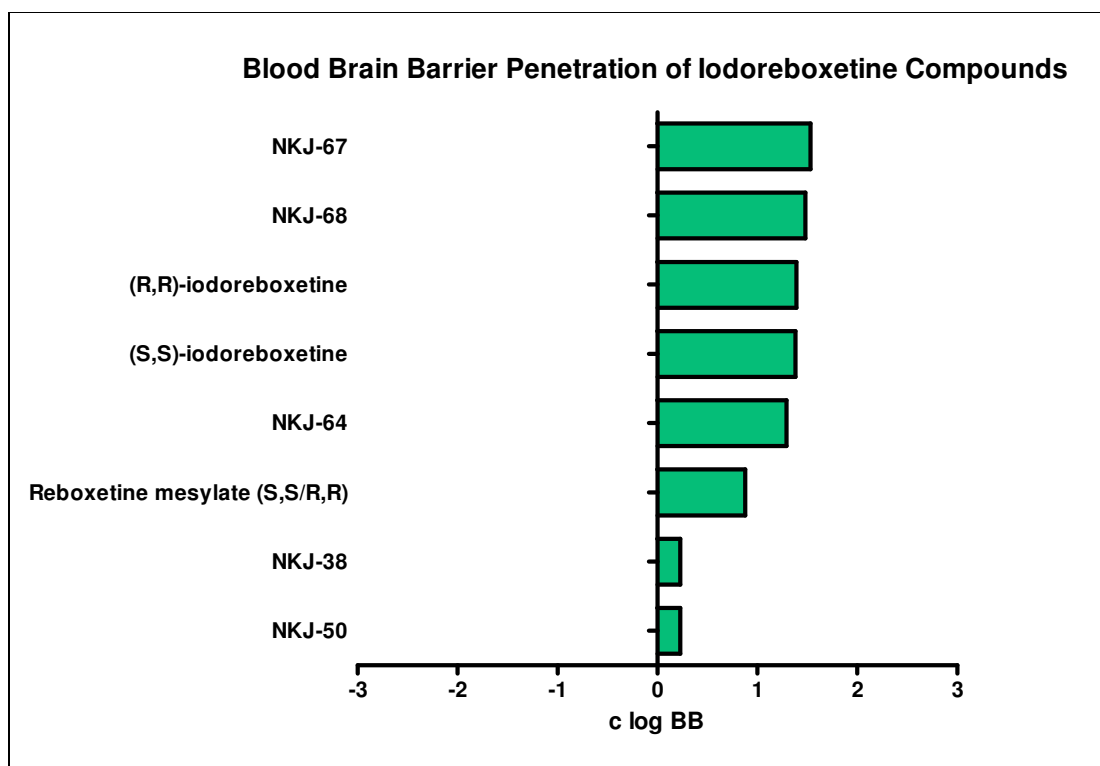


**Figure 5-03:** Measured blood-brain barrier penetration predictors (clog BB) for reboxetine analogues. Higher and lower values indicate greater and lesser brain penetration, respectively. Retention times used in CHI calculations, which were used in log clog BB calculations, were highly reproducible and variance between determinations was not within the sensitivity of the assay.

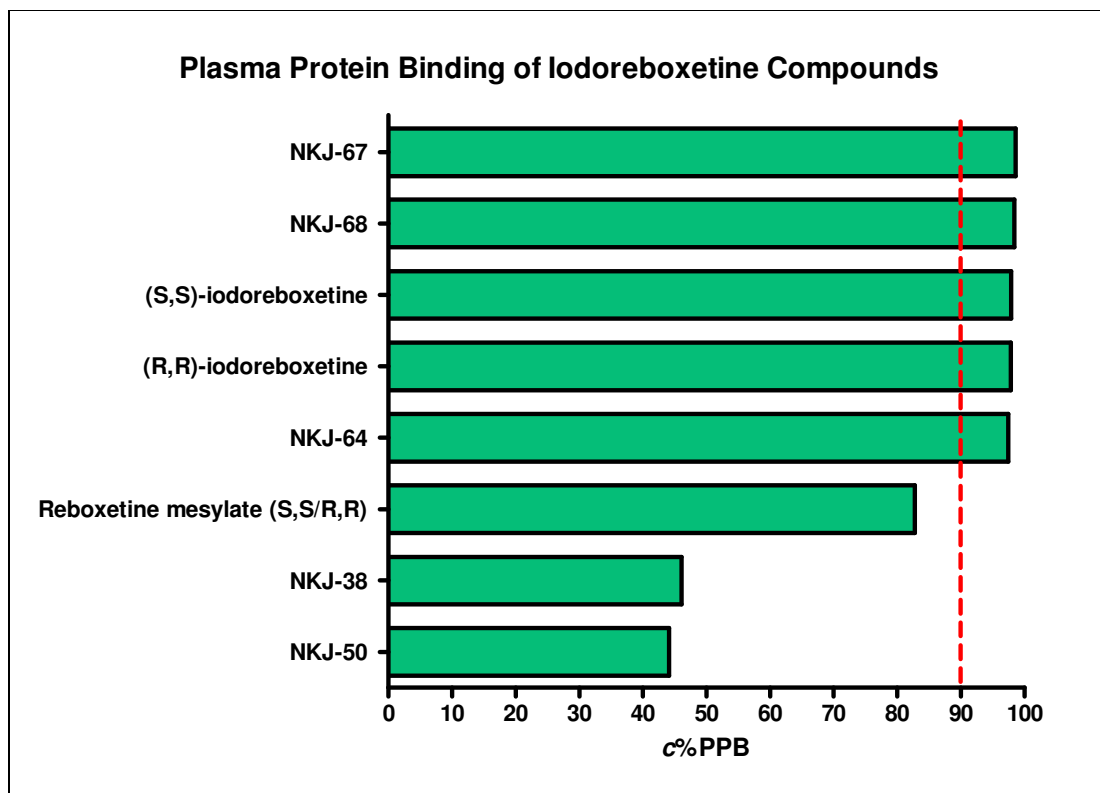


**Figure 5-04:** Plasma protein binding derived from a combination of HSA and AGP affinity determinations for reboxetine analogues. Plasma protein binding is considered inversely proportional to availability of a compound in plasma, although some compounds can use plasma proteins as carrier molecules to more successfully penetrate the brain. Retention times used in CHI calculations, which were used in log *c*%PPB calculations, were highly reproducible and variance between determinations was not within the sensitivity of the assay.

## 5.2.2 Reference Compounds

### 5.2.2.1 Lipophilicity ( $\log P_{OCT}$ )

Reference compounds (Figure 5-05) that fall inside the ideal  $\log P_{OCT}$  range of 1-3.5 (Waterhouse 2003) are MIBG ( $\log P_{OCT}$  2.96), MK-801 ( $\log P_{OCT}$  2.68) 5-I-A-85380 ( $\log P_{OCT}$  2.68) FIAU ( $\log P_{OCT}$  1.24) and  $\alpha$ -3-iodo-2-methyltyrosine ( $\log P_{OCT}$  1.17). Reference compounds that fell outside the ideal  $\log P_{OCT}$  range of 1-3.5 are: I-QNB ( $\log P_{OCT}$  3.55), CNS-1261 ( $\log P_{OCT}$  3.86), PK-11195 ( $\log P_{OCT}$  3.85),  $\beta$ -CIT ( $\log P_{OCT}$  3.84), and 5-iodo-2'-deoxyuridine ( $\log P_{OCT}$  0.97).

### 5.2.2.2 Phospholipophilicity ( $\log D_{7.4 IAM}$ )

The reference compounds that returned relatively moderate values for phospholipophilicity (Figure 5-06) are  $\beta$ -CIT ( $\log D_{7.4 IAM}$  5.55), MK-801 ( $\log D_{7.4 IAM}$  5.45), PK-11195 ( $\log D_{7.4 IAM}$  5.35), 5-I-A-85380 ( $\log D_{7.4 IAM}$  5.01), and  $\alpha$ -3-iodo-2-methyltyrosine ( $\log D_{7.4 IAM}$  2.75). The higher reported reference compound values came from CNS-1261 ( $\log D_{7.4 IAM}$  6.38), MIBG ( $\log D_{7.4 IAM}$  6.75), and I-QNB ( $\log D_{7.4 IAM}$  6.97).

### 5.2.2.3 Blood-Brain Barrier Penetration ( $\text{clog BB}$ )

A high  $\text{clog BB}$  measurement is indicative of likely success for blood-brain barrier penetration and low  $\text{clog BB}$  measurements suggest that blood-brain barrier penetration would be poor (Figure 5-07). Compounds FIAU ( $\text{clog BB}$  -1.56),  $\alpha$ -3-iodo-2-methyltyrosine ( $\text{clog BB}$  -2.81), and 5-iodo-2'-deoxyuridine ( $\text{clog BB}$  -2.98) are all indicated to have unfavourable blood-brain barrier penetration characteristics. Compounds PK11195 ( $\text{clog BB}$  1.62), I-QNB ( $\text{clog BB}$  1.31), CNS-1261 ( $\text{clog BB}$  1.03),  $\beta$ -CIT ( $\text{clog BB}$  0.99), MK-801 ( $\text{clog BB}$  0.87), and MIBG ( $\text{clog BB}$  0.56) are all indicated to have favourable blood-brain barrier penetration characteristics by this predictor. The predictor for 5-I-A-85380 ( $\text{clog BB}$  -0.01) is borderline unfavourable.

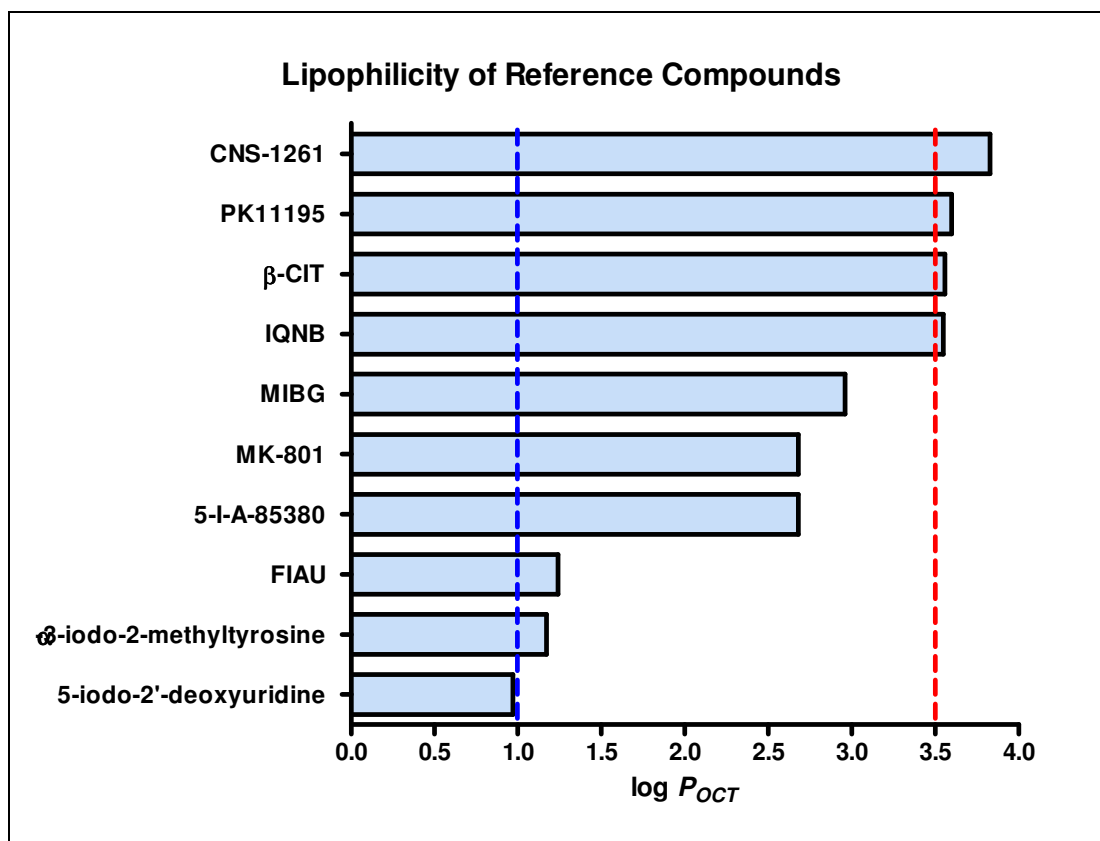


**Figure 5-05:** Measured lipophilicity of the successful and failed imaging tracers comprising the reference compounds. The best blood-brain penetration without problematic non-specific binding is anticipated to be exhibited by compounds with log  $P_{OCT}$  values between 1.0 (dotted blue line) and 3.5 (dotted red line). Retention times used in CHI calculations, which were used in log  $P_{OCT}$  calculations, were highly reproducible and variance between determinations was not within the sensitivity of the assay.

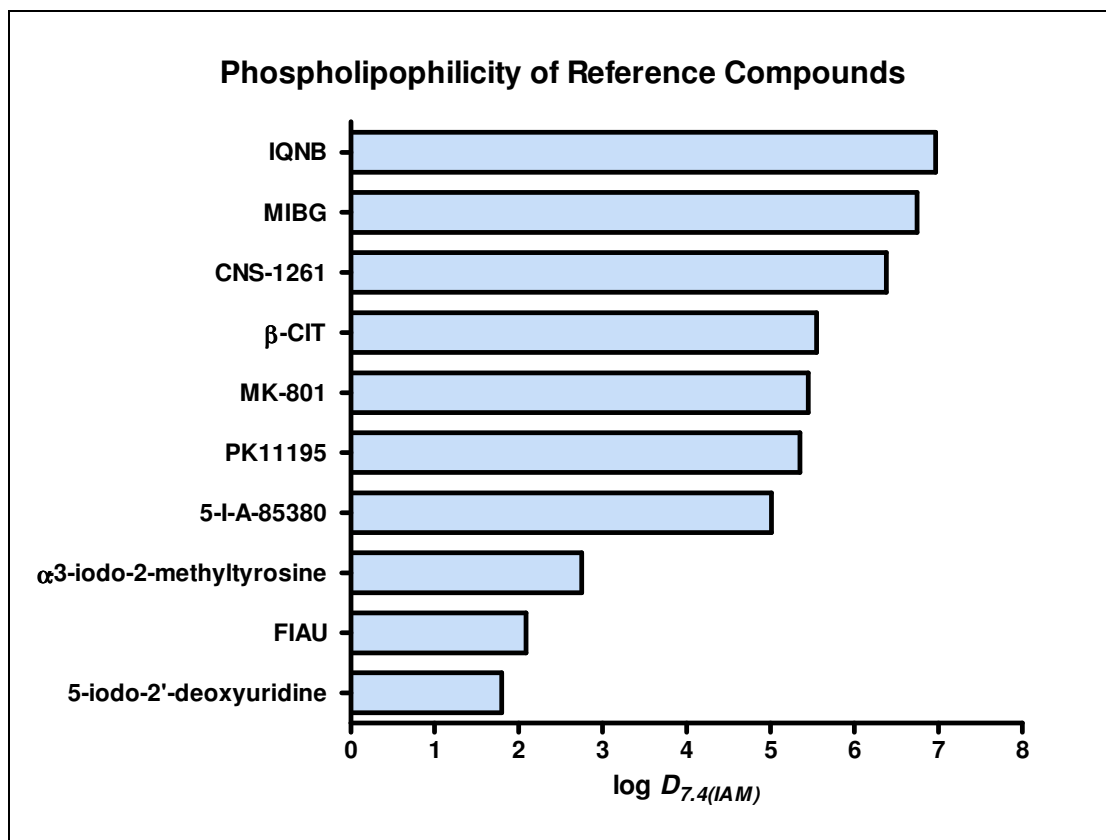


**Figure 5-06:** Measured phospholipophilicity ( $\log D_{7.4(IAM)}$ ) of the successful and failed imaging tracers comprising the reference compounds. Phospholipophilicity is used as a predictor of nonspecific binding and high values indicate higher nonspecific binding. Retention times used in CHI calculations, which were used in  $\log D_{7.4(IAM)}$  calculations, were highly reproducible and variance between determinations was not within the sensitivity of the assay.

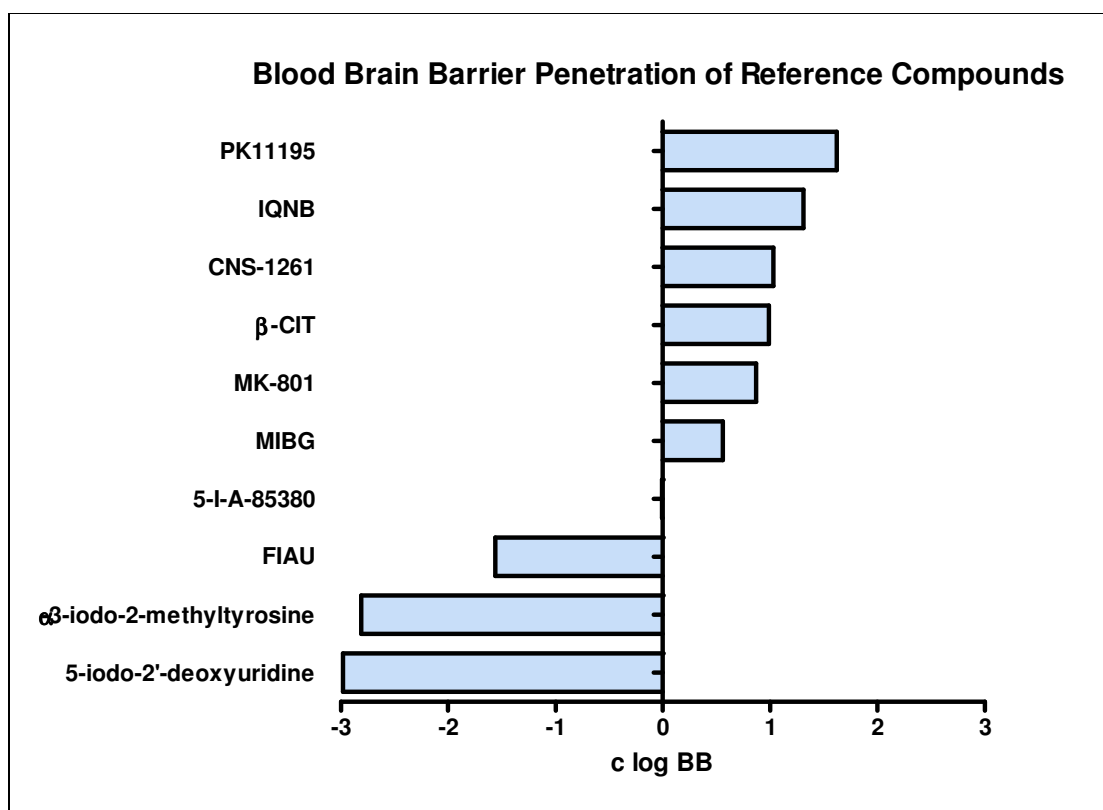


**Figure 5-07:** Measured blood-brain barrier penetration predictors ( $c \log BB$ ) for the successful and failed tracers comprising the reference compounds. Higher and lower values indicate greater and lesser brain penetration, respectively. The negative numbers are theoretical and are interpreted as an inability to penetrate the blood-brain barrier. Retention times used in CHI calculations, which were used in  $c \log BB$  calculations, were highly reproducible and variance between determinations was not within the sensitivity of the assay.

#### 5.2.2.4 Plasma Protein Binding (c%PPB)

I-QNB (c%PPB 97.72), PK-11195 (c%PPB 97.66), posted very similar predictors to the iodinated reboxetine compounds for plasma protein binding, although it is over the defined 95% threshold for desirable levels of plasma protein binding. CNS-1261 (c%PPB 95.84) was also determined to be above the 95% threshold for plasma protein binding (Figure 5-08). MIBG (c%PPB 71.44),  $\alpha$ -3-iodo-2-methyltyrosine (c%PPB 68.97),  $\beta$ -CIT (c%PPB 67.62), MK-801 (c%PPB 48.59), 5-I-A-85380 (c%PPB 27.91), FIAU (c%PPB 19.16), 5-iodo-2'-deoxyuridine (c%PPB 4.31) were well within limits with low predictors for plasma protein binding.

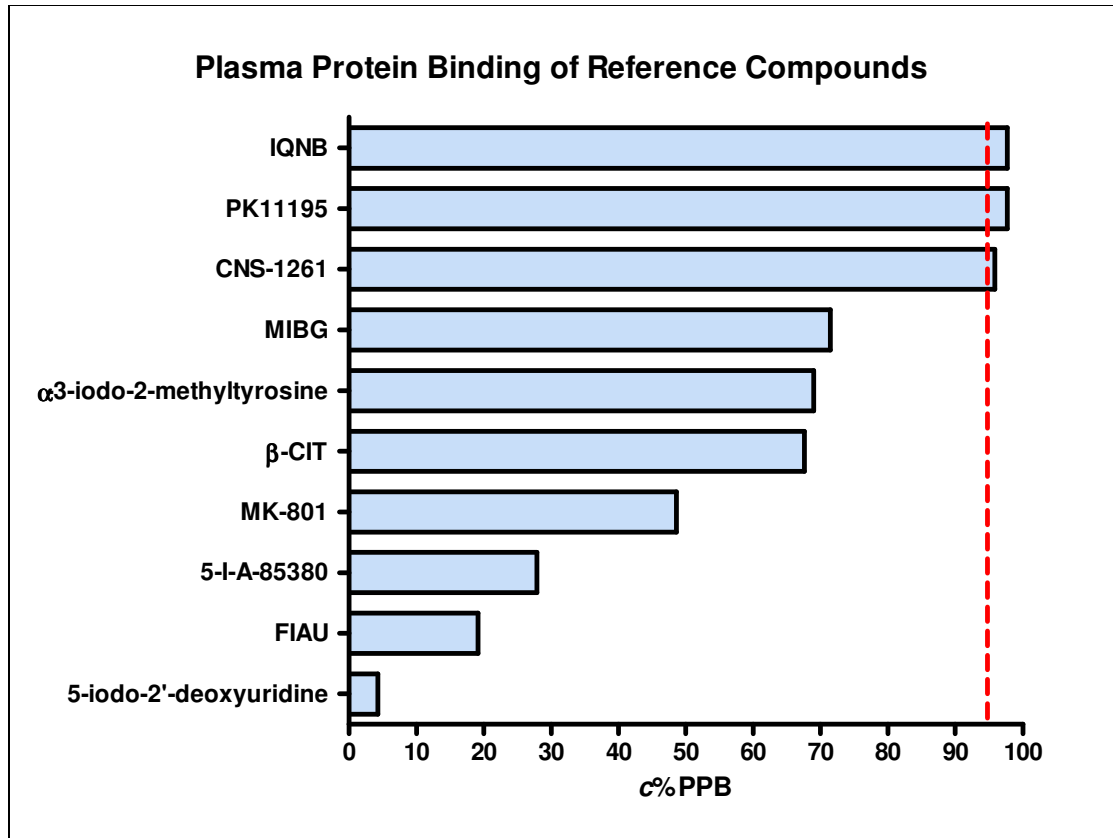


**Figure 5-08:** Plasma protein binding derived from a combination of HSA and AGP affinity determinations for the successful and failed tracers comprising the reference compounds. Plasma protein binding is considered inversely proportional to availability of a compound in plasma, although some compounds can use plasma proteins as carrier molecules to more successfully penetrate the brain. Retention times used in CHI calculations, which were used in c%PPB calculations, were highly reproducible and variance between determinations was not within the sensitivity of the assay.

## 5.2.3 Combined Data Sets

### 5.2.3.1 Lipophilicity ( $\log P_{\text{OCT}}$ )

Relative to reboxetine, the addition of the iodine increased the lipophilicity of the iodoreboxetine compounds (Table 5-01). Out of these, NKJ-64 is the only iodinated reboxetine analogue with favourable pharmacological characteristics (high selectivity and  $K_i < 10\text{nM}$ , see Chapter 4) and is expected to penetrate the brain with moderate/high nonspecific binding. Overall, there is good correlation between the  $\log P_{\text{OCT}}$  predictor and brain penetration as well as nonspecific binding, although there are discrepancies where compounds such as MIBG, FIAU, and  $\alpha$ -3-iodo-2-methyltyrosine do not conform to that trend.

Comparison of the  $\log P_{\text{OCT}}$  data for reboxetine-like compounds with that of the reference compounds indicates that all iodinated reboxetine and iodoamide compounds should cross the blood-brain barrier. The iodinated reboxetine analogues on the whole can be expected to exhibit high nonspecific binding, while the iodoamide compounds are predicted to have low nonspecific binding. Individually, NKJ-64 is the most favourable compound.

### 5.2.3.2 Phospholipophilicity ( $\log D_{7.4 \text{ IAM}}$ )

The iodinated reboxetine compounds have all demonstrated high value  $\log D_{7.4 \text{ IAM}}$  predictors and therefore can be expected to exhibit high nonspecific binding (Table 5-02). Out of the compounds with acceptable NAT affinity (Chapter 4), NKJ-64 has the lowest predictor for nonspecific binding and is similar in determination to that of I-QNB, which exhibits moderate nonspecific binding. However, NKJ-64 also returned higher predictors for nonspecific binding than CNS-1261 and PK11195, both of which are known to have high nonspecific binding when used for imaging.

On the whole, the  $\log D_{7.4 \text{ IAM}}$  predictor was generally well correlated with nonspecific binding demonstrated *in vivo*, however there are no clear-cut thresholds.

Table 5-01: Combined Lipophilicity Results			
Log $P_{OCT}$	Compound	Blood-Brain Barrier Penetration?	Nonspecific Binding
3.83	CNS-1261	Yes	High
3.68	NKJ-67		
3.62	NKJ-68		
3.60	PK11195	Yes	High
3.57	( <i>R,R</i> )-iodoreboxetine		
3.56	$\beta$ -CIT	Yes	Low
3.55	I-QNB	Yes	Moderate
3.54	( <i>S,S</i> )-iodoreboxetine		
3.40	NKJ-64		
2.96	MIBG	No	Not a brain imaging tracer
2.81	Reboxetine	Yes	Not a brain imaging tracer
2.68	MK-801	Yes	
2.68	5-I-A-85380	Yes	Low
1.88	NKJ-38		
1.87	NKJ-50		
1.24	FIAU	No	Not a brain imaging tracer
1.17	$\alpha$ -3-iodo-2-methyltyrosine	Yes (Active Transport)	
0.97	5-iodo-2'-deoxyuridine	No	

**Table 5-01:** Lipophilicity ( $\log P_{OCT}$ ) of reboxetine-like tracer candidate compounds and lipophilicity ( $\log P_{OCT}$ ), blood brain barrier penetration (where known), and nonspecific binding (where known) for the reference compounds that are comprised of both successful and failed tracers. Compounds with measured lipophilicity values that fall within the ideal  $\log P_{OCT}$  range of 1-3.5 are highlighted in green shading.

<b>Table 5-02: Combined Phospholipophilicity Results</b>		
<b>Log <math>D_{7.4 \text{ IAM}}</math></b>	<b>Compound</b>	<b>Nonspecific Binding</b>
7.38	NKJ-67	
7.17	NKJ-68	
7.08	( <i>R,R</i> )-iodoreboxetine	
7.08	( <i>S,S</i> )-iodoreboxetine	
6.97	I-QNB	Moderate
6.87	NKJ-64	
6.75	MIBG	Not a brain imaging tracer
6.38	CNS-1261	High
5.90	Reboxetine	Not a brain imaging tracer
5.55	$\beta$ -CIT	Low
5.45	MK-801	
5.35	PK11195	High
5.01	5-I-A-85380	Low
4.14	NKJ-38	
4.14	NKJ-50	
2.75	$\alpha$ -3-iodo-2-methyltyrosine	Low
2.09	FIAU	Not a brain imaging tracer
1.80	5-iodo-2'-deoxyuridine	

**Table 5-02:** Phospholipophilicity (log  $D_{7.4 \text{ IAM}}$ ) of reboxetine-like compounds and reference compounds comprised of both successful and failed tracers. Higher determined values indicate higher nonspecific binding. Reference compounds have nonspecific binding characteristics listed where known.

### **5.2.3.3 Blood-Brain Barrier Penetration (clog BB)**

The clog BB predictor indicates that all of the reboxetine-like compounds tested will cross the blood-brain barrier (5-03). NKJ-64 returned a very similar predictor to I-QNB, which has been used successfully as a brain imaging tracer. The iodinated reboxetine analogues indicated greater blood-brain barrier penetrability than reboxetine and the iodoamides were determined to have lesser blood-brain barrier penetrability in comparison to reboxetine. Overall, there is good correlation between the clog BB predictor and the known blood-brain barrier penetration of the reference compounds, although there are anomalies such as MIBG which are known not to successfully penetrate the brain.

### **5.2.3.4 Plasma Protein Binding (c%PPB)**

All the predictors for the iodinated reboxetine compounds exceeded the 95% threshold for plasma protein binding (Table 5-04). However the c%PPB value for NKJ-64 is not too dissimilar to I-QNB or PK11195, which have both been used successfully for imaging, so it is not clear whether this will be problematic or not. Reboxetine and the iodoamides were determined to have predictor values well below the 95% however the iodoamides have no notable affinity for the NAT.

<b>Table 5-03: Combined Blood-Brain Barrier Penetration Results</b>		
<b>clog BB</b>	<b>Compound</b>	<b>Blood-Brain Barrier Penetration?</b>
1.62	PK11195	Yes
1.53	NKJ-67	
1.48	NKJ-68	
1.39	( <i>R,R</i> )-iodoreboxetine	
1.38	( <i>S,S</i> )-iodoreboxetine	
1.31	I-QNB	Yes
1.29	NKJ-64	
1.03	CNS-1261	Yes
0.99	$\beta$ -CIT	Yes
0.87	MK-801	
0.88	Reboxetine	Yes
0.56	MIBG	No
0.23	NKJ-38	
0.23	NKJ-50	
-0.01	5-I-A-85380	Yes
-1.56	FIAU	No
-2.81	$\alpha$ -3-iodo-2-methyltyrosine	Yes (Active Transport)
-2.98	5-iodo-2'-deoxyuridine	No

**Table 5-03:** Blood-brain barrier penetration (clog BB) of reboxetine-like compounds and reference compounds comprised of both successful and failed tracers. Higher determined values indicate greater brain penetration and green shading denotes likelihood to cross the blood brain barrier based upon the clog BB value.

<b>Table 5-04: Combined Plasma Protein Binding Results</b>		
<b>c%PPB</b>	<b>Compound</b>	<b>Plasma Protein Binding Below 95%?</b>
98.60%	NKJ-67	
98.37%	NKJ-68	
97.91%	( <i>S,S</i> )-iodoreboxetine	
97.87%	( <i>R,R</i> )-iodoreboxetine	
97.72%	I-QNB	
97.66%	PK11195	Yes
97.49%	NKJ-64	
95.84%	CNS-1261	Yes
82.75%	Reboxetine	
71.44%	MIBG	
68.97%	$\alpha$ -3-iodo-2-methyltyrosine	
67.62%	$\beta$ -CIT	Yes
48.59%	MK-801	Yes
46.09%	NKJ-38	
44.15%	NKJ-50	
29.91%	5-I-A-85380	Yes
19.16%	FIAU	
4.31%	5-iodo-2'-deoxyuridine	Too unstable to measure.

**Table 5-04:** Plasma protein binding (c%PPB) of reboxetine-like compounds and reference compounds comprised of both successful and failed tracers. Determined values above 95% indicate the potential for problematic plasma protein binding, while green shading indicates sufficiently low plasma protein binding to increase likelihood of plasma availability.

### 5.2.3.5 Summary

NKJ-64 displayed good lipophilicity, high phospholipophilicity, high blood-brain barrier penetration, and high plasma protein binding (Tables 5-05 and 5-06). With regard to potentially unfavourable phospholipophilicity and plasma protein binding, examples of successful tracers had similar determinations so the thresholds for these criteria are not absolute.

The predictors of the iodinated reboxetine compounds as a group were generally of good brain penetration, high nonspecific binding, and high plasma protein binding. As tracers, neuroimaging may be difficult if nonspecific binding is too high and availability of the tracer in serum may be reduced if the plasma protein binding proves excessive. The iodoamides generally demonstrated good brain penetration, good nonspecific binding, and low plasma protein binding and thus have demonstrated many of the qualities consistent with the successful tracer. However, the iodoamides have previously been shown to have insufficient affinity at monoamine transporters to be considered as tracers at these sites (Chapter 4).

On the whole, the determined predictor values correlated well with known trends for reference compounds, although there were anomalies (Tables 5-05 and 5-06). Many compounds that have been determined to have a high lipophilicity ( $\log P_{\text{OCT}}$ ) also returned high predictors for phospholipophilicity ( $\log D_{7.4 \text{ IAM}}$ ), calculated blood-brain barrier penetration ( $\text{clog BB}$ ), and calculated plasma protein binding ( $\text{c\%PPB}$ ).

<b>Table: 5-05: HPLC Summary – Predictors of <i>in vivo</i> molecular behaviour</b>					
<b>Categories and Compounds</b>		<b>log <math>P_{OCT}</math></b>	<b>log <math>D_{7.4}^{IAM}</math></b>	<b>clog BB</b>	<b>c%PPB</b>
<i>Ideal Range or Preferable Trend</i>		<i>1 – 3.5</i>	<i>Low</i>	<i>High</i>	<i>&lt;95%</i>
<b>Reboxetine Analogues</b>	Reboxetine mesylate ( <i>S,S/R,R</i> )	2.81	5.90	0.88	82.75
	( <i>S,R</i> )-iodoreboxetine	<i>not tested</i>			
	( <i>R,S</i> )-iodoreboxetine	<i>not tested</i>			
	( <i>S,S</i> )-iodoreboxetine	3.54	7.08	1.38	97.91
	( <i>R,R</i> )-iodoreboxetine	3.57	7.08	1.39	97.87
	NKJ-38	1.88	4.14	0.23	46.09
	NKJ-50	1.87	4.14	0.23	44.15
	NKJ-64	3.40	6.87	1.29	97.49
	NKJ-67	3.68	7.38	1.53	98.60
NKJ-68	3.62	7.17	1.48	98.37	
<b>Reference Compounds</b>	PK11195	3.60	5.35	1.62	97.66
	MIBG	2.96	6.75	0.56	91.44
	$\beta$ -CIT	3.56	5.55	0.99	67.62
	CNS-1261	3.83	6.38	1.03	95.84
	5-I-A-85380	2.68	5.01	-0.01	27.91
	I-QNB	3.55	6.97	1.31	97.72
	$\alpha$ -3-iodo-2-methyltyrosine	1.17	2.75	-2.81	68.97
	5-iodo-2'-deoxyuridine	0.97	1.80	-2.98	4.31
	FIAU	1.24	2.09	-1.56	19.16
	MK-801	2.68	5.45	0.87	48.59

**Table 5-05:** HPLC-measured predictors for *in vivo* molecular behaviour of reboxetine analogues and the successful and failed brain imaging tracers comprising the reference compounds.

<b>Table 5-06: HPLC Summary – Predictors of <i>in vivo</i> molecular behaviour</b>					
<b>Categories and Compounds</b>		<b>log <math>P_{OCT}</math></b>	<b>log <math>D_{7.4}^{IAM}</math></b>	<b>clog BB</b>	<b>c%PPB</b>
<i>Ideal Range or Preferable Trend</i>		<i>Moderate</i>	<i>Low</i>	<i>High</i>	<i>&lt;95%?</i>
<b>Reboxetine Analogues</b>	Reboxetine mesylate ( <i>S,S/R,R</i> )	Moderate	Moderate	Moderate	Yes
	( <i>S,R</i> )-iodoreboxetine	<i>not tested</i>			
	( <i>R,S</i> )-iodoreboxetine	<i>not tested</i>			
	( <i>S,S</i> )-iodoreboxetine	High	High	High	No
	( <i>R,R</i> )-iodoreboxetine	High	High	High	No
	NKJ-38	Moderate	Low	Moderate	Yes
	NKJ-50	Moderate	Low	Moderate	Yes
	NKJ-64	Moderate	High	High	No
	NKJ-67	High	High	High	No
NKJ-68	High	High	High	No	
<b>Reference Compounds</b>	PK11195	High	Moderate	High	No
	MIBG	Moderate	High	Moderate	Yes
	$\beta$ -CIT	High	Moderate	Moderate	Yes
	CNS-1261	High	Moderate	Moderate	No
	5-I-A-85380	Moderate	Moderate	Low	Yes
	I-QNB	High	High	High	No
	$\alpha$ -3-iodo-2-methyltyrosine	Moderate	Low	Very Low	Yes
	5-iodo-2'-deoxyuridine	Low	Low	Very Low	Yes
	FIAU	Moderate	Low	Very Low	Yes
	MK-801	Moderate	Moderate	Moderate	Yes

**Table 5-06:** HPLC-derived predictors for *in vivo* molecular behaviour of reboxetine analogues and the successful and failed brain imaging tracers comprising the reference compounds. Determined values have been converted into general descriptors.

## 5.2 Discussion

### 5.2.1 Iodinated reboxetine compounds

NKJ-64 has displayed many of the HPLC-determined properties that are consistent with successful tracers and has previously been shown to have favourable NAT-specific pharmacology (Chapter 4). Predictors for lipophilicity ( $\log P_{\text{OCT}}$ ) indicated good blood-brain penetration, calculated blood-brain barrier penetration predictors ( $\text{clog BB}$ ) were similarly favourable, and calculated plasma protein binding ( $\text{c\%PPB}$ ) that was high but not dissimilar to successful reference compounds.

The position of the iodine on the iodoreboxetine compounds did not greatly affect lipophilicity, although the only compound within range was NKJ-64 with the iodine in the ortho position. Predictors for phospholipophilicity ( $\log D_{7.4 \text{ IAM}}$ ) indicated that nonspecific binding would be high in all iodinated reboxetine compounds, but the predictor for NKJ-64 was similar to the value returned by reference compound I-QNB, which has moderate nonspecific binding *in vivo*. The iodinated reboxetine analogues ( $\log D_{7.4 \text{ IAM}}$  6.87-7.38) all had higher phospholipophilicity than reboxetine ( $\log D_{7.4 \text{ IAM}}$  5.90). Given the limited library of reference compounds with which to compare, it is difficult to ascertain with certainty whether nonspecific binding will be problematic until an iodinated reboxetine compound is radiolabelled and examined further.

The iodination of reboxetine increased the blood-brain barrier penetrability as determined by the  $\text{clog BB}$  measurement and it was not greatly affected by the position of the iodine. While there is of yet no firmly defined threshold for blood-brain barrier penetrability, a greater library of reference compounds in future studies may yield sufficient data to establish one. One of the reasons the methanol elution may be tried is to improve the peak shape or reproducibility for compounds being eluted from the column when a compound demonstrates low solubility in acetonitrile (Kalendarev et al. 2001) and is a worthwhile technique.

The plasma protein binding measured for the iodinated reboxetine analogues was very high, and plasma protein binding can deplete tracer availability in serum. The lead compound, NKJ-64, had the lowest plasma protein binding predictor of any of

the pharmacologically favourable compounds, although this was still greater than 95%. The location of the iodine, whether on the phenoxy or phenyl ring, seemed to make little difference to the degree of increase in plasma protein binding relative to reboxetine. If indeed plasma protein binding greater than 95% results in a problematic decrease in tracer availability in the serum, then these results could indicate unsuitability from these compounds. However, that is not to say that all compounds with high serum protein binding properties are disadvantaged from entering the brain; the clinical drugs diazepam and fluoxetine exhibit 93.2% and 97.1% binding to HSA, respectively (Hollósy et al. 2006). One such hypothesis to explain this is that plasma proteins can mediate transport of tracers across the blood-brain barrier, as was found with AGP (Lin et al. 1987), and it could be that the plasma protein binding of highly lipophilic compounds prevent their sequestering into peripheral interstitium, muscle, and adipose tissue – thus maintaining compound concentrations in the plasma for brain penetration.

The iodinated amides NKJ-38 and NKJ-50, lacking the phenoxy ring from their molecular structure, had far reduced plasma protein binding predictors of  $c\%PPB$  46.09 and  $c\%PPB$  44.15, respectively. However, the monoamine transporter pharmacology of the amide compounds is extremely poor (Chapter 4) and they would not make suitable brain imaging tracers.

## **5.2.2 Reference compounds (successful and failed tracers)**

The HPLC methodology applied here returns on average a higher log  $P$  value than is recorded in the literature for similar molecules. However, as Waterhouse (2003) took several different types of determination into account for setting out the ideal log  $P$  range of 1-3.5, it is still a reasonable range to apply here to give useful feedback on the suitability of a compound – although perhaps allowing some flexibility in the upper ranges and particular stringency in the lower ranges of returned values would be appropriate for the selection process. Generally, these compounds followed the same trends relative to one another as they do in the literature, with MIBG the most notable of a few exceptions.

MIBG and FIAU are unable to cross the blood-brain barrier (Gourand et al. 2010; Jacobs et al. 2001; respectively) and lipophilicity values for MIBG in the literature

report  $\log P_{OCT}$  -0.51 (DeGrado & Wang 1998) and  $\log P$  0.15 (Raffel & Wieland 2001b) – with a great discrepancy between those values and my predictor of  $\log P_{OCT}$  2.96 for MIBG and a smaller discrepancy for FIAU, for which my predictor was  $P_{OCT}$  1.24. These outlying values from the ideal range suggested by Waterhouse (2003) better reflect what is known about the *in vivo* behaviour of MIBG and FIAU. Perhaps the molecular modelling I used was not accounting for certain characteristics of these molecules, such as strongly electronegative double oxygen bonds in FIAU or polar amine groups in MIBG. Gourand *et al* (2010) demonstrated a lipophilic dihydroquinoline/quinolinium salt could be used as a chemical delivery system to carry MIBG across the blood-brain barrier, perhaps by improving the overall lipophilicity of the temporarily combined molecule. Unfortunately, standardisation is very poor in calculations of  $\log P$  and even  $\log P_{OCT}$ , so perhaps the molecular modelling used by DeGrado & Wang and Raffel & Wieland were better suited to MIBG and FIAU. If it is a case that no model yet exists to encompass all types of compound, then future investigations could examine a larger library of compounds that exhibit similar *in vivo* behaviour to determine if there is a common structural arrangement or feature that means one molecular model should be chosen over another for predicting the behaviour of a particular class of compound.

MK-801 was determined by HPLC measurement to have good lipophilicity and phospholipophilicity, although the iodinated SPECT tracer compound has excessive nonspecific binding manifested through accumulation in white matter (Owens et al. 1997). The compound measured in this thesis is structurally that of the therapeutic drug and not the iodinated SPECT imaging tracer, so this disparity between the predictor for the uniodinated compound and the known binding of the iodinated SPECT tracer is interesting. Assuming that the predictors are a fair reflection of MK-801's *in vivo* behaviour, when combined with the increases in  $\log P_{OCT}$  and  $\log D_{7.4\text{ IAM}}$  that iodination causes to the reboxetine molecule, it supports the hypothesis that iodination will typically increase both lipophilicity and phospholipophilicity. CNS-1261 ( $\log P_{OCT}$  3.86), PK-11195 ( $\log P_{OCT}$  3.85) and  $\beta$ -CIT ( $\log P_{OCT}$  3.84) were all outliers from the ideal range and yet all have been used successfully as imaging tracers (Bressan et al. 2005; Chauveau et al. 2008; Laruelle et al. 2000; respectively). However, these outliers were not outwith of the ideal range by a large degree and so the method's general trend for predicting compound behaviour was maintained.

$\alpha$ -3-iodo-2-methyltyrosine was measured to be favourably lipophilic ( $\log P_{OCT}$  1.17) and although it does get into the brain it has been shown to cross the blood-brain barrier via specific transport (Langen et al. 1991). Consequently, it is unclear to what extent its lipophilicity contributes, if at all, to its brain penetration. Quite clearly in the Waterhouse review (2003), the ideal log P range does not apply to compounds that have an alternative route across the blood-brain barrier such as active transport. Given the time and resources, it would be better to build up a database of tested compounds in order to determine new limits and perhaps improving upon the Waterhouse criteria is something for future investigations to undertake.

For a compound to be successful, an ideal  $\log P_{OCT}$  value appears to be a guideline rather than a rule, so falling within this range does not guarantee successful brain penetration and, conversely, falling outside of this range does not certify blood brain barrier impenetrability – so it is clear that measured lipophilicity is not the quintessential property that exclusively determines tracer success and therefore the other properties of a compound are also important. Lipophilicity is, however, one of the key behavioural properties that may not necessarily be compensated for in the other characteristics of a candidate compound, so those molecules that fall within the ideal range appear to have a greater likelihood of penetrating the blood-brain barrier successfully, while keeping within acceptable limits for nonspecific binding.

High predictors for nonspecific binding in terms of phospholipophilicity were derived for iodinated reboxetine compounds. If indeed these translate into high nonspecific binding *in vivo*, one comparison compound could be CNS-1261, which yielded a not too dissimilar phospholipophilicity of  $\log D_{7.4\text{IAM}}$  6.38. CNS-1261 has been used successfully as a tracer even though *in vivo* nonspecific binding was estimated in white matter to be 60-80% (Erlandsson et al. 2003). 5-I-A-85380 exhibits virtually no nonspecific binding *in vitro* (Pimlott et al. 2004) and has been used successfully for *in vivo* brain imaging (Ogawa et al. 2009) with demonstrated nonspecific binding of 28-30% as ascertained by displacement studies (Fujita et al. 2000).  $\beta$ -CIT has similarly been successfully applied as a brain imaging tracer (Laruelle et al. 2000; Scanley et al. 2000) and demonstrated nonspecific binding of 8% (Al-Tikriti et al. 1995). PK11195 has been used as a successful brain imaging

tracer despite a fairly high demonstrated nonspecific binding of 60% (Petit-Taboue et al. 1991), although this value did include the free fraction during the *in vivo* scans and the nonspecific binding alone was not determined. MK-801 posted a reasonable phospholipophilicity ( $\log D_{7.4 \text{ IAM}} 5.45$ ) in comparison to many other reference compounds used here, but is known to have difficulties with nonspecific binding (Erlandsson et al. 2003).

For clinical imaging purposes, MIBG is predominantly used in the periphery, because it does not cross the blood brain barrier in humans (Guilloteau et al. 1983a; - French language, cited by Baulieu et al. 1990) unless the blood brain barrier is compromised, and the high phospholipophilicity reported here ( $\log D_{7.4 \text{ IAM}} 6.75$ ) is a potential explanation for its inability to penetrate into the brain in light of the acceptable lipophilicity discussed earlier. As a substrate compound, MIBG has found use in treating NAT- and SERT-expressing neuroblastomas and is also taken up by platelets via the SERT (Tytgat et al. 2002), causing thrombocytopenia. Throughout this use, nonspecific binding in the periphery is difficult to quantify given the widespread locations of NAT and SERT. However, quantification seems unnecessary given the immensely amplified level to which tumours over-express monoamine transporters and accumulate MIBG. I-QNB demonstrates the highest phospholipophilicity recorded by any of my chosen reference compounds ( $\log D_{7.4 \text{ IAM}} 6.97$ ) and in practice has shown *in vivo* nonspecific binding of 42-55% in relation to the cerebellum, which was taken as a reference region (Varastet et al. 1992).

FIAU was measured to have a low phospholipophilicity ( $\log D_{7.4 \text{ IAM}} 2.09$ ) and this, in combination with a low lipophilicity (albeit still within the Waterhouse-proposed range) may very well contribute to its inability to effectively cross the blood-brain barrier. However, low phospholipophilicity appears not to always be a disadvantage as  $\alpha$ -3-iodo-2-methyltyrosine ( $\log D_{7.4 \text{ IAM}} 2.75$ ) exhibits, alongside active transport into the brain, a passive blood-brain barrier penetration representing 10% of  $\alpha$ -3-iodo-2-methyltyrosine brain uptake (Riemann et al. 2001).

5-iodo-2'-deoxyuridine ( $\log D_{7.4 \text{ IAM}} 1.80$ ) cannot be assessed for nonspecific binding in the same sense as a ligand because it is a gene marker that becomes incorporated into rapidly proliferating cells where upon a specific signal is measured, while in contact with free serum it succumbs to rapid dehalogenation,

making nonspecific binding *in vivo* extremely difficult to quantify for the parent compound (Khalili et al. 2003). While it was shown to exhibit 40% nonspecific binding in cells, it is unknown how this might relate to the HPLC-derived phospholipophilicity measurement. With such a low aforementioned lipophilicity and phospholipophilicity, it would not be surprising if it was unable to penetrate the brain without the active transport processes that it relies upon for crossing the blood-brain barrier.

So although a high phospholipophilicity is associated with the potential for high nonspecific binding, it is not a characteristic that is unequivocally associated with all failed tracers and lacked by all successful ones. A precise range or threshold is not defined, but generally it would be preferable to observe low phospholipophilicity as it would be a predictor of low nonspecific binding *in vivo*.

The *clog* BB measurement was generally in good agreement with what is known about the ability of each reference compound to cross the blood-brain barrier, however there are no defined thresholds and the library of compounds here was too small to identify one. MIBG and 5-I-A-85380 were exceptions to the trend, with MIBG reporting a *clog* BB of 0.56 while being unable to cross the blood-brain barrier and 5-I-A-85380 measured as -0.01 while penetrating the blood-brain barrier successfully. A value of -2.81 was returned for  $\alpha$ -3-iodo-2-methyltyrosine, however this molecule is actively transported into the brain and thus cannot be said to be an anomaly in a predictor that only applies to passive diffusion across the blood-brain barrier. Furthermore, the process of active transport via amino acid carriers by compounds such as  $\alpha$ -3-iodo-2-methyltyrosine undoubtedly involves some association between blood-brain barrier proteins and plasma proteins to penetrate the brain.

Successful SPECT brain imaging tracers 5-I-A-85380, CNS-1261, and PK-11195 have exhibited greater than 95% plasma protein binding measured via HPLC, despite studies showing that availability in plasma for compounds such as CNS-1261 are below this threshold (Bressan et al. 2004) and PK11195 can be defined as simply >80% (Lockhart et al. 2003). While MIBG is another anomaly that falls beneath the plasma protein binding threshold and fails to penetrate the brain, there may be other reasons for this that are unrelated to the availability of MIBG in the serum. These discrepancies between the plasma protein binding predictions

and the known behaviour of reference compounds in the serum suggest that perhaps the threshold for acceptable plasma protein binding as determined via HPLC requires further optimisation.

It has been previously reported that immobilized AGP, used to derive the  $c\%$ PPB figure, is not suitable as a chromatographic method due to carboxylic groups which are occupied by bonding with the silica support and thus are not available for interaction with positively-charged compounds (Schill et al. 1986). According to C-18 lipophilicity determinations at neutral (near-physiological) pH levels which demonstrated reboxetine-like compound species as being more closely related to the alkali than acidic conditions, at physiological pH levels the reboxetine-like tracer candidate compounds are more likely to assume the negatively charged species than the positively charged species when using these elutions. However, the potential for variability in retention time for compounds that might assume a positively charged species with this column and elution combination means that this data cannot be taken as a guarantee of serum availability for compounds predicted to have  $<95\%$  plasma protein binding and nor does it certify poor availability for blood brain barrier penetration for compounds with  $>95\%$  plasma protein binding predicted.

Across all four measurements, lipophilicity ( $\log P_{\text{OCT}}$ ), phospholipophilicity ( $\log D_{7.4, \text{IAM}}$ ), calculated blood-brain barrier penetration ( $\text{clog BB}$ ), and calculated plasma protein binding ( $c\%$ PPB), the general trend of the reference compounds was indicated correctly. However, there were anomalies in every instance and thus underlines the importance of having a sufficiently large library of reference compounds so as to diminish the impact that individual anomalies have upon the analysis.

### 5.2.3 Conclusions

NKJ-64 displayed predictors for good lipophilicity, high phospholipophilicity, high blood-brain barrier penetration, and high plasma protein binding. With regard to the potentially unfavourable phospholipophilicity and plasma protein binding, examples of successful tracers had similar determinations so the thresholds for these criteria are not absolute. The overall trend was that the addition of the iodine atom to reboxetine increased the values of every HPLC-derived predictor,

which was desirable in the cases of the lipophilicity and blood-brain barrier penetration predictors, but unfavourable in some cases of the phospholipophilicity and plasma protein binding predictors. It was NKJ-64 that most closely demonstrated HPLC-derived properties that were consistent with successful tracers to date, while also possessing favourable monoamine transporter pharmacology (Chapter 4). It is therefore the best candidate from the tested library of iodinated reboxetine compounds for further development as a SPECT tracer.

For this and future studies, when considering all the investigated criteria together they have more value than when examined individually and this overcomes some of the shortcomings of vague thresholds. The reference compounds give meaning to the values in each of the HPLC determinations and so, to define these thresholds more specifically, a greater library of reference compounds with known behaviour *in vivo* is required to further validate the method and increase its usefulness.

## Chapter 6

### General Conclusions

#### 6.1 The NAT is not down-regulated in the PCP model of schizophrenic hypofrontality.

Monoamine transporters were probed with radioligands and their distributions were found to be consistent with those in the published literature (Chapter 3).

In a model of a disease state, I had hypothesised that the probing of monoamine transports in a PCP model of schizophrenic hypofrontality would reveal a down-regulation of the NAT in the prefrontal cortex (Chapter 3). However, no changes were found in the distributions or binding densities of the NAT or the DAT. Selective down-regulation of binding densities to the SERT was observed, although it is unclear whether the very small changes detected would be biologically significant, as biological systems can compensate for small disturbances. For example, in Parkinson's Disease, the onset of motor symptoms does not occur until 70% of nigrostriatal neurons are lost (Przuntek et al. 2004) and until the neurodegeneration reaches that point at which compensation fails, diagnosis is difficult in the absence of motor control symptoms or a neuroimaging scan. There were no significant differences to measured levels of mRNA for any of the monoamine transporters, so the small selective changes observed in SERT density were either not driven by a regulation of gene expression or the ligand binding has greater sensitivity to detect the changes than *in situ* hybridisation. It is possible that PCP was interacting directly with the SERT causing a conformational change to reduce its affinity for autoradiographic ligand binding, or causing it to be internalised into the neuron.

It had been hoped that the PCP model of schizophrenic hypofrontality would provide a model in which to demonstrate the capabilities of a SPECT tracer for the NAT, but the PCP model has no utility in that area. However, since modulation of noradrenergic neurotransmission via the blockade of the NAT has been shown to ease the negative symptoms associated with schizophrenia, the need to be able to image the NAT in both clinical and research scenarios remains. The elucidation of

how the noradrenergic system is able to be used to modulate the brain regions receiving its innervations to mitigate the negative symptoms associated with schizophrenia, and also how the brain reacts to long-term atypical neuroleptic administration, would be aided by a clinical tracer able to image noradrenaline transporter distribution. The competition for receptor occupancy in single scans may reveal mechanisms for successful neuroleptics that are partly mediated by the noradrenergic system. Long-term monitoring may reveal on follow-up scans that long-term stability or long-term deterioration for patients on antipsychotic medication may be achieved by a compensatory up- or down-regulation of sites in the noradrenergic system. Imaging the NAT would provide valuable information on which areas of the brain the noradrenergic system is most strongly innervated over time. Correlating that information with clinical reports would enable any NAT-targeted medications to be adjusted accordingly and provide feedback for future drug development needs.

## **6.2 The best pharmacology was demonstrated by NKJ-64, the ortho-position iodophenoxy ring compound.**

The evaluation of the *in vitro* pharmacology of the various candidate compounds has enabled me to select NKJ-64 as the best available compound to take forward and evaluate for predictors of *in vivo* molecular behaviour.

The greatest affinity for the NAT was demonstrated by NKJ-64 (Chapter 4); this compound compares favourably to the (*S,S*)-isomer in the published literature and affinity was in the same order of magnitude as INER/IPBM (Tamagnan et al. 2007; Kanegawa et al. 2006).

The greatest selectivity for the NAT over other monoamine transporters was demonstrated amongst the iodophenyl ring compounds, however this group of compounds did not have sufficient affinity for the NAT to be used as SPECT imaging tracers. The placement of the iodine on the phenyl ring disturbed the ability of the compounds to fit into the binding site on the noradrenaline transporter. However, the placement of the iodine in the ortho position on the phenoxy ring yielded NKJ-64 and its demonstrated favourable selectivity for the NAT over the DAT and the SERT.

**6.3 The best HPLC-derived predictors of *in vivo* behaviour were demonstrated by NKJ-64, the ortho-position iodophenoxy ring compound.**

Using HPLC-derived predictors of *in vivo* molecular behaviour, NKJ-64 has been selected as the most probable candidate to yield success as a SPECT brain imaging tracer from the array of synthesised compounds (Chapter 5).

The HPLC-derived predictors indicated that the (*S,S*)- and NKJ-50s would have made the best brain imaging tracers, however, these molecules lacked the phenoxy ring and demonstrated no noteworthy affinity for the NAT and therefore were not suitable as NAT brain imaging tracers.

NKJ-64 was determined to have good lipophilicity and predictors of blood-brain barrier penetration, however phospholipophilicity was high and indicates that non-specific binding may be high. Plasma protein binding was also high, although it is uncertain whether this will be an advantage or disadvantage – it remains to be seen whether a strong plasma protein binding association in this case will deplete available tracer for crossing the blood-brain barrier or act as a carrier molecule to slow metabolism in the plasma.

**6.4 Conclusions: NKJ-64, the ortho-position iodophenoxy ring compound, has been identified as the lead candidate for further development.**

This aim of this thesis was to develop a novel SPECT brain tracer for the noradrenaline transporter, and so satisfy the need for an *in vivo* imaging probe for this important monoamine system. The future academic research into the implication of NAT in neurological disease, clinical diagnoses and monitoring, and drug occupancy studies in pharmaceutical development would all greatly benefit from the availability of such a tool. The result is that, from a selection of compounds, a lead candidate has been identified to be taken forward for further development.

NKJ-64, the ortho-position iodo-phenoxy ring compound was identified as having the most favourable pharmacology (Chapter 4) and *in vivo* predictors (Chapter 5)

for imaging the noradrenaline transporter. The data suggests that this compound has suitable affinity for the NAT, selectivity for the NAT over other monoamine transporters, and should be capable of crossing the blood-brain barrier, however data indicates that non-specific binding may be high.

## 6.5 Subsequent Work: radiolabelled compound

The next step for determining this compound's suitability is radiolabelling with a SPECT isotope such as  $^{123}\text{I}$  or  $^{125}\text{I}$  followed by a direct saturation assay on rat brain homogenates to establish a precise  $K_D$  and levels of nonspecific binding. The binding distribution should then be defined with *in vitro* autoradiography and compared to the distribution obtained by [ $^3\text{H}$ ]-nisoxetine, using reboxetine as a displacer to ascertain nonspecific binding throughout the brain. If nonspecific binding for the radiolabelled compound is favourable *in vitro* and acceptable images are achieved with autoradiography, then development could move forward to *ex vivo* autoradiography to determine whether, following intravenous administration, plasma protein binding conditions have allowed for sufficient tracer availability, that blood-brain barrier penetration actually occurs, and that nonspecific binding *in vivo* is not problematic. The *ex vivo* autoradiography could be combined with an attempt at a pilot SPECT scan in the rat model using a micro-SPECT scanner to monitor brain uptake and distribution prior to the schedule 1 kill for brain harvesting, sectioning, and exposure to radiosensitive film.

Recently, these next stages in the development of NKJ-64 were undertaken by Tavares *et al.* (2011), referring to the compound as [ $^{125}\text{I}$ ]-NKJ64 in the literature, and it was determined that *in vitro*  $K_D$  was established as  $4.82 \pm 0.87$  nM in rat brain homogenates, and nonspecific binding defined in the presence of  $10\mu\text{M}$  reboxetine displacer was 77% at a concentration of  $6.25\text{nM}$  [ $^{125}\text{I}$ ]-NKJ-64. This high nonspecific binding correlates with the *in vivo* predictors ascertained by HPLC analysis (Chapter 5), giving validation and confidence to the HPLC technique for use in future tracer development studies. Distribution of [ $^{125}\text{I}$ ]-NKJ-64 throughout coronal rat brain sections matched the known distribution of the noradrenaline transporter (Tavares *et al.* 2011).

*In vivo* experimentation with intravenously administered [ $^{125}\text{I}$ ]-NKJ-64 yielded good brain uptake and *ex vivo* autoradiography demonstrated a good target:non-target

ratio of 2.8, indicating that nonspecific binding was reasonable, although the low density of the NAT in cortical and limbic regions meant that this radiotracer did not have sufficient sensitivity to detect displacement by pre-treatment with reboxetine in cortical or limbic regions. Displacement was demonstrable in the locus coeruleus only and, given the dimensions of the locus coeruleus, a high-resolution modern SPECT scanner will be required to ascertain worthwhile readings of pharmacological displacement or regulatory changes in this brain region should this compound be applied to future imaging studies. Given this data, any neuroimaging study using [<sup>125</sup>I]-NKJ-64 would need to rely on imaging of the locus coeruleus to make a broad observation of the noradrenaline system and more detailed imaging of noradrenaline transporters throughout the brain may not be possible with this tracer.

## Appendix I

### A1.1 Do the groups have equal variances?

The summary of statistically significant differences for the means and variances of the monoamine transporter autoradiograms demonstrates that a parametric analysis of this data set was not appropriate (Table A1-01). The spreads of the data sets for [<sup>3</sup>H]-nisoxetine binding to the NAT, [<sup>3</sup>H]-WIN-35,428 binding to the DAT, and [<sup>3</sup>H]-citalopram binding to the SERT are provided in Tables A1-02, A1-03, and A1-04, respectively.

It had been assumed that the varying expression of monoamine transporters and monoamine transporter-specific mRNA within each group would follow that of a normal distribution. With a P threshold of 0.05 and continuous repetition of the tests, two statistically different means and two statistically different variances could have been expected on pure chance alone. Five statistically different variances indicated that it could not be presumed that each PCP-treated animal is responding to the same degree to the treatment regime, with some rats being affected more than others resulting in the differences in the variances for several important regions. This was particularly evident for the measurement of SERT binding, where most of the differences between the group means were detected. Consequently, a non-parametric technique was deemed necessary and a Mann-Whitney analysis was applied to all data sets to compare the sum of rank order. Assuming the two groups have similar distributions, even if unequal variances, then this comparison of the sum of ranks can be interpreted as a comparison of medians. Analysed data from which interpretations were drawn is therefore expressed graphically as the median  $\pm$  the interquartile range in Chapter 3. As aforementioned, Table A1-01 displays the T-test and F-tests that were used to determine that a parametric analysis would not be appropriate for this data set.

Table: A1-01: Parametric analysis of autoradiographic imaging of monoamine transporters is not appropriate						
Structure	<sup>3</sup> H]-nisoxetine data		<sup>3</sup> H]-WIN-35,428 data		<sup>3</sup> H]-citalopram data	
	Means (T-test)	Variances (F-test)	Means (T-test)	Variances (F-test)	Means (T-test)	Variances (F-test)
PFC	≈	≈	≈	≈	≈	≈
ACg	≈	≈	≈	≈	≠	≈
CPu	≈	≈	≈	≠	≠	≈
N.Acc.	≈	≠	≠	≈	≠	≈
BNST	≈	≈	≈	≈	≈	≠
AVTN	≈	≈	≈	≈	≈	≈
RTN	≈	≈	≈	≈	≈	≠
CA1	≈	≈	No Binding	No Binding	≠	≈
CA2	≈	≈	No Binding	No Binding	≠	≈
CA3	≈	≈	No Binding	No Binding	≠	≈
DG	≈	≈	No Binding	No Binding	≈	≈
VTN	≈	≈	≈	≈	≈	≈
DRN	≈	≈	≈	≈	≈	≈
LC	≈	≈	≈	≈	≈	≠
CBL	≈	≈	No Binding	No Binding	≈	≈

**Table A1-01:** Summary of T-test and F-test to determine statistical differences between means and variances for [<sup>3</sup>H]-ligand binding to monoamine transporters in control and PCP-treated rat brain. The means and variances are designated as either statistically equivalent (≈) or statistically different (≠). Significance was set at a P value of 0.05 for both tests.

**Table A1-02: T-test and F-test of [<sup>3</sup>H]-Nisoxetine Binding Data**

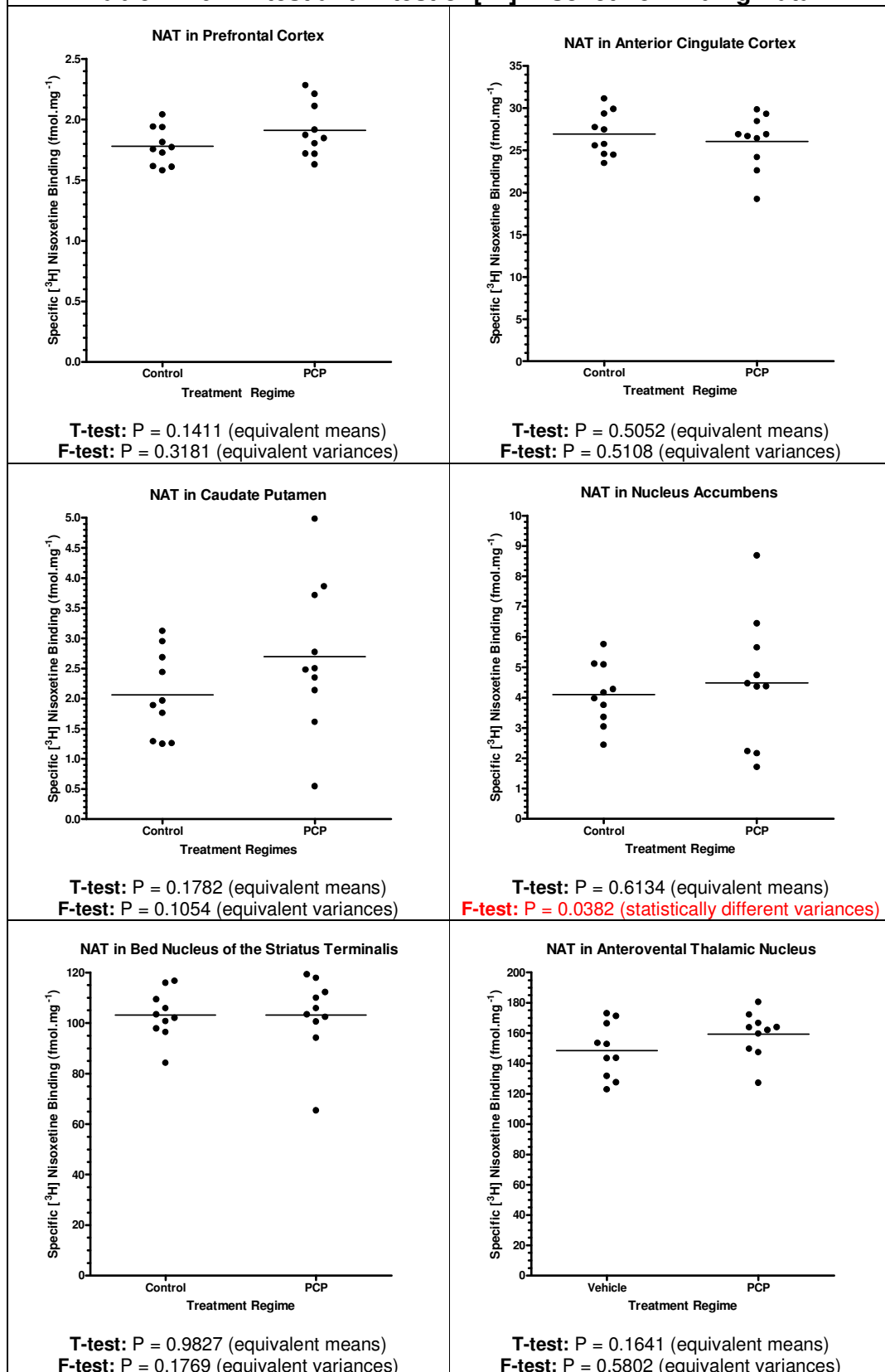


**Table A1-02:** T-test and F-test of [<sup>3</sup>H]-nisoxetine binding data. Control (n=10) and PCP-treated (n=10) data points plotted with mean indicated by bars. Significance threshold set at P < 0.05. Group variances were statistically different in the nucleus accumbens.

**Table A1-02: T-test and F-test of [<sup>3</sup>H]-Nisoxetine Binding Data (continued)**

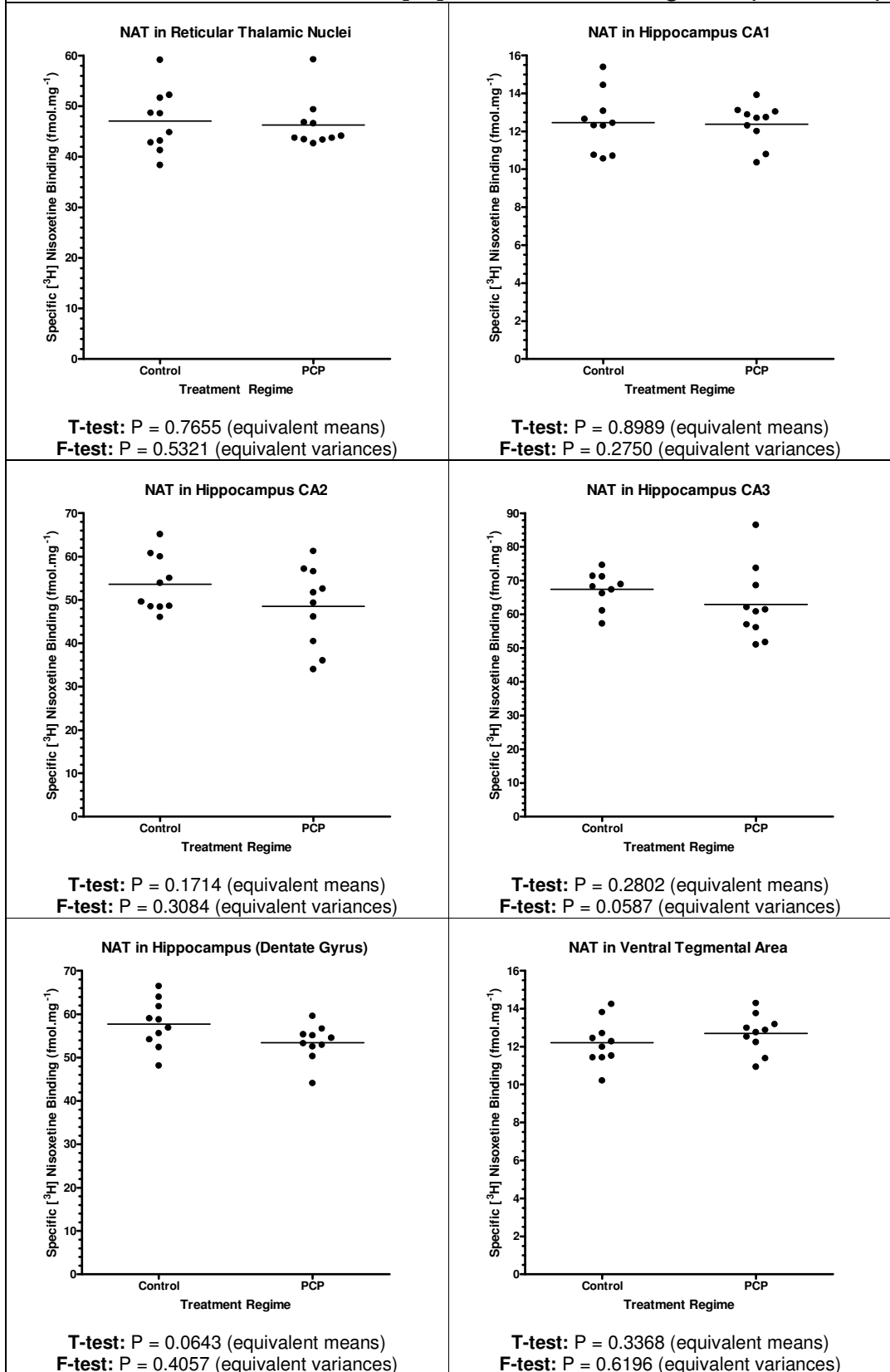


**Table A1-02 (continued):** T-test and F-test of [<sup>3</sup>H]-nisoxetine binding data. Control (n=10) and PCP-treated (n=10) data points plotted with mean indicated by bars. Significance threshold set at P < 0.05.

**Table A1-02: T-test and F-test of [<sup>3</sup>H]-Nisoxetine Binding Data (continued)**

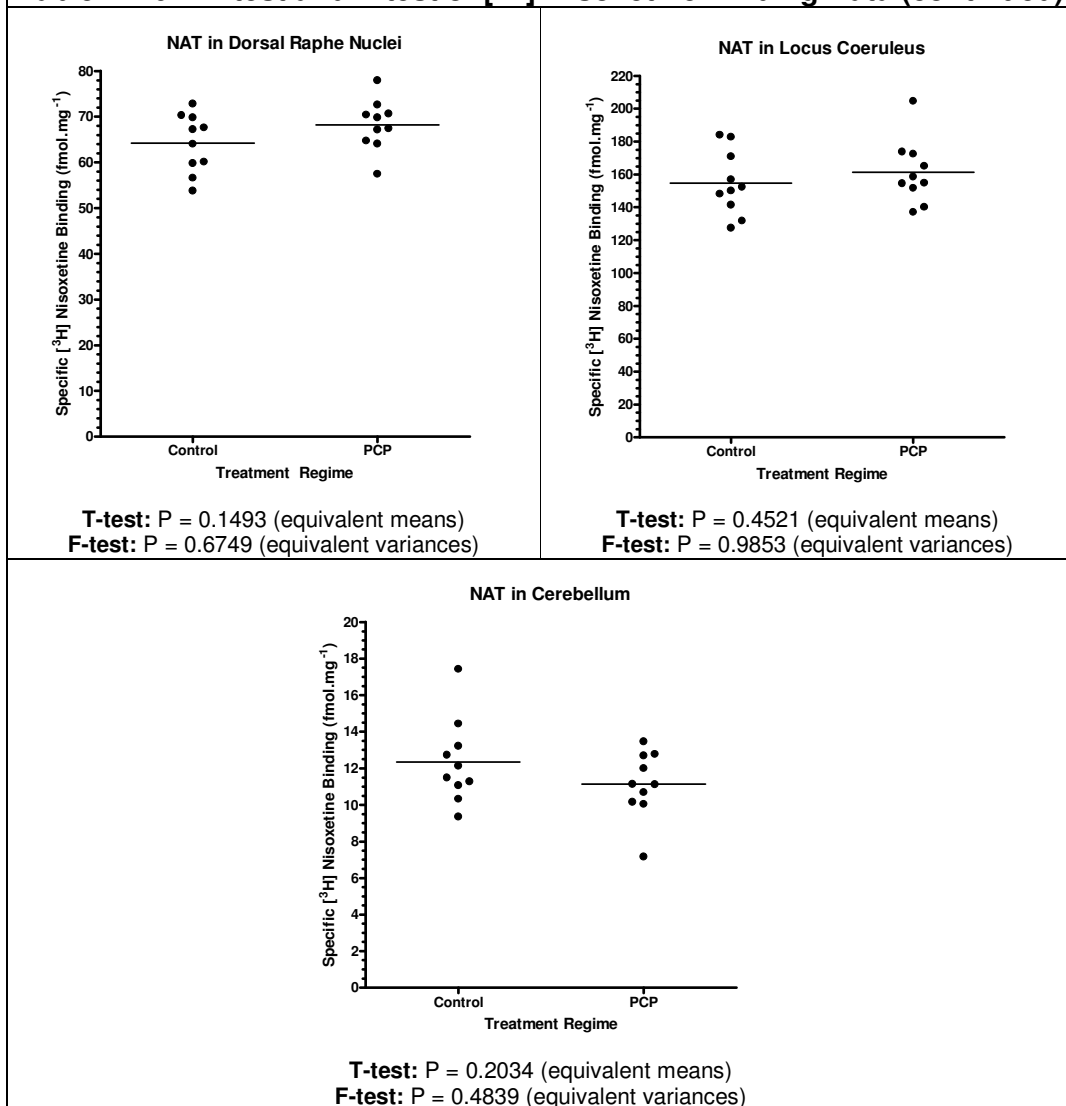


**Table A1-02 (continued):** T-test and F-test of [<sup>3</sup>H]-nisoxetine binding data. Control (n=10) and PCP-treated (n=10) data points plotted with mean indicated by bars. Significance threshold set at P < 0.05.

**Table A1-03: T-test and F-test of [<sup>3</sup>H]-WIN-35,428 Binding Data**

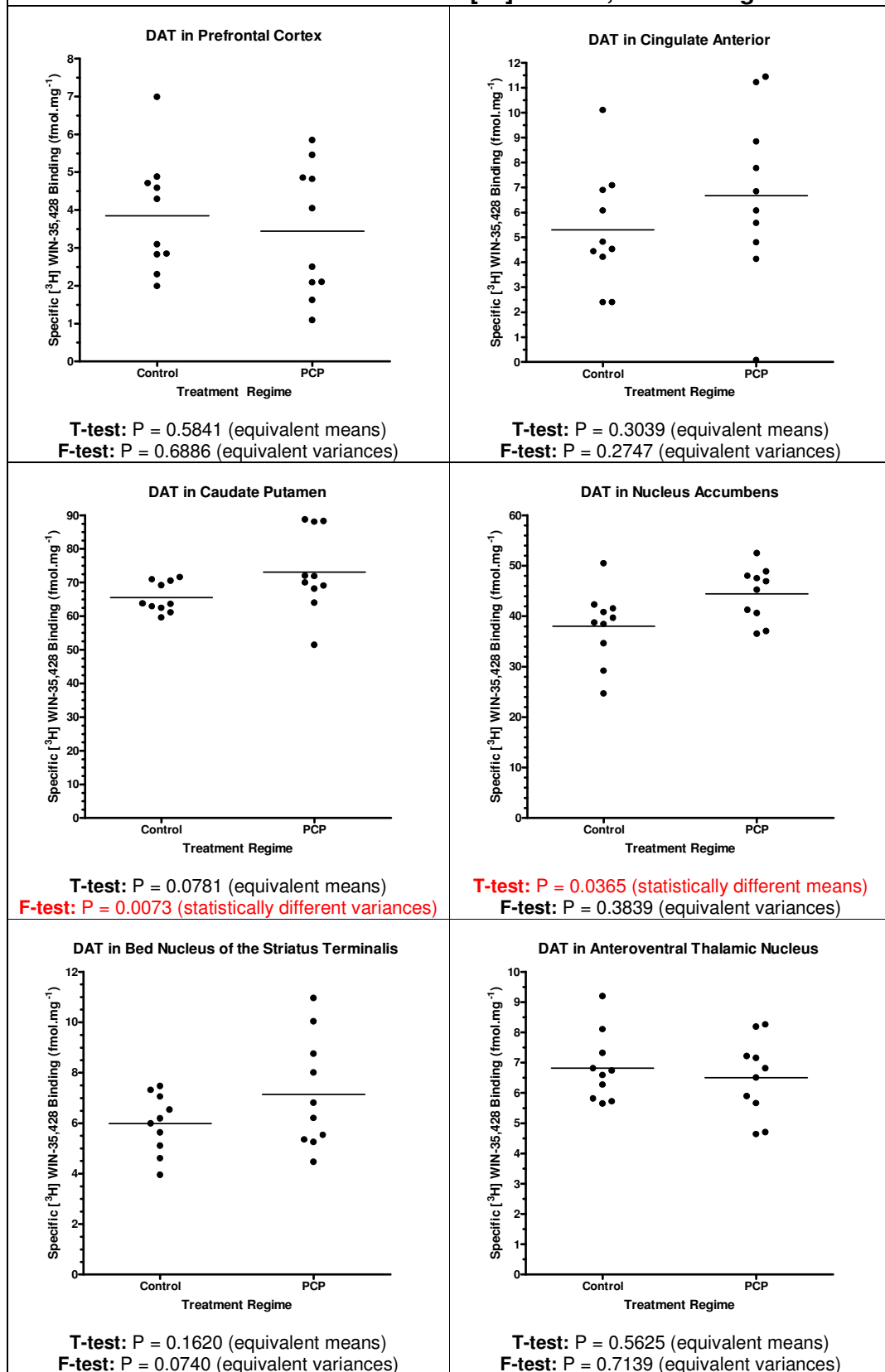


**Table A1-03:** T-test and F-test of [<sup>3</sup>H]-WIN-35,428 binding data. Control (n=10) and PCP-treated (n=10) data points plotted with mean indicated by bars. Significance threshold set at P < 0.05. Group variances were statistically different in the caudate putamen. Group means were statistically different in the nucleus accumbens.

**Table A1-03: T-test and F-test of [<sup>3</sup>H]-WIN-35,428 Binding Data (continued)**

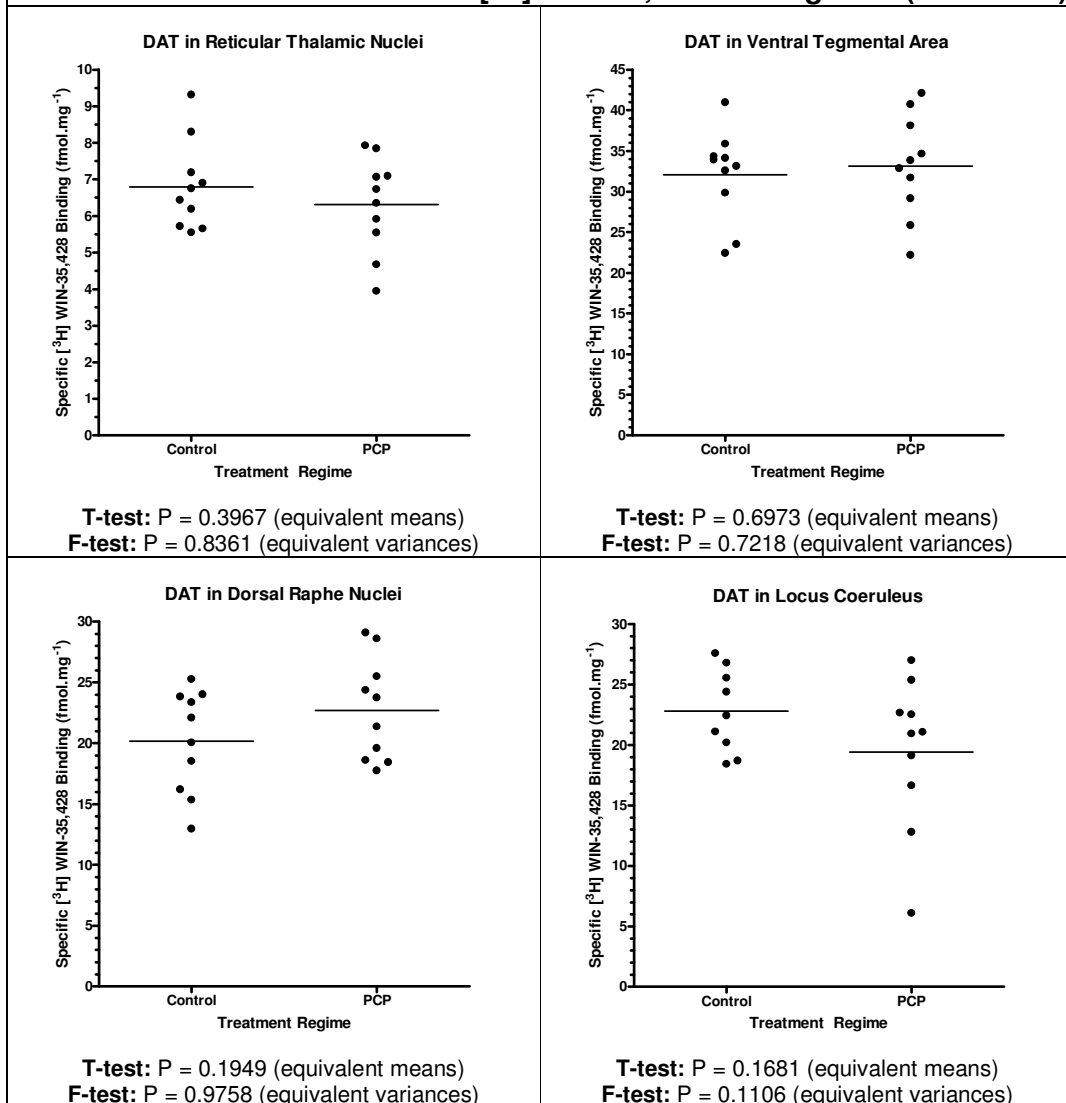


**Table A1-03 (continued):** T-test and F-test of [<sup>3</sup>H]-WIN-35,428 binding data. Control (n=10) and PCP-treated (n=10) data points plotted with mean indicated by bars. Significance threshold set at P < 0.05.

**Table A1-04: T-test and F-test of [<sup>3</sup>H]-Citalopram Binding Data**

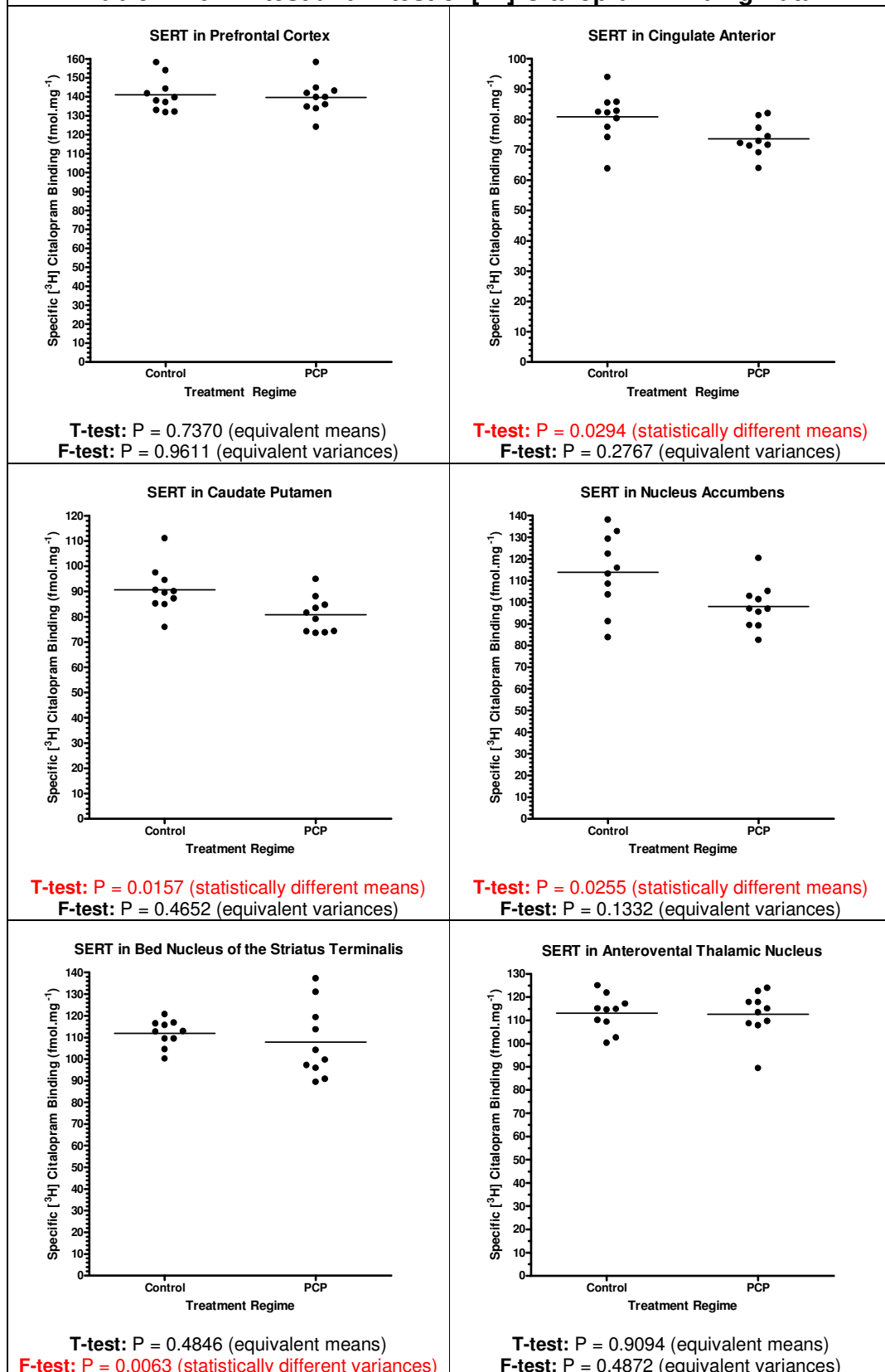


**Table A1-04:** T-test and F-test of [<sup>3</sup>H]-citalopram binding data.

Control (n=10) and PCP-treated (n=10) data points plotted with mean indicated by bars. Significance threshold set at P < 0.05. Group means were statistically different in the cingulate anterior, caudate putamen, and nucleus accumbens. Group variances were statistically different in the bed nucleus of the striatum terminalis.

**Table A1-04: T-test and F-test of [<sup>3</sup>H]-Citalopram Binding Data (continued)**

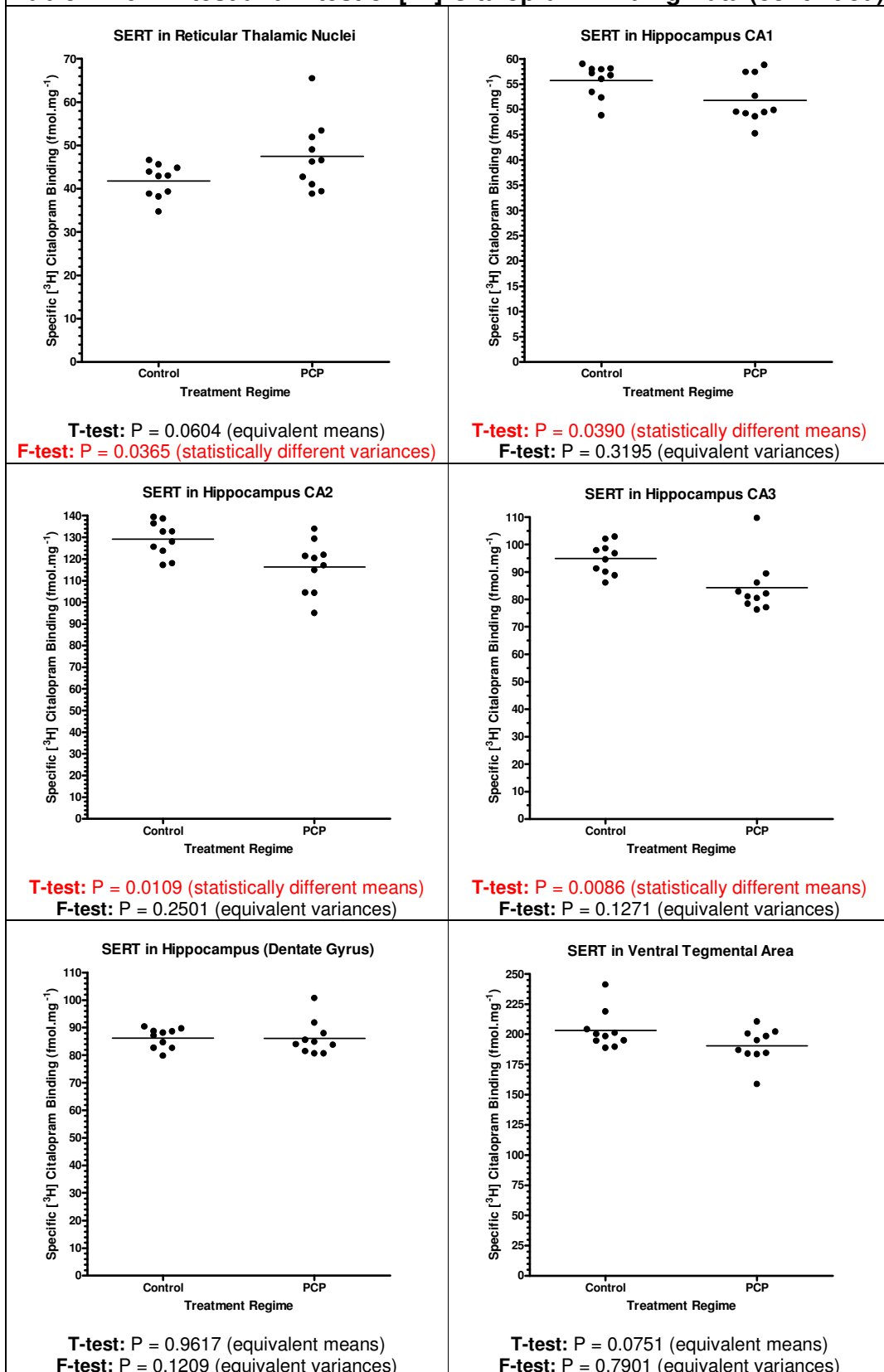


**Table A1-04 (continued):** T-test and F-test of [<sup>3</sup>H]-citalopram binding data. Control (n=10) and PCP-treated (n=10) data points plotted with mean indicated by bars. Significance threshold set at P < 0.05. Group variances were statistically different in the reticular thalamic nuclei. Group means were statistically different in the CA1, CA2, and CA3 regions of the hippocampus.

**Table A1-04: T-test and F-test of [<sup>3</sup>H]-Citalopram Binding Data (continued)**

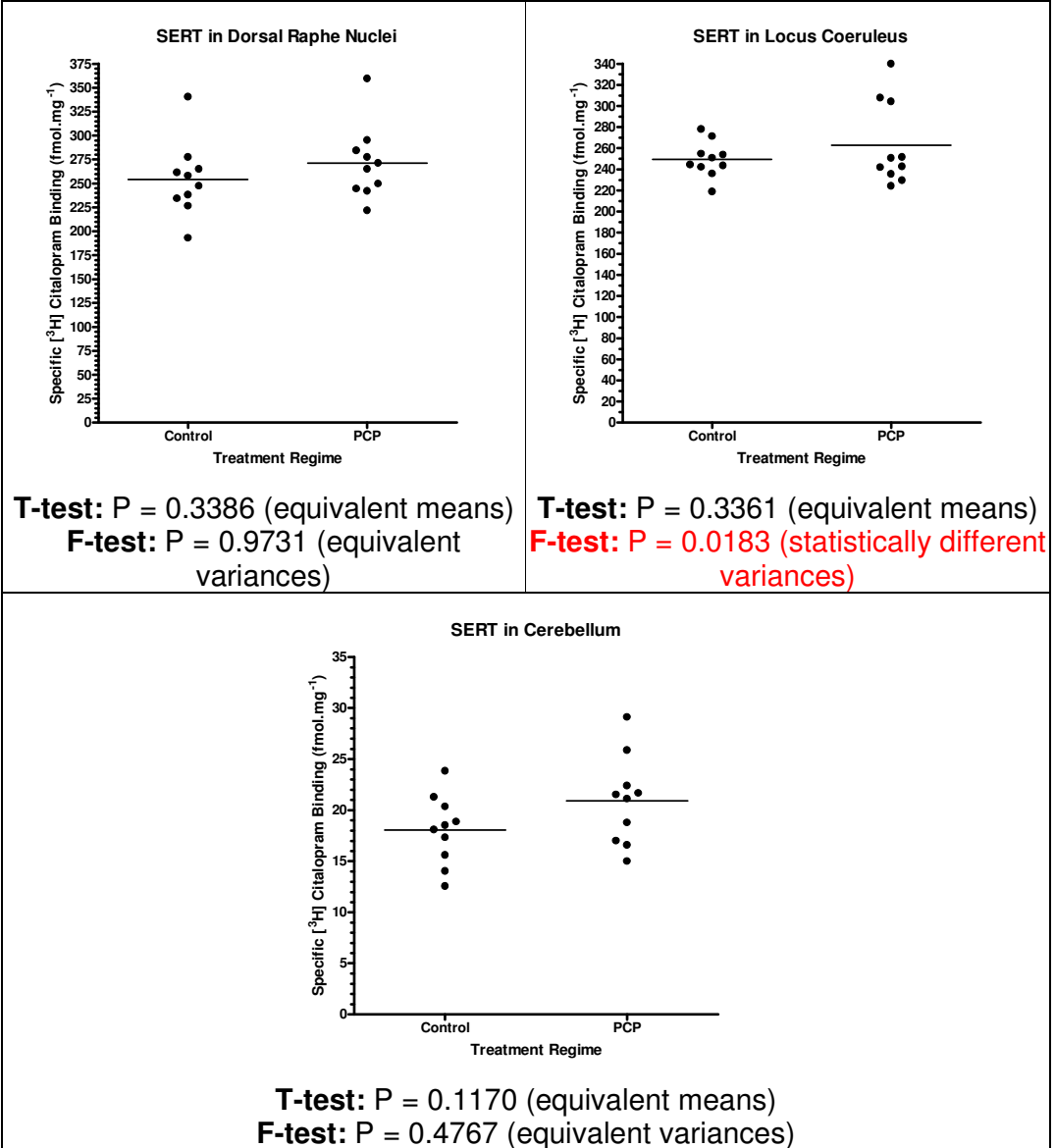


**Table A1-04 (continued):** T-test and F-test of [<sup>3</sup>H]-citalopram binding data. Control (n=10) and PCP-treated (n=10) data points plotted with mean indicated by bars. Significance threshold set at P < 0.05. Group variances were statistically different in the locus coeruleus.

## Appendix II

### A1.1 HPLC system calibrations

Figures A2-01 to A2-07 are the calibration curves for the *in vitro* HPLC methods to predict the *in vivo* characteristics of potential SPECT imaging compounds. Full methodology is described in Chapter 2, Section 2.3.

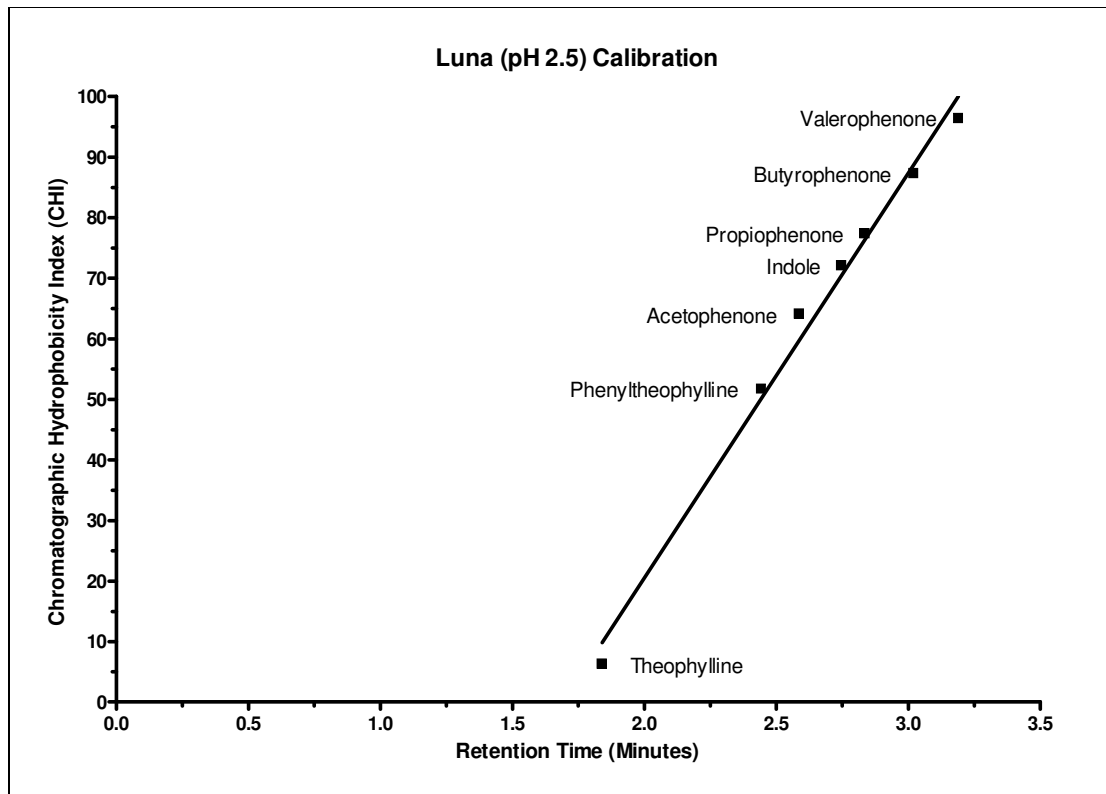


**Figure A2-01:** Calibration curve for the Luna (C-18) lipid column at pH 2.5. The known CHI of standards was used to calibrate retention times to determine the CHI values of samples run on the column.

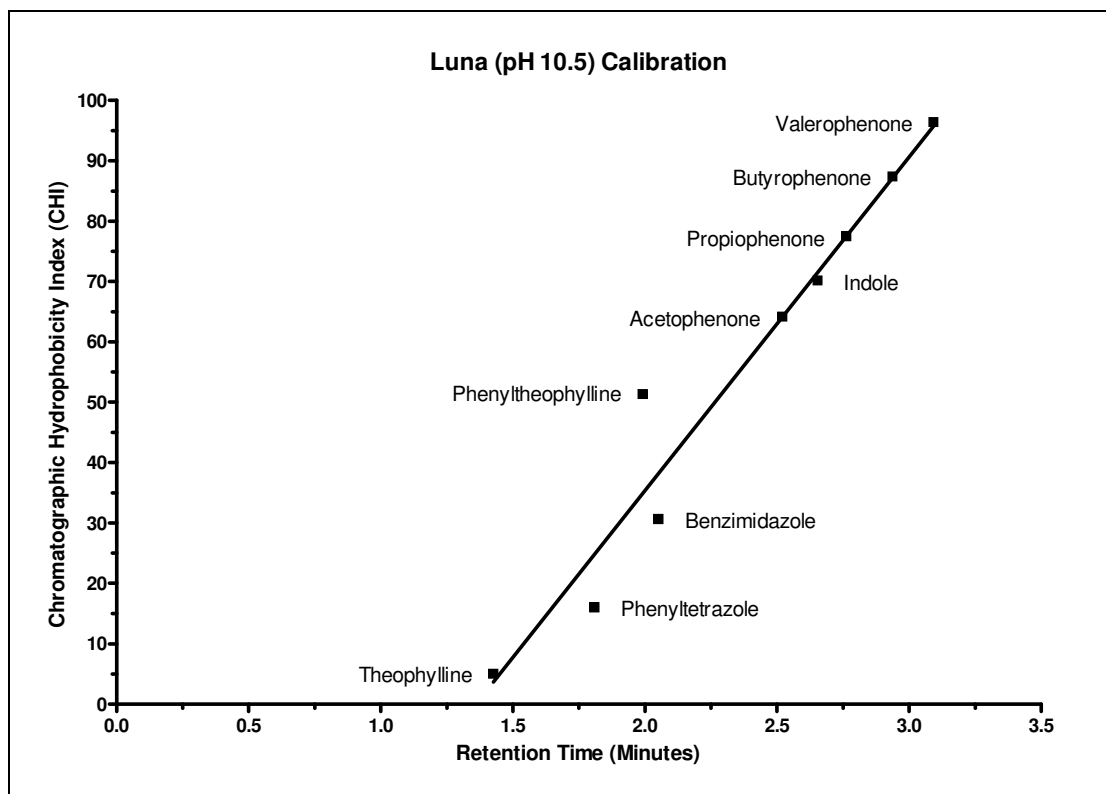


**Figure A2-02:** Calibration curve for the Luna (C-18) lipid column at pH 10.5. The known CHI of standards was used to calibrate retention times to determine the CHI values of samples run on the column.

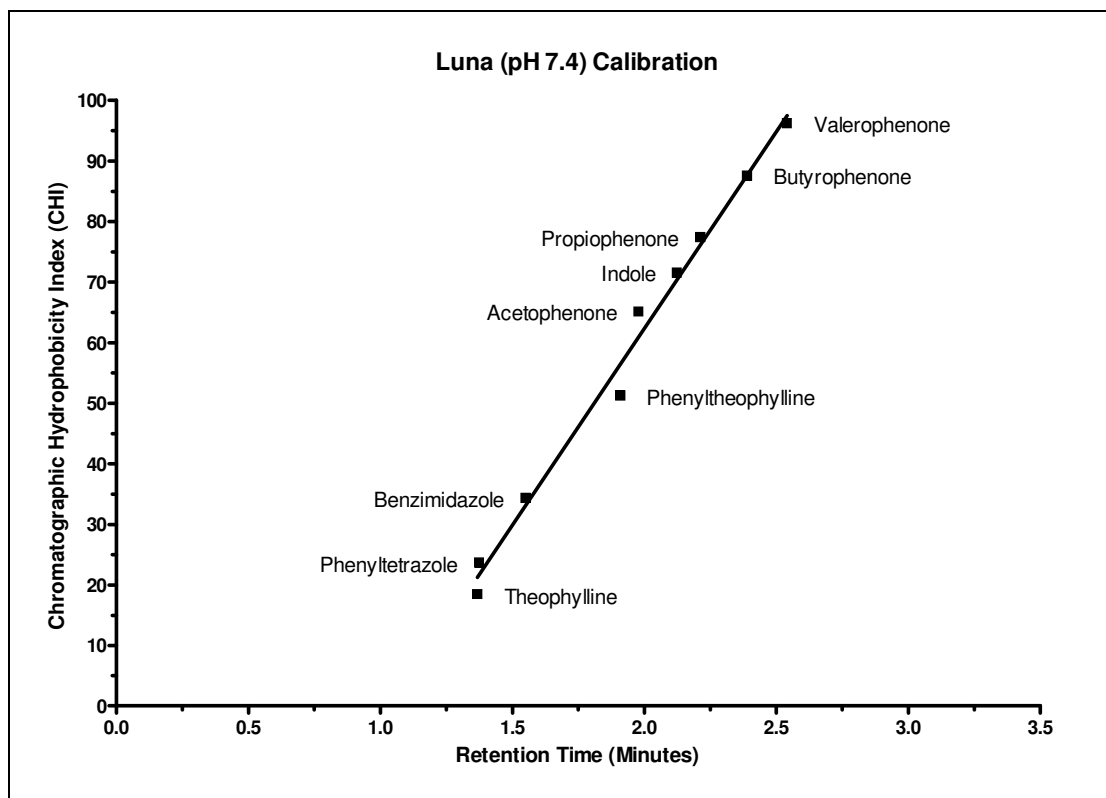


**Figure A2-03:** Calibration curve for the Luna (C-18) lipid column at pH 7.4. The known CHI of standards was used to calibrate retention times to determine the CHI values of samples run on the column.

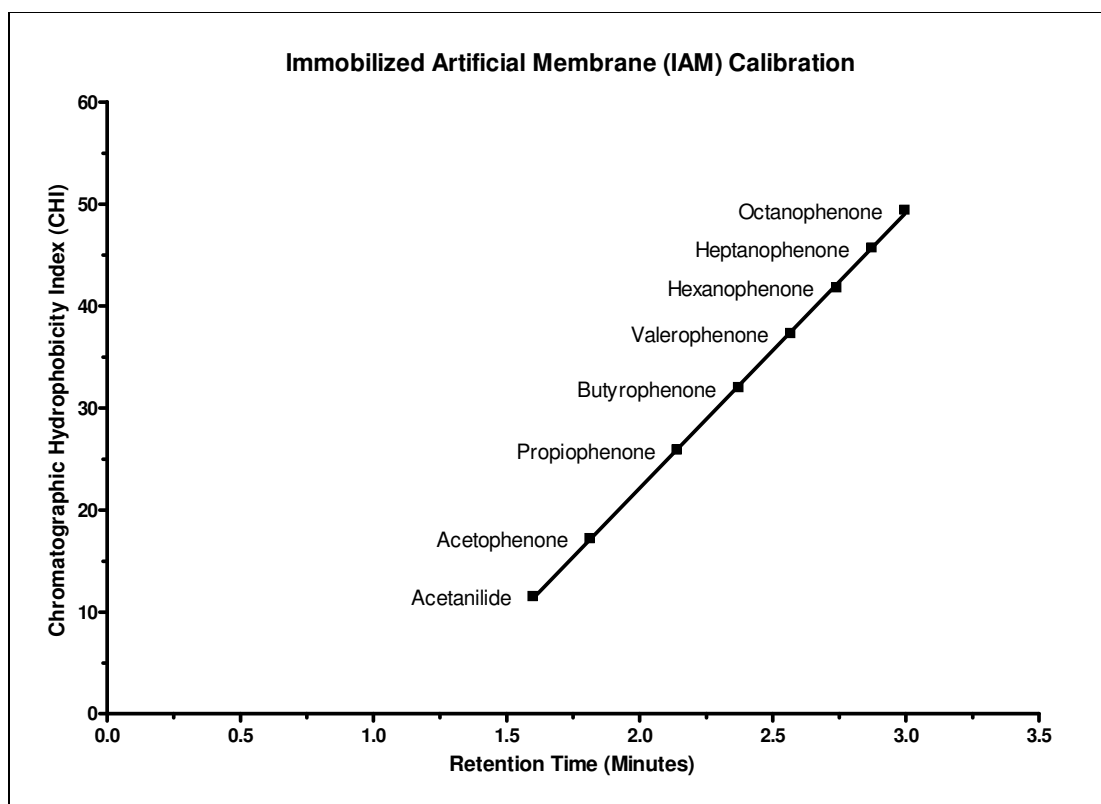


**Figure A2-04:** Calibration curve for the immobilized artificial membrane (IAM) phospholipid column at pH 7.4. The known CHI of standards was used to calibrate retention times to determine the CHI values of samples run on the column.

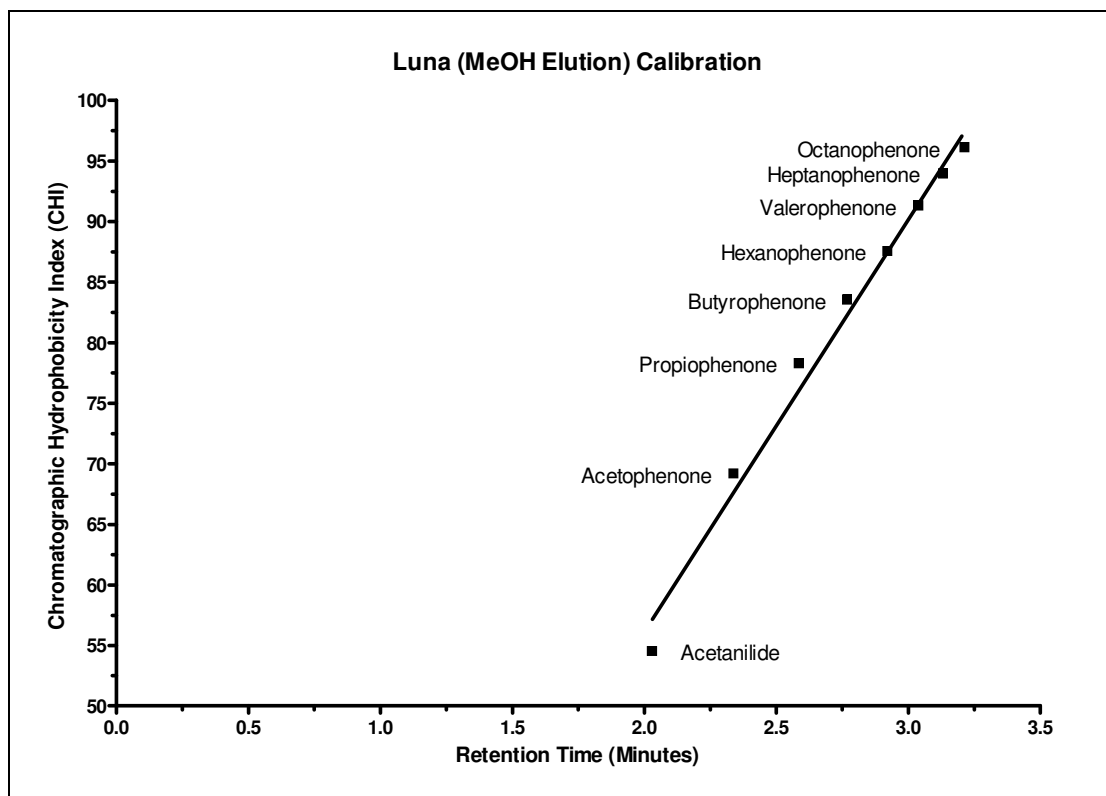


**Figure A2-05:** Calibration curve for the Luna (C-18) column at pH 7.4 with a methanol elution. The known CHI of standards was used to calibrate retention times to determine the CHI values of samples run on the column.

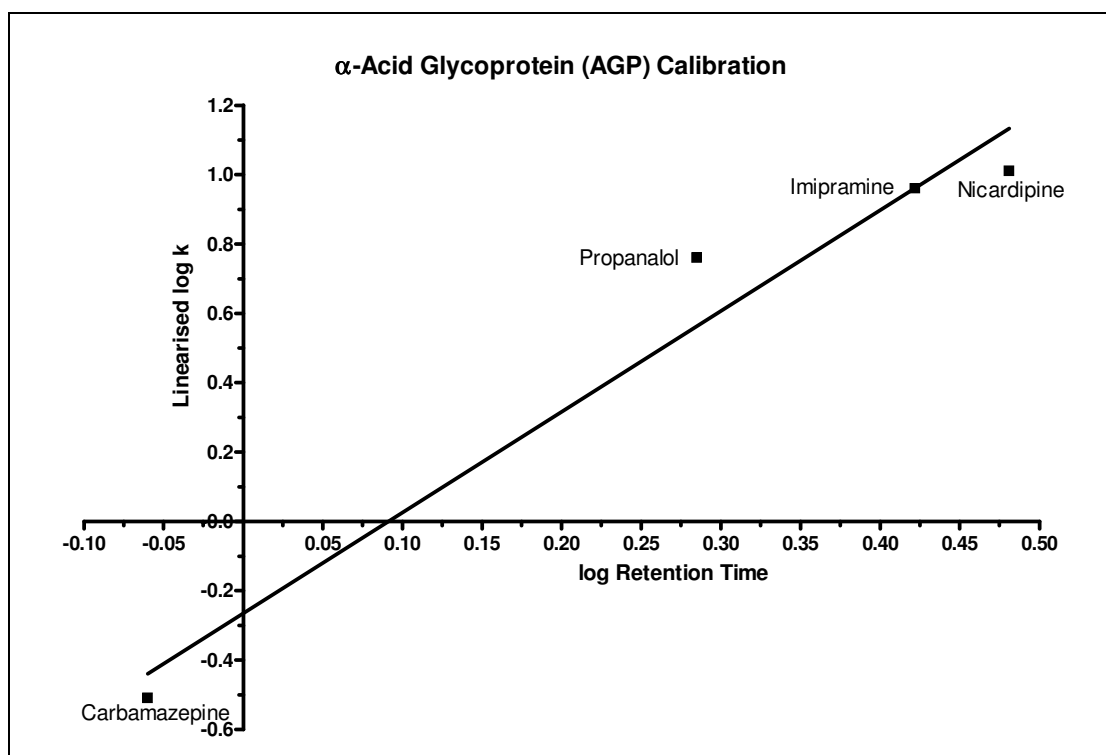


**Figure A2-06:** Calibration curve for the immobilized  $\alpha$ -acid glycoprotein (AGP) column at pH 7.4. The known linearised log  $k$  (measure of protein binding) of standards was used to calibrate retention times to determine the linearised log  $k$  values of samples run on the column.

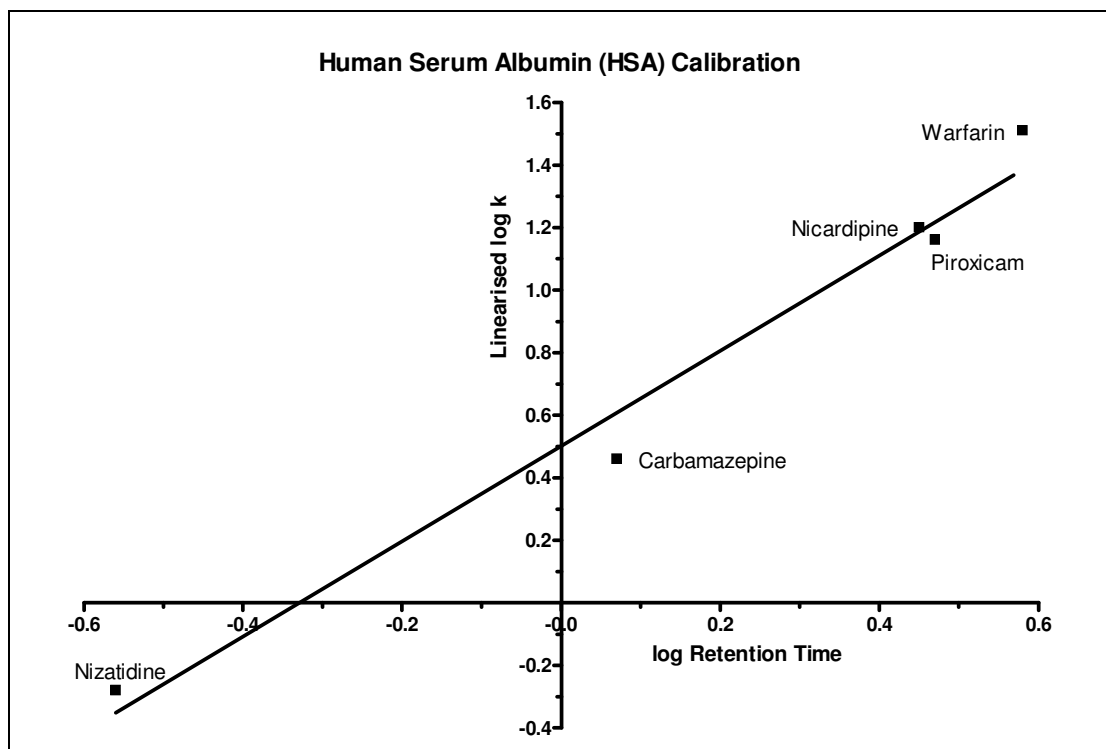


**Figure A2-07:** Calibration curve for the immobilized human serum albumin (HSA) column at pH 7.4. The known linearised log  $k$  (measure of protein binding) of standards was used to calibrate retention times to determine the linearised log  $k$  values of samples run on the column.

## References

- Abi-Dargham, A; (2007). "**Alterations of serotonin transmission in schizophrenia**". *International Review of Neurobiology* 78 (Integrating the Neurobiology of Schizophrenia): 133-164.
- Abi-Dargham, A; (2004). "**Do we still believe in the dopamine hypothesis? New data bring new evidence**". *Int.J Neuropsychopharmacol.* 7 Suppl 1 S1-S5.
- Abi-Dargham, A & Guillin, O; (2007). "**Integrating the neurobiology of schizophrenia - Preface**". *International Review of Neurobiology* 78 (Integrating the Neurobiology of Schizophrenia): XIII-XXVI.
- Abi-Dargham, A & Laruelle, M; (2005). "**Mechanisms of action of second generation antipsychotic drugs in schizophrenia: insights from brain imaging studies.**". *European Psychiatry* 20 15-27.
- Abi-Dargham, A; Mawlawi, O; Lombardo, I; Gil, R; Martinez, D; Huang, YY; Hwang, DR; Keilp, J; Kochan, L; Van Heertum, R; Gorman, JM; & Laruelle, M; (2002). "**Prefrontal dopamine D-1 receptors and working memory in schizophrenia**". *Journal of Neuroscience* 22 (9): 3708-3719.
- Adell, A & Artigas, F; (2004). "**The somatodendritic release of dopamine in the ventral tegmental area and its regulation by afferent transmitter systems**". *Neuroscience and Biobehavioral Reviews* 28 (4): 415-431.
- Adell, A; Celada, P; Abellan, MT; & Artigas, F; (2002). "**Origin and functional role of the extracellular serotonin in the midbrain raphe nuclei**". *Brain Research Reviews* 39 (2-3): 154-180.
- Al-Tikriti, MS; Zea-Ponce, Y; Baldwin, RM; Zoghbi, SS; Laruelle, M; Seibyl, JP; Giddings, SS; Scanley, BE; Charney, DS; Hoffer, PB; & .; (1995). "**Characterization of the dopamine transporter in nonhuman primate brain: homogenate binding, whole body imaging, and ex vivo autoradiography using [125I] and [123I]IPCIT**". *Nucl.Med.Biol.* 22 (5): 649-658.
- Allen, RM & Young, SJ; (1978). "**Phencyclidine-induced psychosis**". *Am.J.Psychiatry* 135 (9): 1081-1084.
- Andersen, ML; Papale, LA; Hipolide, DC; Nobrega, JN; & Tufik, S; (2005). "**Involvement of dopamine receptors in cocaine-induced genital reflexes after paradoxical sleep deprivation**". *Behavioural Brain Research* 160 (1): 44-50.
- Andrews, G; Issakidis, C; Sanderson, K; Corry, J; & Lapsley, H; (2004). "**Utilising survey data to inform public policy: Comparison of the cost-**

**effectiveness of treatment of ten mental disorders".** *British Journal of Psychiatry* 184 526-533.

Avdeef, A & Testa, B; (2002). "**Physicochemical profiling in drug research: a brief survey of the state-of-the-art of experimental techniques**". *Cell Mol.Life Sci.* 59 (10): 1681-1689.

Barnes, NM & Sharp, T; (1999). "**A review of central 5-HT receptors and their function**". *Neuropharmacology* 38 (8): 1083-1152.

Baulieu, JL; Huguet, F; Chalon, S; Gerard, P; Frangin, Y; Besnard, JC; Pourcelot, L; & Guilloteau, D; (1990). "**[I-125] Metaiodobenzylguanidine Uptake and Release in Different Regions of the Rat-Brain**". *Nuclear Medicine and Biology* 17 (5): 511-514.

Bear, MF; Connors, BW; & Raradiso, MA; (2001). "**Neuroscience: Exploring The Brain**" *Lippincott Williams and Wilkins*, United States of America.

Bondy, B; Ackenheil, M; Birzle, W; Elbers, R; & Frohler, M; (1984). "**Catecholamines and their receptors in blood: evidence for alterations in schizophrenia**". *Biol.Psychiatry* 19 (10): 1377-1393.

Bressan, RA; Erlandsson, K; Mulligan, RS; Gunn, RN; Cunningham, VJ; Owens, J; Cullum, ID; Ell, PJ; & Pilowsky, LS; (2004). "**A bolus/infusion paradigm for the novel NMDA receptor SPET tracer [123i]CNS 1261**". *Nuclear Medicine and Biology* 31 (2): 155-164.

Bressan, RA; Erlandsson, K; Stone, JM; Mulligan, RS; Krystal, JH; Ell, PJ; & Pilowsky, LS; (2005). "**Impact of Schizophrenia and Chronic Antipsychotic Treatment on [123i]CNS-1261 Binding to N-Methyl-D-Aspartate Receptors In Vivo**". *Biological Psychiatry* 58 (1): 41-46.

Brunello, N; Mendlewicz, J; Kasper, S; Leonard, B; Montgomery, S; Craig Nelson, J; Paykel, E; Versiani, M; & Racagni, G; (2002). "**The role of noradrenaline and selective noradrenaline reuptake inhibition in depression.**". *European Neuropsychopharmacology* 12 461-475.

Carlsson, A & Lindqvist, M; (1963). "**Effect of chlorpromazine or haloperidol on formation of 3methoxytryamine and normetanephrine in mouse brain**". *Acta Pharmacol.Toxicol.(Copenh)* 20 140-144.

Chauveau, F; Boutin, H; Van, CN; Dolle, F; & Tavitian, B; (2008). "**Nuclear imaging of neuroinflammation: a comprehensive review of [11C]PK11195 challengers**". *Eur.J Nucl.Med.Mol.Imaging* 35 (12): 2304-2319.

Cheng, Y & Prusoff, WH; (1973). "**Relationship between the inhibition constant (K1) and the concentration of inhibitor which causes 50 per cent inhibition \*I50) of an enzymatic reaction.**". *Biochemical Pharmacology* 22 (23): 3099-3108.

- Chumpradit, S; Kung, MP; Panyachotipun, C; Prapansiri, V; Foulon, C; Brooks, BP; Szabo, SA; Tejani-Butt, S; Frazer, A; & Kung, HF; (1992). **"Iodinated tomoxetine derivatives as selective ligands for serotonin and norepinephrine uptake sites"**. *J Med.Chem.* 35 (23): 4492-4497.
- Cochran, SM; Kennedy, M; McKerchar, CE; Steward, LJ; Pratt, JA; & Morris, BJ; (2003). **"Induction of metabolic hypofunction and neurochemical deficits after chronic intermittent exposure to phencyclidine: Differential modulation by antipsychotic drugs"**. *Neuropsychopharmacology* 28 (2): 265-275.
- Cyr, K; (Released: 21 January 2005). **"NASA Inflation Calculator"** Version: 1.0. *National Aeronautics and Space Administration*  
<http://www1.jsc.nasa.gov/bu2/inflation/nasa/inflateNASA.html>  
 Reference Type: Computer Program
- D'Amato, RJ; Largent, BL; Snowman, AM; & Snyder, SH; (1987). **"Selective Labeling of Serotonin Uptake Sites in Rat-Brain by [H-3] Citalopram Contrasted to Labeling of Multiple Sites by [H-3] Imipramine"**. *Journal of Pharmacology and Experimental Therapeutics* 242 (1): 364-371.
- Dajas, F; Barbeito, L; Martinez-Pesquera, G; Lista, A; Puppo, D; & Puppo-Touriz, H; (1983). **"Plasma noradrenaline and clinical psychopathology in schizophrenia. A correlation analysis"**. *Neuropsychobiology* 10 (2-3): 70-74.
- De Sarro, GB; Ascioti, C; Froio, F; Libri, V; & Nistico, G; (1987). **"Evidence that locus coeruleus is the site where clonidine and drugs acting at alpha 1- and alpha 2-adrenoceptors affect sleep and arousal mechanisms"** *Br.J Pharmacol* 90 (4): 675-685.  
 Reference Type: Abstract.
- Dean, B; Opeskin, K; Pavey, G; Naylor, L; Hill, C; Keks, N; & Copolov, DL; (1995). **"[H-3] Paroxetine Binding Is Altered in the Hippocampus But Not the Frontal-Cortex Or Caudate-Nucleus from Subjects with Schizophrenia"**. *Journal of Neurochemistry* 64 (3): 1197-1202.
- DeGrado, TR & Wang, S; (1998). **"Transcapillary transport of metaiodobenzylguanidine (MIBG) in isolated rat heart"**. *Nucl.Med.Biol.* 25 (5): 455-465.
- Deutsch, SI; Mastropaolo, J; Schwartz, BL; Rosse, RB; & Morihisa, JM; (1989). **"A "glutamatergic hypothesis" of schizophrenia. Rationale for pharmacotherapy with glycine"**. *Clin.Neuropharmacol.* 12 (1): 1-13.
- Ding, YS; Lin, KS; Logan, J; Benveniste, H; & Carter, P; (2005). **"Comparative evaluation of positron emission tomography radiotracers for imaging the norepinephrine transporter: (S,S) and (R,R) enantiomers of reboxetine analogs ([C-11]methylreboxetine, 3-Cl-[C-11]methylreboxetine and [F-18]fluororeboxetine), (R)-[C-11]nisoxetine,**

**[C-11]oxaprotiline and [C-11]lortalamine**". *Journal of Neurochemistry* 94 (2): 337-351.

Donnan, GA; Kaczmarczyk, SJ; Paxinos, G; Chilco, PJ; Kalnins, RM; Woodhouse, DG; & Mendelsohn, FAO; (1991). "**Distribution of Catecholamine Uptake Sites in Human Brain As Determined by Quantitative [H-3] Mazindol Autoradiography**". *Journal of Comparative Neurology* 304 (3): 419-434.

Eisenhofer, G; (2001). "**The role of neuronal and extraneuronal plasma membrane transporters in the inactivation of peripheral catecholamines**". *Pharmacol Ther.* 91 (1): 35-62.

Elliott, JM & Beveridge, TJR; (2005). "**Psychostimulants and monoamine transporters: upsetting the balance**". *Current Opinion in Pharmacology* 5 (1): 94-100.

Erlandsson, K; Bressan, RA; Mulligan, RS; Gunn, RN; Cunningham, VJ; Owens, J; Wyper, D; Ell, PJ; & Pilowsky, LS; (2003). "**Kinetic modelling of [123I]CNS 1261--a potential SPET tracer for the NMDA receptor**". *Nucl.Med.Biol.* 30 (4): 441-454.

Farde, L; Nordstrom, AL; Wiesel, FA; Pauli, S; Halldin, C; & Sedvall, G; (1992). "**Positron Emission Tomographic Analysis of Central D1-Dopamine and D2-Dopamine Receptor Occupancy in Patients Treated with Classical Neuroleptics and Clozapine - Relation to Extrapyramidal Side-Effects**". *Archives of General Psychiatry* 49 (7): 538-544.

Frankle, WG; Narendran, R; Huang, Y; Hwang, DR; Lombardo, I; Cangiano, C; Gil, R; Laruelle, M; & Abi-Dargham, A; (2005a). "**Serotonin Transporter Availability in Patients with Schizophrenia: A Positron Emission Tomography Imaging Study with [11C]DASB**". *Biological Psychiatry* 57 (12): 1510-1516.

Frankle, WG; Slifstein, M; Talbot, PS; & Laruelle, M; (2005b). "**Neuroreceptor imaging in psychiatry: theory and applications**". *International Review of Neurobiology* 67 385-440.

Frey, KA; Hichwa, RD; Ehrenkaufer, RLE; & Arganoff, BW; (1985). "**Quantitative in vivo receptor binding III: Tracer kinetic modelling of muscarinic cholinergic receptor-binding**". *Proceedings of the National Academy of Sciences of the United States of America* 82 (19): 6711-6715.

Friedman, SM; (Released: 11 December 2000)(Copyright: 2000). "**The Inflation Calculator**" Version: 1.0. *Westegg.com* <http://www.westegg.com/inflation/>  
Reference Type: Computer Program

Fujita, M; Tamagnan, G; Zoghbi, SS; Al-Tikriti, MS; Baldwin, RM; Seibyl, JP; & Innis, RB; (2000). "**Measurement of alpha4beta2 nicotinic acetylcholine receptors with [123I]5-I-A-85380 SPECT**". *J Nucl.Med.* 41 (9): 1552-1560.

- Garg, P; Verma, J; & Nilanjan, R; (2008). "**In Silico Model for Blood-Brain Barrier Permeability Predictions**" / In: Ehrhardt, C; & Kim, K-J; (2008) "**Drug Absorption Studies: In Situ, In Vitro and In Silico Models**" Pp. 510-556.
- Gehlert, DR; Hemrick-Luecke, SK; Schober, DA; Krushinski, J; Howbert, JJ; Robertson, DW; Wong, DT; & Fuller, RW; (1995). "**(R)-thionisoxetine, a potent and selective inhibitor of central and peripheral norepinephrine uptake**". *Life Sci.* 56 (22): 1915-1920.
- Ghosh, MK & Mitra, AK; (1991). "**Effects of 5'-ester modification on the physicochemical properties and plasma protein binding of 5-iodo-2'-deoxyuridine**". *Pharm.Res.* 8 (6): 771-775.
- Gjedde, A & Wong, DF; (1990). "**Modeling neuroreceptor binding of radioligands in vivo.**" / In: Frost, JJ; & Wagner Jr., HN; (1990) "**Quantitative Imaging: Neuroreceptors, Neurotransmitters, and Enzymes**" *Raven Press*, New York. Pp. 51-79.
- Gomes, UC; Shanley, BC; Potgieter, L; & Roux, JT; (1980). "**Noradrenergic overactivity in chronic schizophrenia: evidence based on cerebrospinal fluid noradrenaline and cyclic nucleotide concentrations**". *Br.J Psychiatry* 137 346-351.
- Goodman, MM; Kilts, CD; Keil, R; Shi, B; Martarello, L; Xing, D; Votaw, J; Ely, TD; Lambert, P; Owens, MJ; Camp, VM; Malveaux, E; & Hoffman, JM; (2000). "**<sup>18</sup>F-Labeled FECNT: A Selective Radioligand for PET Imaging of Brain Dopamine Transporters**". *Nuclear Medicine and Biology* 27 1-12.
- Gourand, F; Mercey, G; Ibazizene, M; Tirel, O; Henry, J; Levacher, V; Perrio, C; & Barre, L; (2010). "**Chemical delivery system of metaiodobenzylguanidine (MIBG) to the central nervous system**". *J Med.Chem.* 53 (3): 1281-1287.
- Graefe, KH & Bönisch, H; (1988). Chapter Four: "**The Transport of Amines Across the Axonal Membranes of Noradrenergic and Dopaminergic Neurons**" / In: Trendelenburg, U; & Weiner, N; (1988) "**Handbook of Experimental Pharmacology**" *Springer-Verlag*, Berlin Heidelberg. Pp. 193-245.
- Guillin, O; Demily, C; & Thibaut, F; (2007). "**Brain-derived neurotrophic factor in schizophrenia and its relation with dopamine**". *International Review of Neurobiology* 78 (Integrating the Neurobiology of Schizophrenia): 377-395.
- Guilloteau, D; Baulieu, J-L; Viel, C; Valat, C; Baulieu, F; Chambon-Deschamps, C; Pourcelot, L; Itti, R; & Besnard, J-C; (1983a). "**Etude préliminaire d'un marqueur de la medullo-surrénale et des terminaisons nerveuses sympathiques: la méta-iodobenzylguanidine = Preliminary study of a tracer for adrenal gland and sympathetic nerves endings: meta-codobenzylguanidine**". *Journal de biophysique & médecine nucléaire* 7 (3): 117-122.

- Guilloteau, D; Baulieu, JL; Viel, C; Valat, C; Baulieu, F; Chambondeschamps, C; Pourcelot, L; Itti, R; & Besnard, JC; (1983b). "**Preliminary-Study of An Adrenomedullary and Sympathetic-Nerves Marker - the Meta-Iodobenzylguanidine**". *Journal de Biophysique & Medecine Nucleaire* 7 (3): 117-122.
- Haavik, J; Blau, N; & Thony, B; (2008). "**Mutations in human monoamine-related neurotransmitter pathway genes**". *Hum.Mutat.* 29 (7): 891-902.
- Hadrich, D; Berthold, F; Steckhan, E; & Bonisch, H; (1999a). "**Synthesis and characterization of fluorescent ligands for the norepinephrine transporter: Potential neuroblastoma imaging agents**". *Journal of Medicinal Chemistry* 42 (16): 3101-3108.
- Hadrich, D; Berthold, F; Steckhan, E; & Bonisch, H; (1999b). "**Synthesis and characterization of fluorescent ligands for the norepinephrine transporter: Potential neuroblastoma imaging agents**". *Journal of Medicinal Chemistry* 42 (16): 3101-3108.
- Hecht, EM & Landy, DC; (2012). "**alpha-2 receptor antagonist add-on therapy in the treatment of schizophrenia; a meta-analysis.**". *Schizophrenia Research* 134 (2-3): 202-206.
- Hellwig, D; Romeike, BFM; Ketter, R; Moringlane, JR; Kirsch, CM; & Samnick, S; (2008). "**Intra-individual comparison of p-[I-123]-iodo-L-phenylalanine and L-3-[I-123]-iodo-alpha-methyl-tyrosine for SPECT imaging of gliomas**". *European Journal of Nuclear Medicine and Molecular Imaging* 35 (1): 24-31.
- Hennah, W; Thomson, P; Peltonen, L; & Porteous, D; (2006). "**Genes and schizophrenia: beyond schizophrenia: the role of DISC1 in major mental illness**". *Schizophr.Bull.* 32 (3): 409-416.
- Hipolide, DC; Moreira, KM; Barlow, KBL; Wilson, AA; Nobrega, JN; & Tufik, S; (2005). "**Distinct effects of sleep deprivation on binding to norepinephrine and serotonin transporters in rat brain**". *Progress in Neuro-Psychopharmacology & Biological Psychiatry* 29 (2): 297-303.
- Hirono, M; Saitow, F; Kudo, M; Suzuki, H; Yanagawa, Y; Yamada, M; Nagao, S; Konishi, S; & Obata, K; (2012). "**Cerebellar globular cells receive monoaminergic excitation and monosynaptic inhibition from Purkinje cells.**". *PLOS ONE* 7 (1): e29663-.
- Hollister, JM; Ballon, J; Barnett, J; Cosgrove, V; Gault, J; JanChan, C; Meier, LY; Rose, D; Schulman, BJ; Ross, M; Roberts, M; Irani, F; Dobervich, J; McGlashan, T; Gottesman, I; Torrey, EF; Pulver, A; Sharma, T; & Chiko, B; (2006). "**Schizophrenia.com - Indepth Schizophrenia News, Information, and Support**" <http://www.schizophrenia.com/>  
Reference Type: Electronic Citation.

- Hollósy, F; Valkó, K; Hersey, A; Nunhuck, S; Kéri, G; & Bevan, C; (2006). **"Estimation of Volume of Distribution in Humans from High Throughput HPLC-Based Measurements of Human Serum Albumin Binding and Immobilized Artificial Membrane Partitioning"**. *Journal of Medical Chemistry* 49 6958-6971.
- Jacobs, A; Braunlich, I; Graf, R; Lercher, M; Sakaki, T; Voges, J; Hesselmann, V; Brandau, W; Wienhard, K; & Heiss, WD; (2001). **"Quantitative kinetics of [124I]FIAU in cat and man"**. *J Nucl.Med.* 42 (3): 467-475.
- Javitt, DC; (1987). **"Negative schizophrenic symptomatology and the PCP (phencyclidine) model of schizophrenia"**. *Hillside.J.Clin.Psychiatry* 9 (1): 12-35.
- Javitt, DC & Zukin, SR; (1991). **"Recent advances in the phencyclidine model of schizophrenia"**. *Am.J.Psychiatry* 148 (10): 1301-1308.
- Jentsch, JD; Redmond, DE; Elsworth, JD; Taylor, JR; Youngren, KD; & Roth, RH; (1997). **"Enduring cognitive deficits and cortical dopamine dysfunction in monkeys after long-term administration of phencyclidine"**. *Science* 277 (5328): 953-955.
- Jimerson, DC; Post, RM; Stoddard, FJ; Gillin, JC; & Bunney, WE; (1980). **"Preliminary trial of the noradrenergic agonist clonidine in psychiatric patients."**. *Biological Psychiatry* 15 (1): 45-57.
- Jobson, NK; (2008). **"The Stereoselective Synthesis of Iodinated Analogues of Reboxetine; New Imaging Agents for the Noradrenaline Transporter"**. *University of Glasgow, Ph.D.Thesis.*
- Jobson, NK; Crawford, AR; Dewar, D; Pimlott, SL; & Sutherland, A; (2008a). **"New iodoreboxetine analogues for SPECT imaging of the noradrenaline transporter"**. *Bioorg.Med.Chem.Lett.* 18 (18): 4940-4943.
- Jobson, NK; Crawford, AR; Dewar, D; Pimlott, SL; & Sutherland, A; (2009). **"Design and synthesis of (2R,3S)-iodoreboxetine analogues for SPECT imaging of the noradrenaline transporter"**. *Bioorganic & Medicinal Chemistry Letters* 19 (17): 4996-4998.
- Jobson, NK; Spike, R; Crawford, AR; Dewar, D; Pimlott, SL; & Sutherland, A; (2008b). **"Stereoselective synthesis of (2S,3R)- and (2R,3S)-iodoreboxetine; potential SPECT imaging agents for the noradrenaline transporter"**. *Org Biomol.Chem.* 6 (13): 2369-2376.
- Johnson, EL & Stevenson, R; (1978). **"Basic Liquid Chromatography"** *Varian Associates Ltd., Palo Alto.*
- Joyce, JN; Shane, A; Lexow, N; Winokur, A; Casanova, MF; & Kleinman, JE; (1993). **"Serotonin Uptake Sites and Serotonin Receptors Are Altered in**

**the Limbic System of Schizophrenics". *Neuropsychopharmacology* 8 (4): 315-336.**

Kalendarev, T; Zupkovitz, G; & Ioffe, V; (2001). **"The unusual gradient elution for reversed phase HPLC of a strong chelator as an active drug substance". *J Pharm.Biomed.Anal.* 24 (5-6): 967-975.**

Kanegawa, N; Kiyono, Y; Kimura, H; Sugita, T; Kajiyama, S; Kawashima, H; Ueda, M; Kuge, Y; & Saji, H; (2006). **"Synthesis and evaluation of radioiodinated (S,S)-2-( $\alpha$ -(2-iodophenoxy)benzyl)morpholine for imaging brain norepinephrine transporters". *European Journal of Nuclear Medicine and Molecular Imaging* 33 639-647.**

Kemali, D; Del, VM; & Maj, M; (1982). **"Increased noradrenaline levels in CSF and plasma of schizophrenic patients". *Biol.Psychiatry* 17 (6): 711-717.**

Kemali, D; Maj, M; Iorio, G; Marciano, F; Nolfi, G; Galderisi, S; & Salvati, A; (1985). **"Relationship between CSF noradrenaline levels, C-EEG indicators of activation and psychosis ratings in drug-free schizophrenic patients". *Acta Psychiatr.Scand.* 71 (1): 19-24.**

Khalili, P; Naimi, E; Sun, WY; Knaus, EE; & Wiebe, LI; (2003). **"Biochemical and pharmacokinetic evaluation of a novel pyrimidine nucleoside nitric oxide donor as a potential anticancer/antiviral agent". *Eur.J Pharm.Sci.* 19 (4): 305-313.**

Kiyono, Y; Kanegawa, N; Kawashima, H; Kitamura, Y; Iida, Y; & Saji, H; (2004). **"Evaluation of radioiodinated (R)-N-methyl-3-(2-iodophenoxy)-3-phenylpropanamine as a ligand for brain norepinephrine transporter imaging". *Nucl.Med.Biol.* 31 (2): 147-153.**

Knol, RJJ; De Bruin, K; Van Eck-Smit, BLF; Pimlott, SL; Wyper, D; & Booij, J; (2009). **"In Vivo [123I]CNS-1261 Binding to D-Serine-Activated and MK801-Blocked NMDA Receptors: A Storage Phosphor Imaging Study in Rats". *Synapse* 67 557-564.**

Kolasiewicz, W; Kuter, K; Nowak, P; Pastuszka, A; & Ossowska, K; (2011). **"Lesion of the cerebellar noradrenergic innervation enhances the harmaline-induced tremor in rats.". *Cerebellum* 10 (2): 267-280.**

Krystal, JH; D'Souza, DC; Karper, LP; Bennett, A; Abi-Dargham, A; Abi-Saab, D; Cassello, K; Bowers, MB; Vegso, S; Heninger, GR; & Charney, DS; (1999). **"Interactive effects of subanesthetic ketamine and haloperidol in healthy humans". *Psychopharmacology* 145 (2): 193-204.**

Kula, NS; Baldessarini, RJ; Tarazi, FI; Fisser, R; Wang, S; Trometer, J; & Neumeyer, JL; (1999). **"[3H]beta-CIT: a radioligand for dopamine transporters in rat brain tissue". *Eur.J Pharmacol* 385 (2-3): 291-294.**

- Kung, MP; Choi, SR; Hou, C; Zhuang, ZP; Foulon, C; & Kung, HF; (2004). **"Selective binding of 2-[125I]iodo-nisoxetine to norepinephrine transporters in the brain"**. *Nucl.Med.Biol.* 31 (5): 533-541.
- Kupers, R; Frokjaer, VG; Erritzoe, D; Naert, A; Budtz-Joergensen, E; Nielsen, FA; Kehlet, H; & Knudsen, GM; (2011). **"Serotonin transporter binding in the hypothalamus correlates negatively with tonic heat pain ratings in healthy subjects: A [(11)C]DASB PET study"**. *Neuroimage* 54 (2): 1336-1343.
- Lake, CR; Sternberg, DE; van Kammen, DP; Ballenger, JC; Ziegler, MG; Post, RM; Kopin, IJ; & Bunney, WE; (1980). **"Schizophrenia: elevated cerebrospinal fluid norepinephrine"**. *Science* 207 (4428): 331-333.
- Lakshmi, B; Kung, MP; Lieberman, B; Zhao, J; Waterhouse, R; & Kung, HF; (2008). **"(R)-N-methyl-3-(3-I-125-pyridin-2-yloxy)-3-phenylpropan-1-amine: a novel probe for norepinephrine transporters"**. *Nuclear Medicine and Biology* 35 (1): 43-52.
- Langen, KJ; Roosen, N; Coenen, HH; Kuikka, JT; Kuwert, T; Herzog, H; Stocklin, G; & Feinendegen, LE; (1991). **"Brain and brain tumor uptake of L-3-[123I]iodo-alpha-methyl tyrosine: competition with natural L-amino acids"**. *J Nucl.Med.* 32 (6): 1225-1229.
- Laruelle, M; Abi-Dargham, A; Casanova, MF; Toti, R; Weinberger, DR; & Kleinman, JE; (1993). **"Selective Abnormalities of Prefrontal Serotonergic Receptors in Schizophrenia - A Postmortem Study"**. *Archives of General Psychiatry* 50 (10): 810-818.
- Laruelle, M; Abi-Dargham, A; van Dyck, C; Gil, R; D'Souza, DC; Krystal, J; Seibyl, J; Baldwin, R; & Innis, R; (2000). **"Dopamine and serotonin transporters in patients with schizophrenia: an imaging study with [123I][beta]-CIT"**. *Biological Psychiatry* 47 (5): 371-379.
- Laruelle, M; Kegeles, LS; Frankle, GW; Narendran, R; Gil, R; Talbot, PS; Hwang, DR; Huang, YY; Cooper, T; Mark, S; & Abi-Dargham, A; (2005). **"Schizophrenia is associated with increased synaptic dopamine in associative rather than limbic regions of the striatum"**. *Neuropsychopharmacology* 30 S196-S196.
- Lee, CM & Snyder, SH; (1981). **"Norepinephrine neuronal uptake binding sites in rat brain membranes labeled with [3H]desipramine"**. *Proc.Natl.Acad.Sci.U.S.A* 78 (8): 5250-5254.
- Lein, ES; Hawrylycz, MJ; Ao, N; Ayres, M; Bensinger, A; Bernard, A; Boe, AF; Boguski, MS; Brockway, KS; Byrnes, EJ; Chen, L; Chen, L; Chen, TM; Chin, MC; Chong, J; Crook, BE; Czaplinska, A; Dang, CN; Datta, S; Dee, NR; Desaki, AL; Desta, T; Diep, E; Dolbeare, TA; Donelan, MJ; Dong, HW; Dougherty, JG; Duncan, BJ; Ebbert, AJ; Eichele, G; Estin, LK; Faber, C; Facer, BA; Fields, R; Fischer, SR; Fliss, TP; Frensley, C; Gates, SN;

Glattfelder, KJ; Halverson, KR; Hart, MR; Hohmann, JG; Howell, MP; Jeung, DP; Johnson, RA; Karr, PT; Kawal, R; Kidney, JM; Knapik, RH; Kuan, CL; Lake, JH; Laramée, AR; Larsen, KD; Lau, C; Lemon, TA; Liang, AJ; Liu, Y; Luong, LT; Michaels, J; Morgan, JJ; Morgan, RJ; Mortrud, MT; Mosqueda, NF; Ng, LL; Ng, R; Orta, GJ; Overly, CC; Pak, TH; Parry, SE; Pathak, SD; Pearson, OC; Puchalski, RB; Riley, ZL; Rockett, HR; Rowland, SA; Royall, JJ; Ruiz, MJ; Sarno, NR; Schaffnit, K; Shapovalova, NV; Sivasay, T; Slaughterbeck, CR; Smith, SC; Smith, KA; Smith, BI; Sodr, AJ; Stewart, NN; Stumpf, KR; Sunkin, SM; Sutram, M; Tam, A; Teemer, CD; Thaller, C; Thompson, CL; Varnam, LR; Visel, A; Whitlock, RM; Wohnoutka, PE; Wolkey, CK; Wong, VY; Wood, M; Yaylaoglu, MB; Young, RC; Youngstrom, BL; Yuan, XF; Zhang, B; Zwingman, TA; & Jones, AR; (2007). "**Genome-wide atlas of gene expression in the adult mouse brain**". *Nature* 445 (7124): 168-176.

Lewis, DA & Hashimoto, T; (2007). "**Deciphering the disease process of schizophrenia: The contribution of cortical GABA neurons**". *International Review of Neurobiology* 78 (Integrating the Neurobiology of Schizophrenia): 109-132.

Lin, TH; Sawada, Y; Sugiyama, Y; Iga, T; & Hanano, M; (1987). "**Effects of albumin and alpha 1-acid glycoprotein on the transport of imipramine and desipramine through the blood-brain barrier in rats**". *Chem.Pharm.Bull.(Tokyo)* 35 (1): 294-301.

Lockhart, A; Davis, B; Matthews, JC; Rahmoune, H; Hong, G; Gee, A; Earnshaw, D; & Brown, J; (2003). "**The peripheral benzodiazepine receptor ligand PK11195 binds with high affinity to the acute phase reactant alpha1-acid glycoprotein: implications for the use of the ligand as a CNS inflammatory marker**". *Nucl.Med.Biol.* 30 (2): 199-206.

Logan, J; Wang, GJ; Telang, F; Fowler, JS; Alexoff, D; Zabroski, J; Jayne, M; Hubbard, B; King, P; Carter, P; Shea, C; Xu, Y; Muench, L; Schlyer, D; Learned-Coughlin, S; Cosson, V; Volkow, ND; & Ding, YS; (2007). "**Imaging the norepinephrine transporter in humans with (S,S)-[C-11]O-methyl reboxetine and PET: problems and progress**". *Nuclear Medicine and Biology* 34 (6): 667-679.

Luby, ED; Cohen, BD; Rosenbaum, G; Gottlieb, JS; & Kelley, R; (1959). "**Study of a new schizophrenomimetic drug; sernyl**". *AMA.Arch.Neurol.Psychiatry* 81 (3): 363-369.

Reference Type: Abstract.

Marek, GJ; (2007). "**Serotonin and dopamine interactions in rodents and primates: Implications for psychosis and antipsychotic drug development**". *International Review of Neurobiology* 78 (Integrating the Neurobiology of Schizophrenia): 165-192.

Martin, LF & Freedman, R; (2007). "**Schizophrenia and the alpha 7 nicotinic acetylcholine receptor**". *International Review of Neurobiology* 78 (Integrating the Neurobiology of Schizophrenia): 225-246.

- Millan, MJ; Gobert, A; Lejeune, F; Newman-Tancredi, A; Rivet, JM; Auclair, A; & Peglioni, JL; (2001). "**S33005, a novel ligand at both serotonin and norepinephrine transporters: I. Receptor binding, electrophysiological, and neurochemical profile in comparison with venlafaxine, reboxetine, citalopram, and clomipramine**". *J Pharmacol Exp. Ther.* 298 (2): 565-580.
- Mintun, MA; Raichle, ME; Kilbourn, MR; Wooten, GF; & Welch, MJ; (1984). "**A quantitative model for the in vivo assessment of drug binding sites with positron emission tomography**". *Annals of Neurology* 15 (3): 217-227.
- Montgomery, SM; (1979). "**Depressive symptoms in acute schizophrenia**". *Progress in Neuropsychopharmacology* 3 (4): 429-433.
- Moore, RY & Bloom, FE; (1979). "**Central catecholamine neuron systems: anatomy and physiology of the norepinephrine and epinephrine systems**". *Annu.Rev.Neurosci.* 2 113-168.
- Morita, T; Sonoda, R; Nakato, K; Koshiya, K; Wanibuchi, F; & Yamaguchi, T; (2000). "**Phencyclidine-induced abnormal behaviors in rats as measured by the hole board apparatus**". *Psychopharmacology (Berl)* 148 (3): 281-288.
- Moron, JA; Brockington, A; Wise, RA; Rocha, BA; & Hope, BT; (2002). "**Dopamine uptake through the norepinephrine transporter in brain regions with low levels of the dopamine transporter: Evidence from knock-out mouse lines**". *Journal of Neuroscience* 22 (2): 389-395.
- Morris, BJ; Cochran, SM; & Pratt, JA; (2005). "**PCP: from pharmacology to modelling schizophrenia**". *Current Opinion in Pharmacology* 5 (1): 101-106.
- Murray, F; Kennedy, J; Hutson, PH; Elliot, J; Huscroft, I; Mohnen, K; Russell, MG; & Grimwood, S; (2000). "**Modulation of [3H]MK-801 binding to NMDA receptors in vivo and in vitro**". *Eur.J Pharmacol* 397 (2-3): 263-270.
- Neal, MJ; (2002). "**Medical Pharmacology at a Glance**" *Blackwell Science Ltd.*, Pp. 60-61.
- Ogawa, M; Tsukada, H; Hatano, K; Ouchi, Y; Saji, H; & Magata, Y; (2009). "**Central in vivo nicotinic acetylcholine receptor imaging agents for positron emission tomography (PET) and single photon emission computed tomography (SPECT)**". *Biol.Pharm.Bull.* 32 (3): 337-340.
- Ohuoha, DC; Hyde, TM; & Kleinman, JE; (1993). "**The Role of Serotonin in Schizophrenia - An Overview of the Nomenclature, Distribution and Alterations of Serotonin Receptors in the Central-Nervous-System**". *Psychopharmacology* 112 (1): S5-S15.
- Oravcová, J; Böhs, B; & Lindner, W; (1996). "**Drug-protein binding studies - New trends in analytical and experimental methodology**". *Journal of Chromatography B: Biomedical Applications* 677 1-28.

- Owens, J; Wyper, DJ; Patterson, J; Brown, DR; Elliott, AT; Teasdale, GM; & McCulloch, J; (1997). "**First SPECT images of glutamate (NMDA) receptor activation in vivo in cerebral ischaemia**". *Nucl.Med.Commun.* 18 (2): 149-158.
- Petit-Taboue, MC; Baron, JC; Barre, L; Travers, JM; Speckel, D; Camsonne, R; & MacKenzie, ET; (1991). "**Brain kinetics and specific binding of [11C]PK 11195 to omega 3 sites in baboons: positron emission tomography study**". *Eur.J Pharmacol* 200 (2-3): 347-351.
- Piggott, MA; Owens, J; O'Brien, J; Colloby, S; Fenwick, J; Wyper, D; Jaros, E; Johnson, M; Perry, RH; & Perry, EK; (2003). "**Muscarinic receptors in basal ganglia in dementia with Lewy bodies, Parkinson's disease and Alzheimer's disease**". *Journal of Chemical Neuroanatomy* 25 (3): 161-173.
- Pimlott, SL; Piggott, M; Owens, J; Grealley, E; Court, JA; Jaros, E; Perry, RH; Perry, EK; & Wyper, D; (2004). "**Nicotinic Acetylcholine Receptor Distribution in Alzheimer's Disease, Dementia with Lewy Bodies, Parkinson's Disease, and Vascular Dementia: In Vitro Binding Study Using 5-[125I]-A-85380**". *Neuropsychopharmacology* 29 108-116.
- Pimlott, SL & Sutherland, A; (2011). "**Molecular tracers for the PET and SPECT imaging of disease**". *Chemical Society Reviews* 40 (1): 149-162.
- Porteous, DJ; Thomson, P; Brandon, NJ; & Millar, JK; (2006). "**The genetics and biology of DISC1--an emerging role in psychosis and cognition**". *Biol.Psychiatry* 60 (2): 123-131.
- Pryma, D & Divgi, C; (2008). "**Meta-iodobenzyl guanidine for detection and staging of neuroendocrine tumors**". *Nuclear Medicine and Biology* 35 S3-S8.
- Przuntek, H; Müller, T; & Riederer, P; (2004). "**Diagnostic staging of Parkinson's disease: conceptual aspects.**". *Journal of Neural Transmission* 111 (2): 201-216.
- Pubill, D; Gasulla, D; Sureda, FX; Camins, A; Pallas, M; Escubedo, E; & Camarasa, J; (1998). "**Characterization of [H-3]nisoxetine binding in rat vas deferens membranes: Modulation by sigma and PCP ligands**". *Life Sciences* 62 (8): 763-773.
- Raffel, DM & Wieland, DM; (2001b). "**Assessment of cardiac sympathetic nerve integrity with positron emission tomography**". *Nucl.Med.Biol.* 28 (5): 541-559.
- Raffel, DM & Wieland, DM; (2001a). "**Assessment of cardiac sympathetic nerve integrity with positron emission tomography**". *Nucl.Med.Biol.* 28 (5): 541-559.

- Rang, HP; Dale, MM; Ritter, JM; & Moore, PK; (2003). "**Pharmacology**" Churchill Livingstone, London.
- Reimann, B; Kopka, K; Stogbauer, F; Halfter, H; Ketteler, S; Vu Phan, TQ; Franzius, C; Weckesser, M; Ringelstein, EB; & Schober, O; (2001). "**Kinetic parameters of 3-[<sup>123</sup>I]iodo-L-a-methyl tyrosine ([<sup>123</sup>I]IMT) transport in human GOS3 glioma cells**". *Nuclear Medicine and Biology* 28 293-297.
- Riemann, B; Kopka, K; Stogbauer, F; Halfter, H; Ketteler, S; Vu Phan, TQ; Franzius, C; Weckesser, M; Ringelstein, EB; & Schober, O; (2001). "**Kinetic parameters of 3-[<sup>123</sup>I]iodo-L-a-methyl tyrosine ([<sup>123</sup>I]IMT) transport in human GOS3 glioma cells**". *Nuclear Medicine and Biology* 28 293-297.
- Rogers, C & Lemaire, S; (1992). "**Characterisation of [<sup>3</sup>H] desmethylinipramine binding in bovine adrenal medulla: interactions with sigma- and (or) phencyclidine-receptor ligands**". *Can J Physiol Pharmacol* 70 (11): 1508-1514.
- Saha, S; Chant, D; Welham, J; & McGrath, J; (2005). "**A systematic review of the prevalence of schizophrenia**". *Plos Medicine* 2 (5): 413-433.
- Scanley, BE; Gandelman, MS; Laruelle, M; Al-Tikriti, MS; Baldwin, RM; Zoghbi, SS; Hoffer, PB; Wang, S; Neumeyer, JL; & Innis, RB; (2000). "**[<sup>123</sup>I]IPCIT and [<sup>123</sup>I]beta-CIT as SPECT tracers for the dopamine transporter: a comparative analysis in nonhuman primates**". *Nucl.Med.Biol.* 27 (1): 13-21.
- Schill, G; Wainer, IR; & Barkan, SA; (1986). "**Chiral separations of cationic and anionic drugs on an alpha1-acid glycoprotein-binded stationary phase (Enantio-Pac) - influence of mobile phase additives and pH on chiral resolution and retention.**". *Journal of Chromatography* 365 73-88.
- Schmitz, J; (2011). "**The production of [(124)I]iodine and [(86)Y]yttrium**". *European Journal of Nuclear Medicine and Molecular Imaging* 38 4-9.
- Schou, M; Pike, VW; & Halldin, C; (2007). "**Development of radioligands for imaging of brain norepinephrine transporters in vivo with positron emission tomography**". *Curr.Top.Med.Chem.* 7 (18): 1806-1816.
- Shikano, N; Kawai, K; Nakajima, S; Nishii, R; Flores, LG2; Kubodera, A; Kubota, N; Ishikawa, N; & Saji, H; (2004). "**Renal accumulation and excretion of radioiodinated 3-iodo-alpha-methyl-L-tyrosine.**" *Ann Nucl Med.* 18 (3): 263-270.  
Reference Type: Abstract.
- Smith, K & Valkó-Slegel, K; (2004). "**Developability Assay - Human Serum Albumin Protein Binding - HPLC - % Bound - ST - sites running assay are ST and UM**".  
Reference Type: GlaxoSmithKline Data File.

- Sora, I; Li, B; Fumushima, S; Fukui, A; Arime, Y; Kasahara, Y; Tomita, H; Ikeda, K; & .; (2009). Chapter 3: "**Chapter 3 Monoamine Transporter as a Target Molecule for Psychostimulants**" / In: Bagetta, G; (2009) "**International Review of Neurobiology** **International Review of Neurobiology - 85**" *Academic Press*, Pp. 29-33.
- Stein, L & Wise, CD; (1971). "**Possible etiology of schizophrenia: progressive damage to the noradrenergic reward system by 6-hydroxydopamine**". *Science* 171 (975): 1032-1036.
- Sternberg, DE; van Kammen, DP; Lake, CR; Ballenger, JC; Marder, SR; & Bunney, WE, Jr.; (1981). "**The effect of pimozide on CSF norepinephrine in schizophrenia**". *Am.J Psychiatry* 138 (8): 1045-1050.
- Suddath, RL; Christison, GW; Torrey, EF; Casanova, MF; & Weinberger, DR; (1990). "**Anatomic Abnormalities in the Brains of Monozygotic Twins Discordant for Schizophrenia**". *New England Journal of Medicine* 322 (12): 789-794.
- Svensson, TH; (2003). "**alpha-Adrenoceptor modulation hypothesis of antipsychotic atypicality**". *Progress in Neuro-Psychopharmacology and Biological Psychiatry* 27 (7): 1145-1158.
- Takano, A; Suzuki, K; Kosaka, J; Ota, M; Nozaki, S; Ikoma, Y; Tanada, S; & Suhara, T; (2006). "**A dose-finding study of duloxetine based on serotonin transporter occupancy**". *Psychopharmacology (Berl)* 185 (3): 395-399.
- Tamagnan, GD; Brenner, E; Alagille, D; Staley, JK; Haile, C; Koren, A; Early, M; Baldwin, RM; Tarazi, FI; Baldessarini, RJ; Jarkas, N; Goodman, MM; & Seibyl, JP; (2007). "**Development of SPECT imaging agents for the norepinephrine transporters: [123I]NER**". *Bioorg.Med.Chem.Lett.* 17 (2): 533-537.
- Tanaka, M; (1999). "**Emotional stress and characteristics of brain noradrenaline release in the rat.**". *Industrial Health* 37 (2): 143-156.
- Tanaka, M; Yoshida, M; Emoto, H; & Ishii, H; (2000). "**Noradrenaline systems in the hypothalamus, amygdala and locus coeruleus are involved in the provocation of anxiety: basic studies.**". *European Journal of Pharmacology* 405 (1-3): 397-406.
- Tatsumi, M; Groshan, K; Blakely, RD; & Richelson, E; (1997). "**Pharmacological profile of antidepressants and related compounds at human monoamine transporters**". *European Journal of Pharmacology* 340 (2-3): 249-258.
- Tatsumi, M; Jansen, K; Blakely, RD; & Richelson, E; (1999). "**Pharmacological profile of neuroleptics at human monoamine transporters**". *Eur.J Pharmacol* 368 (2-3): 277-283.

- Tavares, AAS; Jobson, NK; Dewar, D; Sutherland, A; & Pimlott, SL; (2011). "**123I-NKJ64: A Novel Single Photon Emission Computer Tomography Radiotracer for Imaging the Noradrenaline Transporter in Brain**". *Synapse* 65 658-667.
- Tjuvajev, JG; Macapinlac, HA; Daghighian, F; Scott, AM; Ginos, JZ; Finn, RD; Kothari, P; Desai, R; Zhang, JJ; Beattie, B; Graham, M; Larson, SM; & Blasberg, RG; (1994). "**Imaging of Brain-Tumor Proliferative Activity with Iodine-131-Iododeoxyuridine**". *Journal of Nuclear Medicine* 35 (9): 1407-1417.
- Tonge, SR & Leonard, BE; (1972). "**Interaction of Phencyclidine with Drugs Affecting Noradrenaline Metabolism in the Rat Brain**". *Psychopharmacologia* 23 86-90.
- Tovell, DR; Samuel, J; Mercer, JR; Misra, HK; Xu, L; Wiebe, LI; Tyrrell, DL; & Knaus, EE; (1988). "**The in vitro evaluation of nucleoside analogues as probes for use in the noninvasive diagnosis of herpes simplex encephalitis**". *Drug design and delivery* 3 (3): 213-221.  
Reference Type: Abstract.
- Tytgat, GA; van, dB; Voute, PA; Smets, LA; & Rutgers, M; (2002). "**Human megakaryocytes cultured in vitro accumulate serotonin but not meta-iodobenzylguanidine whereas platelets concentrate both**". *Exp.Hematol.* 30 (6): 555-563.
- United Nations Population Division; (17 November 2006). "**World Population Prospects: The 2004 Revision Population Database**"  
<http://esa.un.org/unpp/>  
Reference Type: Electronic Citation.
- Vaidyanathan, G & Zalutsky, MR; (1998). "**Preparation of 5-[131I]iodo- and 5-[211At]astato-1-(2-deoxy-2-fluoro-beta-D-arabinofuranosyl) uracil by a halodestannylation reaction**". *Nucl.Med.Biol.* 25 (5): 487-496.
- Valentini, V; Frau, R; & Di, CG; (2004). "**Noradrenaline transporter blockers raise extracellular dopamine in medial prefrontal but not parietal and occipital cortex: differences with mianserin and clozapine**"  
*J.Neurochem.* 88 (4): 917-927.  
Reference Type: Abstract.
- Valkó, K.; (2008). "**Personal Communication: HPLC Methodologies**"
- Valkó, K; (2004). "**Application of high-performance liquid chromatography based measurements of lipophilicity to model biological distribution**". *Journal of Chromatography A* 1037 299-310.
- Valkó, K; (2008). "**AGP Column Methodology - GSK AESOP**".  
Reference Type: GlaxoSmithKline Data File.

- Valkó, K; Bevan, C; & Reynolds, D; (1997). "**Chromatographic Hydrophobicity Index by Fast-Gradient RP-HPLC: A High-Throughput Alternative to log P/logD**". *Analytical Chemistry* 69 (11): 2022-2029.
- Valkó, K; Du, CM; Bevan, CD; Reynolds, DP; & Abraham, MH; (2000). "**Rapid-Gradient HPLC Method for Measuring Drug Interactions with Immobilized Artificial Membrane: Comparison with Other Lipophilicity Measures.**". *Journal of Pharmaceutical Sciences* 89 (8): 1085-1096.
- Valkó, KL; Nunhuck, SB; & Hill, AP; (2011). "**Estimating Unbound Volume of Distribution and Tissue Binding by In Vitro HPLC-Based Human Serum Albumin and Immobilised Artificial Membrane-Binding Measurements**". *Journal of Pharmaceutical Sciences* 100 (3): 849-862.
- Valkó-Slegel, K; (2004). "**Developability studies (klv39154) - HPLC - CHI - Lipophilicity - ST - Chromatographic Hydrophobicity Index**".  
Reference Type: GlaxoSmithKline Data File.
- Vallabhajusola, S; (2009). Chapter 9: "**Radiopharmaceuticals**" / In: Anonymous(2009) "**Molecular Imaging - Radiopharmaceuticals for PET and SPECT**" *Springer-Verlag*, Berlin Heidelberg. Pp. 133-149.
- van Rossum, JM; (1966). "**The significance of dopamine-receptor blockade for the mechanism of action of neuroleptic drugs**".  
*Arch.Int.Pharmacodyn. Ther.* 160 (2): 492-494.
- Varastet, M; Brouillet, E; Chavoix, C; Prenant, C; Crouzel, C; Stulzaft, O; Bottlaender, M; Cayla, J; Maziere, B; & Maziere, M; (1992). "**In vivo visualization of central muscarinic receptors using [11C]quinuclidinyl benzilate and positron emission tomography in baboons**". *Eur.J Pharmacol* 213 (2): 275-284.
- Varrone, A & Halldin, C; (2010). "**Molecular Imaging of the Dopamine Transporter**". *Journal of Nuclear Medicine* 51 (9): 1331-1334.
- Waterhouse, RN; (2003). "**Determination of lipophilicity and its use as a predictor of blood-brain barrier penetration of molecular imaging agents**". *Mol.Imaging Biol.* 5 (6): 376-389.
- Whittington, CJ; Kendall, T; Fonagy, P; Cottrell, D; Cotgrove, A; & Boddington, E; (2004). "**Selective serotonin reuptake inhibitors in childhood depression: systematic review of published versus unpublished data**".  
*Lancet* 363 (9418): 1341-1345.
- Wong, EHF; Kemp, JA; Priestley, T; Knight, AR; Woodruff, GN; & Iversen, LL; (1986). "**The Anticonvulsant Mk-801 Is A Potent N-Methyl-D-Aspartate Antagonist**". *Proceedings of the National Academy of Sciences of the United States of America* 83 (18): 7104-7108.

- Wong, EHF; Sonders, MS; Amara, SG; Tinholt, PM; Piercey, MFP; Hoffmann, WP; Hyslop, DK; Franklin, S; Porsolt, RD; Bonsignori, A; Carfagna, N; & McArthur, RA; (2000). "**Reboxetine: A pharmacologically potent, selective, and specific norepinephrine reuptake inhibitor**". *Biological Psychiatry* 47 (9): 818-829.
- Wyatt, RJ; Henter, I; Leary, MC; & Taylor, E; (1995). "**An Economic Evaluation of Schizophrenia - 1991**". *Social Psychiatry and Psychiatric Epidemiology* 30 (5): 196-205.
- Yamamoto, K & Hornykiewicz, O; (2004). "**Proposal for a noradrenaline hypothesis of schizophrenia**". *Progress in Neuro-Psychopharmacology & Biological Psychiatry* 28 (5): 913-922.
- Zeng, F; Jarkas, N; Stehouwer, JS; Voll, RJ; Owens, MJ; Kilts, CD; Nemeroff, CB; & Goodman, MM; (2008). "**Synthesis, in vitro characterization, and radiolabeling of reboxetine analogs as potential PET radioligands for imaging the norepinephrine transporter**". *Bioorganic & Medicinal Chemistry* 16 (2): 783-793.
- Zeng, F; Stehouwer, JS; Jarkas, N; Voll, RJ; Williams, L; Camp, VM; Votaw, JR; Owens, MJ; Kilts, CD; Nemeroff, CB; & Goodman, MM; (2007). "**Synthesis and biological evaluation of 2 beta,3 alpha-(substituted phenyl)nortropanes as potential norepinephrine transporter imaging agents**". *Bioorganic & Medicinal Chemistry Letters* 17 (11): 3044-3047.
- Zoghbi, SS; Tamagnan, G; Baldwin, MF; Al-Tikriti, MS; Amici, L; Seibyl, JP; & Innis, RB; (2001). "**Measurement of plasma metabolites of (S)-5-[123I]iodo-3-(2-azetidylmethoxy)pyridine (5-IA-85380), a nicotinic acetylcholine receptor imaging agent, in nonhuman primates**". *Nucl.Med.Biol.* 28 (1): 91-96.

## Bibliography

Jobson, NK; Spike, R; Crawford, AR; Dewar, D; Pimlott, SL; Sutherland, A (2008).

**“Stereoselective synthesis of (2S,3R)- and (2R,3S)-iodoreboxetine; potential SPECT imaging agents for the noradrenaline transporter.”**

*Organic & Biomolecular Chemistry* 6 (13): 2369-2376.

Jobson, NK; Crawford, AR; Dewar, D; Pimlott, SL; Sutherland, A (2008). “**New**

**iodoreboxetine analogues for SPECT imaging of the noradrenaline**

**transporter.”** *Bioorganic & Medicinal Chemistry Letters* 18 (18): 4940-4943.

Jobson, NK; Crawford, AR; Dewar, D; Pimlott, SL; Sutherland, A (2009). “**Design**

**and synthesis of (3R,3S)-iodoreboxetine analogues for SPECT imaging**

**of the noradrenaline transporter.”** *Bioorganic & Medicinal Chemistry*

*Letters* 19 (17): 4996-4998.

Crawford, AR; Cochran, SM; Morris, BJ; Pratt, JA; Dewar, D (2007). “**Imaging**

**Monoamine Transporters in the PCP-induced Rat Model of the**

**Metabolic Hypofrontality Observed in Schizophrenia”** *Scottish Society*

*for Experimental Medicine Meeting Abstract* pp.36

[http://www.ssem.org.uk/file\\_download.asp?DownloadID=39](http://www.ssem.org.uk/file_download.asp?DownloadID=39)